Influence of Bow-Wave Breaking on the Added Resistance of Fast Ships

Choi, BongJun

DOI
10.4233/uuid:f1e5b2d3-eb4e-4f66-af89-cc5380bef837

Publication date
2018

Document Version
Final published version

Citation (APA)
Choi, B. (2018). *Influence of Bow-Wave Breaking on the Added Resistance of Fast Ships*. [Dissertation (TU Delft), Delft University of Technology]. https://doi.org/10.4233/uuid:f1e5b2d3-eb4e-4f66-af89-cc5380bef837

Influence of Bow-Wave Breaking on the Added Resistance of Fast Ships

BongJun Choi

Influence of Bow-Wave Breaking on the Added Resistance of Fast Ships

Dissertation

for the purpose of obtaining the degree of doctor
at Delft University of Technology
by the authority of the Rector Magnificus prof. dr. ir. T.H.J.J. van der Hagen
chair of the Board for Doctorates
to be defended publicly on
Tuesday 6 March 2018 at 10:00 o'clock

by

BongJun Choi

Master of Science in Naval Architecture and Ocean Engineering
Seoul National University, Republic of Korea
born in Chang-Won, Republic of Korea.

This dissertation has been approved by the promotors.

Composition of the doctoral committee:	
Rector Magnificus,	chairperson
Prof. dr. ir. R. H. M. Huijsmans	Delft University of Technology, promotor
Dr. ir. P. R. Wellens	Delft University of Technology, copromotor
Independent members:	
Prof. dr. Y. H. Kim	Seoul National University, Republic of Korea
Prof. dr. -ing. O. el Moctar	University of Duisburg-Essen, Germany
Prof. dr. ir. C. H. Venner	University of Twente
Prof. dr. P. A. Wilson	University of Southampton, United Kingdom
Prof. ir. J. J. Hopman	Delft University of Technology
Prof. dr. ir. A. P. van't Veer	Delft University of Technology(reserve)

The author of this thesis was financially supported by the Hyundai Heavy Industries (HHI). This research was supported by the Delft University of Technology and the Maritime Research Institute Netherlands (MARIN).

Keywords: added resistance, fast ships, bow-wave breaking, relative wave elevation, non-linearity assessment

Printed by: Gildeprint

Front cover: Plunging breaking of the bow wave in the fast ship

ISBN 978-94-6186-906-7

An electronic version of this dissertation is available at
`http://repository.tudelft.nl/`.

To those
I live with.

SUMMARY

The publication of the Energy Efficiency Design Index (EEDI) by the International Maritime Organization (IMO) has recently stimulated the accurate assessment of actual sea performance of ships, which is evaluated as added resistance in waves. However, a satisfactory consensus on the evaluation method has not yet been reached owing to uncertainty in wave added resistance. This uncertainty can be improved by developing analytical methods that recognize nonlinearities. A typical factor contributing to the uncertainty of added resistance is the breaking of the bow wave. In this study, an evaluation method is developed to explain the nonlinearity of added resistance due to the uncertainty of bow-wave breaking. The accuracy of evaluation of added resistance can be improved by considering the speed of the ship, which affects the stability of the bow wave. This study also confirms that the breaking of the bow wave causes a violation of the linear relation between the pressure and the relative wave elevation of the bow wave.

In order to express the nonlinearity of added resistance due to the breaking of the bow wave, a transfer function including the speed of the ship is proposed because the speed of the ship affects the stability type of bow-wave breaking. By analyzing the results of the added resistance measured in a fast ship series test, it was confirmed that the added resistance should be evaluated by considering the ship's speed. In addition, hull pressures and relative wave elevations are measured for the mother ship of the series test, and analysis tools are developed to represent the nonlinearity between these two signals. This analysis confirms that the nonlinear relationship between the hull pressure and the relative wave elevation, which significantly contributes to the added resistance, is greatly influenced by the speed of the ship.

This study provides important insight into the violation of the linear relation by using the proposed analysis tools. The results show that the nonlinearity due to the plunging breaking of a bow wave is intuitively detected. The nonlinearity is shown to vary with the ship's speed. The findings provide a better understanding of the process of plunging breaking of bow waves.

Based on the above findings, a correction model is proposed to improve the accuracy of numerical calculation performed using the linear potential theory. The calculation of the fast ship is compared with the experimental results. The results reveal that the accuracy of added resistance estimation can be improved through the physics-based correction. Furthermore, a method for improving the reliability of the added resistance estimation is proposed by identifying the nonlinearity of the plunging breaking of the bow wave on a fast displacement ship.

CONTENTS

Summary vii

Contents viii

1 Introduction 1
- 1.1 Motivation . . . 1
- 1.2 Research objective and outline . . . 3

2 Literature review and background 5
- 2.1 Introduction . . . 5
- 2.2 Evaluation of wave added resistance . . . 5
  - 2.2.1 Experimental methods . . . 6
  - 2.2.2 Theoretical and numerical methods . . . 8
  - 2.2.3 Computational fluid dynamics . . . 14
- 2.3 Research trends and limitations . . . 15
  - 2.3.1 Need to improve accuracy . . . 15
  - 2.3.2 Needs for practical estimation methods . . . 16
  - 2.3.3 Elements of wave added resistance . . . 17
- 2.4 Research on bow waves . . . 19
  - 2.4.1 Experimental observation . . . 20
  - 2.4.2 Numerical simulation . . . 22
  - 2.4.3 Theoretical approach . . . 23
  - 2.4.4 Nonlinearity of bow waves . . . 23
  - 2.4.5 Stability type of bow-wave breaking . . . 25
  - 2.4.6 Nonlinear effects on resistance . . . 27
- 2.5 Conclusions . . . 29

3 Influence of plunging breaking of bow wave 31
- 3.1 Introduction . . . 31
- 3.2 Hypothesis . . . 32
- 3.3 Feasibility study on fast ships . . . 34
  - 3.3.1 Model ship . . . 34
  - 3.3.2 Data analysis . . . 36
  - 3.3.3 Performance in calm water . . . 37
  - 3.3.4 Performance in short waves . . . 39
  - 3.3.5 Performance in intermediate waves . . . 41
- 3.4 Interpretation using transfer function . . . 42
- 3.5 Conclusions . . . 46

4 Experimental assessment of effects of bow-wave breaking 49
4.1 Introduction . . . 49
4.2 Measurement of a fast ship . . . 50
4.3 Observation of bow-wave breaking . . . 52
4.4 Development of evaluation template . . . 57
4.4.1 Sequence history of pressure . . . 57
4.4.2 Pressure and relative wave elevation diagram . . . 61
4.5 Analysis of model test results . . . 66
4.5.1 Results in short waves . . . 66
4.5.2 Results in intermediate waves . . . 66
4.5.3 Results in long waves . . . 66
4.5.4 Nonlinearity assessment . . . 70
4.6 Process definition of plunging breaking . . . 71
4.7 Nonlinear influence on added resistance . . . 74
4.7.1 Time average of pressure . . . 74
4.7.2 Vertical integration of pressure . . . 78
4.7.3 Surface integration of pressure . . . 78
4.8 Conclusions . . . 81

5 Numerical implementation of bow-wave breaking effects 83
5.1 Introduction . . . 83
5.2 Linear potential method calculation . . . 85
5.2.1 Model ship and calculation settings . . . 86
5.2.2 Calculation results for FDS-5 . . . 86
5.3 Causes of overestimation of added resistance . . . 91
5.3.1 Contributions to added resistance . . . 91
5.3.2 Analysis of relative wave elevation . . . 95
5.4 Solution of correction model . . . 99
5.5 Validation of the correction model . . . 104
5.5.1 Calculation and correction for FDS-11 . . . 104
5.5.2 Calculation and correction for FDS-20 . . . 106
5.6 Conclusions . . . 108

6 Conclusions 109
6.1 Contribution of the thesis . . . 109
6.2 Recommendations for future work . . . 112

A The sequence history of pressure 117

B Assessment of amplitude effect in short waves 127

C Assessment of amplitude effect in intermediate waves 139

References 151

Nomenclature 159

Acknowledgements 163

Curriculum Vitæ 167

List of Publications **169**

1

INTRODUCTION

1.1. Motivation

Ship designers and operators are interested in reducing fuel consumption and CO_2 production for improving cost efficiency and reducing environmental impact. To that end, the Energy Efficiency Design Index (EEDI) regulation has been adopted by the International Maritime Organization (IMO). The regulation requires that EEDI is applied to new ships built from 2015 in order to reduce CO_2 emissions by 30% by 2030. Furthermore, the IMO will implement a regulation on the monitoring, reporting, and verification (MRV) of fuel usage from 2019 to analyze the status of a ship's greenhouse gas emissions [1].

The reduction of fuel consumption and greenhouse gas emissions by increasing the energy efficiency of a ship is possible by accurately predicting and evaluating the forces required for the ship to move at a constant speed. The force acting on the hull is a resistance when the ship is moving at a constant speed in calm water. The additional force required to maintain a constant speed even when the ship encounters incident waves is called added resistance. The performance of the hullform must be accurately predicted before building the ship because the ship's sea performance is difficult to change after the design has been finalized and building has started [2].

Model tests are thus far the most reliable method to predict the added resistance, since hydrodynamic interactions between the hull and the incoming waves are very complex. Alternatively, a comparative solution in computational fluid dynamics can be obtained using a solver based on the Reynolds-averaged Navier-Stokes (RANS) equation, which includes the viscosity of the fluid and the nonlinear free-surface effect [3, 4].

Nevertheless, neither method is cost-effective in the preliminary design stage. Model tests require much care in preparation and data measurement, and the RANS technique is time-consuming to generate proper grids to capture the detailed phenomena and perform the calculations. Therefore, a more suitable method for estimating added resistance is sought. The linear potential theory method, which has a small calculation requirement, can be used to determine the character of the added resistance quickly. Although the accuracy of the linear potential theory method is limited, it is suitable for grasping the tendency of the added resistance [5]. This is because the motion response of the ship can be estimated relatively accurately [6, 7]. A ship's motion response is a major factor determining the added resistance of the ship navigating in waves. Furthermore, the reflection of waves by the hull plays a significant role. In the linear potential theory method, the influence of a wave reflected on the hull is regarded as a linearized diffraction effect.

While the linear potential theory method is attractive because of the promptness of its calculation, it has a drawback that it does not take into account the influence of viscous resistance by friction. The effect of viscosity is generally neglected because it hardly contributes to the ship's motion response or the reflected wave [8]. Therefore, many studies based on the linear potential theory have ignored the influence of viscosity on the added resistance. However, when the influence of reflection of waves by the hull is dominantly nonlinear (e.g., owing to breaking), the added resistance cannot be calculated accurately by the linear potential theory method. Therefore, if the added resistance can be estimated more accurately by taking into account the generation of nonlinearity between the hull and the incident wave, the linear potential theory method can still be attractive.

The effect of the reflected wave of the hull, especially the wave breaking part, is a typical issue that has hardly been considered in the past in the context of wave added resistance. Previously, the added resistance could be estimated by focusing on the motion responses that make the greatest contribution. However, in addition to the motion response of the ship, the diffraction effect due to the change in hull-form (such as an increase in the length of the ship) in parallel with the issuing of EEDI regulations is important because, for example, the motion response is significantly decreased under normal operating conditions for ships longer than approximatley 300 m. Therefore, understanding the phenomenon of bow-wave breaking, which appears in a complicated form, can improve the evaluation method of added resistance. In order to investigate the effect of the complex wave phenomenon of added resistance, the research subject needs to be confined to a specific breaking phenomenon by clearly defining the influence factors. Moreover, it is necessary to present a method to evaluate the added resistance based on the understanding of the breaking phenomenon.

1.2. Research objective and outline

This thesis presents a method to improve the reliability of added resistance estimation through the identification of nonlinearities caused by breaking of the bow wave on fast ships. This method is motivated by the realization that numerical analysis cannot adequately evaluate the nonlinearity caused by the breaking of the bow wave. Moreover, a correction model is presented to consider the nonlinearity in the added resistance evaluation. An outline of the thesis is shown in Figure 1.1 together with the connections of chapters.

Chapter 2 reviews existing literature and background information on the added resistance and the breaking of the bow wave and analyzes the limitations of existing research results. The existing research results on the breaking of the bow wave are discussed to find a method to consider the bow-wave breaking in the evaluation of added resistance.

Chapter 3 presents a hypothesis that an increase or decrease of the added resistance depends on the stability type of the bow wave and confirms its validity by analyzing model test results. Since the ship's speed can change the type of breaking of the bow wave, the speed is set as an independent variable to test the hypothesis. The transfer function of the added resistance including the speed of the ship is presented and set as a dependent variable. Then, the hypothesis is verified by analyzing a series test of fast ships. This feasibility test confirms that the added resistance evaluation considering the ship's speed is appropriate.

Chapter 4 examines the nonlinearity between the relative wave elevation of the bow wave and the hull pressure that is caused by plunging breaking, which is known to have a relatively small influence on viscosity among the wave types presented in Chapter 3. Analysis templates are proposed to intuitively evaluate the nonlinearity of the elevation of the bow wave and the pressure distribution on the hull surface, which significantly influence the added resistance estimation, and the nonlinearity of the fast ship is analyzed using these tools. In this investigation, it is confirmed that the nonlinearity occurring between the relative wave elevation and the hull pressure closely depends on the speed of the ship.

Chapter 5 confirms that the accuracy of the added resistance estimation by the numerical calculation can be improved by considering the nonlinearity that depends on the speed of the ship, based on the findings of previous chapters. It is also confirmed that the same estimation method can be applied to a similar type of hullform at the same speed of the ship.

Chapter 6 presents the major research findings and suggestions for future studies. It concludes that the reliability of the added resistance estimation can be improved by identifying the nonlinearity that occurs between the ship's hull and the breaking of the bow wave.

1

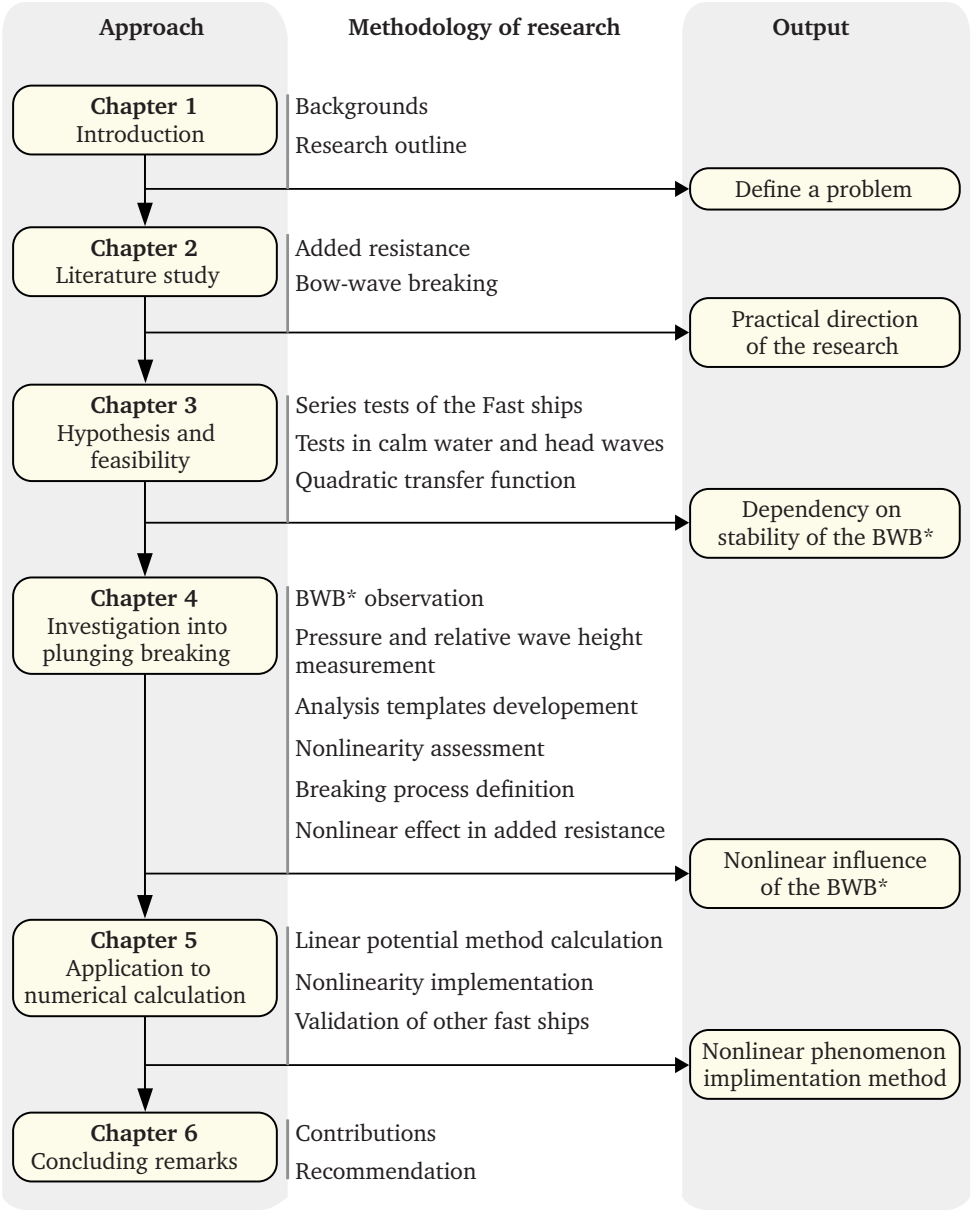

* BWB: Bow-wave breaking

Figure 1.1: Outline of the thesis

2

LITERATURE REVIEW AND BACKGROUND

2.1. Introduction

As discussed in Chapter 1, the influence of bow-wave breaking on the added resistance is not clearly defined. This chapter reviews the literature on methods for evaluating the added resistance, examines the phenomenon of bow-wave breaking, and discusses a realistic solution for predicting the nonlinear influences of bow-wave breaking on the added resistance.

Section 2.2 introduces previous studies on added resistance estimation methods. Section 2.3 identifies the factors to consider for enhancing the accuracy of the added resistance estimation. Section 2.4 analyzes previous research on bow waves. The results of the review are presented as the main question of this thesis in Section 2.5.

2.2. Evaluation of wave added resistance

This section reviews the literature on the evaluation of the wave added resistance of a ship. When a ship sails through waves, the forward speed of the ship is less

than the speed in calm sea for the same power supplied to the engines. The speed difference of the ship can be estimated by evaluating the added resistance, which is the load increase due to the incoming waves. The added resistance in waves has been extensively studied through experimental, theoretical, and numerical methods. The literature on wave-added resistance evaluation provides a variety of solutions.

Research on the added resistance shows a dependency on the properties of the wave (length and height) and the ship (hullform, heading, speed, and motion response). The increase in added resistance due to waves is mainly caused by the phase difference between the motion of the incident wave against the ship and the motion response of the ship. The maximum value of the added resistance is related to the peak of the motion response of the ship.

The added resistance has secondary characteristics. According to the analytical approach of Maruo [9], the added resistance is proportional to the squared of the wave amplitude function (Kochin function), which is given as a superposition of the diffraction wave (ζ_{diff}) and radiation wave(ζ_{rad}). Since ζ_{rad} is proportional to the ship motion amplitude, the square of ζ_{rad} is linearly proportional to the square of the motion response. Strom-Tejsen *et al.* [10] experimentally showed that the added resistance in regular waves changes linearly with the square of the wave amplitude at a constant wavelength.

Blok [11] showed that the vertical relative motion response of the ship is the dominant factor contributing to the added resistance. This is confirmed by the non-dimensionalized added resistance based on the square of the relative motion through experimental and mathematical modeling. He also showed that the upper part of the bow's waterline greatly contributed to the added resistance, while the lower part and stern part have small contributions.

In addition, the added resistance is relatively small compared to the amplitude of oscillating forces acting on the ship since it is the average of the forces. A deviation in the prediction for the relative wave or motion response generally causes a deviation in the added resistance prediction. Therefore, a high accuracy is required for the predictions.

2.2.1. Experimental methods

The hydrodynamic interaction between the hull and the incoming wave is complex. Thus far, the model test has been regarded as the most reliable method for evaluating added resistance. The biggest advantage of the model test is that realistic modeling can adequately simulate significant physical phenomena. This is especially important when applying a concept or a design solution to the application.

Model tests provide reliable benchmark data for the added resistance. Reliable benchmark data helps to understand physical phenomena and to verify the accuracy of numerical calculations. However, the main problem with model testing is that it is difficult to change the modeling conditions during testing. In addition, the measurement of added resistance is sensitive because the amplitude of the measured value is large while the mean value is small.

The strict preparation of test equipment is required for the measurement of added resistance, and the fine calibration of the measurement device is required

Figure 2.1: Model test in waves of a fast ship [12]

for accurate measurements. The measurement reference points must be maintained while measuring oscillating signals. Careful treatments of electrical wires connected to various measuring instruments are essential to reduce noise. Furthermore, there is a possibility of noise in the measured signal due to the vibration of the towing carriage. The limits of the amplitude and wavelength of wave conditions made by the wave generator must be considered in the experiment planning.

Experiments have time limits. After testing one condition, it takes a long time until the waves of the test tank become calm again. In addition, long measurements are advantageous for obtaining reliable data. However, the measurement time is limited by the size of the experiment tank.

In general, the viscosity is known to have no significant effect on motion response and added resistance. However, if the scale factor is large and the ship model is too small, a scale effect due to viscosity or surface tension may occur. Ley *et al.* [4] showed through computational fluid dynamics (CFD) simulations that viscosity plays a role in the evaluation of the added resistance in short waves.

Although these difficulties exist, experimental data are invaluable. In the present research, recent experimental studies are used to develop the analytical techniques in response to new needs. Current trends and new requirements are discussed in Section 2.3.

Gerritsma and Beukelman [13] measured the added resistance on the Series-60 model. Fujii and Takahashi [14] and Nakamura and Naito [15] measured the added resistance with the S175 container ship. Journée [16] measured the added resistance of the Wigley models. These experimental data are still used as a benchmark for numerical calculations.

Tsujimoto [17] presented experiments and calculations on added resistance for a container ship and pure car carrier in short waves. The added resistance due to front reflections in short waves is proposed as an empirical equation considering the effect of the ship's speed.

Kuroda *et al.* [18] experimentally investigated the relationship between the wave added resistance and the bow shape above the waterline of container ships. Experiments on three model ships with different bow shapes were performed. The experimentally determined influence of the bow shape above the waterline is compared with the results of a hybrid calculation method using Tsujimoto's empirical equation with Maruo's formula [19].

Guo and Steen [3] measured the added resistance of KVLCC2, the hullform of a conventional large tanker, in short waves. This experiment divided the ship model into three parts, front, parallel middle, and rear, and inspected the added resistance acting on the model parts. The results show that the added resistance of short waves is small in the rear part and concentrated in the front part. The increase in the frictional resistance measured at the middle is also very small. The total added resistance of the short wave is approximately proportional to the square of the amplitude of the incident wave.

Simonsen *et al.* [20] investigated the added resistance of the KCS container ship in calm water and regular waves. The conditions resulting in the maximum motion response for three velocities were selected. The time series of the resistances of the experiment and calculation were compared. The calculation was performed using CFDSHIP-IOWA and StarCCM+, which are unsteady RANS codes. The results of AEGIR, a potential theory time-domain code [21], were also included in the comparison. The comparison shows that the resistance in calm water and waves can be easily disturbed by experimental and numerical uncertainties.

Park *et al.* [22] measured the vertical motion and added resistance of KVLCC2. The measured data were compared with the results obtained using the strip theory method and Rankine panel method, which are described in Section 2.2.2. This research also summarizes and quantifies the causes of uncertainties in the added resistance.

Park *et al.* [23] measured the added resistance for four draft conditions of a tanker in head waves. Experimental results at full load, ballast, and two intermediate conditions were compared with numerical results.

Abdul Ghani and Wilson [24] showed the experimental study of the sea-going performance for four different bulbous bow of the catamaran. They studied the effect of the bulbous bow to the motion response (heave and pitch) and added resistance in waves. The results shows that ships with minimum resistance in calm water do not exhibit the lowest added resistance in waves.

Recently, experiments have been performed to observe nonlinearity in conventional ships and various off-design conditions in addition to design conditions. These experimental data are necessary for developing and validating appropriate numerical techniques.

2.2.2. Theoretical and numerical methods

The theoretical or numerical solutions of the wave added resistance of a ship can be divided into the potential theory method and CFD method. The main cause of the added resistance is the motion response of the hull due to incoming waves and the influence of reflected waves. The effect of viscous resistance due to friction is

negligible compared to the factors mentioned above. Therefore, there are many conventional studies based on the potential theory of wave added resistance.

Potential theory calculation

The potential theory assumes that the ship is rigid and floating on the surface of an inviscid, incompressible and irrotational fluid. Watanabe [25] and Havelock [26, 27] used the Froude-Krylov approximation to solve the sea-keeping problem. In this approximation, the hull does not diffract the incident wave; rather, the ship's motion in regular waves is calculated. But, It was found in [10] that Havelock [26] is not sufficiently accurate for engineering applications.

The added resistance estimation through methods based on the potential theory has a long history and can be divided into several types [28]. The potential theory is used to calculate the added resistance from the linearized potential processing and pressure solutions. Among the practical methods, linearized potential processing can be divided into the strip and the panel method according to the treatment of singularity (Green's function). This solution is used in integral formulas to obtain hydrodynamic forces. Pressure solutions are divided into near-field and far-field methods. In addition, short-wave solutions are provided with a hybrid method.

Singularity treatment

The strip theory can be used to determine the force and motion of a ship based on the potential theory. The strip theory regards a ship as a cross section of a two-dimensional slice. The mapping of the strips translates the half-circle into strips similar to the ship section through an analytical approach [29], as shown in Figure 2.2(a). Each slice is treated as a section of an infinitely long cylinder. Therefore, the strip theory is also referred to as the thin-ship theory. This treatment assumes that the motion response of the ship in waves is physically small.

To simplify the formulation, the strip theory assumes that the components of the radiation wave and diffraction potential slowly change along the length of the ship. The ship's wave load is obtained by integrating the load of all strips along the ship length. The strip theory describes the hydrodynamic effects of each section below the free surface.

Strip theory assumes that the unsteady wave generated by an oscillating ship propagates in a direction perpendicular to the ship's center plane. The interaction between the strips is ignored owing to the two-dimensional approach of the strip theory.

Maruo [19] developed an analytical solution for the added resistance by using the potential theory. Hosoda [30] developed a modification using an isolated singularity method based on the strip theory of Maruo [19]. But, the theory of Maruo [19] and Hosoda [30] gave accurate results only for cruiser-stern ships without large bulbous bows and that is not applicable to other hull forms.

Salvesen *et al.* [31] described a hull section using a close contour mapping method to define the hydrodynamic potential. Most strip theory methods are variants of the stripping method proposed by Salvesen, Tuck, and Faltinsen [32]. It is also referred to as the STF method according to the initial of each author.

Journée [16] reported a comprehensive comparison between experimental data

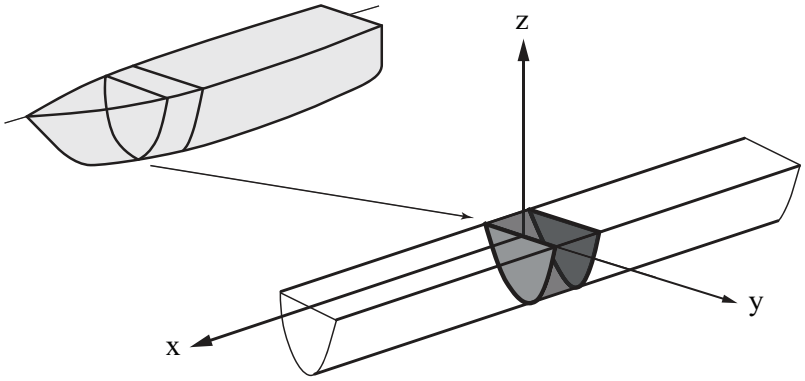

(a) Strip method (adapted from [29])

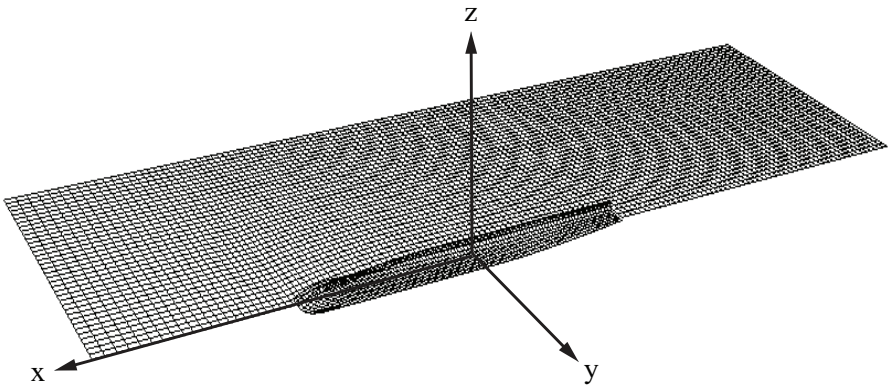

(b) Panel method

Figure 2.2: Representative classification of potential theory methods according to singularity treatment.

and calculated data based on strip theory method. Data on the hydrodynamic coefficients for pitch, vertical motion, wave loading, and added resistance in the form of four Wigley hullforms from experiments performed at the Ship Hydromechanics Laboratory at the Delft University of Technology were compared to the calculated results.

The main advantage of the strip theory method is that the hydrodynamic potential can be solved only by the discretization of the hull. The influence of the wave system around the hullform is ignored, and free-surface conditions are simplified. Therefore, the exact hullform is not simulated. However, the wave system around the actual ship is complex. A breaking of the bow wave is especially important for high-speed or blunt-bow ships. This effect is ignored in the strip theory.

The panel method evaluates the hydrodynamic potential by using a singularity distribution method on the discretized free surface and the hull, instead of evaluation in the strip, as shown in Figure 2.2(b). The panel method uses boundary

conditions to distribute the intensity of the singularity at the boundary of the discretized panels and numerically express the fluid force acting on the ship by using the linear potential theory [33]. The velocity potential of each panel satisfies the Laplace equation, radiation conditions, and simplified free-surface conditions. The nonpenetration condition of the hull is also satisfied for the collocation point of each panel.

The panel method is a numerical method to calculate the hydrodynamic properties around the hull based on Green's integral theorem. A source distribution is expressed by means of the Green's function and is determined by the linear equation for each element. According to this theorem, the three-dimensional Laplace (potential) equation can be transformed into a surface integral equation known as Green's identity [34]. The Green's function is used to find solutions to boundary value problems involving a linear combination of the unknown and its derivatives [35].

Squires and Wilson [36] showed an efficient numerical scheme for evaluating the Green's function. Their approach is based on an alternative form of the pulsating source Green's function of Wu and Taylor [37], a method to subtract the singularity from the integrands of the Green's function, together with an analytical evaluation of the singularity.

Among the panel methods, a widely used method is the Rankine panel method. Gadd [38] and Dawson [39] reported the fundamentals for the boundary element method using Rankine source singularity. They proposed a three-dimensional panel method for a ship's steady resistance problems. The Rankine panel method solves the boundary element problem by distributing Rankine sources as singularities over discrete panels that approximate the underwater surface of the ship. Rankine sources assume singularities with an unknown constant strength, which are expressed as a simple Green's function (l/r) [39] [40].

Sclavounos and Nakos [41] effectively expressed the force and wave of the sea-keeping problem with the Rankine panel method. Their research led to the development of Nakos and Sclavounos [42], a frequency domain panel method called ship wave analysis (SWAN), which can satisfactorily solve a ship's sea-keeping problem.

Raven [43] solved the nonlinear ship resistance problem by moving the singularities generating the flow to a certain height above the free surface while maintaining the collocation points on the exact boundary of the free surface. Bunnik [44] derived the linear discrete dispersion of the reflected and radiated waves of the incident waves based on Raven's results.

One of the advantages of the Rankine panel method is the flexibility to handle complicated shapes and hull surface conditions. In principle, the shape of the hull, created with precision panels, improves the accuracy of the results. This panel method provides a practical estimate of the ship's motion response and resistance. One of the disadvantages is the distortion of the wave system due to free-surface discretization. The handling of numerical radiation conditions can also cause deviations. Linearized free-surface conditions are difficult to be satisfied when nonlinearity occurs because of a blunt hullform at the waterline or high speeds [45].

Fluid pressure solutions

The fluid pressure solution that estimates the added resistance is divided into far-field and near-field methods. The far-field methods include the momentum conservation method [9, 46–48] and the radiated energy method [13, 31]. The near-field method is the direct pressure integration method.

The momentum conservation method is derived from the conservation of energy and momentum of the volume under inspection surrounding the hull. This approach is derived by introducing the slenderness parameter of Joosen [46] into Maruo's equation. Joosen and Newman [49] evaluated added resistance by combining the strip theory with the momentum conservation method to solve for unknowns.

The radiated energy method involves the calculation of added resistance from the generated wave energy and infinite momentum flux. The solution is usually provided in combination with the strip theory. The Gerritsma and Beukelman method (G-B method) [13] is widely used in the literature. This approach evaluates added resistance from the energy contained in the damping wave radiated out of the ship. The radiated energy is calculated by dividing the energy dissipated in one cycle by the distance traveled by the ship in waves.

Salvesen *et al.* [31] applied the two coupled linear equations that govern the heave and pitch motion to the G-B method. Fang and Chen [50] followed Salvesen's approach but used the strip theory in another manner to modify the method and obtained improved results. The calculations are simple and show high correlations with the model tests, especially at the peak values.

The radiated energy method has been extensively used to estimate the added resistance in practical applications. This far-field method is straightforward and robust because it is not necessary to solve a complete boundary value problem for the second-order pressure on the hull surface to obtain the body pressure. However, this approach considers only radiation due to hull motion and has limitations in that it cannot handle the scattering effect. A problem with the use of far-field methods is that the added resistance tends to be zero in short waves because the diffraction effect is not considered. In the case of long waves, it shows a low resistance compared to other methods.

The direct pressure integration method is a near-field method to evaluate added resistance. Boese [51] and Faltinsen *et al.* [52] combined the strip theory method with the direct pressure integration method, while Bunnik [44] and Kim and Kim [53] combined the Ranking panel method with the direct pressure integration method. Boese [51] calculated the added resistance by integrating the pressure on the body surface in the longitudinal direction. The direct pressure integration method involves complicated expressions but simplifies the physical analysis [52].

Grue and Palm [54] and Ye and Hsiung [55] applied the Green's function with the near-field method to the added resistance problem. Joncquez *et al.* [48] extended the AEGIR motion program based on the high-order Rankine panel method to analyze the added resistance problem and apply both far-field and near-field methods.

Kim *et al.* [53, 56] applied higher-order panel methods to added resistance problems by using far-field and near-field methods. They showed that the pressure integration method is more efficient than the G-B method, especially for relatively long or short waves. The pressure integration method can also be successfully used to es-

timate the added resistance peak, but at a high Froude number, the added resistance can be overestimated [45].

Solutions for short waves

In the case of short waves, it is difficult to predict the added resistance without accurately considering the diffraction effect. This is because incident short waves are mostly diffracted, the wavelength of incident short waves is less than the ship length, and the motion response of the ship is almost zero. Much effort has been dedicated to improving the accuracy of this diffraction effect of the added resistance.

Fujii and Takahashi [14] derived semi-empirical formulas for resistance added in the case of short waves. Faltinsen *et al.* [52] derived an asymptotic formula for added resistance in the case of short waves by assuming that the ship has a vertical hullform around the waterline and the incident wave is completely reflected. Both approaches provide good results for a relatively blunt body. However, some results unsatisfactory with high-speed fine-bow ships. To overcome these drawbacks, Kuroda *et al.* [57] proposed a practical correction method for added resistance based on Fujii and Takahashi's method. They modified the existing coefficient using experiment data.

Bingjie and Steen [58] combined the G-B method with Faltinsen's formula to provide a better prediction of the added resistance of KVLCC2 under almost all wavelength conditions. The problem of the G-B method underestimating the added resistance in the case of short waves is solved by applying Faltinsen's formula.

Guo and Steen [3] and Duan and Li [59] developed combined methods to merge effects related to ship motion and reflection. In order to overcome the limitation of the radiated energy method [13] based on ship motion, Guo and Steen [3] applied the asymptotic function of Fujii and Takahashi [14], and Duan and Li [59] applied an extended integral equation in combination with the semi-empirical function of Kuroda *et al.* [57]. These combined methods showed good agreement in all wavelength ranges.

Kashiwagi [60] introduced the enhanced unified theory (EUT) based on Maruo's method to predict the added resistance accurately over the entire range of wavelengths. The evaluation results obtained using the EUT and panel methods are in good agreement with the diffraction effect as well as the radiation. However, the results show a deviation from the measurement when the forward speed of the ship is high. In particular, the deviation is large in the case of short waves, where the wave diffraction near the ship is strengthened, and the nonlinear hydrodynamic effect is prominent.

Seo *et al.* [6, 61] applied three numerical approaches: the strip method, Rankine panel method, and Cartesian grid method. The Cartesian grid method solves the Euler equations to compute the added resistance in waves. The near-field method (direct pressure integration method) and the far-field methods (momentum conservation method and radiated energy method) are adopted for the estimation of added resistance. The added resistance in short waves was also evaluated by an asymptotic approach. The calculated results show a reasonable agreement with the experimental data for the Wigley, Series 60, and S175 container ship.

2.2.3. Computational fluid dynamics

CFD refers to a numerical method that applies field equations such as RANS equations. Codes that use the potential theory have limitations in that they cannot account for turbulence or viscosity, despite extensive work to improve accuracy. As an alternative to overcome these limitations, the CFD solver has been extensively applied to added resistance problems.

The primary purpose of implementing the CFD method in sea-keeping is to solve problems involving strong nonlinear phenomena such as wave breaking, large-amplitude ship motion, and wake flow. CFD is being expanded to complex geometry, and test cases with the RANS method show good results.

Orihara and Miyata [62] analyzed the motion response of the S175 container ship in head waves and evaluated the added resistance by applying the RANS equation in the finite volume method with overlapping grid systems. Simonsen *et al.* [20] obtained good results by estimating movement and added resistance in regular waves for the KCS container ship at the Gothenburg 2010 CFD workshop. Larsson *et al.* [63] compared the performance of various CFD-based methods in an assessment at the Gothenburg 2010 CFD workshop. Various results on the resistance and motion response of ships were compared to experimental data. The three hulls used in the workshop were KVLCC2, KCS, and DTMB 5415. Sadat-Hosseini *et al.* [64] calculated the added resistance for KVLCC2 by using the RANS equation for turbulence modeling and CFDShip-Iowa v4.5, an unsteady RANS (URANS) code with detached eddy simulations [65]. Söding *et al.* [7] calculated the added resistance in head waves from several Froude numbers on the Wigley, a large oil tanker, and a modern container ship. They compared the Rankine panel method with the extended RANS solver. The results are similar in the intermediate and long wavelength regions, but the results for short waves are unsatisfactory with the RANS solver. The comparison results show that the Rankine panel method is still fast and efficient in evaluating the added resistance of a ship in waves.

An open-source and a commercial CFD software are being applied to wave-body interaction issues. Moctar *et al.* [66] applied RANS solvers, OpenFOAM and COMET, to a container carrier and cruise ship. Both methods predict similar values for added resistance. However, RANS solvers need extensive computational effort and have issues such as numerical dispersion in short waves and long waves.

The CFD method has been proved to provide accurate predictions even for complex phenomena. Despite improved computational capabilities, there is still some doubt about the efficiency of the CFD-based method owing to the sensitivity of the grid treatment or time-step interval. Furthermore, it is difficult to apply CFD with special methods for field analysis including the use of turbulence models, free-surface treatment (fluid volume, level set, or particle method), and mesh updates (moving mesh or embedded overset meshing). Even the same approach can produce different results depending on the domain configurations or calculation implementation procedures.

A distinct advantage of certain CFD methods is in the study of nonlinearity. However, compared to potential flow-based methods, CFD is not a time-efficient evaluation method of added resistance. With the help of the development of programs,

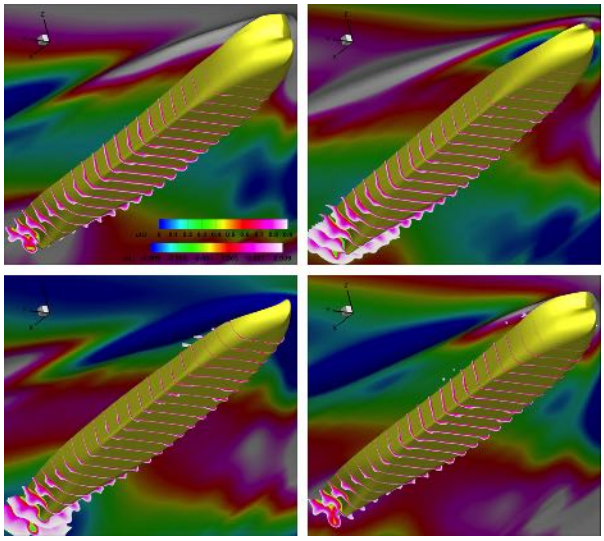

Figure 2.3: CFD solutions of boundary layer represented by slices colored with axial velocity for the four quater encounter periods from Sadat-Hosseini *et al.* [64]

pre-processing and post-processing are becoming simpler, but a large amount of effort is still required to perform calculations.

2.3. Research trends and limitations

Regulations on operational performance have motivated an accurate estimation of added resistance. The accurate estimation of added resistance is a key step in implementing energy-efficiency regulations for ships. The focus of recent research has been to improve and integrate hydrodynamics simulation tools. However, various numerical solutions and multiple operating conditions of ships make it difficult to obtain an integrated solution.

2.3.1. Need to improve accuracy

The Energy Efficiency Design Index (EEDI) and Energy Efficiency Operation Index (EEOI) are important issues in the shipping and shipbuilding industry. Procedures for estimating and identifying CO_2 emissions from ships are being discussed intensively at IMO/Marine Environment Protection Committee (MEPC) [1]. EEDI regulations apply to new ships over 400 GT. EEDI regulations were issued on January 1, 2013.

Regarding the EEDI calculation, the most important parameter in actual operation is the power increase or speed loss in waves. In order to calculate EEDI, these parameters must be predicted by a model test, theoretical calculation, or numerical calculation. The most important aspect in the speed loss calculation is the prediction of the added resistance in waves.

The preceding literature does not cover all the research carried out in this field. However, these studies show various methods and complexities associated with added resistance calculations. Unfortunately, a reliable procedure for calculating the speed loss factor (f_w) in EEDI is not yet available. The decision on a representative method for determining added resistance has been suspended by the International Towing Tank Conference (ITTC) sea-keeping committee [2].

2.3.2. Needs for practical estimation methods

The added resistance can be understood as a combination of various components. Therefore, experimental studies are necessary, but they involve difficulties, as discussed in Section 2.2.1. Numerical approaches estimate the added resistance fairly accurately, but the proper solution applies differently to each problem. In particular, the accuracy of numerical analysis cannot be guaranteed if nonlinear phenomena are involved in a given problem. For example, the numerical analysis of fast ships and large ships in short waves can provide less accurate results. CFD tools, including commercial software, are actively used in the field of sea-keeping. However, the time required for CFD and the quality of results rely heavily on the code developer's technical knowledge and the code operator's proficiency.

A practical solution is required to evaluate the wave added resistance in ship design. Methods of numerical estimation have been extensively reviewed by a consortium of energy efficiency and safety by ship operation (SHOPERA) [5]. SHOPERA is a European research consortium from October 2013 to 2016 with expertise in the maritime industry. The purpose of the consortium was the development of new guidelines on the propulsion and navigation performance required to maintain the performance of a ship under actual sea conditions.

The consortium developed hydrodynamics tools and rules related to experimental techniques, ship design, and operational optimization. SHOPERA studied various types of numerical analysis techniques for various ship types and operating conditions. They mainly considered the potential theory (quasi-2D strip method with possible viscous flow corrections), boundary element method (BEM), 3D panel method with a possible viscous flow, and RANS methods. The reviews show that the BEM method is more suitable than the strip theory, and the RANS method still shows a variation in prediction. Moreover, experimental research is needed to produce reliable benchmark data for the short-wave application.

The complexity of the added resistance can be addressed by applying a better explanation of the nonlinearity of the wave elevation or motion response. Papanikolaou *et al.* [67] corrected the damping coefficient of the potential theory semi-empirically while including viscous flow correction. An understanding of nonlinear phenomena is necessary for problems that are difficult to solve by the numerical method for added resistance. Practical methods for considering nonlinear effects based on an understanding of bow waves should be developed.

2.3.3. Elements of wave added resistance

This section uses the linear potential theory to gain insight into the elements of wave added resistance. The contributing factors are investigated through the direct pressure integration method, which provides a physical understanding. The hydrodynamic force acting on the hull surface can be obtained by integrating the pressure acting on an infinitesimal wetted hull surface (dS), as follows.

$$F\left(\vec{x},t\right) = -\iint_S p\vec{n}dS \tag{2.1}$$

where $\vec{x}$ is the coordinate vector, t is the time, p is the pressure, $\vec{n}$ is the normal vector of the hull and S is the wetted hull surface.

From Bernoulli's equation, the pressure is given by

$$p(\vec{x},t) = -\rho\left(\Psi_t + \frac{1}{2}\nabla\Psi\cdot\nabla\Psi + \frac{1}{2}U^2 + gz\right) + p_{atm} \tag{2.2}$$

where ρ is the fluid density, Ψ is the velocity potential, U is the velocity of the ship, g is the gravity and p_{atm} is the constant atmospheric pressure.

As linear potential flow assumption, a velocity potential Ψ is superposed as follows:

$$\Psi(\vec{x},t) = \Phi(\vec{x}) + \phi(\vec{x}) + \varphi(\vec{x},t) \tag{2.3}$$

where $\Phi(\vec{x})$ is the base-flow potential, $\phi(\vec{x})$ is the steady velocity potential and $\varphi(\vec{x})$ is the unsteady velocity potential.

Using the decomposition of the overall velocity potential, pressure can be divided into a time independent steady part $p_s(\vec{x})$ and a time dependent unsteady part $p_u(\vec{x},t)$.

$$p(\vec{x},t) = p_s(\vec{x}) + p_u(\vec{x},t) \tag{2.4}$$

To obtain the integrals form, a Taylor series and a perturbation series are adapted to the pressure.

$$p = p_0 + \vec{\alpha}\cdot\nabla p_0 + \frac{1}{2}\left(\vec{\alpha}\cdot\nabla\right)^2 p_0 + O\left(|\alpha|^3\right) \tag{2.5}$$

where p_0 is the pressure at average position, the total displacement of $\vec{\alpha} = \vec{\eta} + \vec{\Omega}\times\vec{x}$ with $\vec{\eta}$ is the translational vector and $\vec{\Omega}$ is the rotational motion of the body.

When the formula is further developed, the added resistance, which is the mean value of the second-order force acting on the hull, can be obtained using the following pressure integration approach.

The average of the secondary forces is divided by the components of Equation 2.6 in the following order: velocity squared, the product of angular motion and pressure gradient, the product of linear motion and pressure gradient, the product of angular motion and inertia force, and the waterline contribution of relative wave elevation.

$$\begin{aligned}\left\langle \vec{F}^{(2)} \right\rangle = \Bigg\langle & \frac{1}{2}\rho \iint_{S_0} \nabla\varphi^{(1)} \cdot \nabla\varphi^{(1)} \vec{n} dS \\ & + \iint_{S_0} \Omega^{(1)} \times \left(\Omega^{(1)} \times \vec{x}\right) \cdot \nabla p_s^{(0)} \vec{n} dS \\ & + \iint_{S_0} \left(\vec{\alpha}^{(1)} \cdot \nabla\right) p_u^{(1)} \vec{n} dS \\ & + \Omega^{(1)} \times M\ddot{\vec{x}}_g \\ & - \rho g \int_{wl} \zeta_u^{(1)} \left(\zeta_u^{(1)} - \alpha_3^{(1)}\right) \vec{n} dl + \frac{1}{2}\rho g \int_{wl} \left({\zeta_u^{(1)}}^2 - {\alpha_3^{(1)}}^2\right) \vec{n} dl \Bigg\rangle \end{aligned} \tag{2.6}$$

where $<>$ is a sign to take the mean value, M is the mass, $\ddot{\vec{x}}_g$ is the gravitational body accelerations, α_3 is the heave displacement, ρ is the density of fluid, g is the gravitational acceleration, S_0 is the initial hull surface, wl is the waterline, ζ_u is unsteady relative wave elevation, and the superscripts (0) means the zeroth order and (1) means first order.

The linear potential theory method estimates the motion response relatively accurately. In addition, the terms related to the quadratic term of the motion response in added resistance calculation typically have a small effect for fast displacement ships, as shown in Figure 2.4. Therefore, secondary components related to the motion response are excluded considering the major factors of nonlinearity. Components that contain motion responses in the extended formula, Equation 2.6, are excluded. This condition also corresponds to the short-wave condition without the motion response of the ship. The resulting formula can be reduced to

$$\left\langle \vec{F}^{(2)} \right\rangle = \left\langle \frac{1}{2}\rho \iint_{S_0} \nabla\varphi^{(1)} \cdot \nabla\varphi^{(1)} \vec{n} dS - \frac{1}{2}\rho g \int_{wl} {\zeta_u^{(1)}}^2 \vec{n} l \right\rangle \tag{2.7}$$

In this condition, the influence of the bow wave generated by the advancing ship is significant because there is no motion response of the ship. The height distribution of the bow wave and the velocity field acting on the hull surface near the waterline are the key elements of the added resistance calculation. In this condition, the diffraction caused by the reflected wave of the incident wave is important.

The diffraction boundary condition on the hull for the unsteady potential is given by Equation 2.8. On the hull surface, the velocities on the hull surface due to the diffraction potential (φ_7) must cancel the velocities due to the incident wave potential (φ_0).

$$\frac{\partial\varphi_7}{\partial n} = -\frac{\partial\varphi_0}{\partial n} \qquad on \;\; S_0 \tag{2.8}$$

where φ_0 is the incident wave potential and φ_7 is the diffraction potential and n is the normal vector.

The waterline contribution significantly influences the added resistance estimation in the linear theory method. It is important to estimate the waterline contribution accurately since it is calculated as the square of the relative wave elevation,

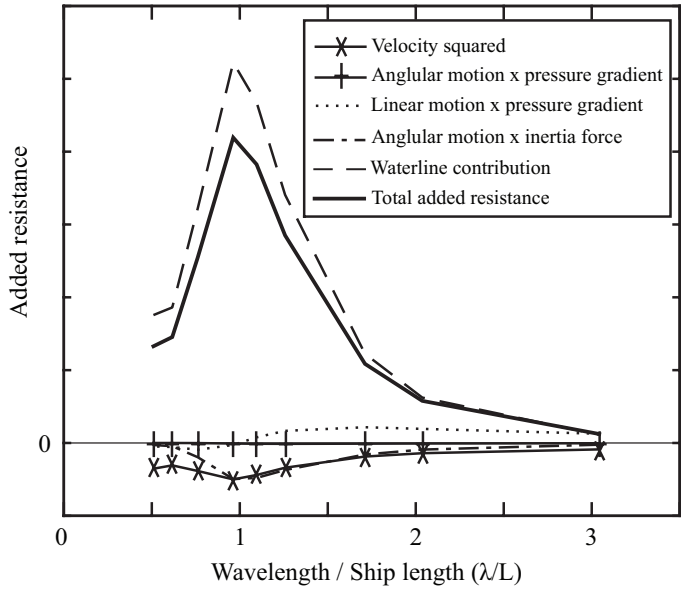

Figure 2.4: Classification of added resistance contributors in the fast displacement ship in a linear potential theory method (This is one of the results presented in Chapter 5 of this thesis.)

which consists of the radiated wave resulting from the ship's motion response and the reflected wave. Although most studies accurately estimate the vertical motion response of a ship, research on the contribution of reflected and radiated waves is still lacking.

2.4. Research on bow waves

This section reviews the literature on bow waves. The nonlinear phenomenon of bow waves is reviewed, and the effect of the bow wave on the added resistance is discussed.

A typical displacement ship displaces a significant amount of water as it moves forward. In this process, surface waves are created. A good description of the wave pattern generated by the ship starts with the Kelvin wave pattern [68]. The Kelvin wave consists of diverging and transverse waves, as shown in Figure 2.5. A single pressure point moves linearly over the free surface and forms a distinctive pattern. Surface waves are one of the causes of ship resistance.

Wave systems are often described with potential theories. However, the waves of a ship are complex fluid motions that cannot be fully explained by the potential theory. In particular, the bow wave is difficult to model theoretically because the bow wave changes continuously through the interaction of air and water with significant differences in properties (e.g., density and viscosity).

In fact, bow waves around the hull are difficult to simulate with numerical algorithms. Reliable experiments from this standpoint are necessary for developing

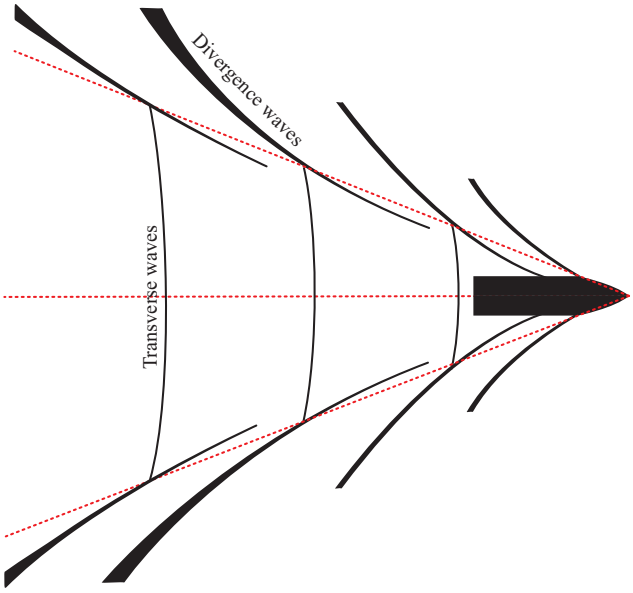

Figure 2.5: Schematic of a Kelvin wave system

mathematical models to understand and simulate the characteristics of bow waves. Advances in computer performance are promoting the development of CFD and the ability to simulate complex waves numerically.

2.4.1. Experimental observation

Experiments on bow waves mainly measure the wave height or the velocity fields. The University of Tokyo Towing Tank has conducted many experimental studies on bow waves [69]. Inui *et al.* [70], Miyata *et al.* [71], Miyata and Inui [72] characterized the structure and flow characteristics of bow waves using surface visualization techniques (aluminum powder and tracking particles). Toda *et al.* [73] measured the wave height and average velocity using a capacitance wire and a 5-hole pitot tube for Series 60. The presence of a bow-wave-induced vortex was observed.

There have been several studies on wave breaking and energy loss. Duncan [74] measured the surface height profile and vertical distributions of velocity behind an underwater hydrofoil at a constant velocity. According to wake investigation measurements, the drag associated with wave breaking at a free surface is thrice the theoretical maximum drag of a nonbreaking wave.

At the David Taylor Model Basin, Dong *et al.* [76] and Roth *et al.* [77] performed PIV measurements and free-surface visualization focused on the early stages of bow-wave development while the bow wave breaks. The flow in the bow wave of the DTMB 4817 model was studied. The results were characterized by Weber and Reynolds numbers. They showed that viscosity and surface tension play a role in the phenomenon of bow-wave breaking.

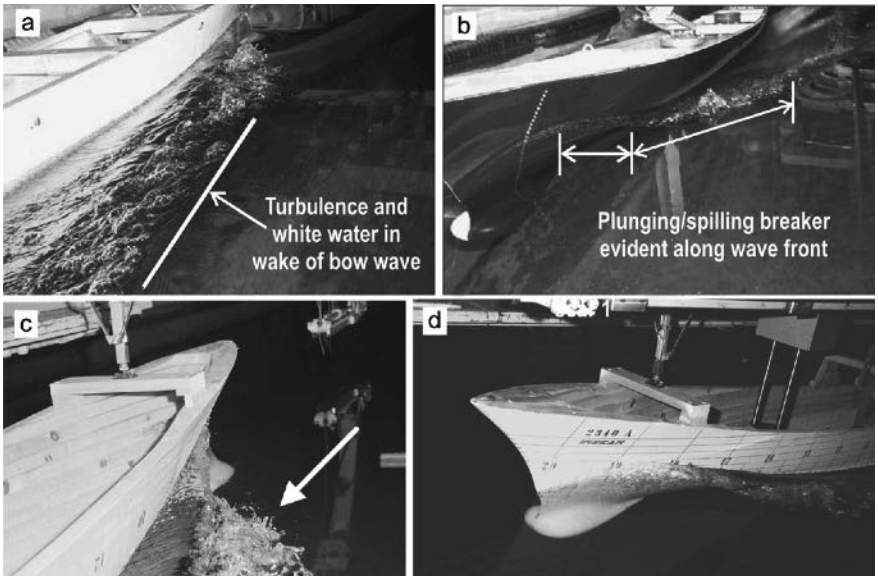

Figure 2.6: Experimental observation of bow waves by Olivieri et al. [75]: Model 5512 side and front views (a) and (b); Model 2340 side and front views (c) and (d)

Waniewski *et al.* [78] investigated the dynamics and air entrainment processes of ship waves. A wedge-shaped bow demonstrates that the bow wave is a nonlinear phenomenon. Olivieri *et al.* [79] researched the bow-wave breaking generated by a naval combatant (INSEAN model 2340). The velocity field was measured using a 5-hole pitot tube downstream of the bow wave. Olivieri *et al.* [75] observed a bow and shoulder wake of a model ship in a subsequent study. The mean velocity measurements showed a complex vortex structure beneath the free surface generated by the breaking waves. The measured data were used to verify the CFD simulation results of the flow. CFD simulation and observations show that high free-surface r.m.s. values are correlated with bubble generation.

Karion *et al.* [80] investigated the size and velocity distribution of the bow-wave breaking generated by a simple wedge-shaped bow through high-speed video analysis. Measurements were made under various Froude, Reynolds, and Weber number conditions. The results show that breaks occur when the Froude and Reynolds numbers exceed a threshold. The study also showed that there exists a critical Weber number to generate the spraying of bow waves. The results are used to examine scaling issues related to bow-wave breaking.

Maxeiner *et al.* [81] investigated the characteristics of a bow wave by using a two-dimensional plus time (2D+T) approximation method using a flexible wave board designed to simulate one side of bow waves for an advancing ship with a simple bow shape. The characteristics of the bow wave were investigated considering the height of the bow wave and shape of the crest. Wave parameters such as maximum wave height and wave velocity were found to correlate strongly with the motion of a wave generator simulating the shape and speed of the ship.

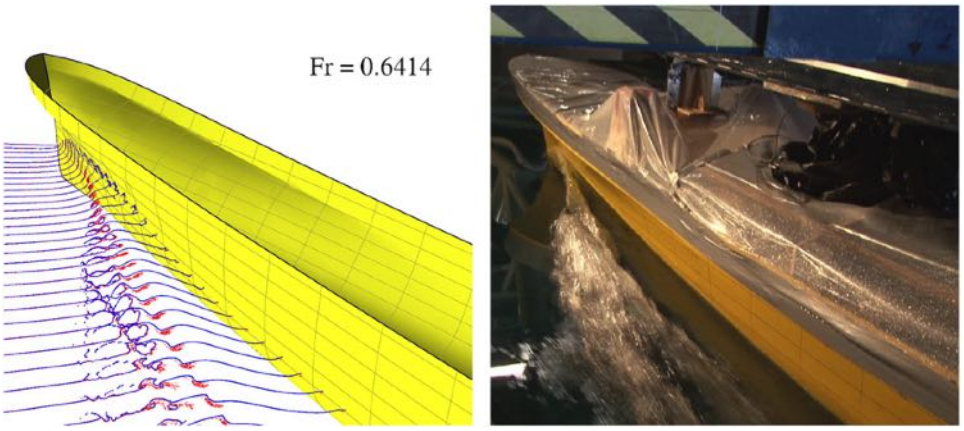

Figure 2.7: Numerical simulation and comparision with experimental observation for the bow wave breaking in the CNR-INSEAN by Marrone *et al.* [82]

2.4.2. Numerical simulation

Numerical studies on bow waves are reviewed here. The complex interaction between bow waves and incident waves requires good solvers. Efforts have been made to understand bow waves numerically using RANS-based codes. Many technologies have been applied to abnormal applications, and satisfactory progress has been achieved. For example, many studies have been conducted on the diffraction of bow waves when the ship has an advancing speed [62, 62, 83, 84].

Dommermuth *et al.* [85] simulated the flow around a ship model by using an immersive body and volumetric methods that can calculate the flow with spilling breaking. Carrica *et al.* [86] numerically analyzed the forward diffraction problem using the RANS approach. A mixed turbulence model for the turbulent viscosity and the level set method to calculate the free surface were used. Analysis of the flow indicates that the force of the wave can cause nonlinear behavior. Olivieri *et al.* [75] provided an analysis of vortices generated by wave breaking using the RANS method.

Weymouth *et al.* [87] used a high-resolution direct numerical simulation (DNS) of the Navier-Stokes equation to simulate unsteady breaking waves. The results show that vorticity or surface tension plays a major role in the strength of wave breaking.

Colagrossi and Landrini [88] and Marrone *et al.* [82] applied the smoothed particle hydrodynamics (SPH) model to the wave pattern generated by a fast ship with a fine bow. This method allows the ship motion to be approximated by a mathematically equivalent set of equations that governs the abnormal 2D free-surface flow created by the deformable body on a vertical plane across the ship. These studies simulated the shape of the bow waves. Complex phenomena can be realistically simulated using RANS or DNS. However, each calculation is time-consuming.

2.4.3. Theoretical approach

The studies that achieved theoretical and straightforward descriptions are noteworthy. Longuet-Higgins *et al.* [89] introduced numerical techniques for nonlinear and unsteady free surface waves. By focusing on the simpler and larger features of the wave flow, ignoring the viscosity and surface tension, he studied the spatial dependence of motion at each time interval.

Noblesse *et al.* [90, 91] and Delhommeau *et al.* [92] used the thin-ship theory to approximate the bow-wave characteristics by observing empirically simulated bow waves on a flat plate. They focused on the waterline entrance angle of the wedge-shaped hull and the depth-based Froude number. Several simple relationships have been developed to calculate the bow-wave height, crest location, and steepness. Noblesse's findings, especially the expressions of stability of the bow wave, are discussed further in Section 2.4.4.

2.4.4. Nonlinearity of bow waves

A phenomenon that can affect the added resistance is the nonlinear behavior of the bow wave. Pile-up and swell-up are important phenomena to be considered in the analysis of added resistance as they affect the increase of the relative wave elevation of the bow wave.

Pile-up, shown in Figure 2.8(a), is a phenomenon in which water splashes up when a wedge is dropped into the water. Pile-up is described by Payne [93] as a function of the hull bow's deadrise. It is an important concept related to the nonlinearity of the bow wave with respect to the flare angle of ships. Pile-up occurs when the relative motion between the incident wave and the bow increases and is connected to the breaking of the bow wave. A similar phenomenon can occur in the case of a relatively high wave steepness and rapid variation of the relative wave elevation.

Swell-up, shown in Figure 2.8 (b), is an increase in the relative wave elevation compared to undisturbed incident waves, and it occurs even when considering a stationary bow wave. The peak wave height measured in a model test is greater than the sum of the undisturbed incident wave height and motion response [94, 95]. Swell-up is caused by the increase in waterline entrance angle with increasing draft. This can be understood from the fact that the stationary bow wave increases at high drafts in general. The increase in bow-wave amplitude also affects the estimation of added resistance [11].

Ferguson and Dand [96] provided a discussion of the validity of the linear superposition of wave profiles of the hullform and the bulb. Each wave profile of the hullform and the bulb were discussed to be nonlinearly superposed due to the complex interaction of turbulence and boundary layer growth and to be able to account for energy dissipation due to disturbance and breaking.

Lloyd *et al.* [97] investigated the effect of variations in above waterline bow shapes on deck wetness. They showed an experimental study of nine bow shapes that had the same waterline entrance angle but different flare, stem overhang, and knuckle. The effect of bow shape on deck wetness in regular waves was compared.

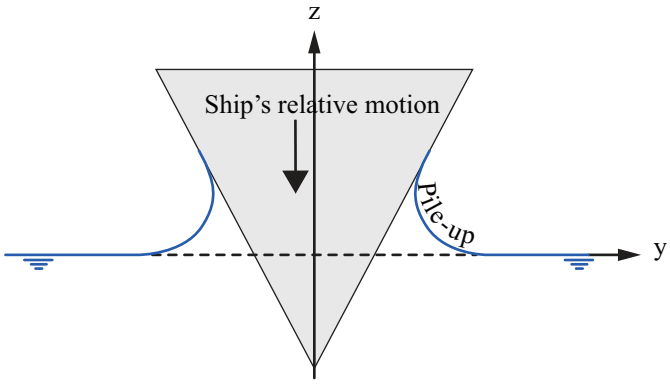

(a) Pile-up

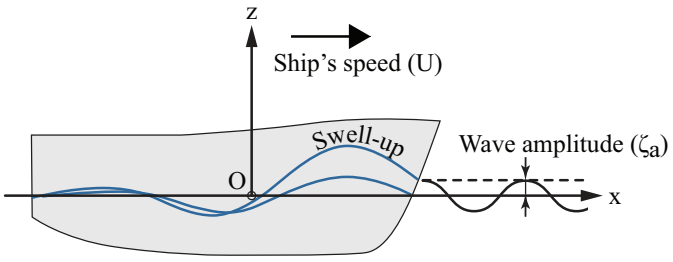

(b) Swell-up

Figure 2.8: Nonlinear height increase of bow wave

The effect of different bow shapes was explained with the swell-up coefficient defined by Blok and Huisman [98] as the ratio of the actual and notional relative motion amplitudes. The swell-up coefficient generally increases to reflect the increase in flare angle and relative motion.

Although there is uncertainty in their results, the frequency of freeboard exceedances and deck wetness were low for small flare angle and long stem overhang. And the reduction of freeboard exceedances caused by the knuckle was evident. This was considered to be the result of the knuckle suppressing the swell-up by promoting the detachment of bow waves. However, the knuckle effect on deck wetness was not significant.

In addition, in the form of excessive flare angle (55 degrees), the relative motion was large while the deck wetness was less. This was interpreted as a result of the large relative motion and the effect of flare throwing impressive sheets of water aside.

Squires [99] showed the connection between the swell-up of bow waves and deck wetness. The phase difference was compared between the experimental relative motion and the theoretical relative motion. From experimental and theoretical studies, he showed that diffraction and radiation can have a significant influence on the relative motion. And the swell-up coefficient can be used to improve the accuracy of the amplitude of the calculated motion response.

In his study, the peak of the swell-up coefficient was found to shift aftward as Froude number increased. And the steady potential at which the wave profile calculation can play an important role in determining the characteristics of incident wave distortion and diffraction swell-up coefficient. This swell-up coefficient has a phase difference because there is a phase change between the actual and the theoretical relative motion.

Wu and Taylor [37] also showed the nonlinearity by coupling of steady and unsteady potentials. They derived a mathematical formula of linearized potential theory for slowly moving vessels based on a perturbation series of forward velocities. They included a degree of nonlinearity by coupling effects between the steady and unsteady potentials in the free surface boundary conditions to improve reverse flow prediction around a submerged circular cylinder and a floating semicircular cylinder.

2.4.5. Stability type of bow-wave breaking

Bow-wave breaking occurs on most ships operating in waves with different strengths and types. The type of breaking is divided into plunging and spilling depending on the stability appearance at the crest, as shown in Figure 2.9. Plunging is a type of breaking that appears as an overturning detachment on the crest of the bow wave. This type is mainly found in a hullform with a narrow bow angle. Spilling is a type of turbulent form that disturbs the adjacent flow field. This type is predominant in a hullform with a blunt bow angle.

In the study by Maxeiner *et al.* [81], the breaking type of the bow wave was estimated to be significantly influenced by the waterline entrance angle and the ship's speed. Moreover, a narrow range of transition regions where two types of breaking overlap were found. The transition region of the bow wave with the change

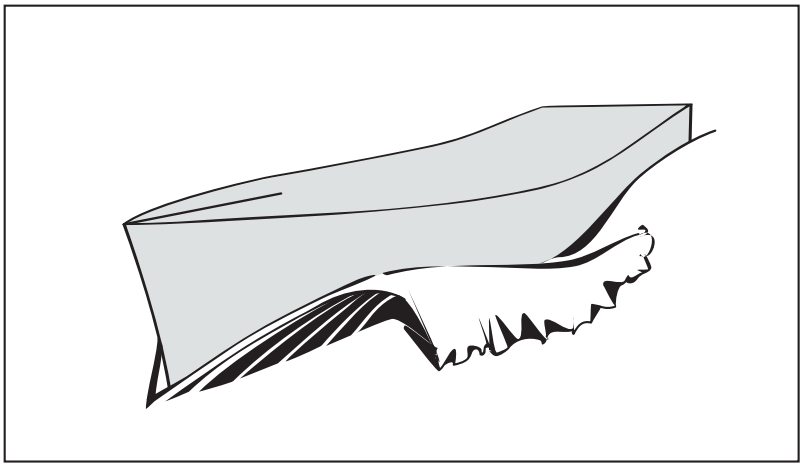

(a) Plunging breaking

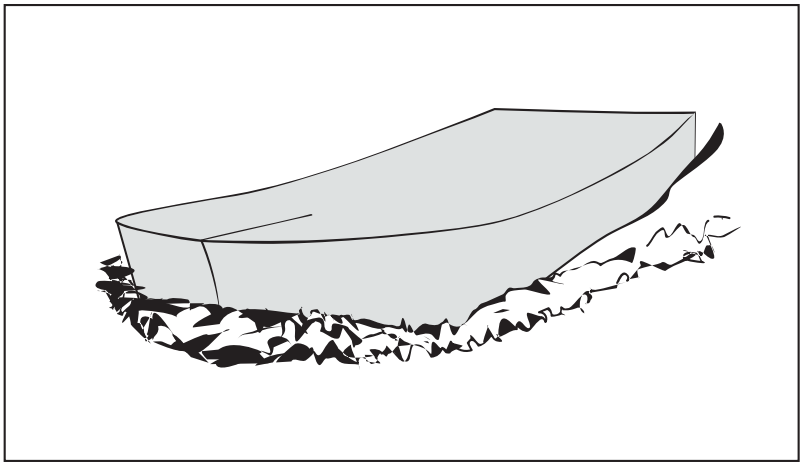

(b) Spilling breaking

Figure 2.9: Classification of the bow-wave breaking by stability on the crest

of speed was also found in Karion's experimental study using a simple wedge shape [80].

Noblesse *et al.* [91] approximated a simple analytical equation for a wedge-shaped ship without a bulbous bow in calm water that divides the types of the bow wave with the boundary shown in Equation 2.9. This analytical expression has been applied to the Bernoulli's equation for the bow wave and by the experimental approximation method. The major parameters that affect the stability of the bow-wave crest are the depth-based Froude number (F_D) and the waterline entrance angle (α_E) defined by Figure 2.10.

$$F_D = \frac{4.4}{(1 - q_b^2)} \frac{\tan \alpha_E}{\cos \alpha_E} - 1 \tag{2.9}$$

where q_b is the total flow velocity at a bow wave crest and α_E is the half waterline entrance angle and F_D is the ship draft D based Froude number $F_D = U/\sqrt{(gD)}$.

Figure 2.11 shows this boundary for various flow velocities at the crest q_0. Figure 2.11 shows that, when the test is conducted at the left-hand side of the boundary, an overturning bow wave (stable) is expected. On the other hand, when the test is conducted at the right-hand side of the boundary, an unstable (corresponding to unsteady in his description) spilling-type bow wave is expected. From this boundary, it can be deduced that the characteristics of the bow wave can be changed dynamically when the speed of the ship or the depth of the ship is changed.

2.4.6. Nonlinear effects on resistance

Some previous experimental studies provide a link between the resistance and the type of wave breaking. Rapp and Melville [100] analyzed the loss of momentum due to the breaking of deep-water waves through an experimental approach. They showed that the loss of momentum depends on the type of wave breaking, and plunging breaking causes more energy loss than spilling breaking because of the large difference in wave height before and after breaking. This study shows that energy dissipation depends on the type of breaking.

Kayo and Takekuma [101] described the increase in resistance of a ship with a blunt bow by controlling the shear flow of the free surface. They showed that an increased shear flow of the free surface of the ship in the advancing direction induces a high residual resistance. This study clarifies the resistance change due to the shear-flow change of spilling breaking. In addition, Ali *et al.* [102] investigated the bow wave for a ship moving at a slow speed, typically the wave in front of a bow. They described the correlation between wave resistance and energy dissipation by the breaking of the bow wave and the disturbance of the free surface for a hullform with a large block coefficient. The goal of that study was to investigate the relationship between free-surface disturbances and bow-wave breaking, which can be used to determine parameters for numerical analysis. The results of that study show that the wave-breaking area increases with the increase of the Froude number and block coefficient and with the increase of the surface integral of the square of the free-surface disturbance function.

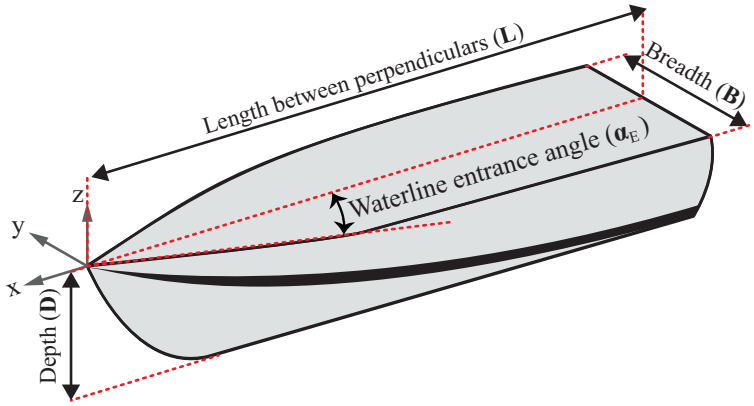

Figure 2.10: Definitions of ship parameters

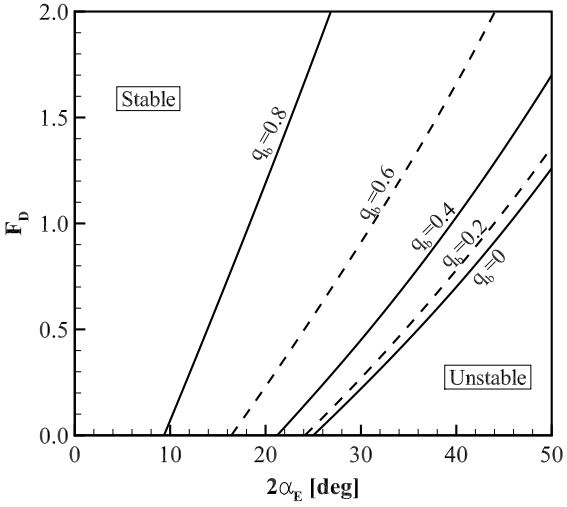

Figure 2.11: Stability boundary of the bow wave from Equation 2.9 for the various number of the flow velocity on the crest q_b (adapted from [91])

An experimental study was also reported on the nonlinear effects of bow-wave breaking on the added resistance. Kashiwagi *et al.* [103] performed model tests to find the nonlinearity of the bow wave using the unsteady wave analysis method at various wavelengths for the modified Wigley model. They showed that, as the ship's motion response is increased in intermediate waves, the added resistance can be significantly different between direct measurements and wave analysis because of nonlinear local waves. This nonlinearity is prominent near the forefront of the ship.

2.5. Conclusions

The existing literature on estimation methods of the added resistance of a ship has been reviewed. Experimental and numerical studies on the added resistance and nonlinearity of the bow wave have been discussed. The added resistance requires accurate estimation owing to regulations on operational performance.

Experimental measurements are the most accurate method to evaluate added resistance. However, it is difficult to measure the added resistance for all ships experimentally. Experiments to measure added resistance depend on experimental conditions (wavelength, wave height, and ship's velocity) and involve time-consuming procedures for test preparation (ship model, instrument, and tank schedule).

Numerical studies are suitable as alternatives to experimental measurements. Since the added resistance is proportional to the square of the motion response, it is important to estimate the motion response accurately. Most numerical studies aim to estimate the accurate vertical motion response of a ship. Numerical approaches estimate the added resistance based on accurately evaluated motion responses. However, the suitable solution is different for each problem. In particular, the accuracy of numerical analysis cannot be guaranteed if nonlinear phenomena are involved in a given problem. Therefore, if the experimental information can complement the numerical evaluation, it can be an effective solution.

The waterline contribution due to the relative wave elevation is closely linked to the added resistance. For the relative wave elevation, accurate estimation of the radiation component due to the motion response and the diffraction component due to the reflection of waves by the ship is required. Therefore, the nonlinear effect of the relative wave elevation due to the bow-wave breaking is an interesting topic.

A typical example of the nonlinear phenomenon of the relative wave elevation is the swell-up that the actual wave elevation is larger than the theoretical wave elevation. A small flare that effectively sheds water can reduce the swell-up. And the knuckle suppresses the swell-up and physically promotes the detachment of the bow wave [97].

As the Froude number increases, the maximum swell-up coefficient of the fast ship moves aftward [99]. The stability of the bow-wave crest is related to the speed of the ship [81, 90, 91]. From these results, it can be inferred that if the nonlinearity of the bow wave (swell-up and stability) can be related to the pressure distribution over the hull, this may yield a practical approach to correcting added resistance calculations.

The review also focused on the influence of bow waves on the added resistance.

Bow-wave breaking occurs on most ships operating in waves. There is a lack of research on the effect of breaking waves on the added resistance. The loss of energy that occurs in this process is a factor that contributes to the added resistance.

A realistic option for the accurate estimation of this effect is to include a practical implementation of the nonlinear effect of the bow wave in the analysis, which is typically a CFD analysis using the RANS formula. This method is also effectively applied to the solution of the added resistance in short waves, in which the motion response of the ship is small.

However, another method is to incorporate the experimentally confirmed nonlinear characteristics into a numerical calculation using the linear potential theory. This method can be a realistic solution that reflects physical properties. Considering the advantage of rapid computation, the linear potential theory method, which accurately estimates the motion response, is suitable for added resistance evaluation in the hullform development stage. Techniques are still needed to account for nonlinear phenomena in cases where the linear theory is not applicable.

A typical problem related to the nonlinearity is the breaking of bow waves. The most important issue in this problem is the specific perception of nonlinear phenomena and the application of appropriate solutions. A similar solution can be applied to ships showing similar nonlinear phenomena.

The review of literature shows that the effect of bow-wave breaking on added resistance in waves is an interesting topic. Among the types of bow-wave breaking, this thesis will focus on the plunging breaking phenomenon. Plunging breaking is relatively free from the effects of viscosity. Based on experimental investigations, this thesis attempts to investigate effective perspectives that can be applied to numerical analysis.

3

INFLUENCE OF PLUNGING BREAKING OF BOW WAVE

3.1. Introduction

From the literature review in Chapter 2, bow-wave breaking is classified according to the stability at the crest of the bow wave. The stability changes of bow-wave breaking depend on the water entrance angle and the speed of the ship. The stability of bow-wave breaking may vary with speed for a given hullform.

There are many factors to consider for clarifying the impact of bow-wave breaking on added resistance. Excluding the motion response of the ship, which is estimated relatively accurately through theoretical or numerical analysis, the squared relative wave elevation along the waterline and the squared velocity around the hull significantly influence the added resistance, as expressed in Equation 2.7.

Gerritsma and Beukelman [13] assumed that the added resistance changes linearly with the squared wave height at constant wavelength and a constant forward speed. This assumption has been verified by the experiment of Journée [104]. However, in his experiment, it was shown that the assumption of wave amplitude squared can be broken if the nonlinearity is significant.

Bow-wave breaking directly affects the relative wave elevation, which is a major component of the added resistance because it affects the hull pressure distribution. The nonlinear phenomenon of bow-wave breaking is too complex, but the prospect of analysis in relation to the stability of the bow wave is examined. The investigation also starts with the assumption that the stability of the bow wave is affected by the speed of the ship.

This chapter examines the nonlinear response of the added resistance with respect to the ship's speed, in conjunction with changes in the characteristics of plunging breaking of bow waves. Insight into the connectivity is verified by analyzing model test results of the added resistance for a series of fast displacement ships.

Section 2.3.3 investigates the uncertain factors that violate the linear theory of added resistance regarding bow-wave breaking. A hypothesis is suggested that the influence of bow-wave breaking on the added resistance depends on its stability type. For testing the feasibility of the hypothesis, the speed of the ship is set as an independent variable because the ship's speed affects the stability type of bow-wave breaking. Moreover, a transfer function of the added resistance is proposed that includes the squared speed of the ship as a dependent variable. The hypothesis is given in Section 3.2, and the feasibility is tested using test results for a series of fast ships in Section 3.3. Section 3.4 provides verification results of the hypothesis.

3.2. Hypothesis

The intensity of breaking of bow waves in a given ship is related to the ship's speed. The influence of bow-wave breaking is investigated by connecting the speed of the ship to the added resistance analysis.

For a given hullform, the breaking phenomenon of the bow wave can be classified into two types. One is plunging breaking, which appears as an overturning detachment of the bow wave. The other is spilling breaking, which appears as a disturbance of the flow field around the hull. The detachment of the bow wave can make the relative wave elevation less than the value predicted by the linear theory, and the disturbance of the flow field around the hull can weaken the suction effect of the incident wave. Therefore, this section proposes a hypothesis that the type of bow-wave breaking, which is distinguished by the stability of the crest of the bow wave, affects the added resistance.

Figure 3.1 shows a conceptual representation of the proposed hypothesis. If the plunging breaking of the bow wave becomes strong, the height of the bow wave may not reach the value given the linear relation owing to the detachment of the bow wave. Thus, the added resistance will be less than that predicted by the linear theory. On the other hand, if the bow wave exhibits a relatively unstable spilling breaking, the disturbance of the velocity field around the hull weakens the pressure suction effect of the incoming waves, and the added resistance can be greater than that predicted by the linear theory.

The added resistance is a second-order hydrodynamic parameter known to be proportional to the squared amplitude of the incident wave under the non-breaking condition [105]. The result is often expressed as a quadratic transfer function (QTF).

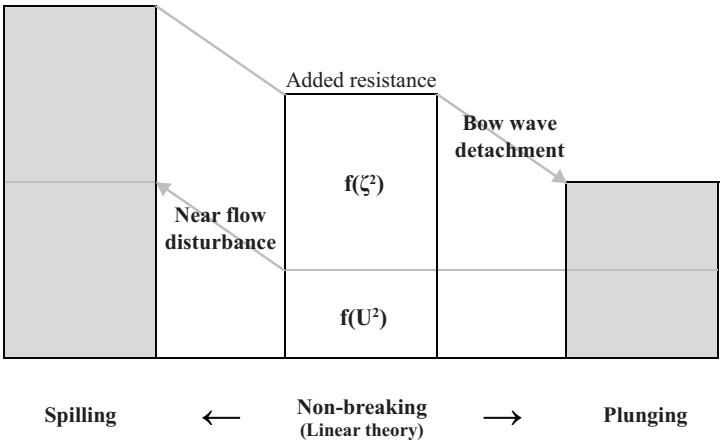

Figure 3.1: The concept of a hypothesis that the type of bow-wave breaking has a different influence on the added resistance

However, the conventional QTF of the added resistance expressed by Equation 3.1 has weak compatibility to grasp the nonlinear effects of the bow wave because this transfer function is derived considering linear sea-keeping.

$$C_{aw} = \frac{R_{aw}}{\rho g B^2 \zeta_a^2 / L} \tag{3.1}$$

in which R_{aw} is the measured added resistance, ρ is the water density, g is the acceleration of gravity, B is the maximum breadth of the waterline, ζ_a is the amplitude of the incident wave, and L is the length between perpendiculars.

To test the feasibility of the hypothesis, the speed of the ship is set as an independent variable. It is necessary to analyze the added resistance based on the speed of the ship to understand the nonlinearity of the added resistance because the stability type of bow-wave breaking depends on the ship's speed as well as the waterline entrance angle. Therefore, this section proposes a transfer function of the added resistance including the ship's speed as a dependent variable, and the proposed hypothesis is verified through this variable expressed by Equation 3.2.

$$C_{ra} = \frac{R_{aw}}{\rho \zeta_a^2 U^2} \tag{3.2}$$

where U is the speed of the ship.

3.3. Feasibility study on fast ships

3.3.1. Model ship

The feasibility of the hypotheses presented in the previous section was tested using experimental data from a series test of fast displacement ships (FDSs). In order to limit the impact parameters as much as possible, the test data-set of a simple FDS hullform was chosen. The hullforms of the chosen FDSs have a relatively small flare angle and waterline entrance angle. Therefore, the influence of viscosity and surface tension on these hullforms is low compared to their influence on conventional hullforms with complex shapes. In the case of low speed, it was considered that the effect of viscosity is not negligible; therefore, the results of the high-speed test were judged to be valid. Moreover, the bow wave is expected to be dominated by the form of plunging breaking.

A systematic series of model tests on a FDSs was conducted as a Joint Industry Project in 1979-1989 [94, 106]. The model tests were performed in a deep-water towing tank measuring 250 x 10.5 x 5.5 m and a high-speed towing tank measuring 220 x 4 x 3.6 m in length, width, and depth, respectively, at the Maritime Research Institute Netherlands (MARIN). The resistance of the ship in calm water and the added resistance in regular waves were measured along with the motion response. The model ship was secured to the towing carriage by universal joints, which limit sway, yaw, and surge motions. The joint is attached to an air-lubricated cylinder so that the ship can freely move up and down.

For all experiments measuring physical quantities, uncertainty analysis of the measurements is important. A contemporary experimental program conducted between 1986 and 1990. The experimental set-up for testing comprises the model; the measurement set-up; and the system for acquiring, amplifying, and digitizing data. All experiments were conducted based on a measurement system meeting the experiment organization's acceptable standards. The measurement system was evaluated formally, and the accuracy due to random error was found to be on the order of 1.2%.

Nine hullforms, which consisted of three waterline entrance angles and three block coefficients (C_B = 0.35, 0.4, and 0.5), were selected in the series tests. Hullforms were developed to have the same bodyplan when the block coefficient is the same, but they have different waterline entrance angles because of the difference in L/B. The main parameters of the model are listed in Table 3.1, and the bodyplans are shown in Figure 3.2.

The dimensions of ships are slightly different because the series test was originally designed to examine the sea-keeping performance against various nondimensional parameters of ships. However, because the experiment was conducted according to Froude similarity, the similarity between the resistance component related to the bow wave and the dynamic motion response of the ship is preserved in the experiment region. Therefore, the model test data of this study are suitable to investigate the dependence of the added resistance on the stability type of bow-wave breaking.

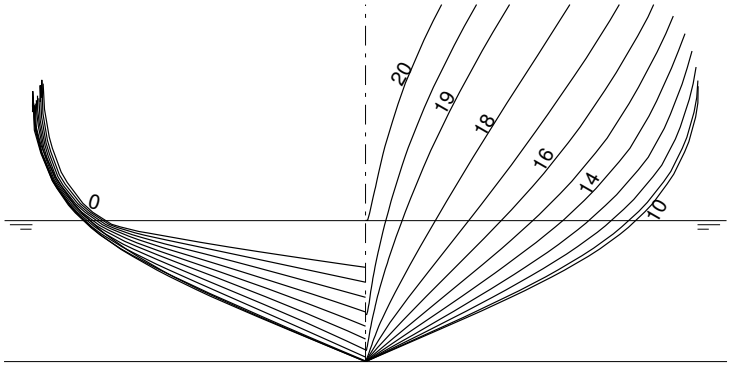

(a) C_B = 0.35

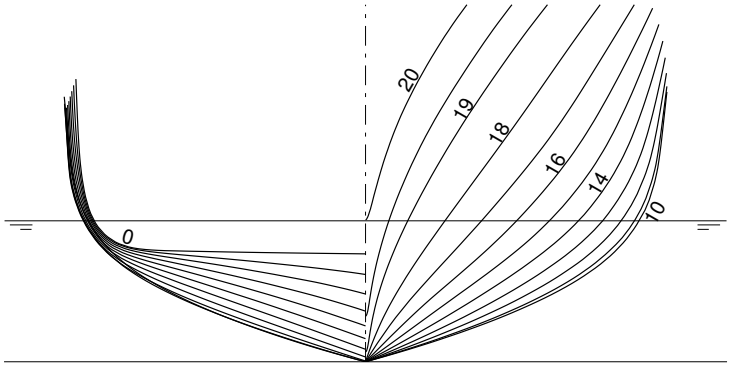

(b) C_B = 0.4

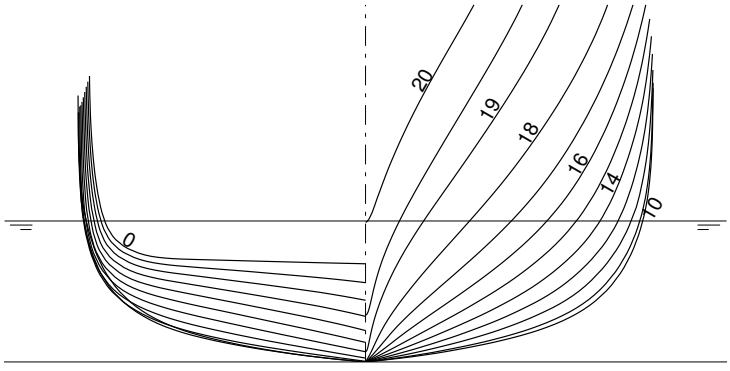

(c) C_B = 0.5

Figure 3.2: Bodyplans of fast displacement ships

3.3.2. Data analysis

The measured resistances of nine hullforms in calm water are analyzed according to the two-dimensional performance prediction method established at the International Towing Tank Conference in 1978 (ITTC-78), which divides the total resistance C_t into the frictional resistance C_f and the residual resistance C_r.

The total resistance coefficient is given by:

$$C_t = \frac{R_t}{\frac{1}{2}\rho S U^2} \tag{3.3}$$

where R_t is the total resistance, S is the wetted surface area and U is the ship speed.

The frictional resistance is treated in the same manner as the measured resistance of a flat plate with the same wetted surface area under the wave-free condition. A typical formula was provided by the International Towing Tank Conference in 1957 [107].

$$C_f = \frac{0.075}{\{log(Rn) - 2\}^2} \tag{3.4}$$

where Rn is Reynolds number for the ship.

The rest resistance of the total resistance of the ship except the frictional resistance is the residual resistance C_r.

$$C_r = C_t - C_f \tag{3.5}$$

The added resistances for nine hullforms in regular waves of wavelength ratio λ/L = 0.4 and 1.2 were measured for Fn = 0.285, 0.430, 0.570, 0.855 and 1.140. Some measurement points are missing because of the experimental conditions. In the shortwave condition, the wave slope ($2\zeta_a/\lambda$) was up to 4%. The waves of intermediate and long waves had a constant wave height of $0.02L$.

The measured added resistance in regular waves is compared with the conventional QTF (Equation 3.1) and the proposed transfer function (Equation 3.2). First, experimental data for short waves are investigated. A short wave causes little motion response of the ship, and the wave diffraction effect is important. Then, experimental data for intermediate waves with significant motion response of the ship and high added resistance are investigated.

Table 3.1: Main particulars for nine hullforms of fast displacement ships

Ship ID	15	12	16	9	5	10	19	11	20
Length [m]	4	5	6	4	5	6	4	5	6
Breadth [m]	1	0.625	0.5	1	0.625	0.5	1	0.625	0.5
Depth [m]	0.25	0.156	0.125	0.25	0.156	0.125	0.25	0.156	0.125
C_B	0.5	0.5	0.5	0.40	0.40	0.40	0.35	0.35	0.35
Lpp/Breadth	4	8	12	4	8	12	4	8	12

3.3.3. Performance in calm water

The resistances in calm water are analyzed for the selected nine hullforms. Figure 3.3 and Figure 3.4 show experimental data for the nine hullforms as a combination of shapes and lines. C_B = 0.5 is a circle, C_B = 0.4 is a diamond, and C_B = 0.35 is an inverted triangle. The results of hullforms of L/B = 4, 8 and 12 are indicated by solid line, dash-dot line, and dashed line, respectively.

Figure 3.3 shows the total resistance coefficients C_{tm} of Equation 3.3 and the frictional resistance coefficients of ITTC-57 in Equation 3.4 of each hullform as functions of $log(Rn)$. Figure 3.4 shows the residual resistance coefficient of each hullform as a function of the Froude number (Fn). In Figure 3.3 and Figure 3.4, the resistance coefficients are divided into three groups illustrated by different colors in the order of L/B of the hullform, which is the magnitude of the waterline entrance angle.

In Figure 3.4 at the ship's speed is less than Fn = 0.5, the value and slope of residual resistance coefficient C_r are large for hullforms having a small L/B with a large waterline entrance angle. The residual resistance coefficient of all hullforms has a maximum at approximately Fn = 0.5. Moreover, all the residual resistance coefficients converge to a specific value as the Froude number increases to a very high speed.

The residual resistance is greatly influenced by the change of wetted surface area due to the dynamic squat of the ship. However, the residual resistance may reflect the effect of shifts in the stability of the ship's bow wave, which may change with the speed of the ship. The dynamic squat (trim and sinkage), which is affected by the speed of the ship, changes the dynamic waterline entrance angle of the ship. The variation of the waterline entrance angle of the ship due to the squat can cause stability transients in the bow wave. If a stability transient occurs and the characteristics of the bow wave change, the residual resistance will show a different response.

Therefore, with the generation of the bow wave along the ship's speed, the variation of the draft by the dynamic squat and the change of the waterline entrance angle can be treated as factors contributing to the residual resistance. These factors are also closely related to the stability of the bow wave.

The connectivity of the residual resistance and the dynamic squat of FDS-19 with C_B = 0.35, L/B = 4 is investigated. Figure 3.5 shows the trim and sinkage as well as the residual resistance coefficients as functions of the Froude number of FDS-19. This hullform has a relatively large incident angle of 33.2 °. At a Froude number less than 0.5, there is a small dynamic squat change of the ship, but C_r increases greatly. Trim changes drastically around Fn = 0.5, and C_r shows a peak. At speeds greater than Fn = 0.6, Cr tends to decrease without substantial changes in the dynamic squat.

The relationship between the residual resistance due to the change of Froude number and the change of stability type of the bow wave can be interpreted as follows. From the viewpoint of the stability boundary presented in Figure 2.11, the residual resistance responds greatly to the speed because of the relatively unstable

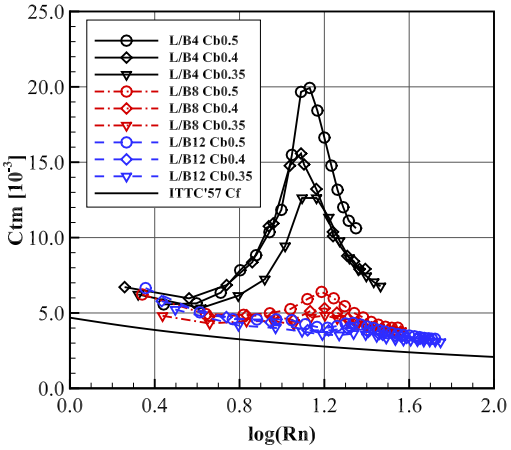

Figure 3.3: The total resistance coefficients of nine hullforms against log(Rn) with the frictional resistance coefficient of ITTC-57

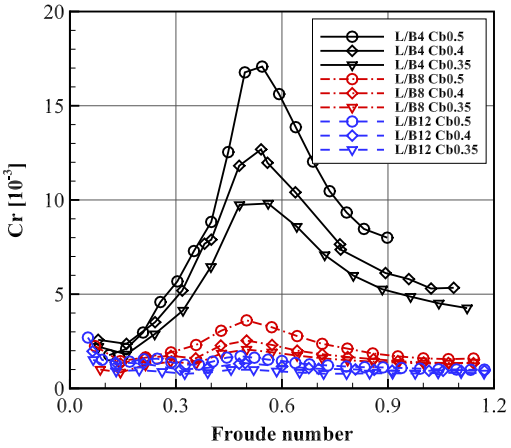

Figure 3.4: The residual resistance coefficients of nine hullforms against Froude number

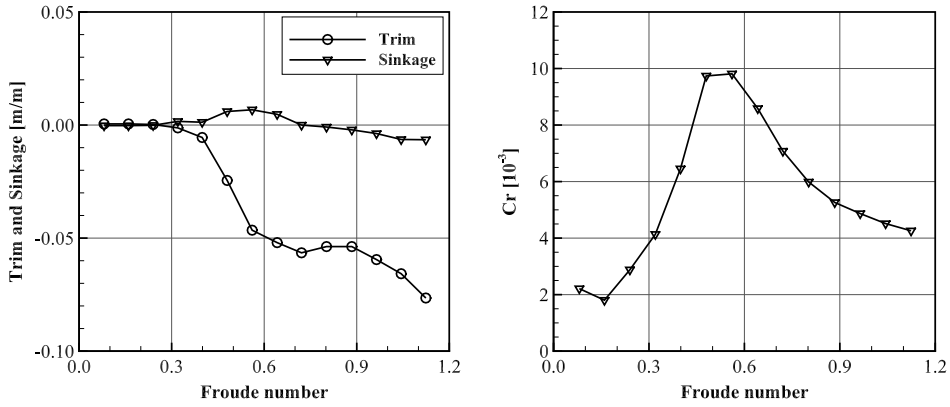

(a) Trim and sinkage (b) Residual resistance coefficients

Figure 3.5: Results according to Froude number of FDS-19

bow wave with a large entrance angle and the low speed with a Froude number less than 0.5. At approximately $Fn = 0.5$, the speed increase and the large squat change induce a change of stability type of the bow wave; therefore, the residual resistance shows its maximum value at this Froude number. When the Froude number is greater than 0.6, the response of the residual resistance to the ship's speed is reduced by a stronger plunging breaking, as the detachment of the bow wave increases at very high speeds.

Therefore, the residual resistance coefficient can be interpreted to reflect the characteristics of the bow wave formed by the change of the dynamic squat and the waterline entrance angle with the change of the ship's speed. As the speed of the ship can change the stability of the bow wave, it is the main parameter to be considered when interpreting the added resistance related to the bow wave.

3.3.4. Performance in short waves

The added resistance of the ships advancing with little motion response in short waves of $\lambda/L = 0.4$ is investigated. The added resistance in this condition is mainly caused by the diffraction of the bow wave. From the perspective of the bow wave, the added resistance of the short waves can be interpreted as a resistance added to the calm-water resistance because of the interaction with the incident wave. Under the same wave amplitude, a wave of short wavelength has a relatively high steepness, which is expressed by the ratio of the wave length to the wave amplitude. When the ship encounters relatively short waves, the interaction increases the steepness of the bow wave and, in turn, enhances the probability of bow-wave breaking.

Figure 3.6 and Figure 3.7 show the experimental data for the nine hullforms as a combination of shapes and lines with the same rule as Figure 3.4. Figure 3.6 shows the heave and pitch of the motion response at $\lambda/L = 0.4$. In this figure, the response

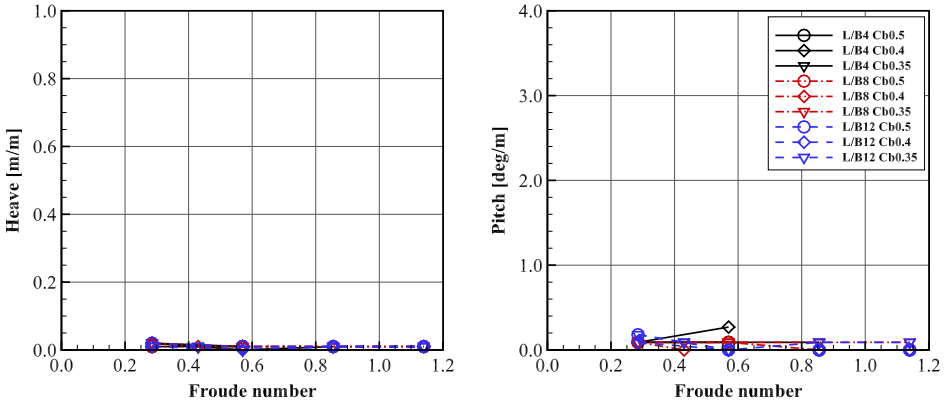

(a) Heave (b) Pitch

Figure 3.6: Motion response against Froude number for nine hullforms in short waves ($\lambda/L = 0.4$)

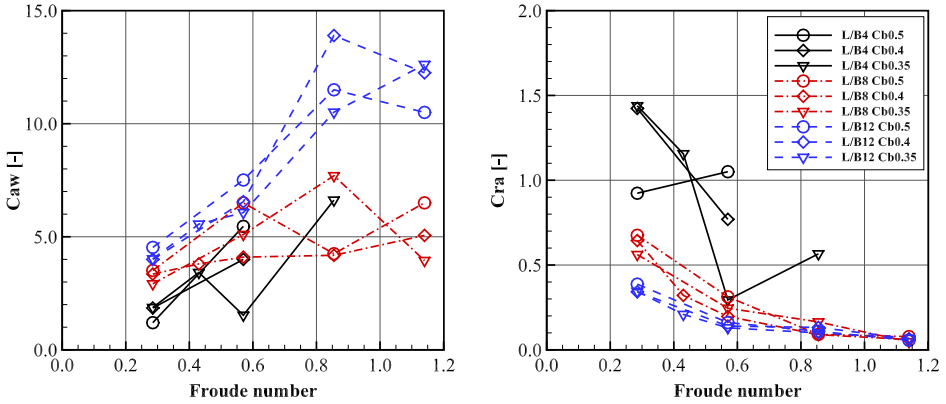

(a) C_{aw} of Equation 3.1 (b) C_{ra} of Equation 3.2

Figure 3.7: Quadratic transfer functions of added resistance against Froude number for nine hullforms in short waves ($\lambda/L = 0.4$)

amplitude operators (RAO) are close to zero, and there is little motion response of the ship in the entire speed range. The absence of motion response implies that the dynamic squat of the ship at a given speed is the same as that in calm water, even though the ship encounters waves. The added resistance measured in the short waves of $\lambda/L = 0.4$ is analyzed by using the conventional QTF of Equation 3.1 and proposed transfer function expressed by Equation 3.2.

Figure 3.7 (a) shows that the added resistance for the nine hull forms is generally proportional to the Froude number. However, it is difficult to define a meaningful relationship between the geometric element (e.g., C_B or L/B) and the added resistance coefficient (C_{aw}). On the other hand, Figure 3.7 (b) showing the proposed transfer function of added resistance, shows a clearer relationship of the added resistance coefficient (C_{ra}) with the Froude number. In Figure 3.7 (b), as the speed of ship increases, all the C_{ra} values decrease. The C_{ra} of a hullform with a relatively large waterline incident angle ($L/B = 4$), expressed by a solid line, is higher than those of the others. It is expected that a bow wave formed on the ship with a large waterline entrance angle and slow speed will be relatively unstable in comparison with the other hulls. An unstable bow wave causes an unstable reflected wave propagating in the direction normal to the hull surface, which disturbs the fluid field around the hull. Consequently, the suction effect is reduced because of disturbed velocity fields in the ship with a large waterline entrance angle, which may cause a higher resistance compared to those of other hullforms.

Figure 3.7 (b) reveals that a steep decrease in C_{ra} occurs between $Fn = 0.430$ and $Fn = 0.570$ for $C_B = 0.35$ and $L/B = 4$ (FDS-19), as shown with an inverted triangle and solid line. This abrupt change region coincides with the peak-value region of the residual resistance in calm water shown in Figure 3.5. In this region, the dynamic squat due to the increase in the ship's speed is greatly changed, and the stability of the stationary bow wave may change. The stability change due to the increase in the ship's speed induces a more stable bow wave, which can be deduced from Noblesse's relation shown in Figure 2.11. A steep decrease in C_{ra} due to an increase in the speed, therefore, can be explained as a transient region of the stability of the bow wave, where the detachment of the bow wave occurs by adding a stable plunging to the unstable bow wave. Consequently, the added resistance decreases because of the detached contribution of the relative wave elevation.

3.3.5. Performance in intermediate waves

This section investigates the response of the added resistance for intermediate wavelengths of $\lambda/L = 1.2$, at which the ship's motion response is significant. The response of the ship is highest at a wavelength similar to the length of the ship, and the added resistance is closely linked with the square of the motion response in the absence of wave breaking [11].

The model test data are analyzed considering the changes in stability of the bow wave due to the increased vertical motion response. As the vertical movement of the ship increases, the velocity of vertical motion is added to the velocity of the water particles at the crest of the bow wave, which can cause the bow wave to detach.

Therefore, the vertical movement of the ship increases the strength of the plunging breaking of the bow wave.

Figure 3.8 and Figure 3.9 show the experimental data for the nine hullforms as a combination of shapes and lines with the same rules as in Figure 3.4. Figure 3.8 shows the heave and pitch as well as the motion response of hullforms advancing at λ/L = 1.2. The motion response is significantly increased compared to the case of short waves. The added resistance measured for intermediate wavelengths of λ/L = 1.2 is analyzed using the conventional QTF of Equation 3.1 and the proposed transfer function of Equation 3.2. The added resistance in Figure 3.9 is significantly greater than that in Figure 3.7 for short waves.

The C_{aw} analysis of Figure 3.9 (a) shows that the peak of the added resistance does not match the motion response of the hullform with a small waterline entrance angle (L/B = 8 and 12). It is difficult to define a relationship between the added resistance and hull-related parameters, such as the ship's speed, C_B, or L/B. On the other hand, a meaningful relationship can be established in the C_{ra} analysis of Figure 3.9 (b). In the hullform with a small waterline entrance angle, the motion response of heave and pitch at Fn = 0.570 is greater than those at other speeds, but C_{ra} values are smaller. The increase in vertical motion response enhances the plunging breaking of the bow wave, which detaches the bow wave and weakens the contribution of the relative wave elevation to the added resistance. Therefore, the added resistance does not increase in proportion to the squared ship's speed and the motion response; rather, it decreases.

In addition, the C_{ra} values of all block coefficients and L/B = 4 with large incident angles at Fn = 0.570 are significantly lower than those of Fn = 0.285. The slope of this abrupt decrease is greater than the slope at the same speed for short waves shown in Figure 3.7. In Figure 3.7, the C_{ra} of a ship with a large entrance angle sometimes maintained a large value even if the speed increased. However, in the case of intermediate wavelengths, for which the vertical motion response of the ship is added, the C_{ra} values of all hullforms tend to decrease as the speed increases. This tendency of abrupt decrease in C_{ra} with an increase in the ship's speed may be associated with a decrease in the motion response of heave and pitch. However, it can also be interpreted to result from a reduction in the contribution of the relative wave elevation to the added resistance due to the detachment of the bow wave.

3.4. Interpretation using transfer function

In Section 3.3, a feasibility test was performed with the hypothesis that the two breaking types, spilling and plunging, affect the nonlinearity of the added resistance in different ways. The response of the added resistance was investigated according to the variation of stability type, especially for the plunging breaking of the bow wave deduced from the waterline entrance angle and the speed of the ship. The plunging breaking, which causes the detachment of the bow wave, affects the relative wave elevation of the bow wave. On the other hand, spilling breaking causes the disturbance of the velocity field around the hull.

In the process of stability change of the bow wave, the speed of the ship is the

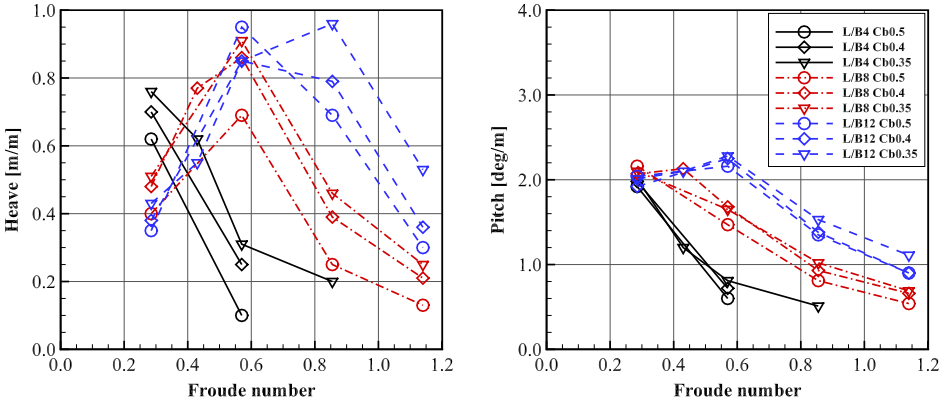

(a) Heave (b) Pitch

Figure 3.8: Motion response against Froude number for the nine hullforms in intermediate waves (λ/L = 1.2)

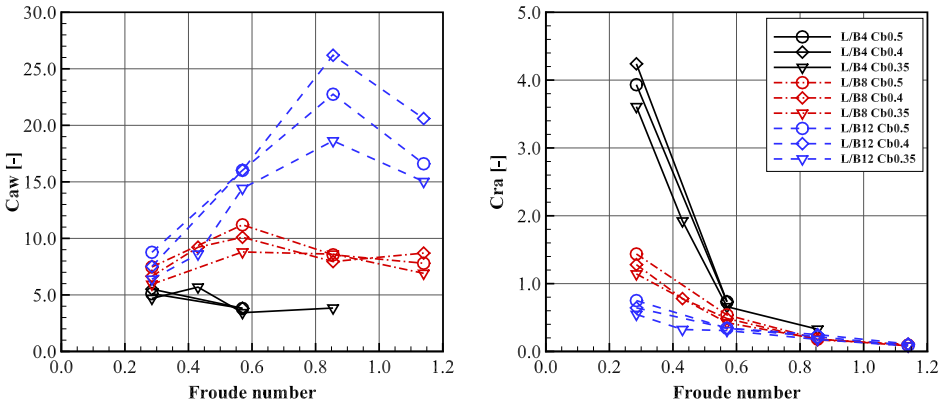

(a) C_{aw} of Equation 3.1 (b) C_{ra} of Equation 3.2

Figure 3.9: Quadratic transfer functions of added resistance against Froude number for nine hullforms in intermediate waves (λ/L = 1.2)

primary variable to be considered. The change of the ship's speed affects not only the ship's dynamic squat but also the stability of the crest of the bow wave. As shown in Figure 3.7 (b), the added resistance at adjacent speeds can have a significant impact, which can be explained by the resulting difference in the stability of the bow wave.

In Figure 3.8 (a), the resonant frequency varies with speed. Nevertheless, Figure 3.9 (b) showing the proposed transfer function of added resistance, demonstrates a clearer relationship of the added resistance coefficient with the Froude number. The speed discrimination power can be evaluated as too strong.

Nevertheless, the C_{ra} analysis can also be interpreted as a decrease of the added resistance due to threshold passing near $Fn = 0.5$ in Figure 3.7 (b) for short waves. C_{ra} abruptly decreases around $Fn = 0.5$ in the hullform with a relatively large entrance angle. This decrease can be interpreted to be caused by a decrease in contribution of the wave height of the added resistance by the detachment of the bow wave in the transient process, in which the plunging breaking of the bow wave suddenly increases because of the increased vertical motion response of the ship. These transient regions of C_{ra} occur in a region similar to the maximum point of the residual resistance curve in calm water shown in Figure 3.5.

Figure 3.9 (b) for intermediate waves shows an analysis for consistency with the analysis of Figure 3.7 (b) for short waves. In other words, it can be interpreted as a decrease in the contribution of added resistance due to the detachment of the bow wave. The decrease in C_{ra} with increasing ship speed in Figure 3.7 (b) is interpreted to be caused by the relative wave elevation being lower than that predicted by the linear theory owing to the detachment of the bow wave.

The interpretation of the added resistance with the proposed transfer function C_{ra}, which includes the squared ship's speed, effectively explains the hypothesis presented in Section 3.2. This effectiveness implies that the nonlinear response of the added resistance presented in the hypothesis can be identified by the change in the stability of the bow wave inferred from the speed change and the motion response of the ship.

Figure 3.10 and Figure 3.11 show the added resistance expressed by the conventional QTF of Equation 3.1 and the proposed transfer function expressed by Equation 3.2 with respect to the waterline entrance angle for three hullforms of $C_B = 0.35$ in short waves and intermediate waves, respectively. The C_{aw} in Figure 3.10 (a) for short waves and that in Figure 3.11 (a) for intermediate waves show a decreasing trend with increasing waterline entrance angle. This decreasing trend is considered to be due to differences in the length of the model in experiments performed according to the Froude similarity. The reason for this decrease is that the speed difference between the model ships in the experiment is not reflected in the analysis. Model ships with a large waterline entrance angle are constructed to have shorter lengths. Thus, their speed is less than that of other model ships for the same Froude number. Additional scientific interpretations for this decreasing trend are not possible.

However, in the analysis using C_{ra} proposed in Section 3.2, it is feasible to interpret the different diffraction effects on the bow wave, assuming that the similarity of the bow wave is preserved in the experiment. The C_{ra} of Figure 3.10 (b) and Figure 3.11 (b) is generally proportional to the waterline entrance angle at each speed.

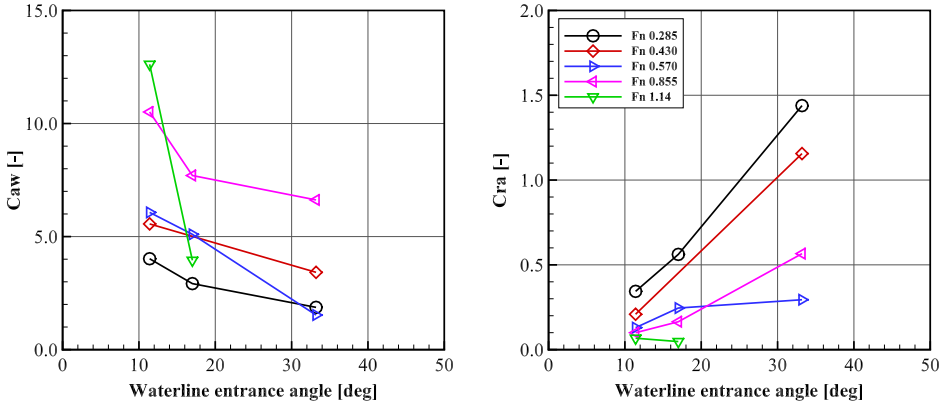

(a) C_{aw} of Equation 3.1 (b) C_{ra} of Equation 3.2

Figure 3.10: Quadratic transfer functions of added resistance against waterline entrance angle for three hullforms of the $C_B = 0.35$ in short waves ($\lambda/L = 0.4$)

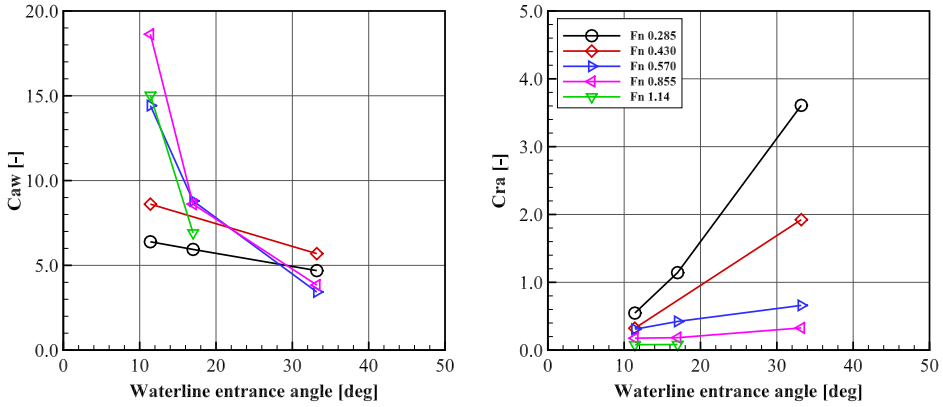

(a) C_{aw} of Equation 3.1 (b) C_{ra} of Equation 3.2

Figure 3.11: Quadratic transfer functions of added resistance against waterline entrance angle for three hullforms of the $C_B = 0.35$ in intermediate waves ($\lambda/L = 1.2$)

In these figures, a smaller C_{ra} is obtained at a faster speed or a smaller waterline entrance angle of the ship. This result can be interpreted following the hypothesis presented in Section 3.2 that the ship having a greater speed or smaller entrance angle will have a relatively stable breaking of the bow wave; thus, the resulting added resistance will be smaller than that predicted by the linear theory. This relationship can prove to be useful as it allows an intuitive interpretation by analyzing the nonlinearity of the added resistance depending on the speed of the ship.

3

3.5. Conclusions

This chapter investigated the response of the added resistance to the stability of the bow wave to understand the influence of bow-wave breaking for fast ships in which plunging breaking dominates. A hypothesis that the increase or decrease of added resistance depends on the stability type of bow-wave breaking was presented, and its feasibility was verified through the analysis of the model test results.

Since the speed can change the stability type of breaking of the bow wave, the ship's speed was selected as an independent variable to test the hypothesis. A transfer function of the added resistance including the squared ship's speed was presented and set as a dependent variable.

In the feasibility test, the hypothesis that the change of the added resistance depends on the stability of the bow wave was confirmed to be effective to interpret the nonlinearity observed in the model test results. To understand the nonlinearity of the added resistance due to the bow-wave breaking, the added resistance should be analyzed according to the speed of the ship. There is a transient region where sudden resistance changes occur. It was determined that there exists a boundary where the influence of the bow-wave breaking changes. The shift of the dominant influence of the bow wave induces a sudden change in the resistance. This was confirmed in the response of the added resistance through the proposed QTF including the squared ship speed. The transient region corresponds to the peak of the residual resistance coefficient in calm water as well. As the speed changes, the trend of the residual resistance coefficient and the added resistance changes at a specific speed region.

Understanding the phenomenon of bow-wave breaking, which appears in a complicated form, can improve the evaluation of added resistance. The results of this section show that a solution in the form of a method to evaluate the added resistance based on an understanding of the breaking phenomenon is necessary. Further research is needed to analyze the breaking phenomenon quantitatively and link it with the added resistance. Moreover, research to understand the nonlinear phenomena physically through the observation of a specific subject should be continued. Although the phenomena vary for different conditions of ships, phenomena that have similar physical characteristics must be explored continuously. The solution for the added resistance evaluation should be based on an understanding of the specific phenomena. Understanding the physical phenomena allows for a better estimation of the added resistance.

This chapter focused on the fact that the added resistance depends on the stability of the bow wave, which in turn depends on the speed of the ship. This chapter

suggests that the ship speed should be considered for the analysis of nonlinear phenomena. In order to verify this suggestions in detail, by measuring the hull surface pressure and relative wave elevation, the effect of the ship speed on the added resistance is investigated in the next chapter.

4

EXPERIMENTAL ASSESSMENT OF EFFECTS OF BOW-WAVE BREAKING

4.1. Introduction

In the review in Chapter 2, it was discussed that the behavior of the relative wave elevation of a ship is important to understand its effect on added resistance. Chapter 4 experimentally investigates the cause of plunging breaking of the bow wave and its effect on the added resistance by assessing the nonlinearity. Experiments have been conducted on a fast ship, which clearly shows the plunging breaking phenomenon. The relationship between the pressure of the hull and the relative height of the bow wave is examined. Templates have been proposed to evaluate the nonlinear relationship between the bow-wave height and the hull pressure, which has a decisive influence on the added resistance evaluation. The results show that the overturning detachment of the bow wave induces a pressure drop during the rise of the relative wave elevation. This pressure drop results in a lower wave added resistance compared to that predicted by the linear theory, which is based on a linear relationship

Table 4.1: Main particulars of FDS-5

Description	Ship	Model
Length $[m]$	100	6.667
Breadth $[m]$	12.502	0.833
Submerged draft $[m]$	3.125	0.208
Displacement $[m^3]$	1568.4	6.971
Wetted surface $[m^2]$	1212.3	0.359
Block coefficient C_B [-]	0.40	0.40

between pressure and wave height. The effect of this pressure drop on the added resistance is examined by the integration of measured pressures. The nonlinearity between the pressure and the relative wave elevation due to plunging breaking is closely related to the speed of the ship. Furthermore, the process of plunging breaking is defined in three stages: bow-wave development stage, pile-up, and breaking stage, and bow-wave absent stage.

The fast ship model used in the experiment and a video observation of the model test are introduced in Section 4.2 and 4.3, respectively. Section 4.4 proposes techniques to evaluate the breaking effect by investigating the relationship between the pressure on the hull surface and the relative wave elevation of bow waves. Section 4.5 assesses the effect of bow-wave breaking. Section 4.6 defines the process of plunging breaking considering its nonlinear effect on the added resistance. Section 4.7 assesses the cause of the nonlinearity due to plunging breaking and its influence on the added resistance. The conclusions of this chapter are presented in Section 4.8.

4.2. Measurement of a fast ship

Model tests with a fast ship were performed to measure the hull surface pressure and the relative wave elevation to clarify the relationship between them. The model ship has a length of 6.7 m, and the experiments were conducted at the Maritime Research Institute Netherlands (MARIN)'s Seakeeping and Maneuvering Basin (SMB), which has a length, width, and depth of 170 m, 40 m, 5 m, respectively. The hullform used in the experiment is the parent hullform of the systematic series of fast displacement ships (FDSs) of the Joint Industry Project from 1979-1989 [94, 106, 108]. The hullform has a simple triangular V-shaped front part and a nearly flat bottom stern, as shown in Figure 4.1. The main parameters of the model are listed in Table 4.1, and the scale factor is 15.0. The model test was performed with the ship in the free-running mode and equipped with the propeller, rudder, and autopilot system at three speeds (Fn = 0.285, 0.430, and 0.570).

As shown in Figure 4.2, the model ship is equipped with diaphragm-type pressure transducers and resistance-type wave height transducers at vertical intervals of 0.525 m at five stations (16, 17, 18, 18.75, and 19.5). Technically, there is a distance difference of 0.1 stations between the two types of transducers installed on the model ship. However, this difference, corresponding to 3.3 cm, is ignored because

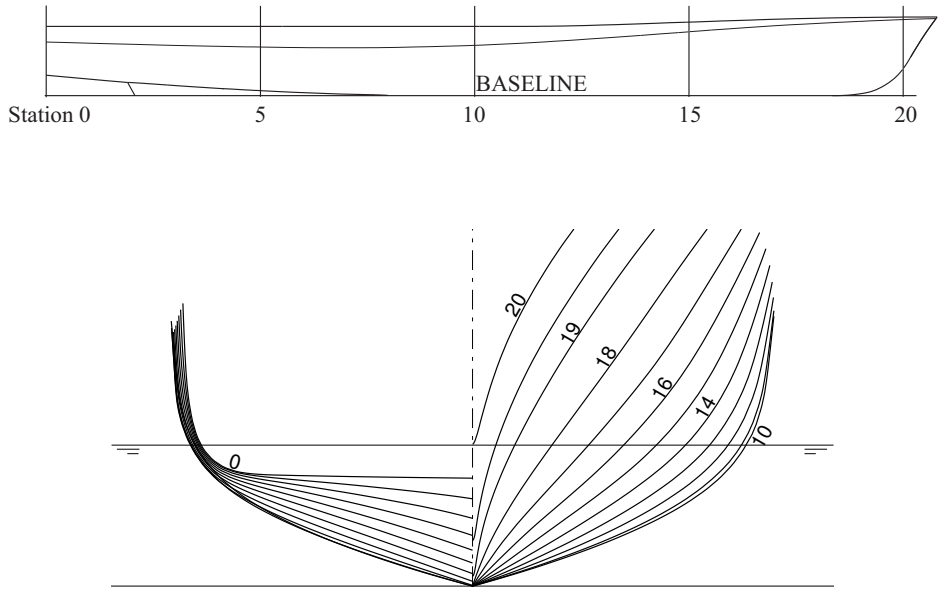

Figure 4.1: Profile and bodyplan of FDS-5

Figure 4.2: Photograph of the model ship

it does not play a decisive role in determining the effect of unsteady bow waves. Pressures and the relative wave elevation on the hull surface are measured for the ship advancing at a constant speed in calm water and regular waves (λ/L = 0.5, 1.1 and 2.0) with an amplitude of 1.0 m.

4.3. Observation of bow-wave breaking

Videos of the model tests are captured to show the behavior of the bow waves. Figure 4.3~4.6 show the instantaneous bow waves at three speeds in calm water, short waves (λ/L = 0.5), intermediate waves (λ/L = 1.1) and long waves (λ/L = 2.0). The left-hand side photographs of Figure 4.4~4.6 show the highest wave height at station 18. The photographs on the right-hand side in Figures 4.4~4.6 show the lowest wave height at station 18.

Bow waves appear as sheet-shaped overturning detachment because the ship is fast and has a simple fine bow shape with a small waterline entrance angle. Model tests on the fast ship can focus on the influence of wave elevation on the hull-surface pressure due to the bow-wave breaking, in contrast to conventional ships (e.g., blunt bow or bulbous bow), which are known to be influenced by viscosity [4].

In Figure 4.3~4.6, an overturning thin sheet of the plunging breaking of bow waves is observed. As the speed of the ship increases, the size of the sheet increases. At Fn = 0.285 in the figures, the bow wave is observed to break relatively less. When the ship's speed increased to Fn = 0.430, the bow wave clearly breaks with overturning motion. At the maximum speed of Fn = 0.570, the longitudinal length of the region where the overturning detachment of the thin sheet occurs is considerably increased.

The left-hand side of Figure 4.4 shows the highest wave height of the bow wave in short waves. It is observed that the overturning detachment of the bow wave is greatly increased compared to that at the same speed in calm water. At the right-hand side of Figure 4.4, which shows the lowest wave height, the stationary wave, which is a fundamental element of the wave resistance of the ship, disappears.

The left-hand side of Figure 4.5 shows the highest wave height of the bow wave in intermediate waves. The bow wave is significantly broken. It is observed that the breaking area also increases as the speed increases. In the photographs on the right-hand side, where the wave height is the lowest after the bow wave breaks, the bow wave has disappeared.

In the left-hand side of Figure 4.6, the overturning detachment is also observed in long waves. At each speed, however, the breaking form of the bow wave is milder than in the short-wave condition of Figure 4.4, in which the ship shows no motion response.

The plunging breaking in the fast ship is observed as two phenomena. The first is the overturning detachment on the crest of the bow wave. The second is the disappearance of the stationary bow wave. These breaking phenomena of the bow wave are more clearly observed as the speed of the ship increases.

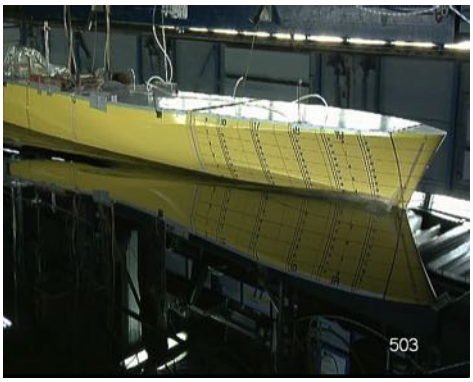

(a) $Fn = 0.285$

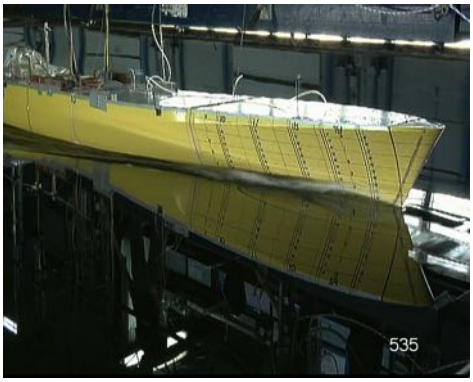

(b) $Fn = 0.430$

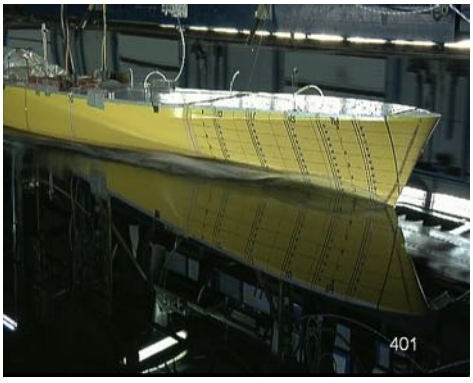

(c) $Fn = 0.570$

Figure 4.3: Stationary bow waves in calm water for three speeds

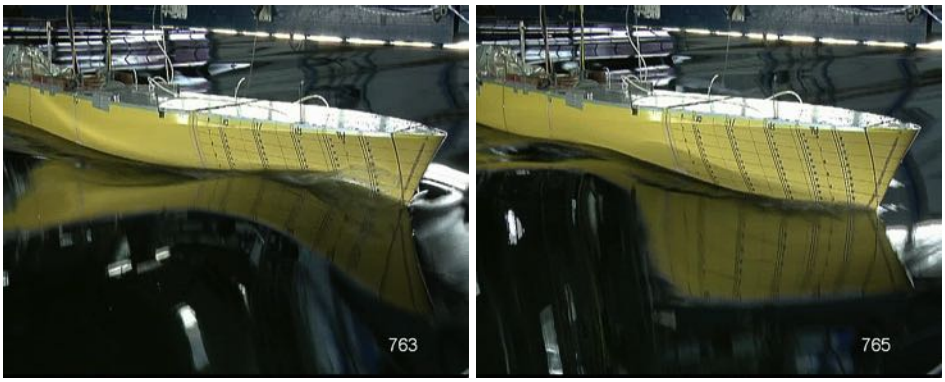

(a) $Fn = 0.285$

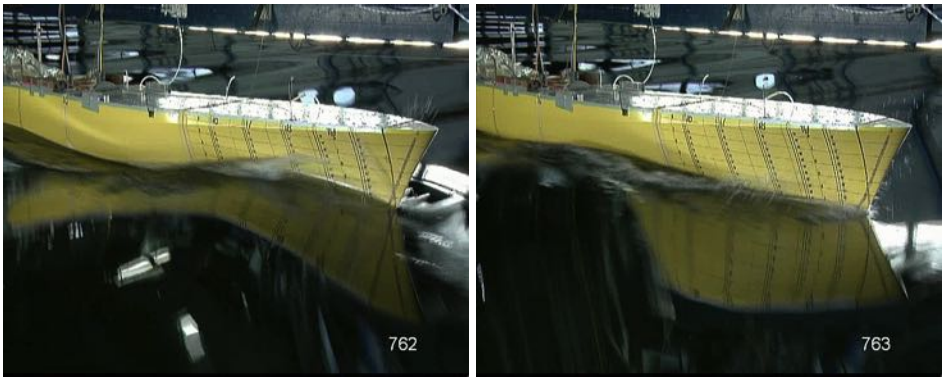

(b) $Fn = 0.430$

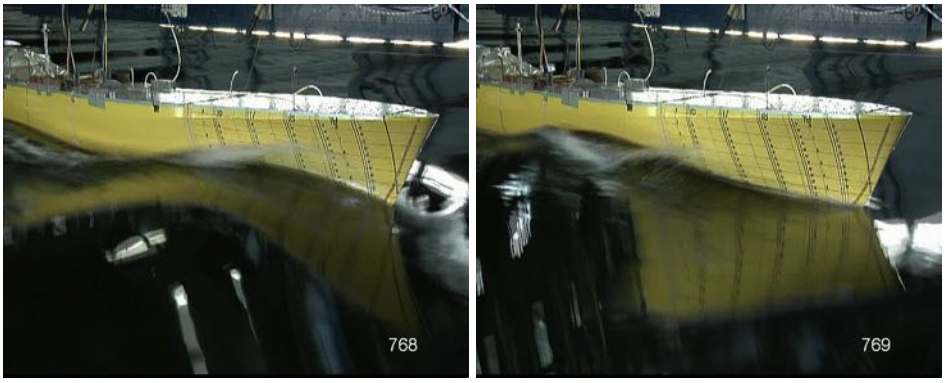

(c) $Fn = 0.570$

Figure 4.4: Instantaneous bow waves for three speeds in short waves ($\lambda/L = 0.5$). The left-hand side photos show the highest height of the bow wave and the right-hand side photos show the lowest wave height at station 18.

(a) $Fn = 0.285$

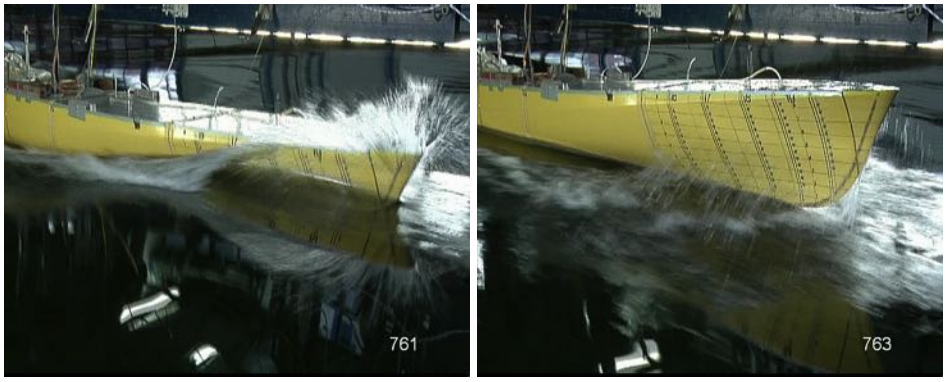

(b) $Fn = 0.430$

(c) $Fn = 0.570$

Figure 4.5: Instantaneous bow waves for three speeds in intermediate waves ($\lambda/L = 1.1$). The left-hand side photos show the highest height of the bow wave and the right-hand side photos show the lowest wave height at station 18.

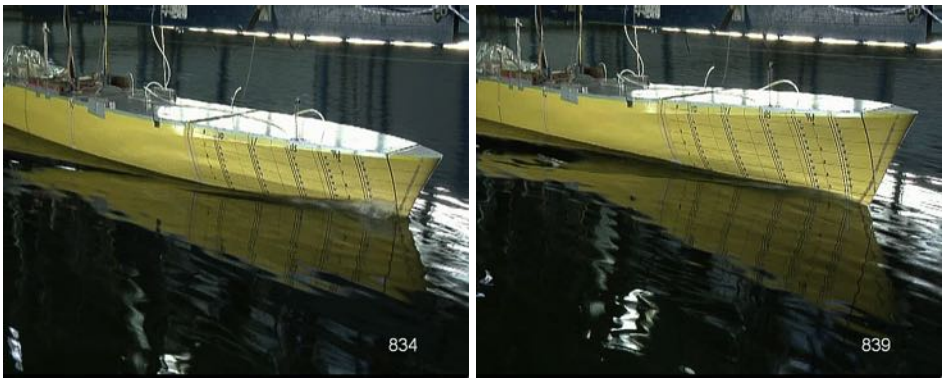

(a) $Fn = 0.285$

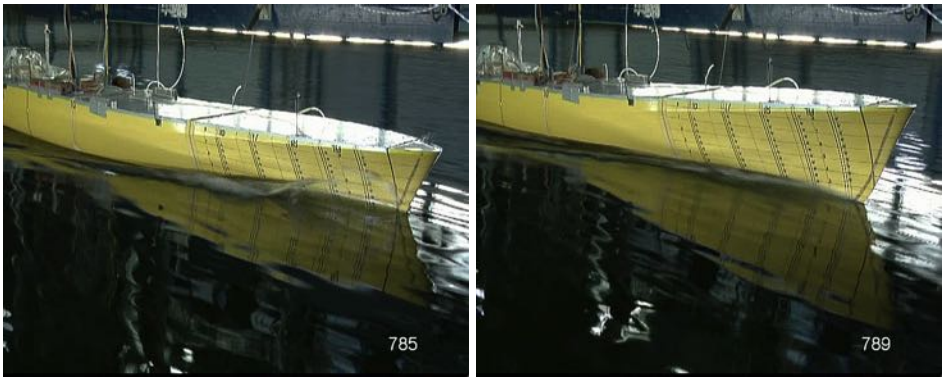

(b) $Fn = 0.430$

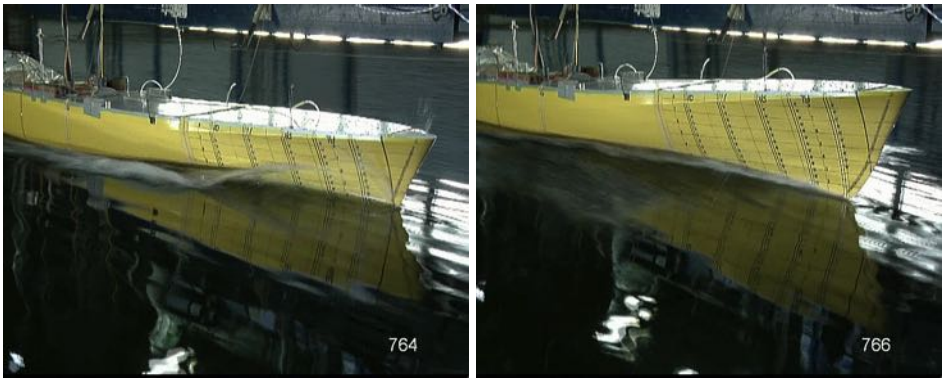

(c) $Fn = 0.570$

Figure 4.6: Instantaneous bow waves for three speeds in long waves ($\lambda/L = 2.0$). The left-hand side photos show the highest height of the bow wave and the right-hand side photos show the lowest wave height at station 18.

4.4. Development of evaluation template

In Chapter 2, various studies successfully simulated the dynamics of the bow wave. However, little research has been performed on basic physical models to help understand the impact of bow-wave breaking on the added resistance.

The waterline contribution of the added resistance has an important significance, especially in the fast displacement ship. The waterline contribution is proportional to the square of the relative wave elevation in Equation 2.7. Therefore, it is important to evaluate the relative wave elevation accurately. In addition to accurately evaluating the relative wave elevation, it is necessary to pay attention to the particular changes in the hull pressure when the bow wave is breaking. In particular, it is important to evaluate the relationship between the relative wave elevation and the unsteady pressure of a ship concerning the nonlinearity of the wave added resistance.

Pressure measurements are needed to identify physical phenomena that affect the added resistance. In the analysis of the measured signals, it is difficult to correlate the time-domain signals of each pressure gauge and wave transducer. The measurement of the hull-surface pressure in waves is an expensive experiment, which involves difficult-to-install pressure gauges and signal processing. The measured results should be carefully analyzed and evaluated. It is necessary to develop an efficient method for processing a large amount of measurement data.

This section presents analytical templates to evaluate the effect of the bow-wave breaking by using the relative wave elevation and the pressure of the hull surface measured in the model test. Two types of templates are introduced: the sequence history of pressure and the pressure and relative wave elevation diagram (P-R diagram) of the bow wave. These templates have been developed to investigate the effect of bow-wave breaking. The two templates proposed in this chapter have the advantage of capturing the relationship between the time series of pressure and the relative wave elevation into a simple synthesized form.

4.4.1. Sequence history of pressure

Figure 4.7∼4.9 show the sequence history for one cycle of the signals measured from twelve pressure gauges installed in sequence at a vertical interval of 0.525 m at station 18. Each box represents the time-series pressure for one of twelve sequences from left to right. These figures show the pressure trend in the order of the pressure gauges installed at constant vertical intervals along the y-axis. The pressure measured at zero speed in calm water is selected as the reference zero value for each run. The unsteady pressure measured for the advancing ship is corrected by the pressure of the still water.

The sequence history of pressure shows the compression of the relationship among each pressure signal. Consequently, the development and disappearance of the bow wave are captured in this figure. Figure 4.7∼4.9 show the results for $\lambda/L =$ 0.5, 1.1, and 2.0, respectively. In these figures, when the elevation of the bow wave is high, pressure is generally high, but this is not the case at high speed.

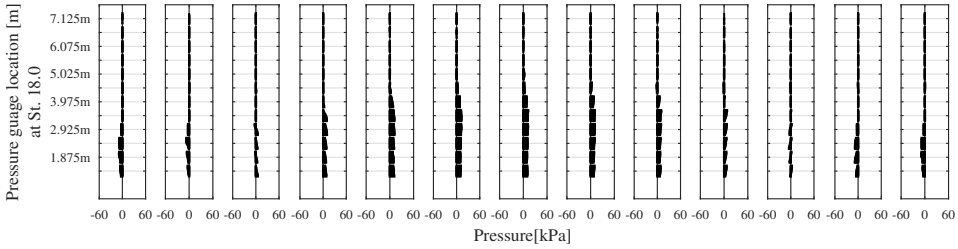

(a) $Fn = 0.285$

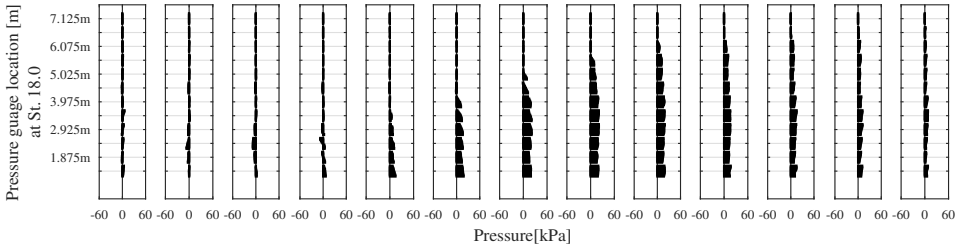

(b) $Fn = 0.430$

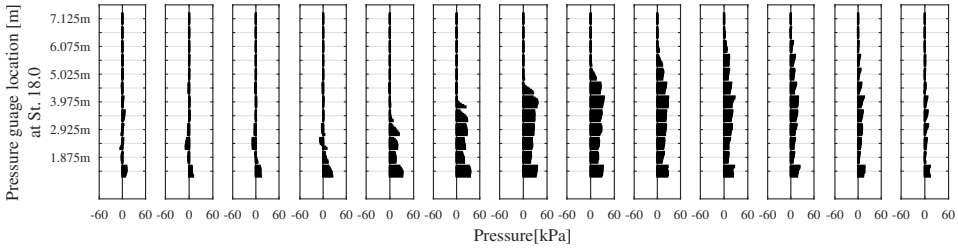

(c) $Fn = 0.570$

Figure 4.7: The sequence history of pressure at station 18 in short waves ($\lambda/L = 0.5$)

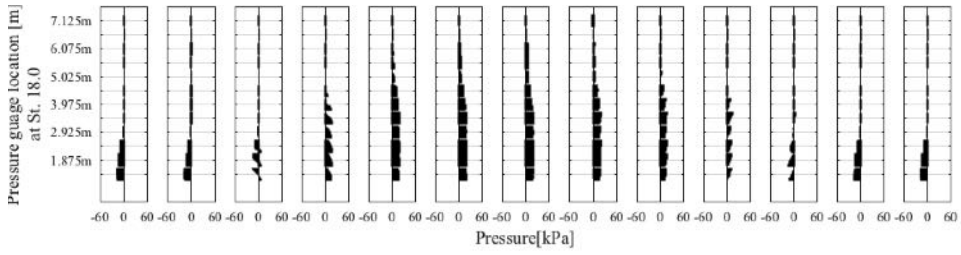

(a) $Fn = 0.285$

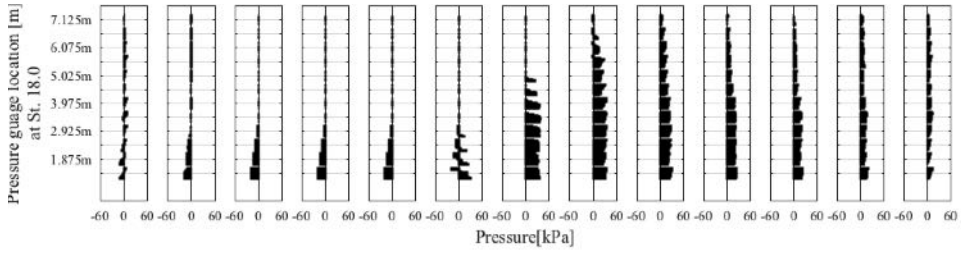

(b) $Fn = 0.430$

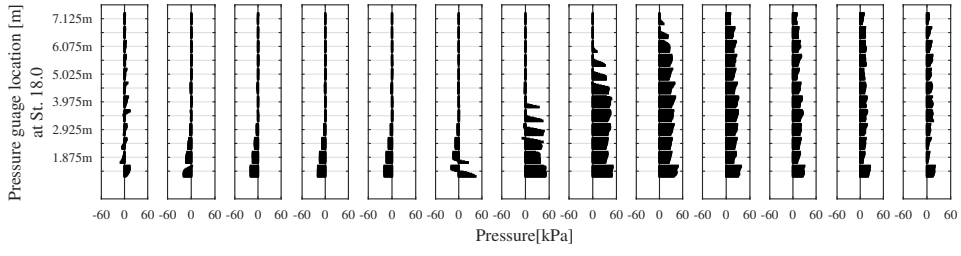

(c) $Fn = 0.570$

Figure 4.8: The sequence history of pressure at station 18 in intermediate waves ($\lambda/L = 1.1$)

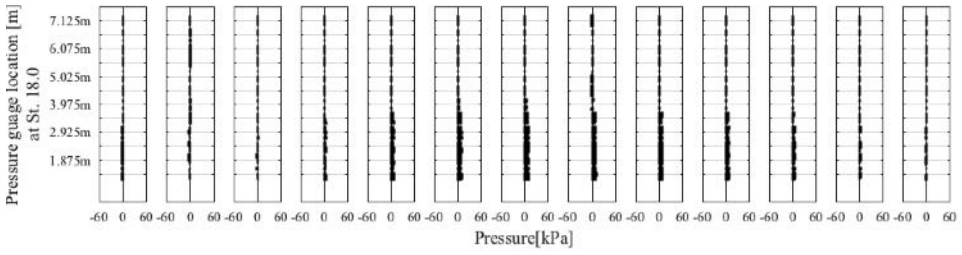

(a) $Fn = 0.285$

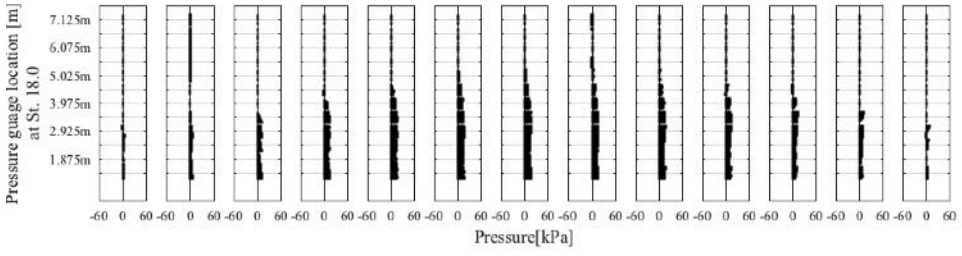

(b) $Fn = 0.430$

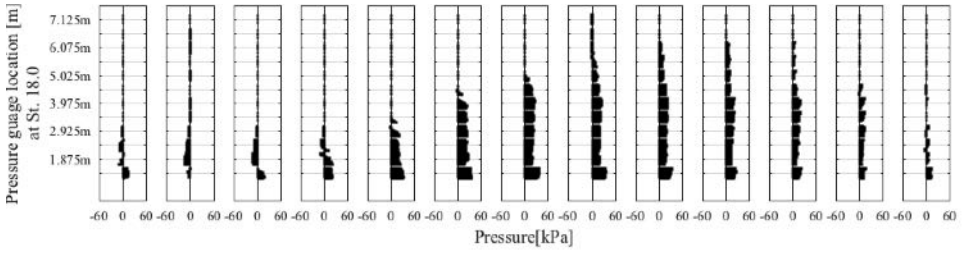

(c) $Fn = 0.570$

Figure 4.9: The sequence history of pressure at station 18 in long waves ($\lambda/L = 2.0$)

At Fn = 0.570 in each figure, the pressure acting on station 18 at the sequence of the maximum wave elevation is not the greatest. This discrepancy in pressure is usually significant at high speeds. The pressure trend described by the sequence history is consistent with the detachment phenomenon of the bow wave observed in the experiment video.

This comparison demonstrates that the pressure contribution of the bow wave is not linearly proportional to the wave height. The nonlinear relationship between these two signals is also related to the speed of the ship. The association of these two signals is explained in detail in the next section.

4.4.2. Pressure and relative wave elevation diagram

In regular waves, the pressure and relative wave elevation signals in the time domain at station 18 for three periods are shown in Figure 4.10~4.12. The measured time-domain pressure signals are smoothed with a time-based moving average filter of a five-point span. Figures 4.10~4.12 show the smoothed pressure data with a solid line, the raw data with circles, and the relative wave elevation with a dashed line. The figures show that the smoothed pressure signal removes the local high-frequency signal and preserves the response of the original signal well. Each measured value in calm water is subtracted from the measured signals (pressure and relative wave elevation) in regular waves to focus only on an unsteady bow wave. Therefore, the subtracted signal represents the unsteady phenomenon in regular waves. As the ship's speed increases, it is observed that the sinusoidal tendency of the signal decreases.

An analysis tool called pressure and relative wave elevation diagram (P-R diagram) is proposed. The measured pressure is non-dimensionalized by the square of the speed in Equation 4.1.

$$C_p = \frac{P}{\frac{1}{2}\rho U^2} \tag{4.1}$$

where P is the measured pressure, ρ is the water density and U is the speed of the ship.

The pressure measured by the fixed pressure gauge and the relative wave elevation measured by the wave height transducer at a specific location on the hull show a repeated signal in the same period. Figure 4.13 shows a schematic X-Y plot for three cycles, with the smoothed pressure on the x-axis and the corresponding relative wave elevation on the y-axis. The P-R diagram shows a closed shape by directly matching these two terms but not the time term. In the P-R diagram, the center of the graph is the origin (0, 0) because the corresponding values of the pressure and the relative wave elevation in calm water are subtracted from the measured signals in waves.

Figure 4.13 depicts the periodic history of the development and disappearance of the bow wave and the instantaneous pressure contribution on the hull surface in the order of the numbered dashed-line arrows. The number '1' is the process of linearly

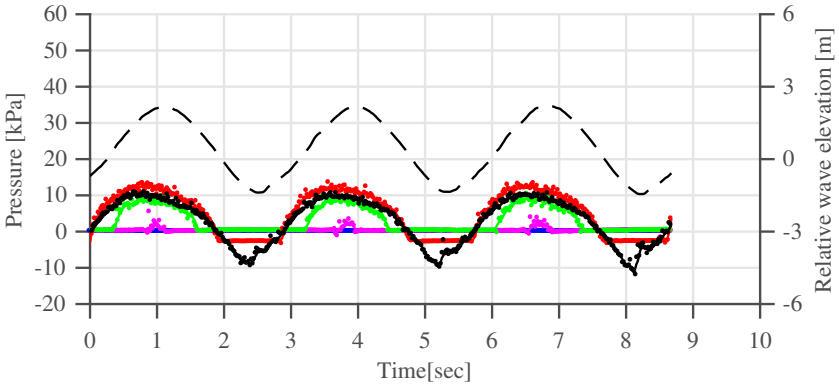

(a) $Fn = 0.285$

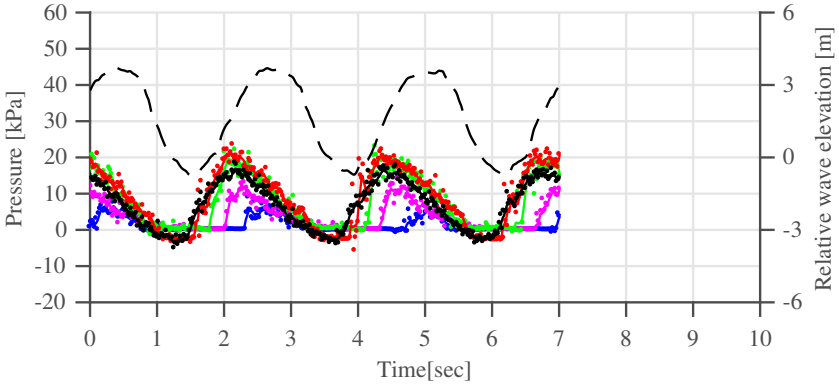

(b) $Fn = 0.430$

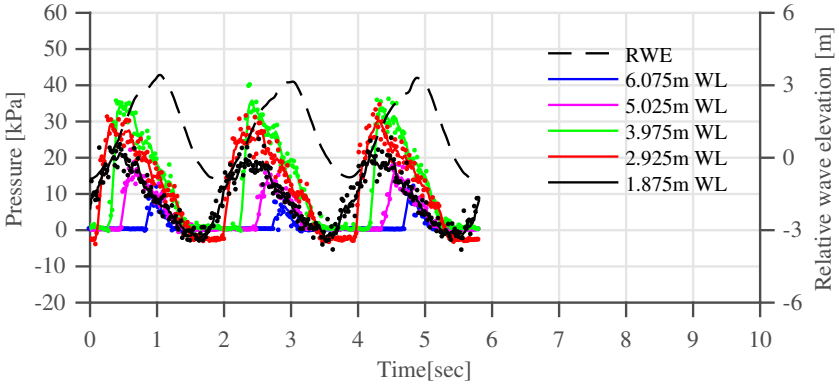

(c) $Fn = 0.570$

Figure 4.10: An example of relative wave elevation (RWE) and pressure signals for three cycles. Pressure signals are smoothed with a time-based moving average filter of a five-point span over three speeds at station 18 in short waves ($\lambda/L = 0.5$).

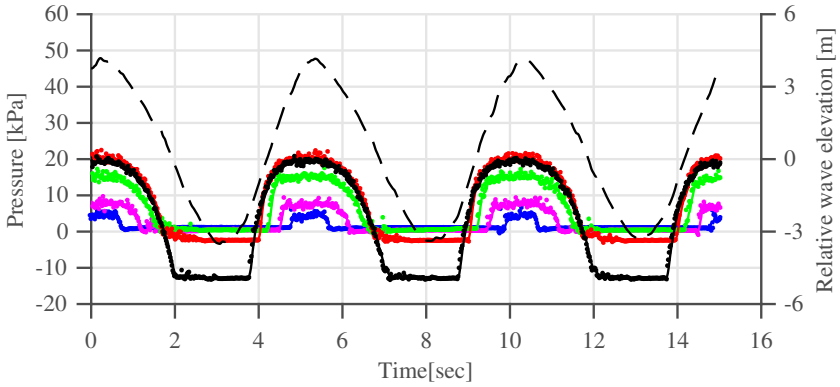

(a) Fn = 0.285

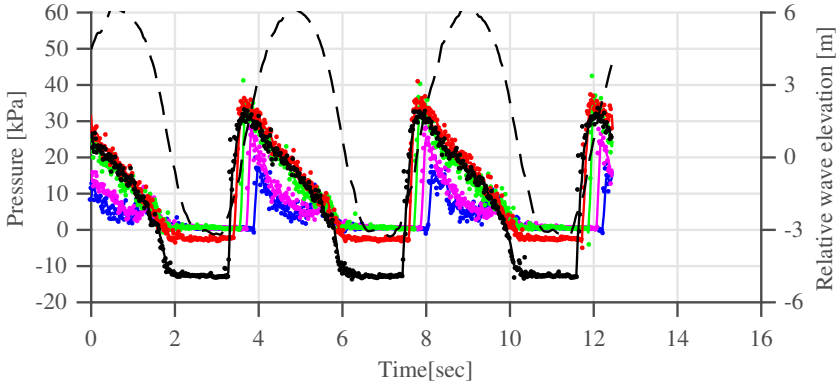

(b) Fn = 0.430

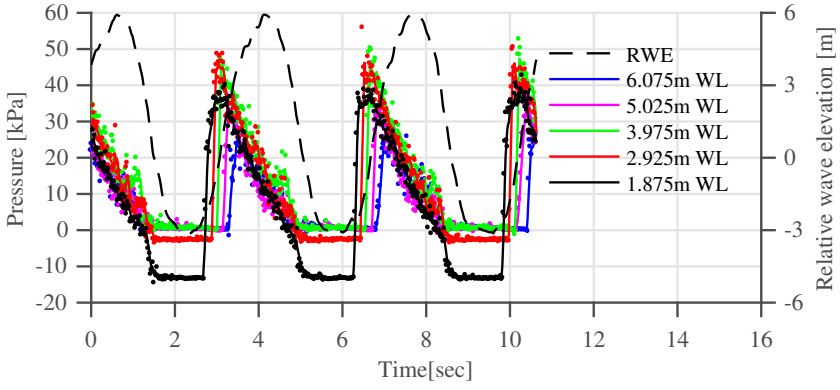

(c) Fn = 0.570

Figure 4.11: An example of relative wave elevation (RWE) and pressure signals for three cycles. Pressure signals are smoothed with a time-based moving average filter of a five-point span over three speeds at station 18 in intermediate waves ($\lambda/L = 1.1$)

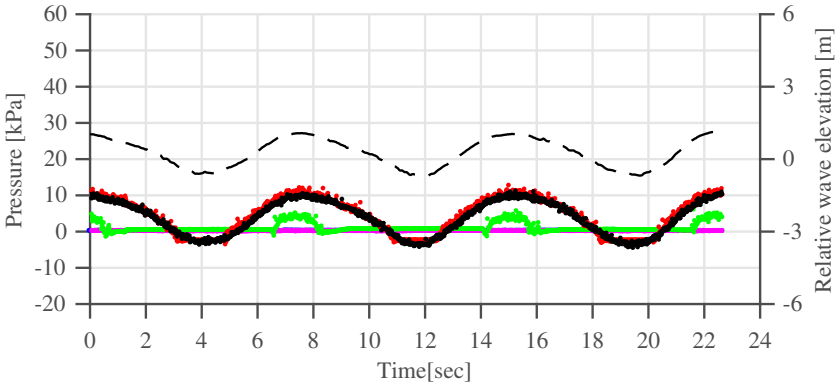

(a) $Fn = 0.285$

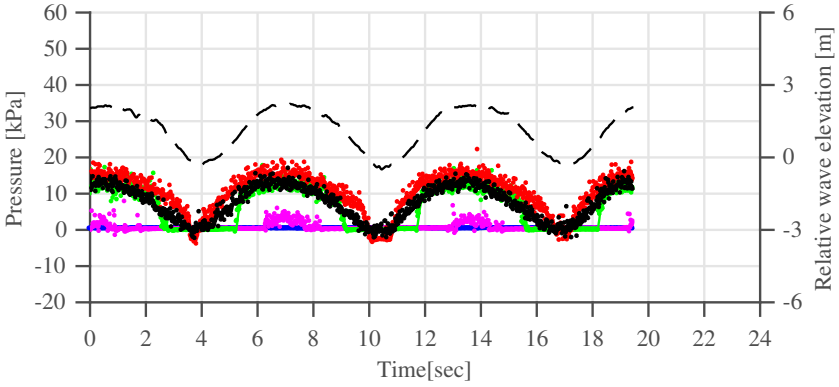

(b) $Fn = 0.430$

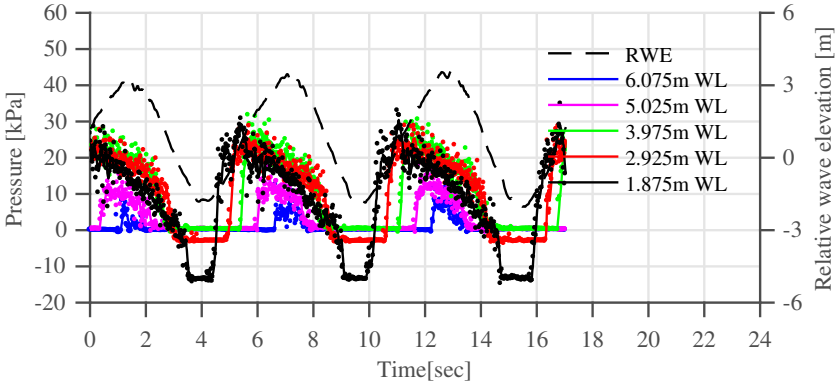

(c) $Fn = 0.570$

Figure 4.12: An example of relative wave elevation (RWE) and pressure signals for three cycles. Pressure signals are smoothed with a time-based moving average filter of a five-point span over three speeds at station 18 in long waves ($\lambda/L = 2.0$)

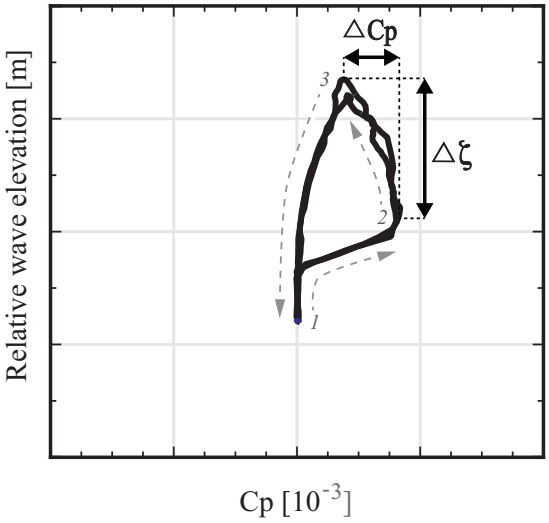

Figure 4.13: Schematic drawing of the pressure and relative wave elevation diagram (P-R diagram) with the characterization of the upwash of the relative wave elevation ($\Delta\zeta$) and the pressure drop (ΔCp) during the upwash. The development and disappearance of the bow wave and the instantaneous pressure contribution on the hull surface are indicated by the order of the dashed-line arrows.

increasing the pressure as the relative wave elevation increases. The number '2' is the process where the relative wave elevation increases but the pressure decreases. The number '3' is the subsequent process where the relative wave elevation and pressure are reduced. At the end of this process, pressure absence is observed. This P-R diagram shows the hysteresis of the repeated signal at the same time.

In the linear theory, a linear relationship exists between the pressure and the relative wave elevation. If the linear theory is valid, a linear relationship between these two signals should be identified about the origin of the P-R diagram. Otherwise, if a nonlinear relationship occurs between the two signals, the P-R diagram will have a distorted shape due to the discrepancy between the maximum points of the pressure and the relative wave elevation. Therefore, the distortion can be considered evidence of nonlinearity.

Here, the peak of the relative wave elevation is followed by the pressure peak, which violates the linear relation between the pressure and relative wave elevation. To investigate this discrepancy further, the counter-gradient of each pressure gauge is described with the upwash of relative wave elevation ($\Delta\zeta$) after the pressure peak and the pressure drop (ΔCp) during this upwash, as shown in Figure 4.13. These two characteristic values are discussed in detail in Section 4.5.4.

4.5. Analysis of model test results

4.5.1. Results in short waves

Figure 4.14 shows the relationship between the pressure acting on the hull and the relative wave elevation measured at five stations at three speeds (Fn = 0.285, 0.430 and 0.570) in short waves (λ/L = 0.5) with little motion response. The figure shows that the linear relationship between pressure and wave elevation becomes weaker as the ship's speed increases. The bulge of the shape of the diagram at Fn = 0.430 is greater than that at Fn = 0.285. In Figure 4.14 (c) Fn = 0.570, it is difficult to find a linear relation between the pressure and the relative wave elevation. The pressure drop during pile-up is more pronounced as the ship's speed increases.

As the ship's speed increases, the longitudinal position where the highest pressure drop occurs during the growth of the bow wave is shifted to the back of the ship. This phenomenon occurs at station 19.5 for Fn = 0.285, at station 18.75 for Fn = 0.430, and at station 18.0 for Fn = 0.570. The nonlinear phenomenon identified in the P-R diagram is consistent with the plunging breaking phenomenon identified in the captured video of Figure 4.4. The shape of the P-R diagram expands as the ship's speed increases. Moreover, as the ship's speed increases, the longitudinal range of the bulging shape in the P-R diagram increases.

4.5.2. Results in intermediate waves

Figure 4.15 shows the relationship between the pressure acting on the hull and the relative wave elevation measured at five stations at three speeds (Fn = 0.285, 0.430, and 0.570) in intermediate waves (λ/L = 1.1) with significant motion response. The figure shows a significant increase in the relative wave elevation due to the increase in the ship's motion response.

The bulging of the P-R diagram is also increased. In contrast to the short-wave condition, the bulging shape of the P-R diagram at the representative stations 16 and 17 is obvious at intermediate waves, as shown in Figure 4.15. A pressure drop is clearly observed in the process of increasing the bow-wave height.

This difference is explained by the greater vertical motion response of the ship. Owing to the larger response, the increased relative velocity in the flow field around the hull induces a stronger breaking of the bow wave. On the other hand, this is also the result of an interaction of the incoming waves with the local geometric features of the hullform, such as a flare that changes the dynamic waterline entrance angle.

4.5.3. Results in long waves

Figure 4.16 shows the relationship between the pressure and the relative wave elevation measured at five stations at three speeds (Fn = 0.285, 0.430, and 0.570) for the movement of the ship along the free surface in long waves (λ/L = 2.0).

The shape of the P-R diagram in this wavelength condition shows a more linear

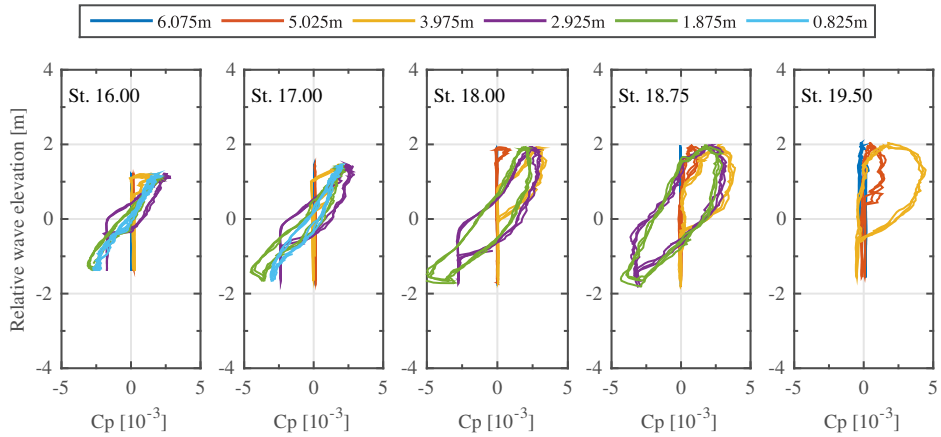

(a) $Fn = 0.285$

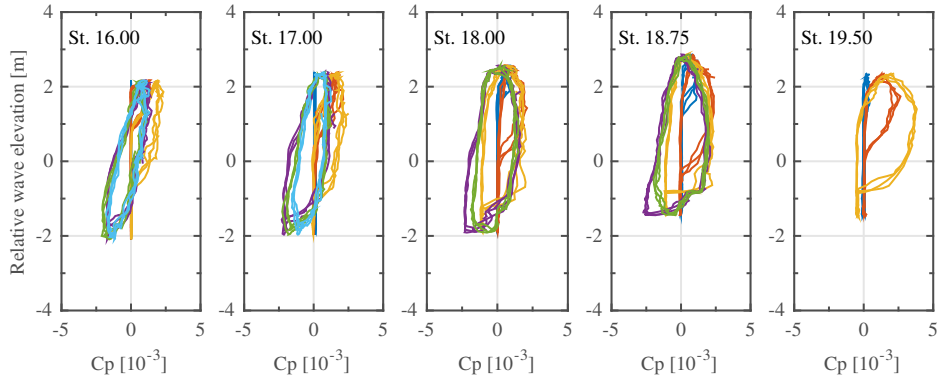

(b) $Fn = 0.430$

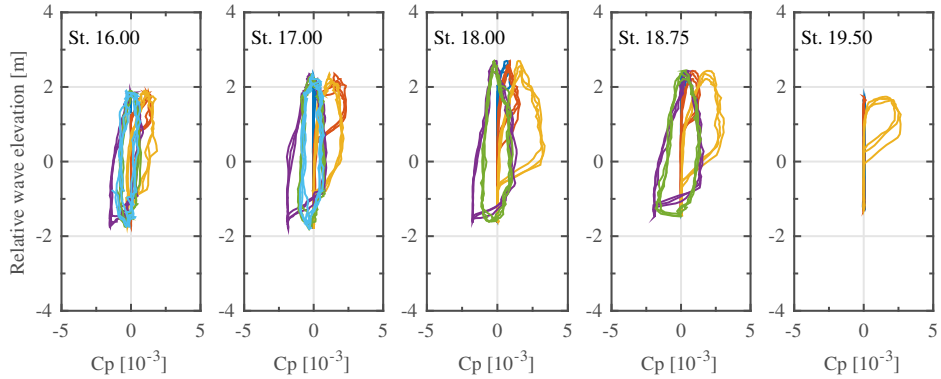

(c) $Fn = 0.570$

Figure 4.14: The pressure and relative wave elevation diagram (P-R diagram) for three ship's speeds in short waves ($\lambda/L = 0.5$)

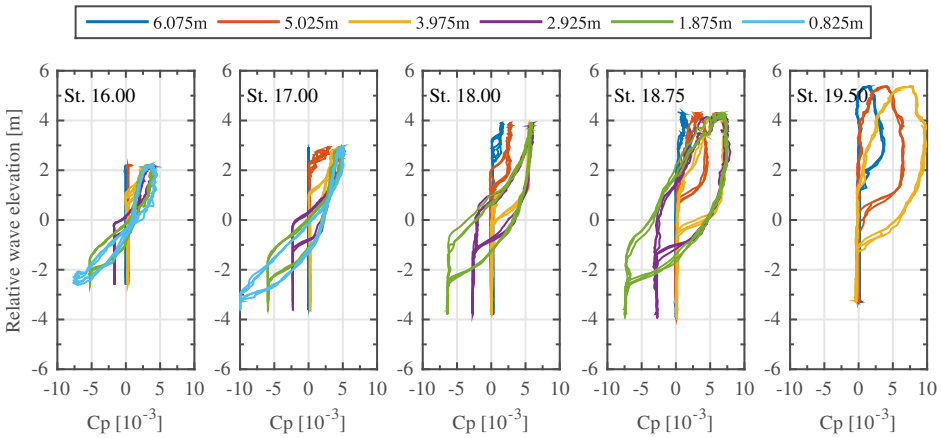

(a) $Fn = 0.285$

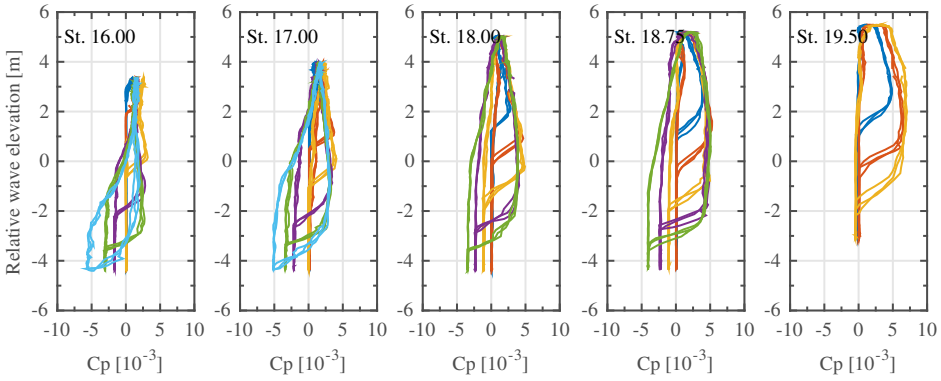

(b) $Fn = 0.430$

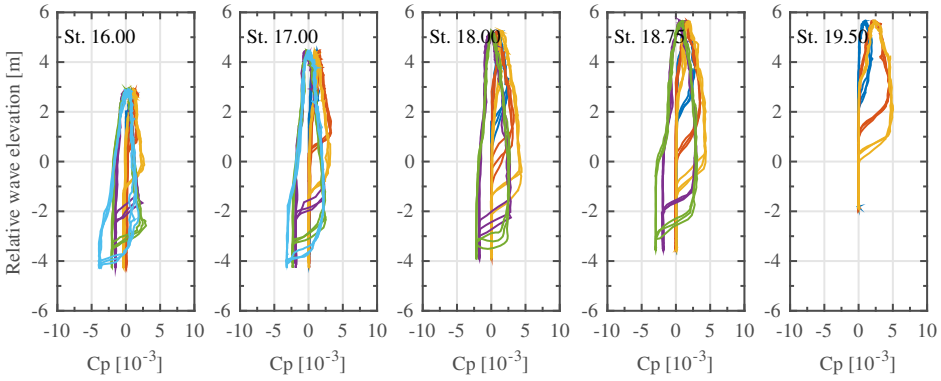

(c) $Fn = 0.570$

Figure 4.15: The pressure and relative wave elevation diagram (P-R diagram) for three ship's speeds in intermediate waves ($\lambda/L = 1.1$)

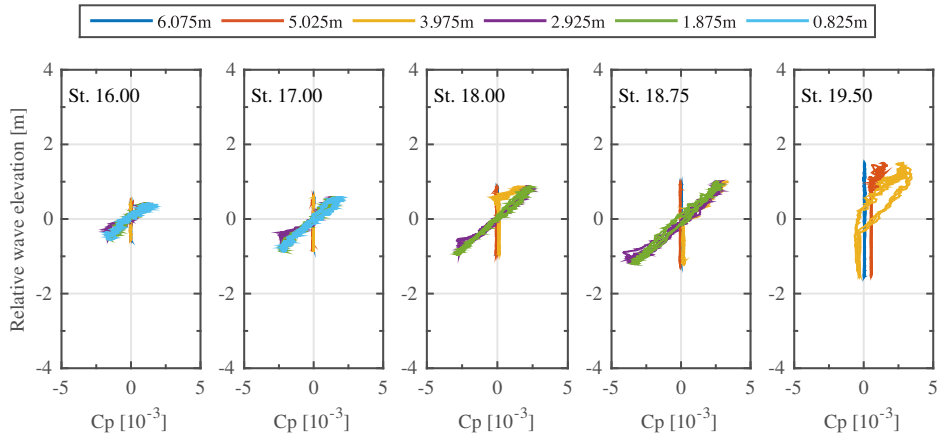

(a) $Fn = 0.285$

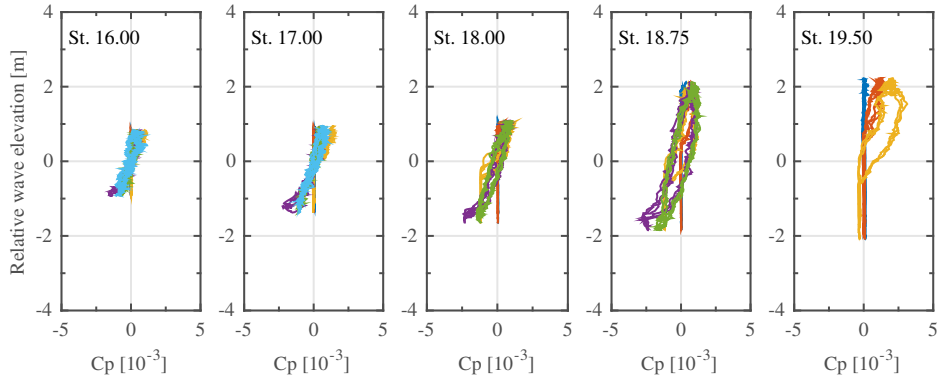

(b) $Fn = 0.430$

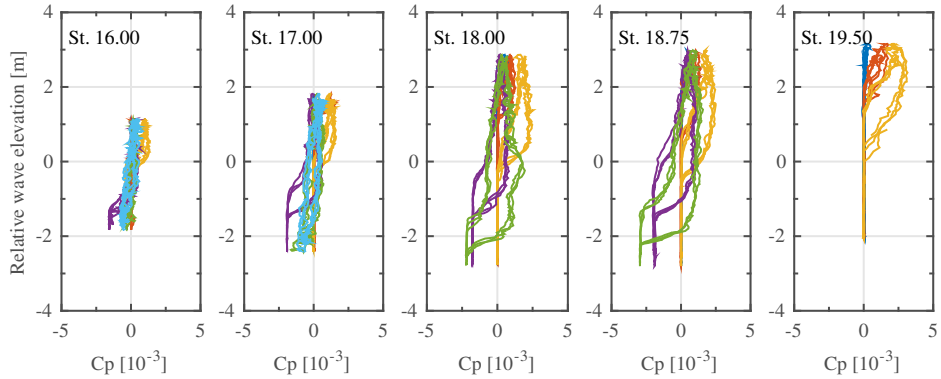

(c) $Fn = 0.570$

Figure 4.16: The pressure and relative wave elevation diagram (P-R diagram) for three ship's speeds in long waves ($\lambda/L = 2.0$)

relationship at all speeds compared to the previous wavelength conditions (λ/L = 0.5 and 1.1). The width of the graph envelope is greatly reduced. This indicates improved linearity between the two signals. This increased linearity of the diagram results from the preservation of the proportional relationship between the pressure and the relative wave elevation, thereby reducing the pressure difference between the rising and falling relative wave elevation. This indicates that the bow wave is preserved to a greater degree in long waves than in other wavelength conditions.

In summary, the generation and disappearance of the bow wave have been effectively shown and analyzed by the P-R diagram, which is presented in Section 4.4.2, at three wavelengths (λ/L = 0.5, 1.1, and 2.0). The P-R diagram shows the history of pressure acting on the hull during the periodic operation of the bow wave. The P-R diagram allows the nonlinear relationship between the pressure and the relative wave elevation of the bow wave to be intuitively captured by the bulging shape. The plunging breaking, which appears as a detachment of the bow wave, produces a nonlinear relationship between the pressure on the hull surface and the relative wave elevation of the bow wave. The intensity of the plunging breaking is large when the ship's speed or motion response is large.

4.5.4. Nonlinearity assessment

The shape of the P-R diagram is influenced by the maximum value of phase difference between the relative bow wave elevation and the pressure signal. As shown in Figure 4.13, the pressure development process when the bow wave is detached can be described as follows. The bow wave develops with the increase of height and pressure. When the bow wave detaches, the pressure begins to decrease past the maximum value while the height of the bow wave is still increasing. When the relative height is maximum, the pressure is already considerably reduced.

During the bow-wave development process, the phase mismatch between the maximum values of the relative wave elevation and the pressure is the result of detachment of the bow wave by plunging breaking. The phase difference between the pressure and relative wave elevation destroys the linear relationship represented in the P-R diagram. When the breaking phenomenon of the bow wave becomes stronger, the phase difference between the maximum values of the two signals increases. Moreover, the shape of the P-R diagram bulges.

The nonlinear relationship between the pressure and relative wave elevation can be characterized with the upwash of relative wave elevation ($\Delta\zeta$) after the pressure peak as well as the pressure drop (ΔCp) during this upwash, as shown in Figure 4.13.

Figures 4.17 and 4.18 show the nonlinear characteristics of the P-R diagram at five stations installed with the series of pressure gauges. Each graph shows the analysis results of the signals from pressure gauges installed with vertical intervals of 0.525 m in each station. The black solid line, red dotted line, and blue dotted line correspond to Fn = 0.285, 0.430, and 0.570, respectively. The analysis results of the P-R diagrams of short waves, intermediate waves, and long waves are shown in (a), (b), and (c), respectively.

Upwash of relative wave elevation ($\Delta\zeta$)
Figure 4.17 shows the difference between the maximum height at the station and the height corresponding to the maximum pressure of each gauge. Figure 4.17 (a) shows that the $\Delta\zeta$ of short waves depends on the longitudinal position and Froude number. Figure 4.17 (b), the $\Delta\zeta$ values of intermediate waves increase significantly from Fn = 0.285 to Fn = 0.430, but show similar values for further increase to Fn = 0.570. Large values are maintained until station 16, which is the aft-boundary where measurement is performed. In Figure 4.17 (c), the $\Delta\zeta$ of long waves shows meaningful values related to breaking only at station 18 with Fn = 0.570.

Pressure drop during upwash (ΔCp)
At each station, the pressure drop during the increase in the relative wave elevation is shown in Figure 4.18. In Figure 4.18 (a), the ΔCp of short waves tends to be generally proportional to the ship's speed after station 18. At the front of station 18, the maximum value of ΔCp appears at a different speed. The largest ΔCp appears at Fn = 0.285 for station 19.5, Fn = 0.430 for station 18.75, and Fn = 0.570 for station 18. The station with the maximum value of ΔCp moves backward as the speed increases. The ΔCp of intermediate waves in Figure 4.18 (b) is significantly greater than that of short waves. The increase in the ΔCp at Fn = 0.430 is particularly evident. At each speed, the position at which the maximum value of ΔCp appears moves backward as the speed increases. However, at Fn = 0.285, the region with significant values is limited to the foremost station. ΔCp is greatly reduced at station 16 at Fn = 0.430, but remains large at station 16 at Fn = 0.570. In Figure 4.18 (c), the ΔCp of long waves is considerably less than the values at the other wavelengths, making meaningful comparisons difficult.

By integrating the analysis results, as the ship's speed increases, the positions of the maximum value of nonlinearity properties ($\Delta\zeta$ and ΔCp) appear to move backward. Particularly, in the intermediate wave analysis, in which the characteristic values are large, the area of the region with substantial characteristic values increases as the ship speed increases. The area decreases sharply from station 18.75 at Fn = 0.280, it starts to decrease from station 17 at Fn = 0.430, and it begins to decrease from station 16 at Fn = 0.570. The above analysis characterizes the bow-wave breaking. Thus, the P-R diagram intuitively detects the plunging breaking phenomenon through shape distortion.

4.6. Process definition of plunging breaking

Taking into account the behavior of the pressure and the relative wave elevation investigated through the P-R diagram proposed in this chapter, the process of plunging-type breaking of waves can be divided into three stages. The first (the number '1' in Figure 4.13) is the bow-wave developing stage, in which the ship's surface pressure increases with the relative wave elevation. The second (the number '2' in Figure 4.13) is the pile-up and breaking stage, in which the height of the bow wave increases but the surface pressure of the hull decreases. The pile-up of the bow wave occurs, but the pressure starts to decrease owing to the detachment of the bow wave.

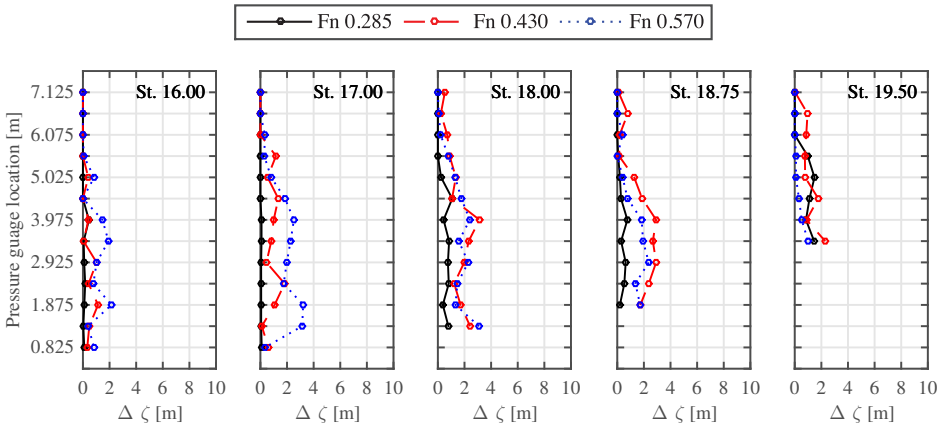

(a) $\lambda/L = 0.5$

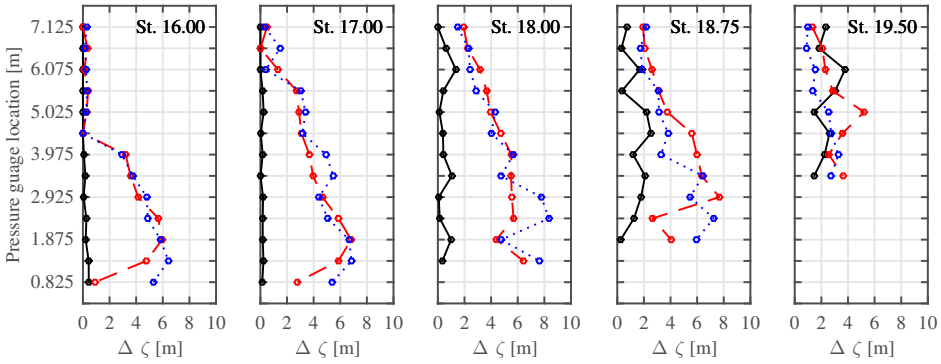

(b) $\lambda/L = 1.1$

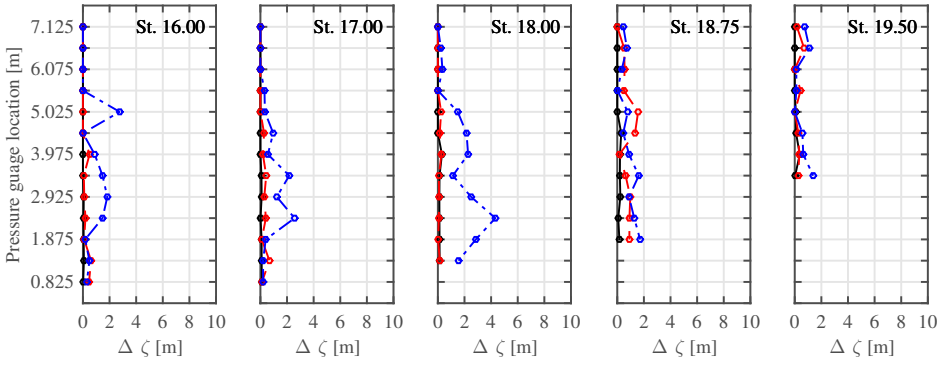

(c) $\lambda/L = 2.0$

Figure 4.17: The height difference ($\Delta\zeta$) between the highest relative wave elevation and the wave height on the maximum pressure.

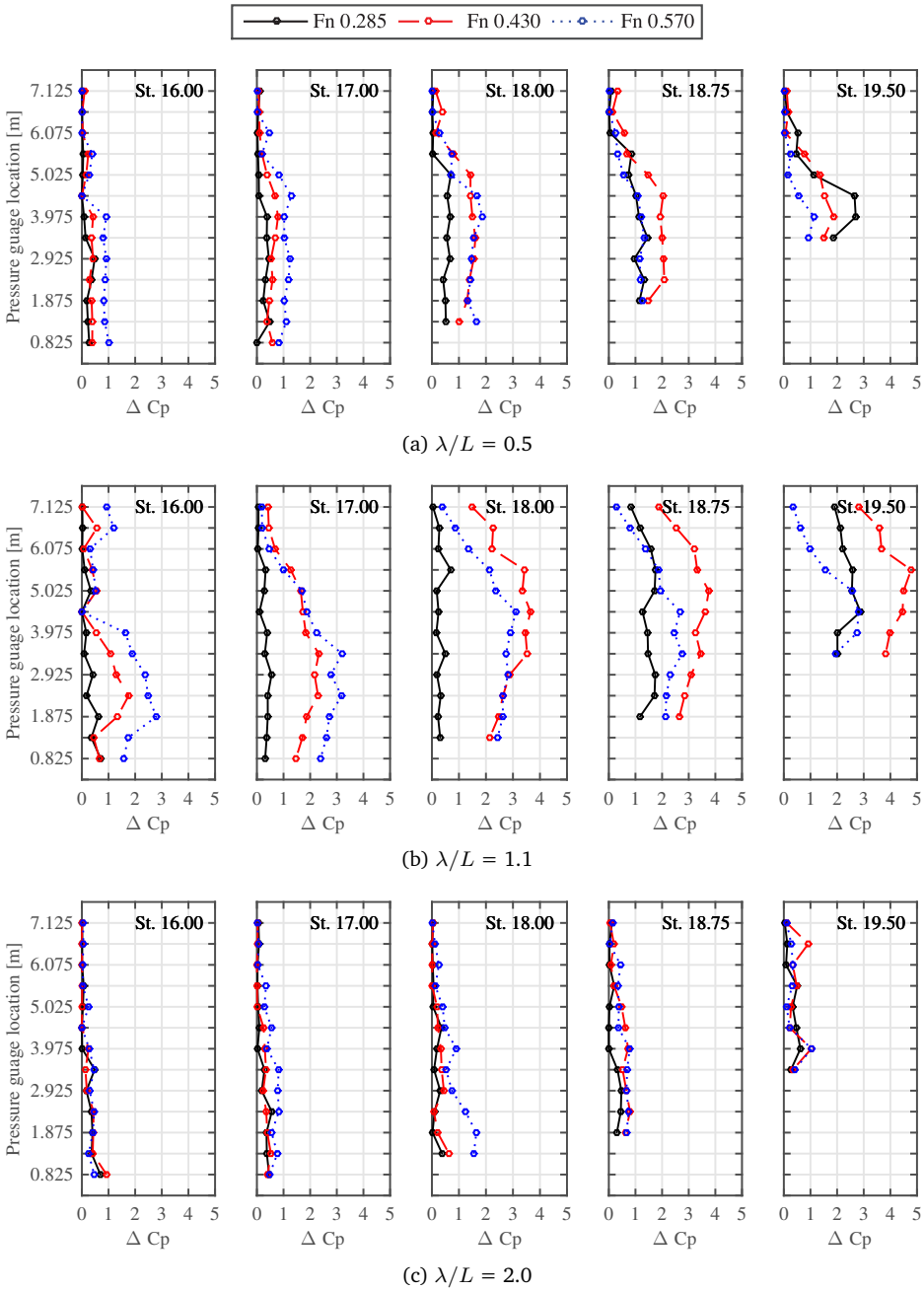

(a) $\lambda/L = 0.5$

(b) $\lambda/L = 1.1$

(c) $\lambda/L = 2.0$

Figure 4.18: The pressure drop (ΔCp) between the maximum pressure and the pressure at the highest relative wave elevation during upwash

4

This process is skipped when the bow wave is not breaking. The third (the number '3' in Figure 4.13) is the bow-wave absent stage, in which the pressure and relative wave elevation drop rapidly. It may be a natural phenomenon related to the generation and disappearance of the bow wave, but when the bow wave breaks in the previous stage, the bow wave that acts as a resistance to the hull disappears. This process is clearly detected when the breaking of the bow wave is evident.

The second step, in which the pressure drop is found, can be explained based on Bernoulli's equation by the pressure suction due to the increase in amplitude of the incident wave. However, this pressure drop is also related to the detachment of the bow wave, which is the cause of the disappearance of the stationary bow wave, observed in the photographs on the right-hand side of Figures 4.4~4.6.

The detachment of the bow wave is indicated in the P-R diagram (Figure 4.13) by different pressures at the same wave height. When the height of the bow wave returns to the same height after detachment, the pressure acting on the ship, indicated as the number '3' in Figure 4.13, is significantly reduced compared to the maximum pressure of the development stage, indicated as the number '1' in Figure 4.13. A pressure that is not proportional to height is another perspective for interpreting the nonlinearity of added resistance.

4.7. Nonlinear influence on added resistance

The previous section investigated the nonlinear relationship between the pressure and the relative wave elevation due to the plunging breaking of the bow wave. This section compares integrated pressures to determine the effect of the breaking waves on the added resistance.

4.7.1. Time average of pressure

The periodic pressure measured in a specific area of the forward part of the hull is time averaged by Equation 4.2, and a contour plot is constructed. This distribution represents the mean pressure acting on the ship advancing in waves.

$$C_{px_{mean}} = \frac{1}{T}\int C_p(t) n_x dt \tag{4.2}$$

where $C_p(t)$ is the unsteady pressure subtracted by the steady pressure in the time domain, T is the measured time and n_x is the normal vector in the longitudinal direction.

Figure 4.19~4.21 show the time-averaged distribution of pressures in short, intermediate, and long waves. Each figure shows the results at three speeds of Fn = 0.285, 0.430, and 0.570, as indicated in (a), (b), and (c), respectively. In the figures, the installed pressure gauges are shown by red circles, and the profile of the ship and the still waterline are shown together by blue solid lines. The greater the pressure on the hull surface, the redder is the color displayed in the figure.

Positive averaged pressures are concentrated in the upper vicinity of the still waterline (3.125 m) under all conditions. The averaged pressure of the intermediate

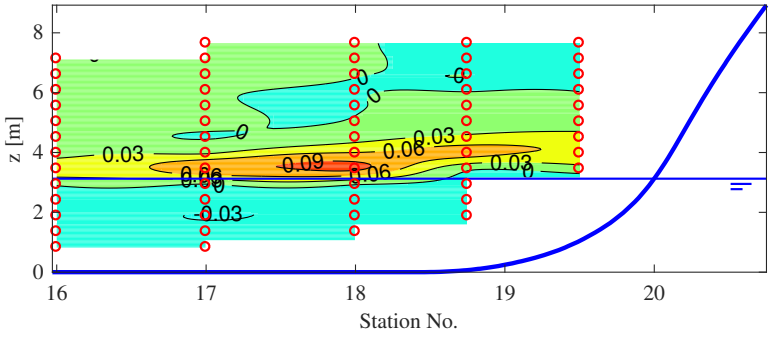

(a) $Fn = 0.285$

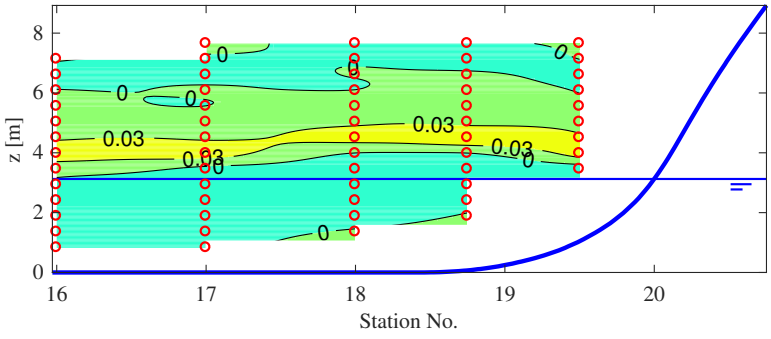

(b) $Fn = 0.430$

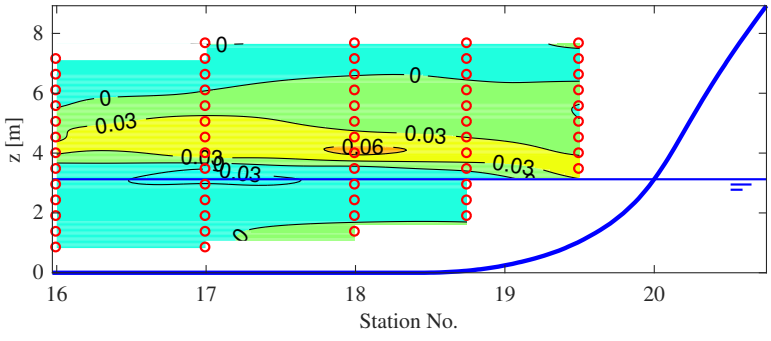

(c) $Fn = 0.570$

Figure 4.19: Contours of mean unsteady pressure $C_{px_{mean}}$ in longitudinal direction of the ship for three ship's speeds in intermediate waves ($\lambda/L = 0.5$)

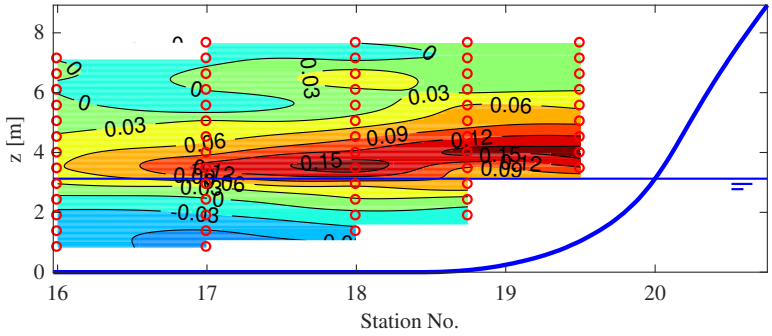

(a) $Fn = 0.285$

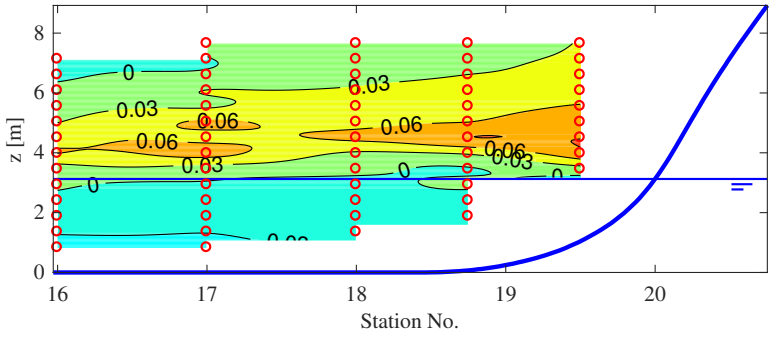

(b) $Fn = 0.430$

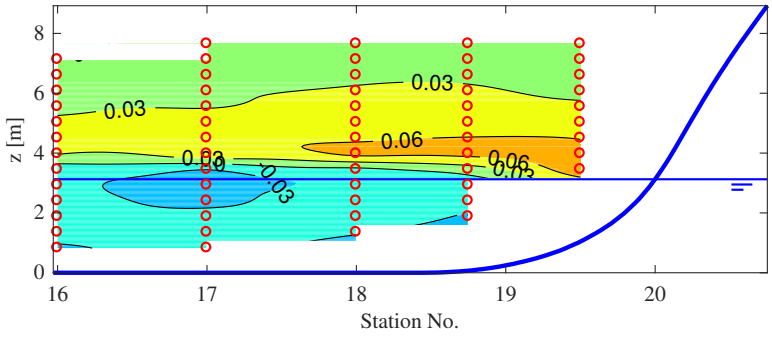

(c) $Fn = 0.570$

Figure 4.20: Contours of mean unsteady pressure $C_{px_{mean}}$ in longitudinal direction of the ship for three ship's speeds in intermediate waves ($\lambda/L = 1.1$)

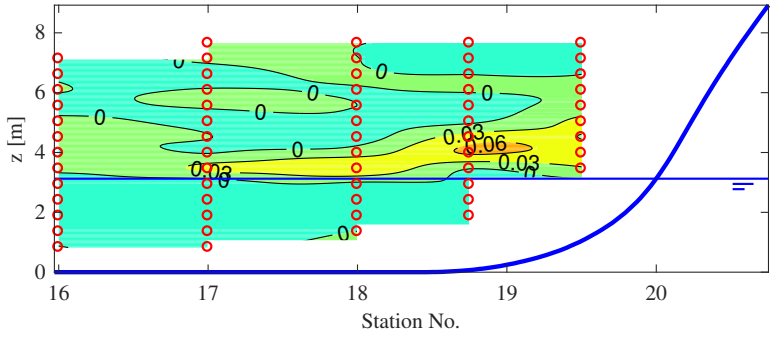

(a) Fn = 0.285

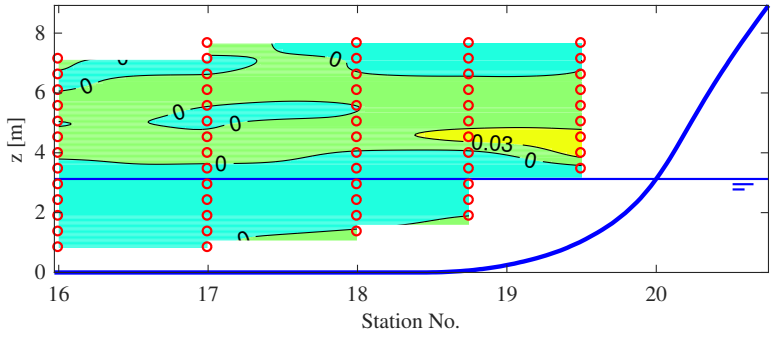

(b) Fn = 0.430

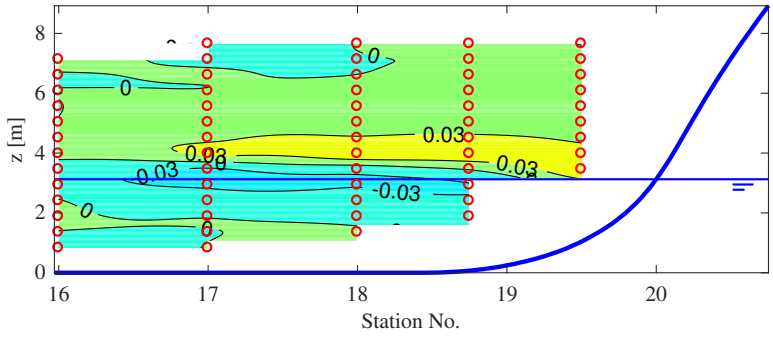

(c) Fn = 0.570

Figure 4.21: Contours of mean unsteady pressure $C_{px_{mean}}$ in longitudinal direction of the ship for three ship's speeds in long waves (λ/L = 2.0)

waves of Figure 4.20 appears larger in a wider area compared to the other wavelength conditions. This is primarily due to the large motion response. The average pressures of the short waves are greater than that of the long waves. This is because the incident waves act more strongly on the hull in the case of short waves, for which the relative motion of the ship is small.

The pressure at Fn = 0.285 in each figure is greater than those at other speeds. This corresponds to the growing nonlinear relationship between the pressure and the relative wave elevation as the ship's speed increases, as observed in Section 4.5.4. Therefore, it is confirmed that the ship's speed affects the average pressure on the ship due to the bow wave. A negative pressure is found under the still waterline. In particular, a negative pressure is clearly found under the intermediate waves condition of Figure 4.20, for which strong plunging breaking occurs. This is also related to the disappearance of the bow wave presented in Section 4.6.

4.7.2. Vertical integration of pressure

The time-mean pressures by Equation 4.3 are integrated vertically upwards according to the trapezoidal rule at each station.

$$\int C_{px_{mean}} dz \tag{4.3}$$

The time-averaged pressures obtained from Equation 4.2 are integrated vertically upwards according to the trapezoidal rule at each station. The integrated values for each station, given by Equation 4.3, are shown in Figure 4.22. The values corresponding to Fn = 0.285, 0.430, and 0.570 are shown by circles, diamonds, and gradients, respectively. Figures (a), (b), and (c) show the results for short, intermediate, and long waves, respectively.

Figure 4.22 (a) and (c), corresponding to the short and long waves, respectively, are less likely to confirm the effect of bow-wave breaking because the variation in the integrated pressure value is small. However, Figure 4.22 (b), corresponding to the intermediate wave condition, shows a large variation in the integrated pressure. Especially at stations 18 and 19, the large integral value at Fn = 0.285 drops to a small value at Fn = 0.430. At Fn = 0.570, the values decrease further at stations 16 and 17. This tendency can be interpreted to agree with the nonlinear relationship between the pressure and the relative wave elevation of Figure 4.15. The P-R diagrams at Fn = 0.430 and Fn = 0.570 shown in Figure 4.15 (b) and (c) provide evidence of the plunging breaking in the upper-right corner by counter gradient, which is defined as the nonlinearity due to the wave breaking in Section 4.5.4.

4.7.3. Surface integration of pressure

Figure 4.23 shows the integral value according to the trapezoidal rule in the longitudinal direction of the ship with the values shown in Figure 4.22. The pressure integrals acting on the hull in the intermediate, short, and long waves are represented by circles, diamonds, and gradients, respectively. These values, expressed by

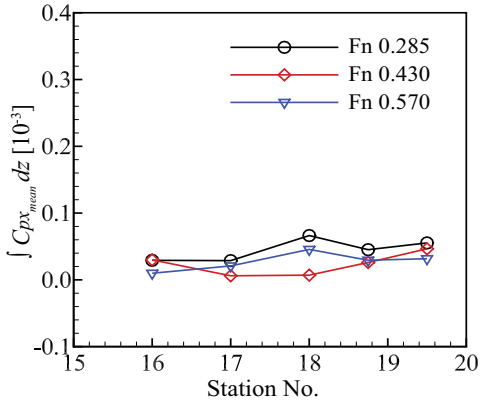

(a) $\lambda/L = 0.5$

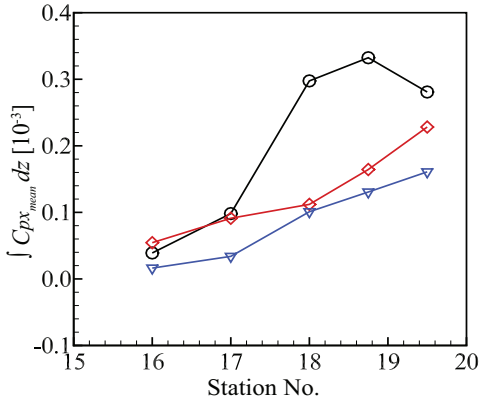

(b) $\lambda/L = 1.1$

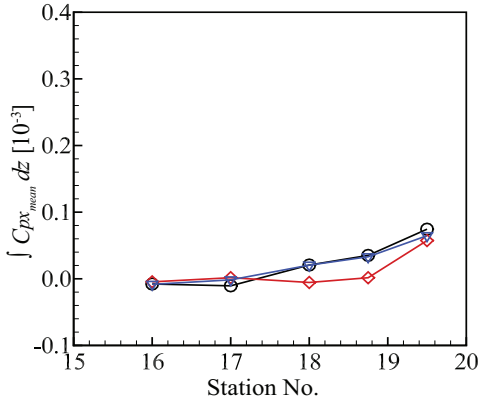

(c) $\lambda/L = 2.0$

Figure 4.22: Mean unsteady pressure acting on the stations for three ship's speeds

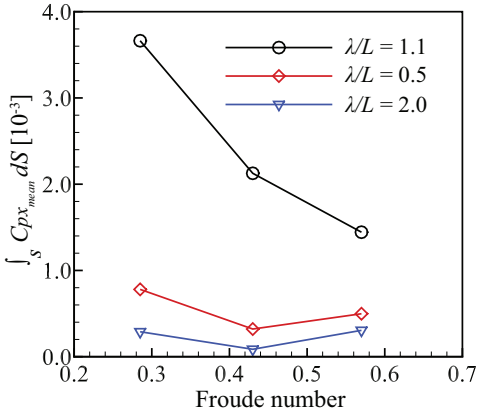

Figure 4.23: Pressure integral acting on a specific area of the forefront part of the hull for three wavelengths

Equation 4.4, represent the pressure acting on a particular area and are interpreted as the force acting on the hull.

$$\int_S C_{px_{mean}} dS \tag{4.4}$$

The added resistance can be obtained by numerically integrating the second-order pressure acting on the entire surface of the hull. The integrated pressure in Figure 4.23 is the force acting on a particular area of the hull's bow surface. Although these values are not representative of the entire surface of the hull, they can reveal the effect on the added resistance by comparison. This is because most of the added resistance occurs at the front part of the hull [109]. Therefore, Figure 4.23 clarifies that the nonlinearity of the added resistance depends on the wavelength of the incident wave or the speed of the ship.

In intermediate waves, as indicated by the circles in Figure 4.23, the integrated pressure progressively decreases as the speed of the ship increases. Under this condition, the plunging breaking appears to become stronger as the speed increases, as confirmed by the P-R diagram of Figure 4.15. The pressure drop occurs during the relative rise of the wave height. Therefore, the declining tendency of integrated pressure can be interpreted to be the result of the pressure drop due to the plunging breaking. However, it is difficult to determine the effect under the short and long wave conditions because the integrated values are small. Furthermore, it is not possible to completely exclude other influences, such as the effect of viscosity and stern shape [4, 110, 111].

4.8. Conclusions

The aim of this chapter was to identify the effect of the bow-wave breaking for fast ships to improve the reliability of the added resistance estimation. Model tests of the fast ship were conducted to investigate the influence of the hull pressure and the relative wave elevation of the bow wave caused by the plunging breaking. This chapter proposed templates that can be used to intuitively evaluate the nonlinear relationship between the pressure and the relative wave elevation, which significantly influences the wave added resistance.

Using the P-R diagram proposed in this study, this chapter confirmed that the overturning detachment of the bow wave induces a pressure drop during the rise of the relative wave elevation. The nonlinearity occurring between the pressure and the relative wave elevation is closely related to the speed of the ship. Furthermore, it is concluded that the plunging breaking of the bow wave induces less wave added resistance compared to that calculated from the linear consideration owing to the pressure drop caused by the detachment of the bow wave. In addition, the process of the plunging breaking of the bow wave can be divided into three stages at which different physical phenomena occur: the bow-wave development stage, pile-up and breaking stage, and bow-wave absent stage.

However, the results of this chapter are not applicable to all types of breaking of the bow wave, as they are derived only for plunging-type breaking in the fast ship. In this regard, further research is necessary to establish the impact of spilling-type breaking on the added resistance quantitatively. If the understanding of the nonlinearity between the hull and the bow wave can be taken into account in a numerical analysis method, the reliability of the added resistance estimation can be improved.

5

NUMERICAL IMPLEMENTATION OF BOW-WAVE BREAKING EFFECTS

5.1. Introduction

Chapter 4 experimentally showed that the pressure exerted on the hull can be weaker than the value calculated from linear considerations because of plunging breaking. The decrease in pressure occurs because the linear Bernoulli theory between the hull pressure and relative wave elevation is not valid. When the bow wave is detached, the surface pressure of the hull is decreased even if the relative wave elevation is high. This nonlinear effect is introduced in this chapter as a correction model based on experimental assessment that can be applied to the linear potential theory method. The purpose of this chapter is to develop a correction method to improve the accuracy for evaluating added resistance using the linear potential method calculation.

Linear potential method calculations have the advantage of fewer requirements and shorter computation times compared to experiments or CFD calculation. The quick calculation offered by the linear theory method is useful for evaluating the tendency of hull performance in the initial design of a ship. However, the disadvantage of linear theory calculations is that the results are not accurate when a nonlinear phenomenon (e.g., breaking of a bow wave) occurs on a ship. Accurate estimates are limited to conditions in which the nonlinearity does not affect the performance

of the ship. The nonlinearity covered in this chapter is confined to the nonlinear effects occurring between the relative wave elevation and the hull-surface pressure. This chapter deals with plunging breaking, which is a typical nonlinear phenomenon involving the detachment of the bow wave.

The plunging type of bow-wave breaking with a stable detachment of the bow wave is observed in a ship with a relatively high speed and a small waterline incidence angle. Typical ships of this type are navy frigates, cruise ships, ferry ships, and container ships. It has been reported that linear theory calculations for these ships can overestimate the added resistance in the resonance region of motion response [59, 110].

The added resistance is proportional to the square of the ship's motion response [9, 11]. Therefore, it is important to estimate the motion response accurately, since an error in motion prediction may cause a significant deviation in the added resistance.

However, the problem of overestimation of the added resistance is difficult to address by limiting the motion response because the added resistance is determined by the sum of the correlation of the motion components and the waterline component in a complicated manner. Nevertheless, among these components, the waterline contribution is decisive in determining the added resistance. The complexity of added resistance contributions can be simplified to the dominant waterline contribution in a fast ship with a simple hullform.

For ships with large bow waves, the reflection and radiation effects of bow waves are important when estimating added resistance. Furthermore, the relative wave elevation is affected by nonlinearity due to bow-wave breaking. The significant nonlinearity of the relative wave elevation causes errors in the added resistance estimation. The rational estimation of the relative wave elevation considering the nonlinearity is directly related to the reliability of the added resistance estimation.

This chapter compares the added resistance of fast ships calculated by the linear potential method to the experimental measurements. Then, this chapter investigates the computational error that can be accounted for by the nonlinearity of bow-wave breaking. Based on this investigation, a correction method to improve the accuracy of the calculation is proposed. The method for improving the accuracy of the calculation is investigated by applying the nonlinearity assessed in Chapter 4 to the numerical calculation results. The aim of Chapter 5 is to provide a solution to the problem of overestimating the added resistance of a fast ship while maintaining the advantages of the linear potential method. This solution provides a method to improve the accuracy of the contribution of the relative wave elevation calculated with the linear potential method.

Section 5.2 describes the unsteady linear potential method calculation and results for FDS-5, which is used as the hullform in Chapter 4. Section 5.3 shows an analysis of the calculated contributions to the added resistance, including the contribution of the relative wave elevation. Section 5.4 proposes a correction method for the calculation based on the experimental results and shows the results of applying it to the computation of the fast ship. The correction method is also applied to other fast ships of a similar hullform in Section 5.5. The conclusions of this chapter are presented in Section 5.6.

5.2. Linear potential method calculation

Numerical calculations for added resistance were performed using the linear potential method calculation (LPMC) developed by Bunnik [44]. The calculation estimates the motion responses and added resistance of a ship based on the linear potential theory in the frequency domain. The special feature of LPMC is that the nonlinear steady flow is a basis for linearization. The application of the nonlinear steady flow allows nonlinear effects to be considered in the amplitude of the unsteady wave caused by the incident wave [43]. The nonlinear effect of the steady flow caused by the ship's speed is taken into account in the unsteady calculation.

LPMC solves the problem with the boundary element method, which consists of the Laplace equation and linearized boundary conditions. The unknowns of panels distributed on the submerged hull and the free surface are calculated by applying the Rankine panel method. Oscillating unsteady flows (incidence, diffraction, and radiation) and ship motions are linearized with respect to the nonlinear steady flow, which is obtained by the nonlinear potential method code. LPMC considers the dispersion of the reflected waves by the ship and the interference with the relative wave elevation. In particular, the LPMC used in this chapter linearizes with respect to the actual hull immersion for the steady flow estimated using the nonlinear potential flow code, instead of a calm surface with zero speed.

LPMC provides information on the flow around the hull, the ship's motion response, and the added resistance in regular waves. The motion response is calculated by applying the steady pressure gradients from the nonlinear steady flow to the wave-induced load distribution [45]. The relative wave elevation takes into account the diffraction of the radiated and reflected waves for each of the six motion responses of the ship, in addition to the vertical motion of the ship relative to the undisturbed incident wave. The relative wave elevation of the ship is estimated to be more realistic considering the effect of the nonlinear steady flow due to the speed of the ship.

LPMC is a useful tool for calculating the sea-keeping performance of a forward-advancing ship, but it has limitations. LPMC cannot consider common nonlinear phenomena such as the breaking of the bow wave. The viscosity effect is ignored in the calculation, although a custom viscous damping is used.

LPMC calculates the wave added resistance by integrating the secondary pressure on the hull. The integration formula determines the added resistance as the sum of the contributions. The interconnections between these contributions make it difficult to treat added resistance problems. In LPMC, added resistance can be offered in the following five contributions in Equation 5.1: velocity squared (I), products of angular motion and pressure gradient (II), products of linear motion and pressure gradient (III), products of angular motions and inertia force (IV), and waterline contribution of relative wave elevation (V). In particular, the waterline contribution (Contribution V) is obtained by applying the vertical pressure gradient of steady flow obtained from the nonlinear potential method calculation.

$$
\begin{aligned}
Raw = \quad & \tfrac{1}{2}\rho \iint_S \nabla\varphi \cdot \nabla\varphi \vec{n} dS && (I) \\
& + \iint_S \left(\vec{\Omega} \times \left(\vec{\Omega} \times (\vec{x} - \vec{x_g}) \right) \right) \cdot \nabla p_s \vec{n} dS && (II) \\
& + \iint_S (\vec{\alpha} \cdot \nabla) p \vec{n} dS && (III) \\
& + \vec{\Omega} \times \left(M \frac{\partial^2 \vec{X}}{\partial t^2} \right) && (IV) \\
& - \tfrac{1}{2} \int_{wl} \frac{\partial p_s}{\partial z} \eta_{rel}^2 \vec{n} dl && (V)
\end{aligned}
\tag{5.1}
$$

5.2.1. Model ship and calculation settings

5

Nonlinear steady calculations were performed for the linearization of the unsteady LPMC. The computation is performed for FDS-5, which is the parent model of the series test in Chapter 3 and the model used in the experimental measurement in Chapter 4. The hullform of FDS-5 has a fine bow, as shown in Figure 3.2 (b).

The full-scale length of the hull used in the calculation is 100 m. The hull consists of 1100 panels for calculation. The free-surface mesh and domain size are chosen according to the speed of the ship. The domain sizes of the free surface are listed in Table 5.1. The free surface consists of approximately 6000 to 11000 panels, depending on the speed. The size of the domain increases as the speed increases.

Table 5.1: Domain of the free-surface mesh for FDS-5 as length between perpendiculars (Lpp)

Froude number	Forward of the bow	Backward of the stern	Half-width
0.285	0.5 Lpp	1.0 Lpp	0.8 Lpp
0.430	0.5 Lpp	2.0 Lpp	1.1 Lpp
0.570	0.5 Lpp	3.0 Lpp	1.3 Lpp

Figure 5.1 shows the hull and free-surface panels used in LPMCs. The number of panels per wavelength was intended to be maintained at 15. The calculations were executed using four 2 GHz Intel Core i7 processors operating in parallel. The typical calculation time is less than 5 min for one frequency of incident waves.

5.2.2. Calculation results for FDS-5

The calculations were performed at speeds of Fn = 0.285, 0.430, and 0.570. The range of the wavelength ratio (λ/L) for each Fn is from 0.5 to 3.0. The calculated motion response and added resistance are shown in Figures 5.2 ~5.7 as functions of λ/L. The calculated motion responses at Fn = 0.285 are similar to the experimentally measured data. Although the heave in the intermediate waves range is underpredicted as the speed increases, the overall trend is similar to that obtained through the experiment.

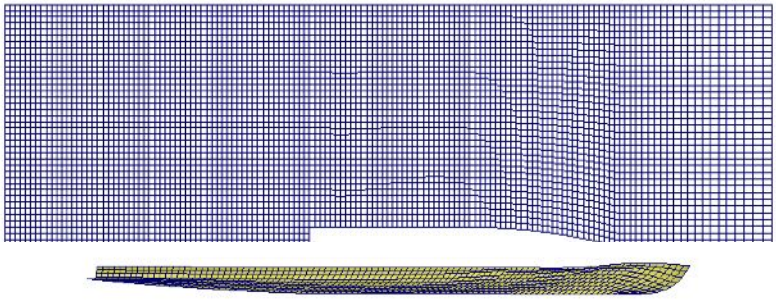

(a) $Fn = 0.285$

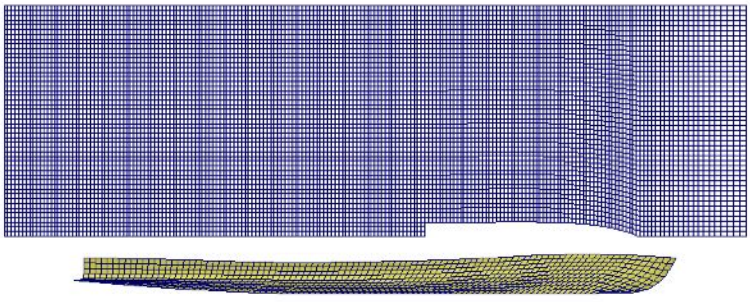

(b) $Fn = 0.430$

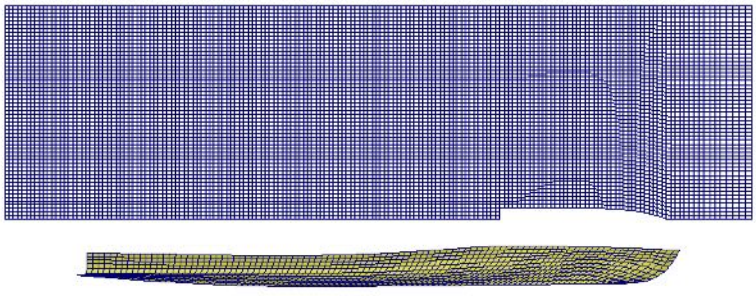

(c) $Fn = 0.570$

Figure 5.1: Hull and free-surface panels for FDS-5

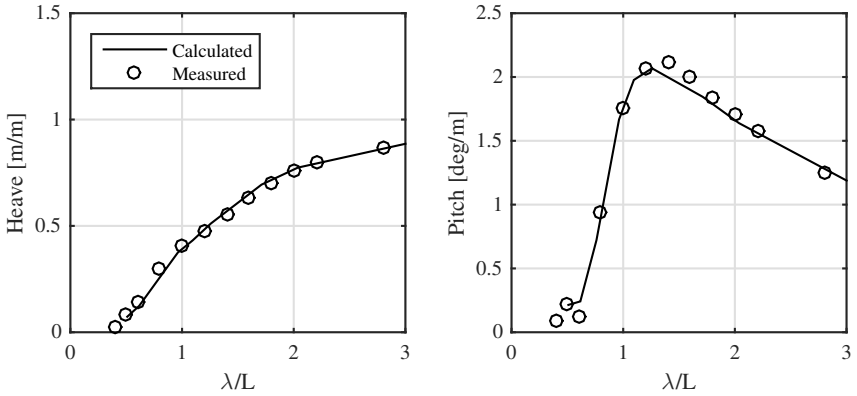

Figure 5.2: Motion responses of heave and pitch of FDS-5 at $Fn = 0.285$

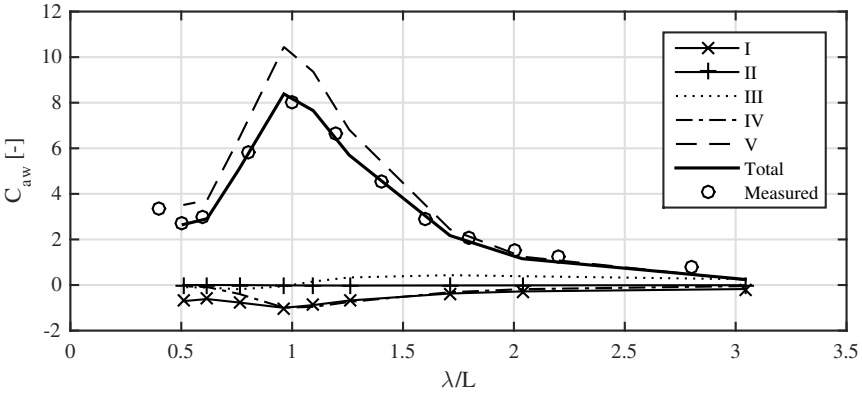

Figure 5.3: The contributions of added resistance in waves of FDS-5 at $Fn = 0.285$

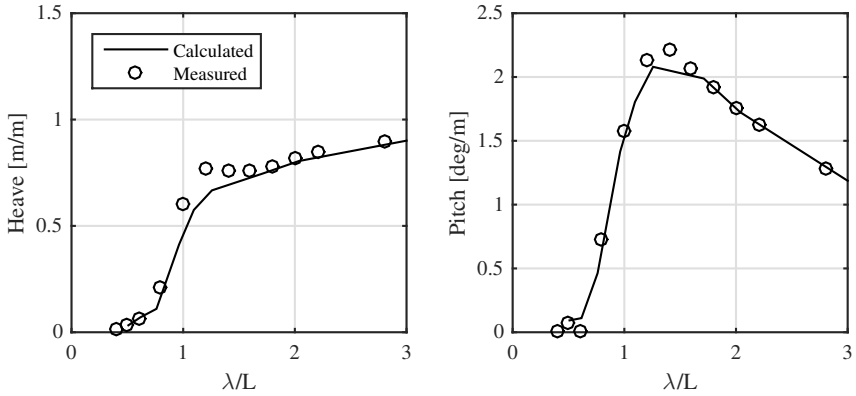

Figure 5.4: Motion responses of heave and pitch of FDS-5 at $Fn = 0.430$

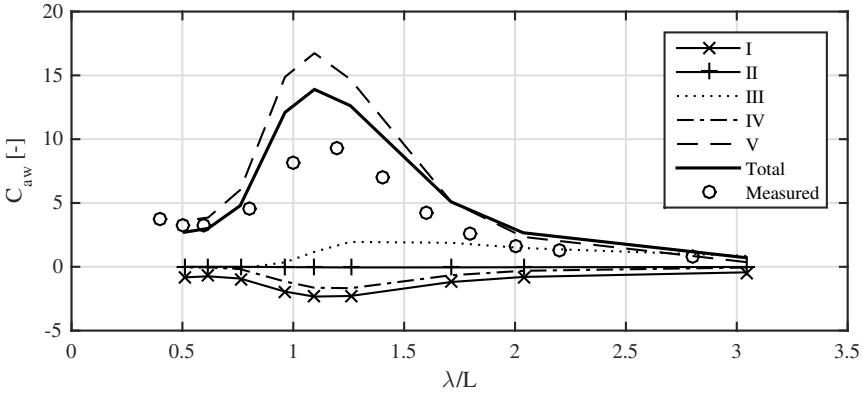

Figure 5.5: The contributions of added resistance in waves of FDS-5 at $Fn = 0.430$

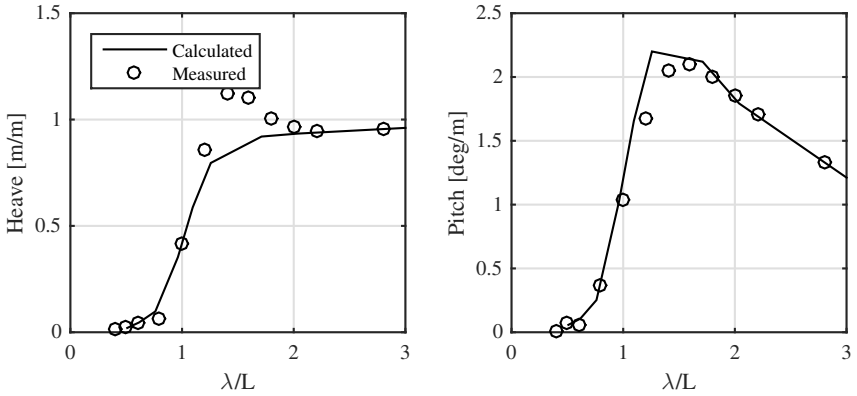

Figure 5.6: Motion responses of heave and pitch of FDS-5 at $Fn = 0.570$

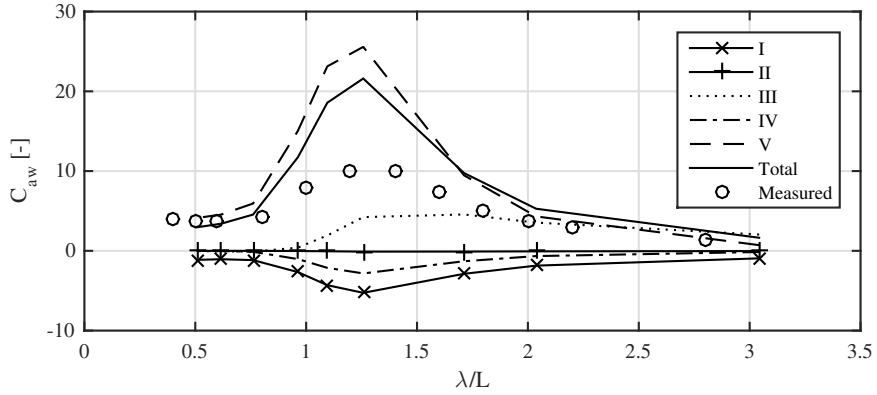

Figure 5.7: The contributions of added resistance in waves of FDS-5 at $Fn = 0.570$

The added resistance is shown by the QTF (C_{aw}) in Figures 5.3, 5.5, and 5.7 as a function of λ/L. The figures show the total added resistance, the five contributions to added resistance, and measured values. Each contribution is shown by combinations of symbols and lines. The solid line shows the calculated total added resistance, and circles indicate the measured added resistance. The total added resistance is the sum of the five contributions. The most significant contribution in this calculation is the waterline contribution (Contribution V; in Equation 5.1) expressed as a squared relative wave elevation.

The calculated C_{aw} at Fn = 0.285 is in good agreement with the experimental measurements. However, as the speed increases, the C_{aw} in the intermediate-wave region becomes larger than that obtained from the experimental measurement. Although the motion response of the calculation is underestimated compared to that obtained from the experiment in Figures 5.4 and 5.6, the added resistance is overestimated in Figure 5.5 and 5.7. Contributions II, III and IV including the motion component are much smaller than Contribution V of the relative wave elevation. The cause of the overestimation of the added resistance is analyzed in the next section in terms of the nonlinear relationship between the pressure and the relative wave elevation.

5.3. Causes of overestimation of added resistance

The calculation results for three wavelengths are analyzed: short waves (λ/L = 0.5), intermediate waves (λ/L = 1.1), and long waves (λ/L = 2.0). These wavelengths are consistent with the conditions used in Chapter 4, which analyzed the relationship between the hull-surface pressure and the relative wave elevation.

5.3.1. Contributions to added resistance

Figure 5.8∼5.10 show the distribution of five components of the added resistance against longitudinal direction of the ship for three speeds and three wavelengths. Each contribution is obtained from Equation 5.1. In the figures, each contribution is expressed as a percentage of the total added resistance.

Each contribution to the added resistance mainly acts at the forward position of the ship at all speeds and wavelengths. In the short-wave condition (λ/L = 0.5) of Figure 5.8, the waterline contribution (Contribution V) is the largest at 8.0%, 6.4%, and 5.7% for Fn = 0.285, 0.430, and 0.570, respectively.

Pressure suction by velocity (Contribution I) is approximately 2%. In the intermediate wave condition (λ/L = 1.1) of Figure 5.9, the maximum of Contribution V is at station 19, with percentages of 11.5%, 9.0%, and 7.2% for Fn = 0.285, 0.430, and 0.570, respectively. Other contributions are approximately 1%. In the long-wave condition (λ/L = 2.0) of Figure 5.10, the maximum values of Contribution V are 13.0%, 8.5%, and 6.4% for Fn = 0.285, 0.430, and 0.570 respectively.

In long waves, contributions other than Contribution V have values in the range of 3%∼5%. Contribution III is maximum at Fn = 0.570, but it appears only in a

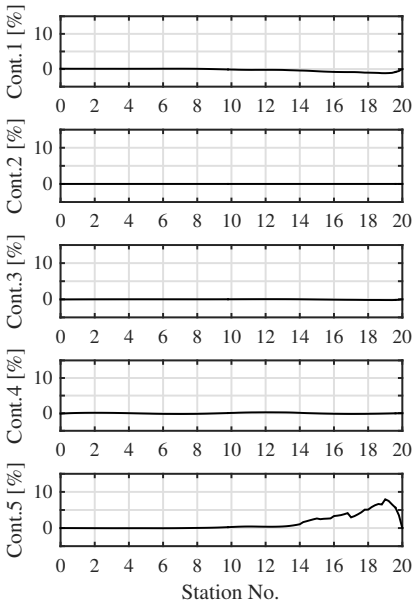

(a) Fn = 0.285

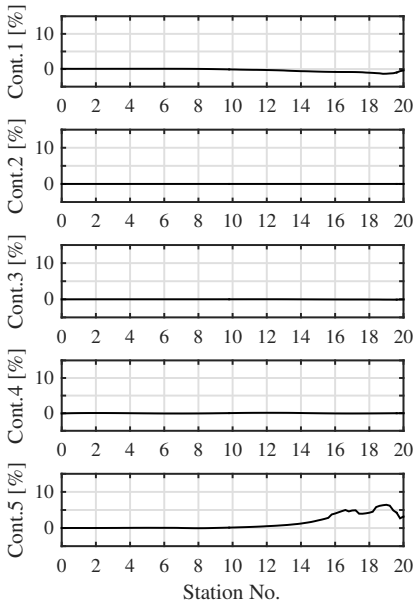

(b) Fn = 0.430

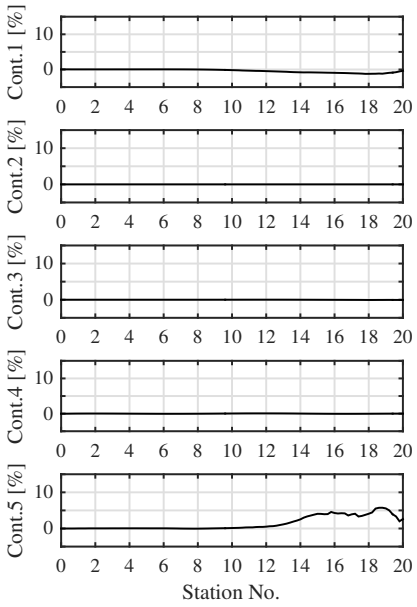

(c) Fn = 0.570

Figure 5.8: Distributions of five components of added resistance against longitudinal position of the ship in short waves (λ/L = 0.5)

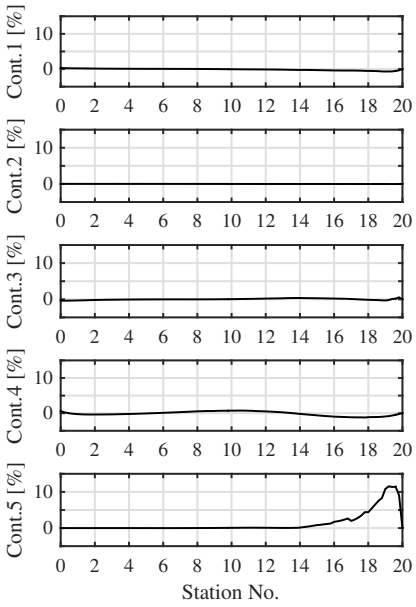

(a) Fn = 0.285

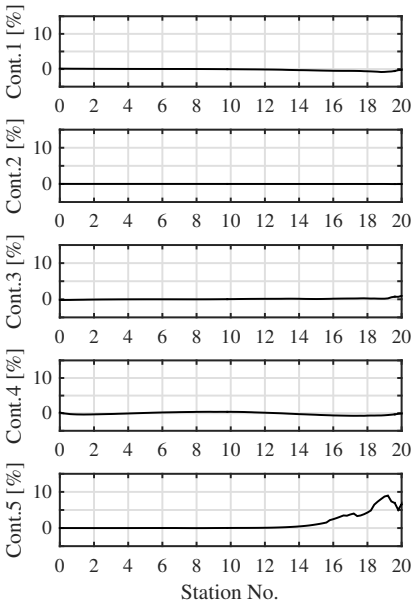

(b) Fn = 0.430

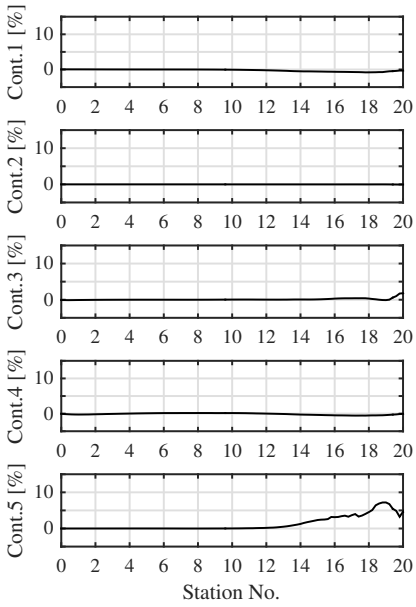

(c) Fn = 0.570

Figure 5.9: Distributions of five components of added resistance against longitudinal position of the ship in intermediate waves (λ/L = 1.1)

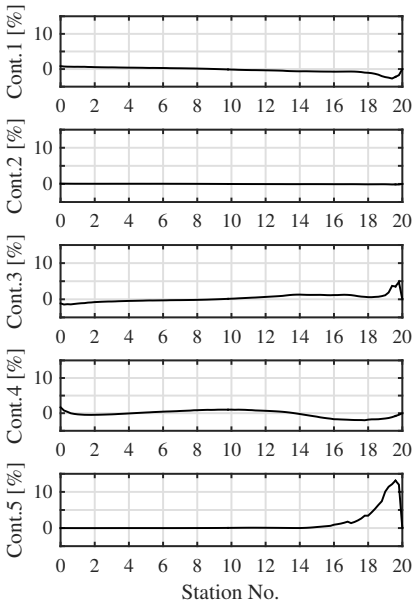

(a) Fn = 0.285

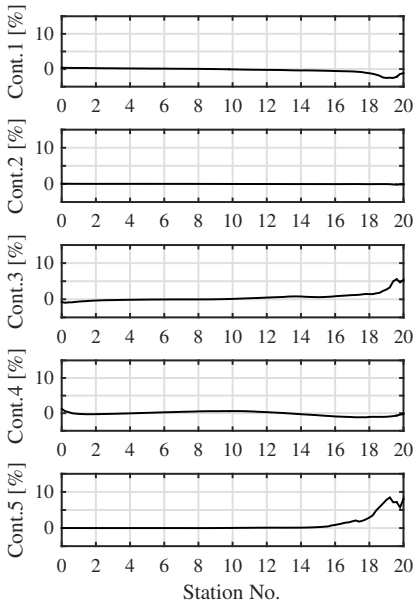

(b) Fn = 0.430

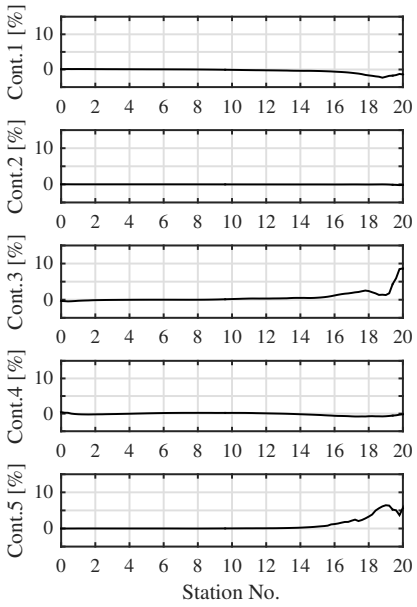

(c) Fn = 0.570

Figure 5.10: Distributions of five components of added resistance against longitudinal position of the ship in long waves (λ/L = 2.0)

narrow region at the stem. Moreover, the total added resistance for long waves is smaller than that for other wavelengths.

Contribution III reflects the influence of linear motion response and pressure gradient distribution. Pressure gradient distribution is likly to be affected by the nonlinear bow-wave breaking. However, the influence of this component on added resistance is not particularly large and narrowly concentrated on the stem part, except for the long-wave condition (λ/L = 2.0). Therefore, Contribution III does not have a decisive effect.

Thus, it can be concluded that the influence of the waterline contribution is the largest at all speeds and wavelengths. Contribution V shows the highest percentage on the bow, which implies that the influence of the bow wave is greatest in the calculated fast ship. The fast ship allows analysis to focus on the effects of relative wave elevation, among all contributions, on the added resistance. Furthermore, the effective influence region of Contribution V, which is concentrated on the bow part, widens as the speed increases. The representative boundaries for intermediate draft are formed in front of station 16 at Fn = 0.285, in front of station 15 at Fn = 0.470, and in front of station 14 at Fn = 0.570.

The waterline contribution (Contribution V) in Equation 5.1 includes the square of the relative wave elevation. The next section investigates the cause of the overestimation of the added resistance in the waterline contribution.

5.3.2. Analysis of relative wave elevation

Figures 5.11∼5.13 show the total relative wave elevation and the undisturbed relative wave elevation calculated for three speeds and three wavelengths. The total relative wave elevation includes the contributions of diffraction of the reflected and radiated components for each of the six motion responses minus the vertical displacement due to heave, roll and pitch. The undisturbed component excludes the radiation and diffraction components from the total relative wave elevation. Each relative wave elevation is numerically calculated using Equations 5.2 and 5.3, and denoted by the subscripts 'total' and 'undisturbed.'

$$\zeta_{rel\_total} = \zeta_{inc} + \zeta_{rad} + \zeta_{diff} - (\alpha_{heave} - \theta_{pitch} \cdot (x - x_g) + \theta_{roll} \cdot (y - y_g)) \quad (5.2)$$

$$\zeta_{rel\_undisturbed}(x) = \zeta_{inc}(x) - (\alpha_{heave} - \theta_{pitch} \cdot (x - x_g) + \theta_{roll} \cdot (y - y_g)) \quad (5.3)$$

where ζ_{rel} is the relative wave elevation, ζ_{inc} is the incident wave elevation, ζ_{rad} is the radiated wave elevation, ζ_{diff} is the diffracted wave elevation, α_{heave} is the vertical motion displacement by heave, θ_{pitch} is the pitch angle, θ_{roll} is the roll angle,x_g is the longitudinal center of gravity, and y_g is the horizontal center of gravity.

In the case of a symmetrical ship in head waves, the contribution due to roll motion is absent.

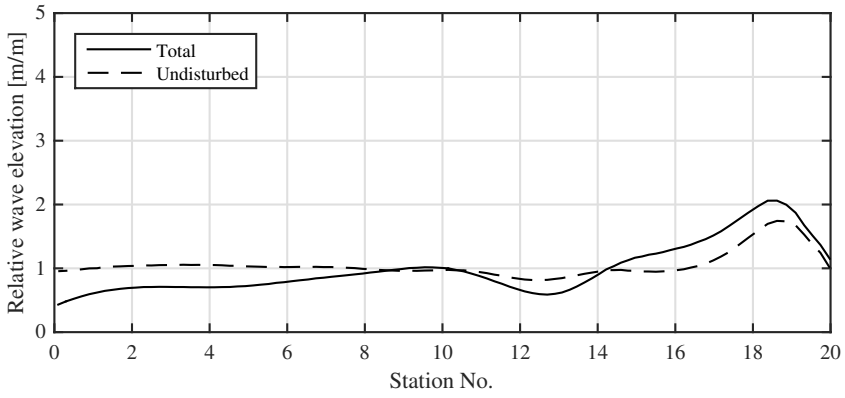

(a) Short waves (λ/L = 0.5)

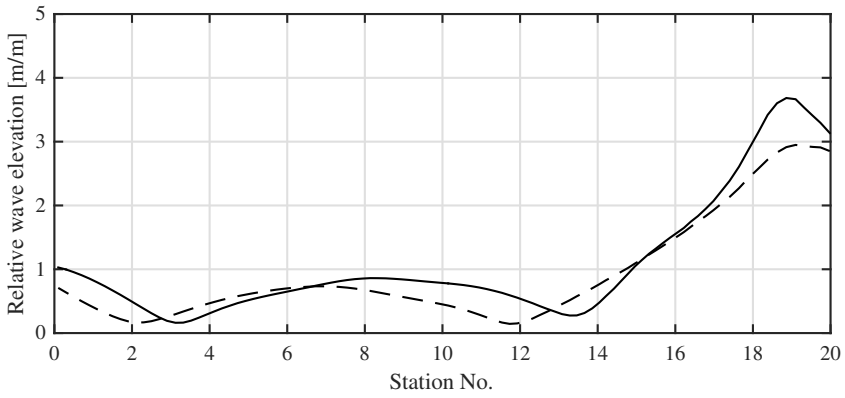

(b) Intermediate waves (λ/L = 1.1)

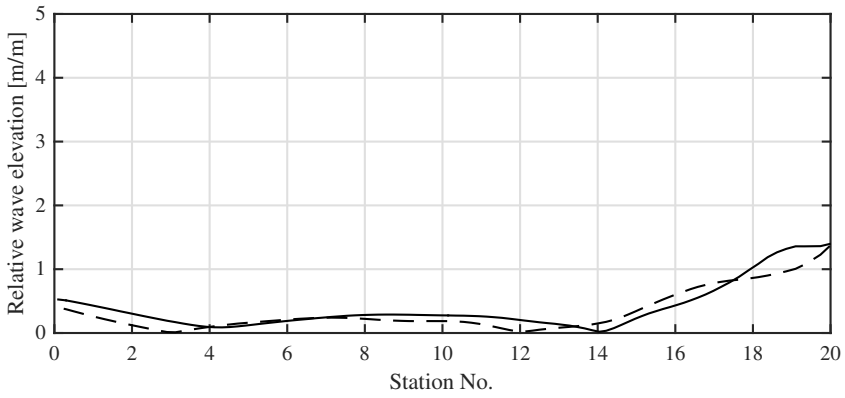

(c) Long waves (λ/L = 2.0)

Figure 5.11: Total and undisturbed relative wave elevation of FDS-5 at Fn = 0.285

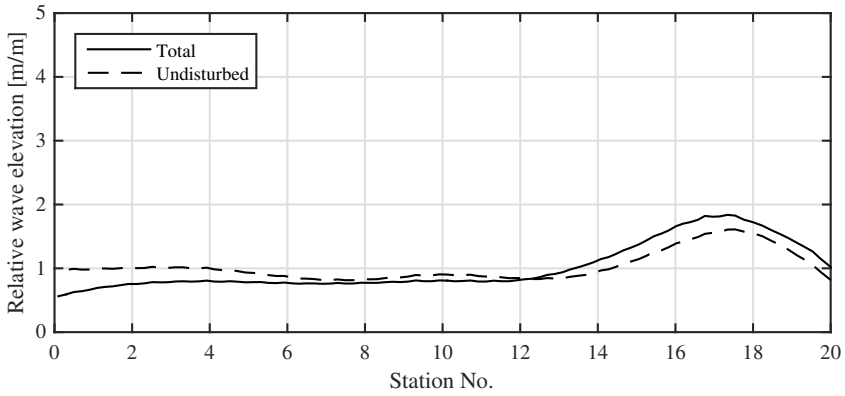

(a) Short waves (λ/L = 0.5)

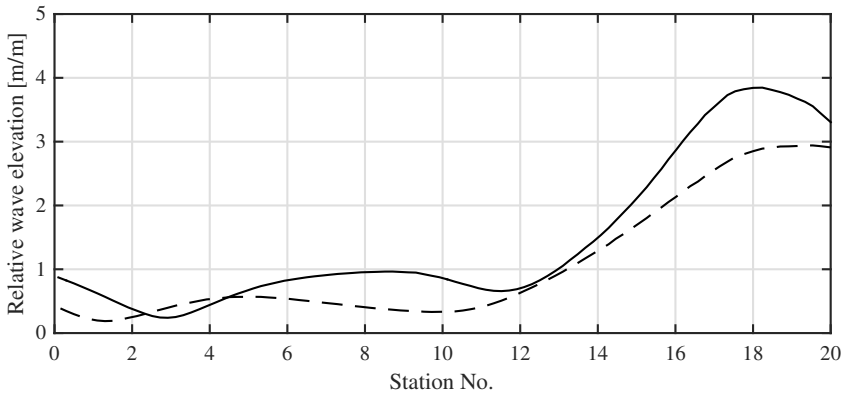

(b) Intermediate waves (λ/L = 1.1)

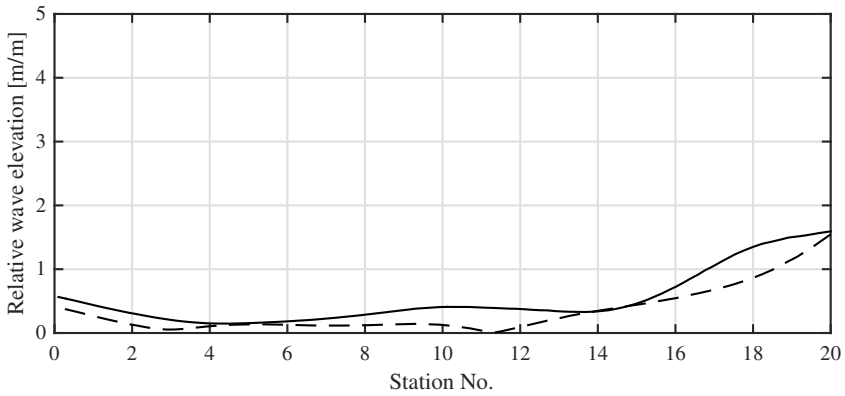

(c) Long waves (λ/L = 2.0)

Figure 5.12: Total and undisturbed relative wave elevation of FDS-5 at Fn = 0.430

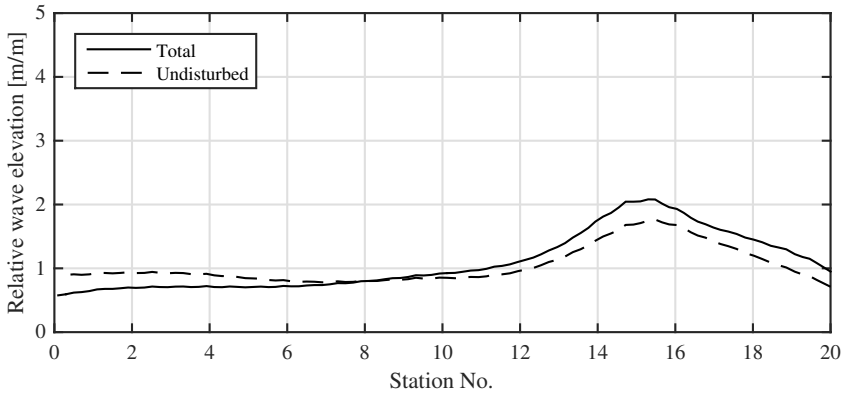

(a) Short waves (λ/L = 0.5)

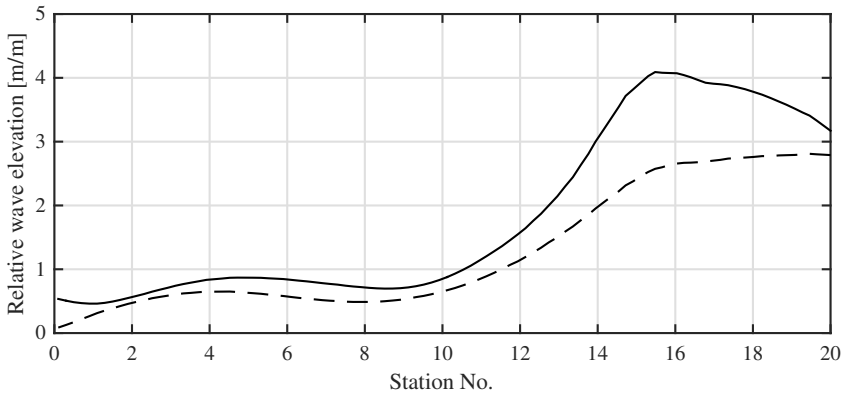

(b) Intermediate waves (λ/L = 1.1)

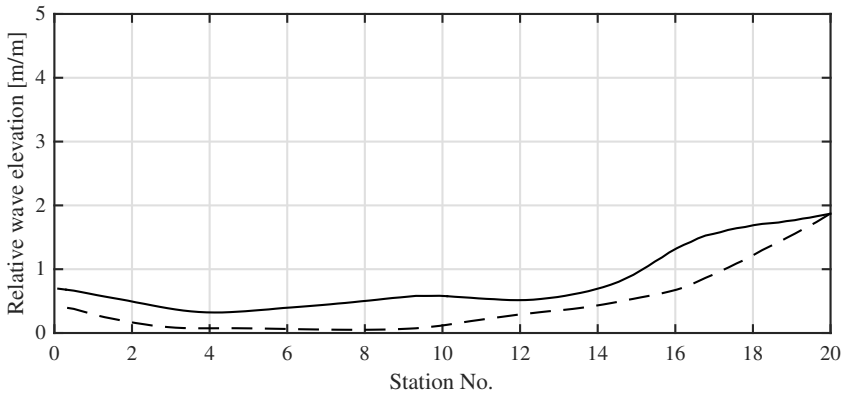

(c) Long waves (λ/L = 2.0)

Figure 5.13: Total and undisturbed relative wave elevation of FDS-5 at Fn = 0.570

The motion response affects the relative wave elevation. At all values of Fn, the relative wave elevation at the front part of the ship for intermediate waves is significantly higher than that for short or long waves. In particular, the total relative wave elevation for intermediate waves at Fn = 0.570 maintains a significant value of 4 m/m over a wide region from station 15 to the stem in Figure 5.13 (b). In this region, there is a large difference between the undisturbed and the total relative wave elevation. On the other hand, this difference is small at all speeds for short and long waves.

It is noted that a large difference between the total and undisturbed relative wave elevation occurs for intermediate waves at Fn = 0.570. Under this condition, the analysis of the P-R diagram in Figure 4.15 (c) reveals a significant shape bulge in which the pressure decreases during the increase of the wave height. In this condition, the bow-wave breaking is clearly observed in Figure 4.5 (c).

The bow-wave breaking of the fast ship is indicated by the detachment of the bow wave, which weakens the effects of reflected and radiated waves from the ship on the relative wave elevation. The detachment of the bow wave leads to the loss of reflected and radiated waves without being accumulated on the incident wave. Consequently, if a significant plunging breaking of the bow wave occurs, the difference between the total and undisturbed relative wave elevation should be small because the reflected and radiated diffraction due to the motion response is weak.

However, the calculated result of Fn = 0.570 in intermediate waves in Figure 5.13 (b) shows that the total relative wave elevation is much higher than the undisturbed relative wave elevation. This difference constitutes evidence that the nonlinear phenomena due to breaking are not reflected in LPMCs.

Therefore, the linear potential method can overestimate the contribution of reflected and radiated waves from the fast ship. If this nonlinear phenomenon can be reflected in the determination of the relative wave elevation, the problem of overestimating the added resistance in the calculation can be solved. When calculating the waterline contribution, the excessive contribution of the reflected and radiated diffraction due to the motion response can be eliminated by applying the undisturbed relative wave elevation at the region where the bow-wave breaking is assessed.

5.4. Solution of correction model

This section proposes a method to enhance the accuracy of the waterline contribution by solving the overestimation of the relative wave elevation in the linear potential method. The method is proposed to obtain the waterline contribution using the undisturbed relative wave elevation in a partial region where the detachment of the bow wave is evident through the video observation and the nonlinearity assessment introduced in Chapter 4.

The overestimation of the added resistance is solved by applying the phenomenon that the reflected and radiated component is weakened by the bow-wave breaking in the decision of relative wave elevation. The undisturbed relative wave elevation is applied in the decision of the relative wave elevation at the region where the de-

tachment of bow wave and the bulge shape of the P-R diagram (Figure 4.13) are detected. A method to apply this corrected relative wave elevation to the waterline contribution in the added resistance calculation is proposed.

Correction model for FDS-5 at Fn = 0.570

The correction model is provided for Fn = 0.570, and intermediate waves (λ/L = 1.1), for which the added resistance is significant and plunging breaking is observed. Under this condition, the plunging breaking of the bow wave is assessed by the pressure and relative wave elevation diagram up to station 16 in Figure 4.15 (c). The data were measured in front of station 16. Moreover, a strong detachment of the bow-wave is observed up to station 15 in the video observation shown in Figure 4.5 (c). Taking these results into consideration, the influence region of the plunging breaking is determined to range from the ship's stem to station 15.

Based on this decision, the relative wave elevation is corrected. The calculated total relative wave elevation is corrected to the undisturbed one at the front of station 15. The corrected relative wave elevation is used to recalculate the waterline contribution of the added resistance. The discrete range of the relative wave elevation is connected smoothly by a simple method. This method is numerically implemented as a smooth transition function (s) using the hyperbolic tangent of Equation 5.4.

$$s(x) = 0.5 + 0.5 \tanh\left((x - a)/b\right) \tag{5.4}$$

where x is the longitudinal position, a is the intersection position, and b is the relaxation parameter.

The intersection point specifies the boundary at which the breaking occurs, and the relaxation parameter smoothly connects the transition of the boundary. In this chapter, the relaxation (b) is designated as '1.' The relaxation value is not determined theoretically or numerically. The relaxation value can be empirically determined to have a value between 0.5 and 1.5 for smooth coupling of the relative wave elevation. However, a difference in this value does not cause a large difference in the added resistance.

Figure 5.14 shows the smooth transition formed in the longitudinal direction of the ship. In this calculation for Fn = 0.570, a = 15 and b = 1 are used in Equation 5.4. The smooth transfer function divides the contribution of relative wave elevation at station 15, determined as the boundary of the plunging breaking. The smooth transfer function determines the corrected relative wave elevation numerically by using Equation 5.5.

$$\zeta_{rel\_corrected} = s \times \zeta_{rel\_total} + (1 - s) \times \zeta_{rel\_undisturbed} \tag{5.5}$$

where ζ_{rel} is the relative wave elevation, the subscript 'corrected' means the corrected result with Equation 5.5, and the subscripts 'total' and 'undisturbed' means the component of the relative wave elevation defined at the beginning of the Section 5.3.2.

Consequently, the corrected relative wave elevation is smoothly connected with the undisturbed and total relative wave elevation. The corrected relative wave elevation with a smooth transition is shown in Figure 5.15 with a red line.

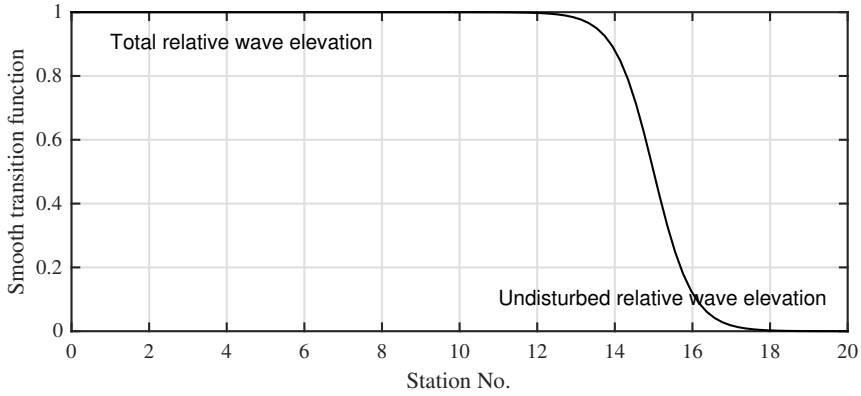

Figure 5.14: The smooth transition function with the hyperbolic tangent at $Fn = 0.570$ ($a = 15$ and $b = 1$ is used in Equation 5.4)

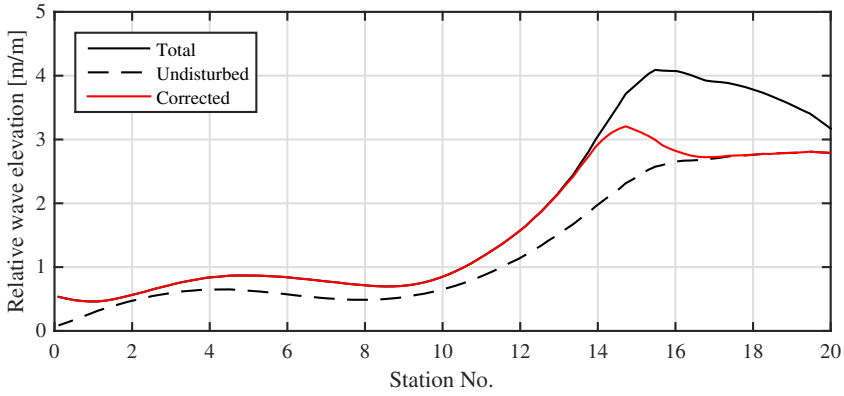

Figure 5.15: Comparison of total, undisturbed, and corrected relative wave elevation of FDS-5 of intermediate waves (λ/L = 1.1) at $Fn = 0.570$

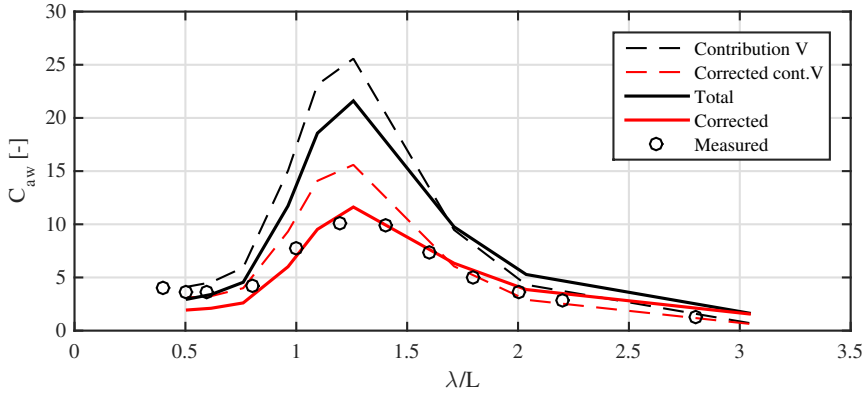

Figure 5.16: Corrected added resistance of FDS-5 at $Fn = 0.570$

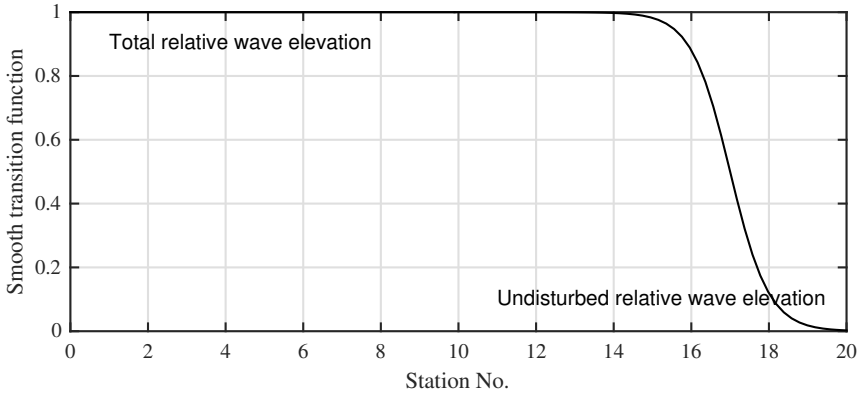

Figure 5.17: The smooth transition function with hyperbolic tangent at $Fn = 0.430$ ($a = 17$ and $b = 1$ is used in Equation 5.4)

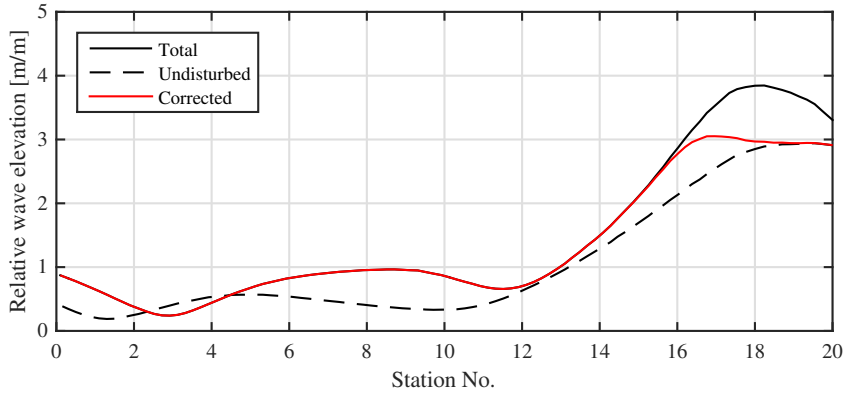

Figure 5.18: Comparison of total, undisturbed, and corrected relative wave elevation of FDS-5 of intermediate waves (λ/L = 1.1) at $Fn = 0.430$

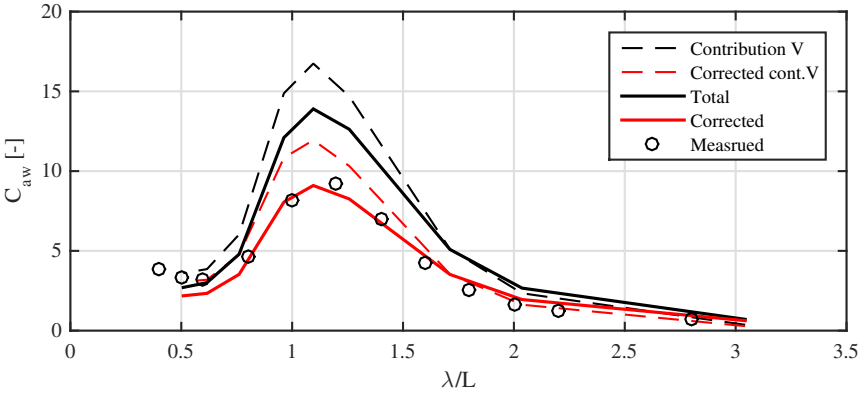

Figure 5.19: Corrected added resistance of FDS-5 at $Fn = 0.430$

Figure 5.16 shows the recalculated waterline contribution and the added resistance based on the corrected relative wave elevation. The corrected Contribution V and the corrected added resistance are shown by a red dashed line and solid line, respectively. The corrected added resistance agrees well with measured results in the intermediate-wave region. Thus, the overestimation of the added resistance in the resonant region of motion response has been effectively resolved.

Correction model for FDS-5 at Fn = 0.430

The previous correction method also applies to the results at Fn = 0.430. However, the intersection position of the smooth transition function is adjusted based on the experimental observation. It is inferred from the photograph in Figure 4.5 (b) and P-R diagram in Figure 4.15 (b) that the bow wave is broken at the front of station 17. The intersection position is determined as station 17 at Fn = 0.430. In this calculation, a = 17 and b = 1 are used in Equation 5.4.

Figure 5.17 shows the smooth transition function with station 17 as the intersection position. Figure 5.18 shows the corrected relative wave elevation obtained from Equation 5.5 with a smooth transition by a red solid line. The corrected Contribution V and the added resistance based on the corrected relative wave elevation are shown in Figure 5.19. The corrected Contribution V and the corrected added resistance are shown by a red dashed line and solid line, respectively. The corrected added resistance in the intermediate-wave region is also in good agreement with the experimental results.

The correction method of the added resistance is applied to the calculation of other ships with a hullform similar to that of FDS-5 in Section 5.5.

5.5. Validation of the correction model

5.5.1. Calculation and correction for FDS-11

In order to ensure that the correction method presented in the previous section also applies to other ships with a similar hullform, the same method is applied to FDS-11 with a different C_B = 0.35. The bodyplan and parameters used for the calculation are shown in Figure 3.2 (a) and listed in Table 3.1, respectively. FDS-11 has not been experimentally measured for hull pressures and relative wave elevations but the added resistance was measured in [106]. The added resistance calculated using LPMC has a problem in that it is overestimated compared with the experimental value in the intermediate-wave region at Fn = 0.570.

The calculation was performed for a full scale with Lpp of 100 m. Hull consists of 1000 panels. The domain of the free surface is made by 0.5 Lpp forward of the bow, 2.5 Lpp backward of the stern, and a half-width of 1.32 Lpp in the transverse direction for the calculation at Fn = 0.570. There are 8020 panels on the free surface. The panels of the hull and free surface used in the calculations are shown in Figure 5.20.

Figure 5.21 shows the calculated motion response along with the experimental results. The calculated added resistance of FDS-11 overestimated the measured value, especially in the intermediate-wave region. The intersection position of the smooth transition function in the correction is designated as station 15 at Fn = 0.570 for FDS-5. In this calculation, a = 15 and b = 1 are used in Equation 5.4. The corrected relative wave elevation with the smooth transition is shown by a red solid line in Figure 5.22. Figure 5.23 shows the corrected contribution 5 and the corrected added resistance by a red dashed line and solid line, respectively. The calculation results obtained for FDS-11 using the same correction method as for FDS-5 are very similar to the experimental data. Thus, the problem of overestimating added resistance is resolved.

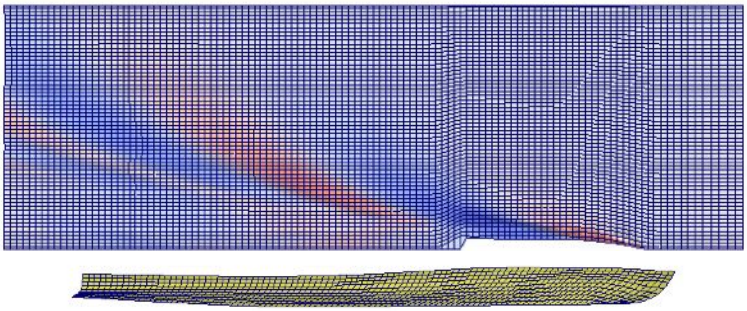

Figure 5.20: Hull and free-surface panels of FDS-11 for Fn = 0.570

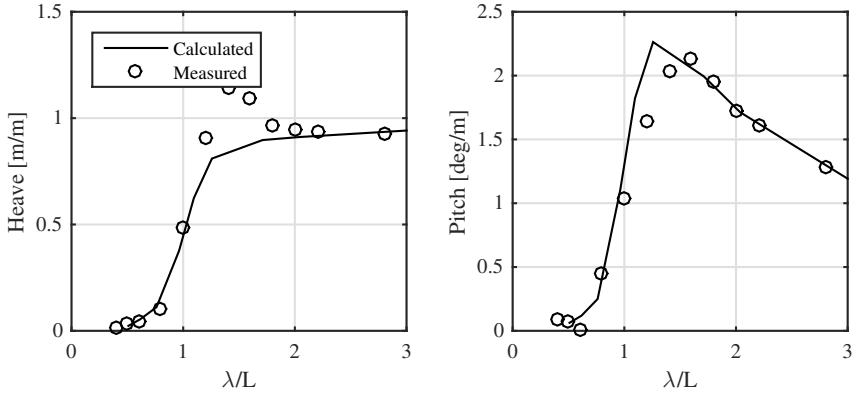

Figure 5.21: Motion responses of heave and pitch of FDS-11 at $Fn = 0.570$

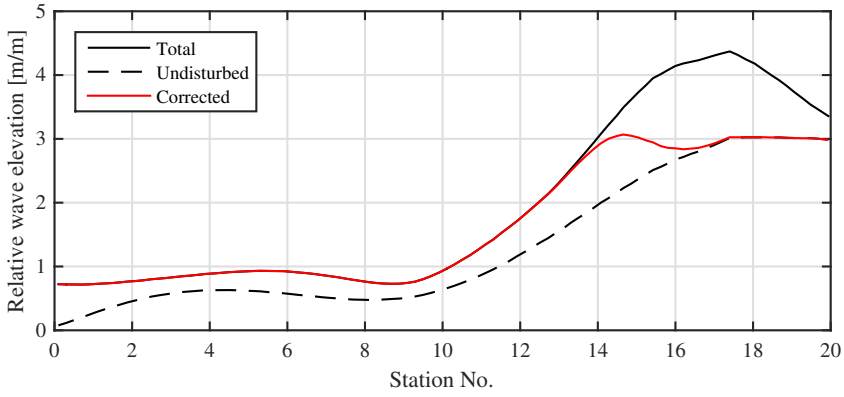

Figure 5.22: Comparison of total, undisturbed, and corrected relative wave elevation of FDS-11 of intermediate waves (λ/L = 1.1) at $Fn = 0.570$ ($a = 15$ and $b = 1$ is used in Equation 5.4)

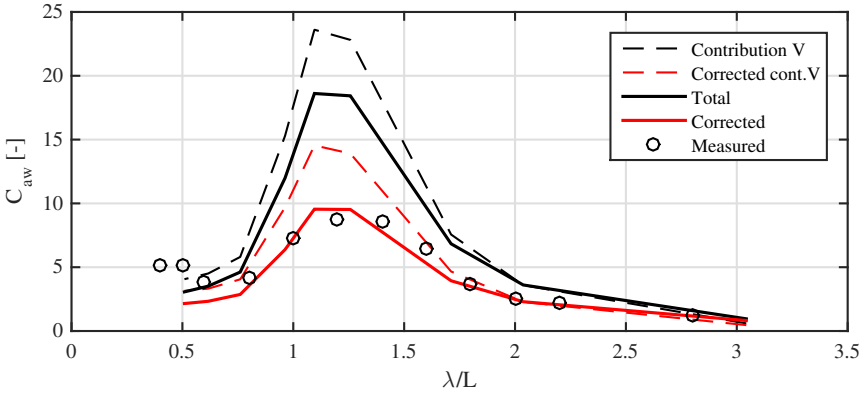

Figure 5.23: Corrected added resistance of FDS-11 at $Fn = 0.570$

5.5.2. Calculation and correction for FDS-20

The correction method is applied to FDS-20, which has the same bodyplan and C_B as FDS-11. However, FDS-20 has a smaller waterline entrance angle owing to the larger L/B. The hullform and parameters are shown in Figure 3.2 (a) and listed in Table 3.1, respectively.

The calculation is performed for a full scale with Lpp of 100 m. The hull consists of 1100 panels. The domain of the free surface is made by 0.5 Lpp forward of the bow, 2.5 Lpp backward of the stern, and a half-width of 1.32 Lpp in the transverse direction for the calculation at Fn = 0.570. There are 8120 panels on the free surface. The panels of the hull and free surface used in the calculations are shown in Figure 5.24.

The calculated motion responses are shown in Figure 5.25 along with the measured data. As in the previous calculations, the added resistance is overestimated compared to the measured data in the intermediate-wave region. Station 15 at Fn = 0.570, which is the same as that for FDS-5 and FDS-11, is applied as the intersection position of smooth transition functions in the correction. In this calculation, a = 15 and b = 1 are used in Equation 5.4.

The corrected relative wave elevation with the smooth transition is shown by a red line in Figure 5.26. The difference between the total and undisturbed relative wave elevation in FDS-20 is not significant, indicating that the waterline entrance angle of FDS-20 is so small that the effect of reflection and radiation of the hull is small. Figure 5.27 shows the calculated waterline contribution for the corrected relative wave elevation and the corrected added resistance with a red dashed line and solid line, respectively. The results for FDS-20's added resistance is corrected by the same method as that applied for FDS-5 and FDS-11. The corrected added resistance for FDS-20 is also similar to the measured data in the intermediate-wave region.

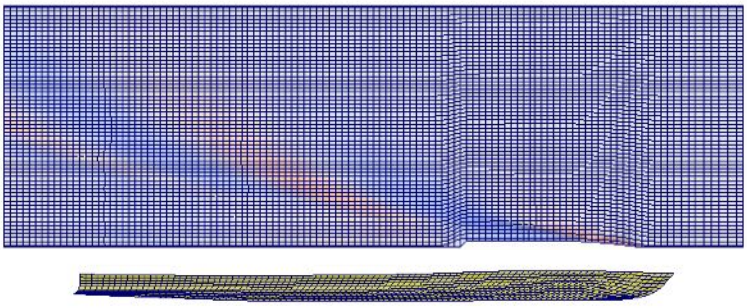

Figure 5.24: Hull and free-surface panels of FDS-20 for Fn = 0.570

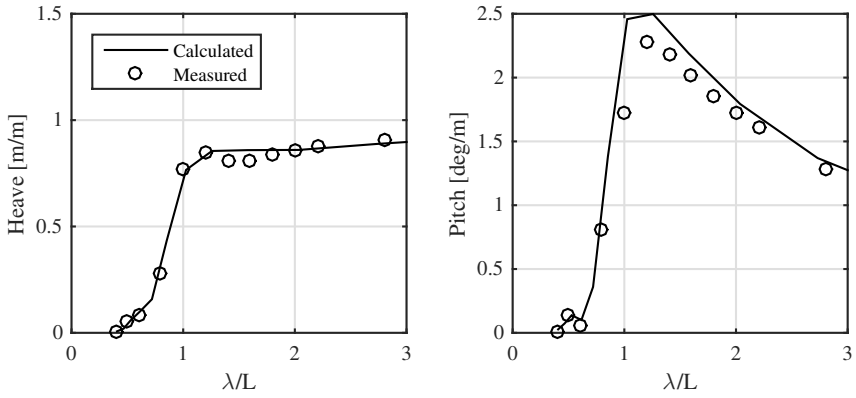

Figure 5.25: Motion responses of heave and pitch of FDS-20 at $Fn = 0.570$

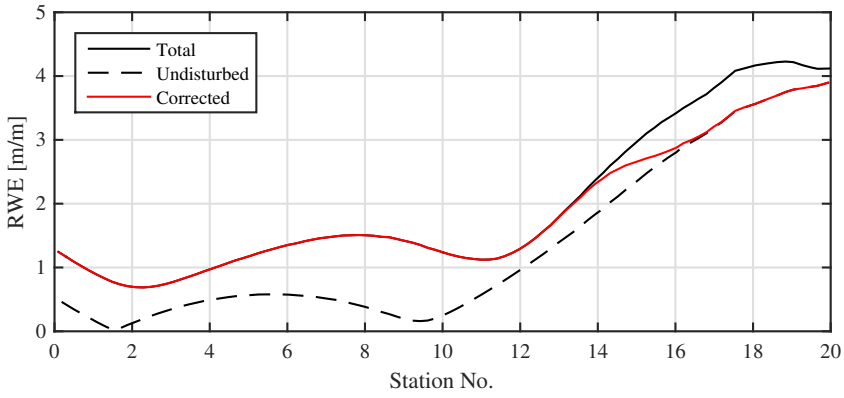

Figure 5.26: Comparison of total, undisturbed, and corrected relative wave elevation of FDS-20 of intermediate waves (λ/L = 1.0) at $Fn = 0.570$ ($a = 15$ and $b = 1$ is used in Equation 5.4)

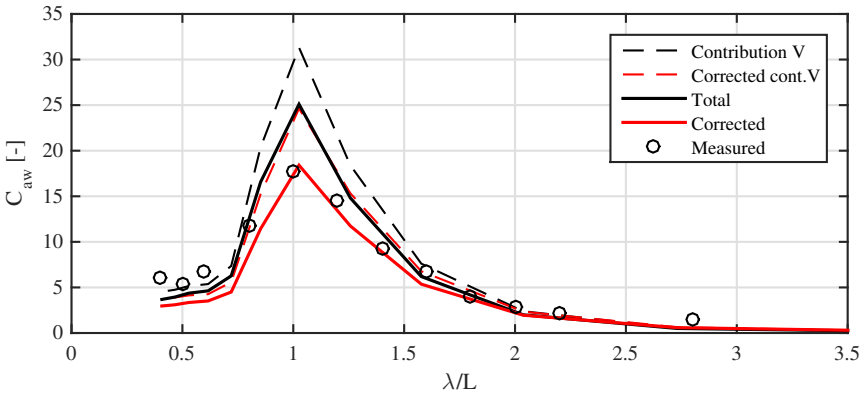

Figure 5.27: Corrected added resistance of FDS-20 at $Fn = 0.570$

5.6. Conclusions

This chapter proposed a correction method to solve the overestimation of the wave added resistance of a fast ship in the linear potential method calculation. The solution accounts for the nonlinearity of plunging braking, which is the detachment of the bow wave.

The correction method adjusts the relative wave elevation calculated by the linear potential method to the undisturbed relative wave elevation ahead of the position where the plunging breaking occurs. This method is based on the fact that detaching the bow wave weakens the influence of the reflected and radiated waves on the relative wave elevation. The region where the bow wave breaks was determined based on an experimental analysis.

A solution was developed for a fast ship in intermediate waves, for which the influence of the bow wave is greatest. The corrected relative wave elevation was used to recalculate the waterline contribution to the added resistance. The corrected added resistance solves the problem of overestimation of the added resistance in the intermediate-wave region of the fast ship by the linear potential method calculation. The longitudinal position where the plunging breaking occurs depends on the speed of the ship.

However, the calculation results underestimated the added resistance of short waves. For short waves, additional nonlinear effects such as the viscosity and stern shape, as reported by Liu *et al.* [111], should also be considered.

The linear potential method can be a useful tool to quickly determine the tendency of added resistance due to parameter changes at the hullform development stage. However, numerical calculations based on the linear theory can overestimate the added resistance by overestimating the waterline contribution. In particular, the calculation of ships with plunging breaking requires careful attention to determine whether the waterline contribution is overestimated. The accuracy of the calculation can be improved by considering the nonlinear phenomena in the calculation according to the characteristics of the bow wave.

6

CONCLUSIONS

This chapter presents the major research findings in Section 6.1 and recommendations for future research in Section 6.2. The research findings and recommendations presented in this chapter answer the following main question.

How can the reliability of added resistance estimation be improved?

6.1. Contribution of the thesis

This thesis presented a method to improve the reliability of added resistance estimation by identifying the nonlinearity caused by the plunging breaking of the bow wave on a fast ship. The method was motivated by the limitations of numerical analysis of the linear potential theory, which has the advantage of rapid computation but cannot adequately evaluate nonlinearity due to the breaking of the bow wave.

A method considering bow-wave breaking in the evaluation of added resistance was proposed by investigating the relationship between the pressure and relative wave elevation. The influence of bow-wave breaking on the added resistance was investigated by integration of the secondary pressure. This thesis proposed a correction method that takes into account the nonlinear effect of the bow wave into the linear potential method calculation of the added resistance.

The stability type of breaking is divided into plunging and spilling. Plunging is a type of breaking that appears as an overturning detachment on the crest of the bow wave. Spilling is a type of turbulent form that disturbs the adjacent flow field.

This thesis makes three important contributions to the analysis of the effects of bow-wave breaking on wave added resistance. First, a hypothesis was suggested that the added resistance depends on the stability type of bow-wave breaking, and the feasibility of the hypothesis was confirmed by analyzing the results of model tests. The hypothesis was presented by estimating the effect of increasing or decreasing the added resistance depending on the stability type of the bow wave. In particular, because the type of breaking depends on the speed of the ship, the speed was set as an independent variable to test the hypothesis. A transfer function of the added resistance including the speed of the ship was presented and set as a dependent variable. Then, the hypothesis was verified by analyzing the change in added resistance with a series of nine fast ships with different waterline entrance angles at several high speeds. In this feasibility test, it was verified that the added resistance evaluation based on the ship's speed is appropriate.

There is a transient region where sudden resistance changes occur. It was determined that there exists a boundary where the influence of the bow-wave breaking changes. The shift of the dominant influence of the bow wave induces a sudden change in the resistance. This was confirmed in the response of the added resistance through the proposed QTF including the squared ship speed. The transient region corresponds to the peak of the residual resistance coefficient in calm water as well. As the speed changes, the trend of the residual resistance coefficient and the added resistance changes at a specific speed region.

The second contribution is unique techniques for intuitively assessing the nonlinear relationship between the hull pressure and the relative wave elevation, which significantly influences the added resistance. The nonlinearity of the plunging breaking was experimentally investigated for a fast ship with a simple bow shape. The relative elevation of the bow wave and the pressure on the hull were measured. The model test results of the fast ship were analyzed using proposed templates. Theoretically, when the bow wave breaks, nonlinearity occurs and Bernoulli's equation is invalid.

The sequence history of pressure, which was proposed in Chapter 4, represents the dynamics of the bow wave into a simple graph. The history of the pressure signal can be intuitively analyzed by placing them according to the measured vertical position. In addition, the P-R diagram, which was also proposed in Chapter 4, correlates the time-series data of the pressure and the relative wave elevation into a closed graph without the time term. The nonlinearity between the pressure and the relative wave elevation is determined by a bulge shape of the closed graph.

Through the analysis using these techniques, the overturning detachment of the bow wave was confirmed to induce a pressure drop during the relative increase of the bow-wave height. The process of plunging breaking of the bow wave can be divided into three stages: the bow-wave development stage, pile-up and breaking stage, and bow-wave absent stage. The latter two stages are associated with the nonlinearity of the bow wave. The nonlinearity between the pressure and the relative wave elevation is closely related to the speed of the ship. It was also concluded that the plunging breaking of the bow wave results in lower wave added resistance compared to that predicted by the linear theory owing to the drop in pressure while the relative wave elevation is increasing, which is caused by the detachment of the

bow wave.

The third contribution is a method to improve the accuracy of the added resistance estimation by applying the results of the experimental analysis of nonlinear phenomena to the linear potential theory method. A correction model for the waterline contribution of the added resistance was proposed to overcome the shortcomings of the linear potential theory method and to improve the accuracy of the numerical calculation. The correction method adjusts the relative wave elevation of the region where the plunging breaking occurs to the undisturbed wave height calculated by the linear potential theory method. The corrected relative wave elevation is used to recalculate the waterline contribution of the added resistance. The regions where the bow wave breaks were determined based on the experimental analysis. The longitudinal position where the plunging breaking occurs depends on the speed of the ship. This method is based on the interpretation that the detachment of the bow wave decreases the influence of the relative wave elevation on the hull pressure.

The effectiveness of this solution was confirmed in intermediate waves for ships advancing at high-speed (Fn = 0.570), which are affected by the plunging breaking of the bow wave. The corrected added resistance solves the problem of the linear potential method calculation, which overestimates the added resistance. It was confirmed that the accuracy of the added resistance calculation by the linear potential theory method can be improved by considering the speed-dependent nonlinearity of the bow wave.

However, the results of this thesis are not applicable to all types of bow waves, because only fast ships at relatively high speeds were investigated. Therefore, further research is needed on the effect of spilling breaking, which occurs for blunt-bow ships at relatively slow speeds. In addition, it can be applied to numerical analysis if it is complemented with studies to quantify the nonlinearity of bow wave which changes with hullform change. If the understanding of the nonlinearity between hull and bow waves can be taken into account in the numerical analysis method, the reliability of the added resistance estimation can be improved.

The linear potential theory method can be a useful tool to quickly determine the trend of added resistance due to parameter changes in the initial hullform development stage. However, numerical calculations based on the linear potential theory can overestimate the added resistance, especially in intermediate waves, for which the motion response of the ship is significant. It is necessary to pay close attention to whether the waterline contribution is overestimated. It is possible to increase the accuracy by integrating into the calculation a limitation function based on the nonlinear phenomenon according to the characteristics of the bow wave.

Recent regulations for ship operation require that the added resistance be accurately evaluated. Therefore, it is necessary to improve and integrate hydrodynamic simulation tools. However, the various numerical solutions and multiple operating conditions of the ship make it difficult to determine a synthesized solution. The accurate estimation of the wave added resistance is a key step towards implementing regulations related to ships' energy efficiency. Previously, the added resistance could be estimated by focusing on the motion response of ships, which makes the greatest contribution. However, changes in hullform (such as increasing ship length) and diverse operating conditions for implementing regulations cannot be explained by the

ship's motion response alone. The influence of hull-reflected waves, especially the bow-wave breaking, is a typical problem that was rarely considered in the context of added resistance in the past.

Model tests provide reliable benchmark data for the added resistance. Reliable benchmark data help in understanding physical phenomena and verifying the accuracy of numerical calculations. However, the main problem of the model test is that there are limitations to changing the modeling conditions during the testing. Furthermore, the measurement of the added resistance requires caution because the amplitude of the measured value is large, while the average value is small. CFD calculations (e.g., RANS solution) also help in understanding complex breaking phenomena, but they are limited to specific problems. It takes much effort to prepare the calculations, and CFD still has a long calculation time.

The linear potential theory method is attractive because of the cost-effective solution. The effect of viscosity is neglected because it does not contribute much to the motion response of the ship or the effect of reflected waves under conditions where linearity is maintained. Thus, when the breaking of the reflected wave by the hull is a dominant effect, the added resistance cannot be accurately calculated by the linear potential theory method. The nonlinear relationship between the hull and the bow wave must be taken into account in a manner different to the linear potential theory method. Therefore, through the development of a method to account for the nonlinearity between the hull pressure and bow wave in the added resistance evaluation, the linear potential theory method can still be used.

The understanding of nonlinear phenomena is important for problems that are difficult to explain with the linear potential theory of added resistance. The most significant problem is the distinctive recognition of nonlinear phenomena and the application of appropriate solutions. Similar solutions can be applied to vessels with similar nonlinear phenomena.

The incorporation of experimentally verified nonlinear characteristics into numerical calculations, as demonstrated in the present study, is a practical solution. This approach can be a realistic solution based on the physical properties. Techniques describing nonlinear phenomena that cannot be described by the linear theory are still needed. In particular, to understand the nonlinearity of the added resistance due to the breaking of the bow wave, the analysis must carefully consider the change in added resistance depending on the speed of the ship.

6.2. Recommendations for future work

In order to enhance the accuracy of evaluation of the added resistance further, it is necessary to develop a solution based on the understanding of nonlinear phenomena. Directions for future research are suggested as follows.

The practical application of this thesis is the improvement of the prediction method of added resistance. The phenomenon of bow-wave breaking is instantaneous and complex. It is recommended to consider at least the bow-wave breaking when the ship has extreme motion responses or high speeds. A small waterline entrance angle of the ship may cause plunging breaking due to the detachment of the

bow wave. Changes in the ship's speed or an increase in the dynamic waterline entrance angle by the motion response can induce plunging breaking phenomena in combination with spilling breaking. A correlation function based on observations of phenomena or a reliable analysis can be applied for the numerical calculation of such complex phenomena.

Complex solutions that consider complex phenomena simultaneously have limited application. Physics-based correlation practically reduces the error of numerical calculation. The most influential element should be isolated, and a suitable solution should be developed for each phenomenon. Turbulence spilling breaking of bow waves is a common phenomenon, and future research is needed to correlate it with the added resistance. A better understanding and explanation of these effects can improve the accuracy of added resistance calculations.

The current research can be elaborated through a comparison of further experiments and numerical studies. The results presented in this thesis are applied to the linear potential theory method by simplifying the nonlinearities of the breaking phenomena observed through the experiments. From the perspective of nonlinear phenomena, a better insight into the intersection between experimental limits and numerical calculations is needed. Research to quantify this intersection is also necessary.

Research needs a specific definition of the nonlinearity. The term nonlinearity covers a broad range of factors, making it difficult to establish an integrated interpretation for the added resistance. This thesis investigated the nonlinearity of the relationship between the hull pressure and the relative wave elevation, which directly affects the added resistance. Changes in linear relationships due to the ship's speed were also investigated.

Velocity conditions and dynamic squats are essential to be considered for the evaluation of the added resistance of a ship. The nonlinear effects of the bow wave depend on the speed in the added resistance evaluation of a given ship. Further research for tracking the shifts of a nonlinear phenomenon by speed change in actual operation is also required.

Further research to understand the nonlinear phenomena physically through the observation of a specific subject should be continued. Although the phenomena vary for different conditions of ships, phenomena that have similar physical characteristics must be explored continuously. The solution of the added resistance evaluation should be based on an understanding of the specific phenomena. Understanding the physical phenomena allows for a better estimation of the added resistance.

For blunt-bow ships, additional nonlinear effects such as viscosity must be considered simultaneously because the hull reflections that cause the rise of the bow wave in front of the hull and the resulting turbulence of spilling breaking also affects the wake field of the bow wave around the hull. This problem is still difficult to explain using numerical solutions. Careful research is needed because scale effects can influence this phenomenon.

Appendices

A

THE SEQUENCE HISTORY OF PRESSURE

In the analysis of Chapter 4, the sequence histories of the pressure of station 18 are compared in Figures 4.7, 4.8 and 4.9. Appendix A shows additional sequence histories for the five stations (16, 17, 18, 18,75 and 19.5) of the experimental data used in the analysis in Chapter 4.

The list of the additional figures is shown in Table 1.

Table A.1: List of figures in Appendix A

No.	Type	Fn	λ/L	ζ_a [m]
Figure A.1	The sequence history of pressure	0.285	0.5	1.0
Figure A.2	The sequence history of pressure	0.430	0.5	1.0
Figure A.3	The sequence history of pressure	0.570	0.5	1.0
Figure A.4	The sequence history of pressure	0.285	1.1	1.0
Figure A.5	The sequence history of pressure	0.430	1.1	1.0
Figure A.6	The sequence history of pressure	0.570	1.1	1.0
Figure A.7	The sequence history of pressure	0.285	2.0	1.0
Figure A.8	The sequence history of pressure	0.430	2.0	1.0
Figure A.9	The sequence history of pressure	0.570	2.0	1.0

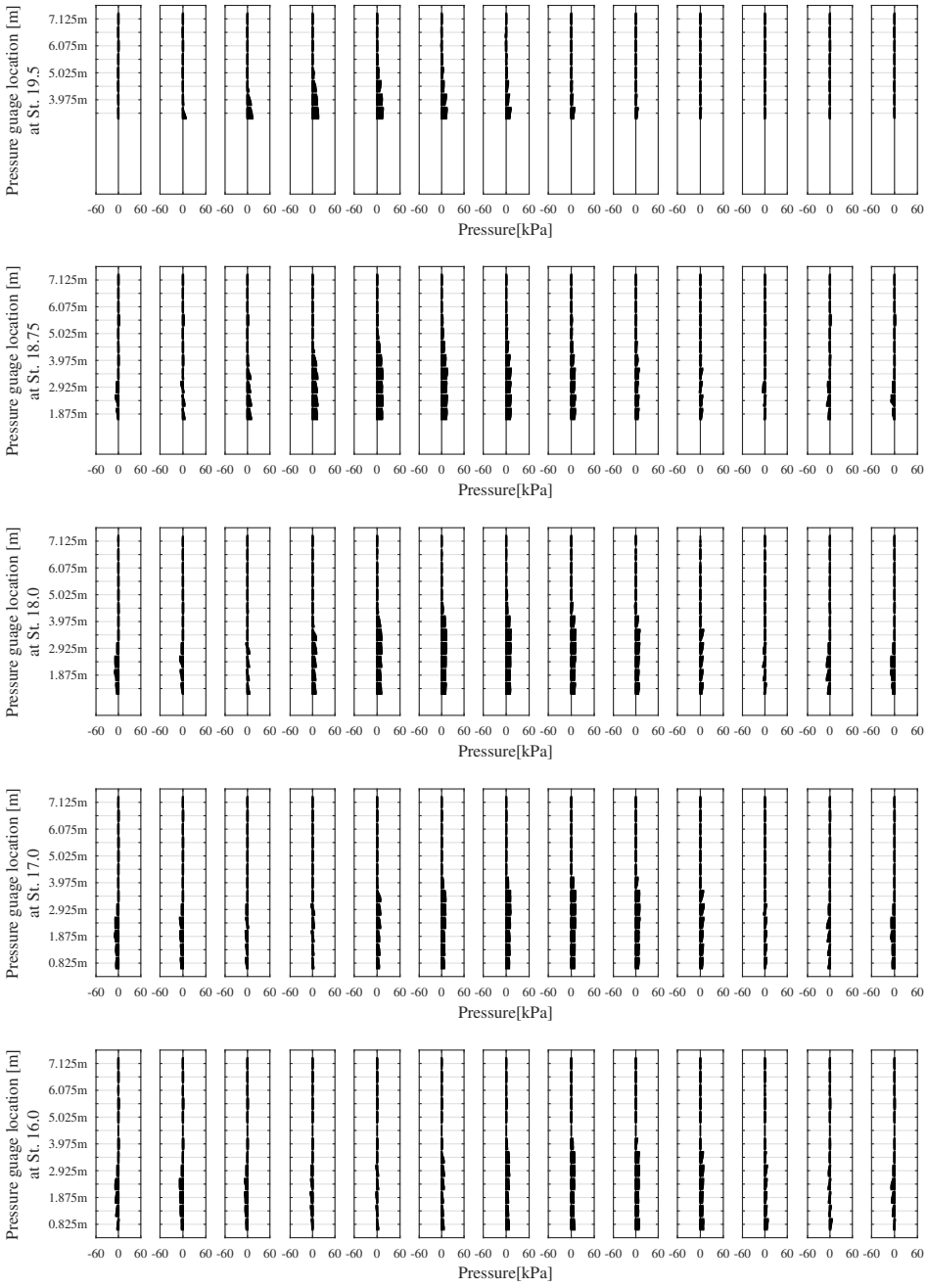

Figure A.1: The sequence history of pressure of the bow wave in short waves (λ/L = 0.5) at Fn = 0.285

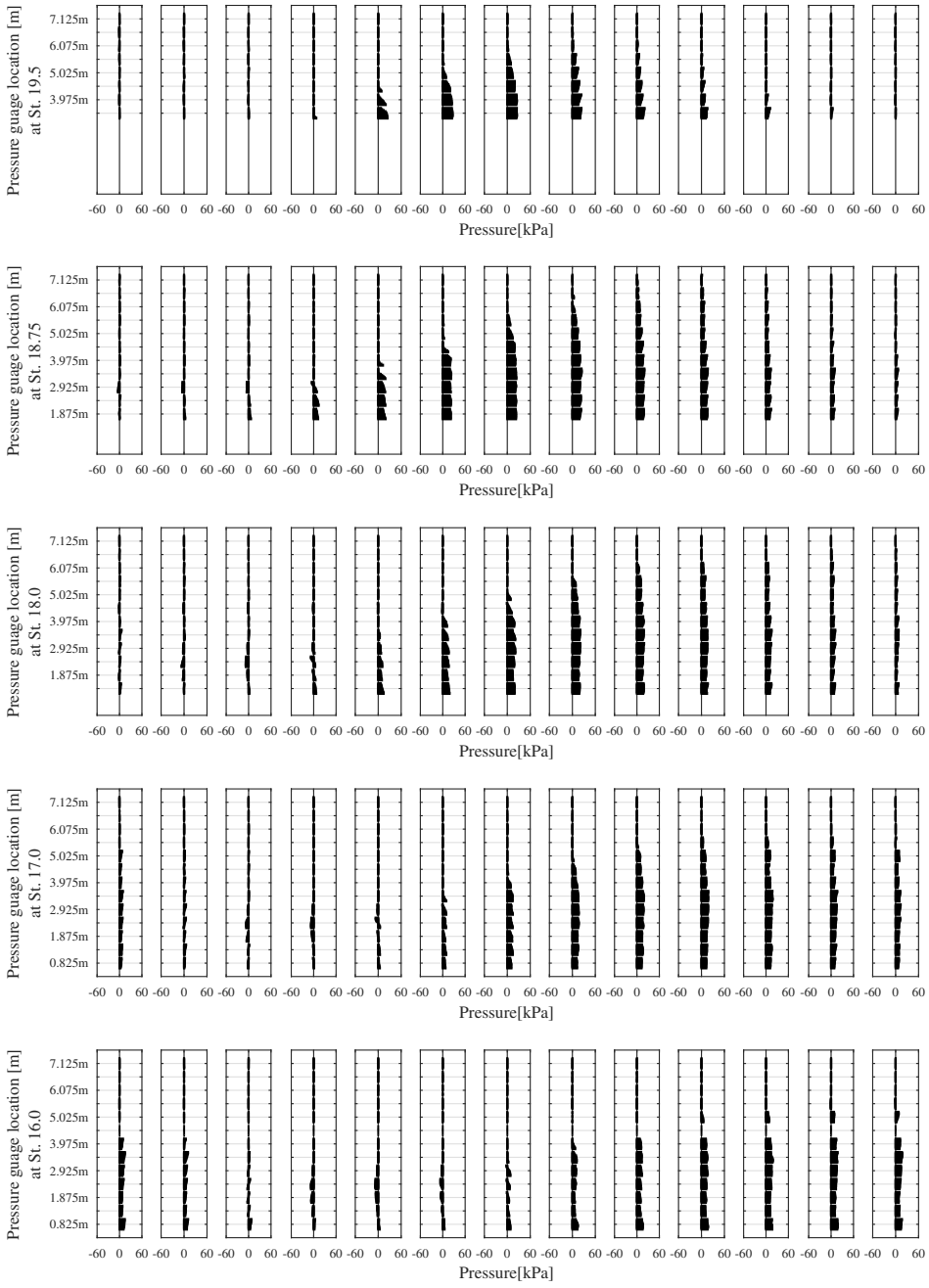

Figure A.2: The sequence history of pressure of the bow wave in short waves (λ/L = 0.5) at Fn = 0.430

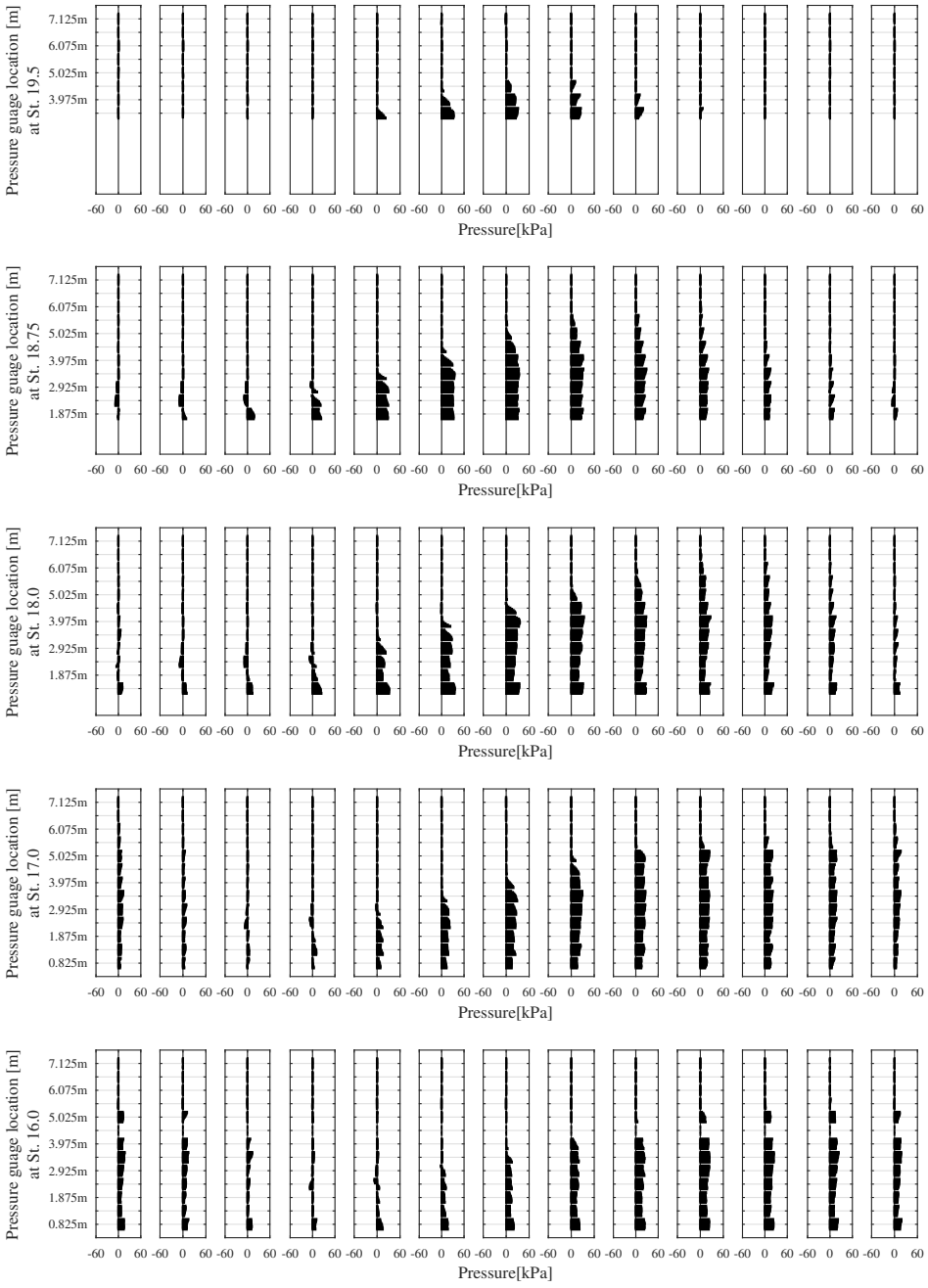

Figure A.3: The sequence history of pressure of the bow wave in short waves (λ/L = 0.5) at Fn = 0.570

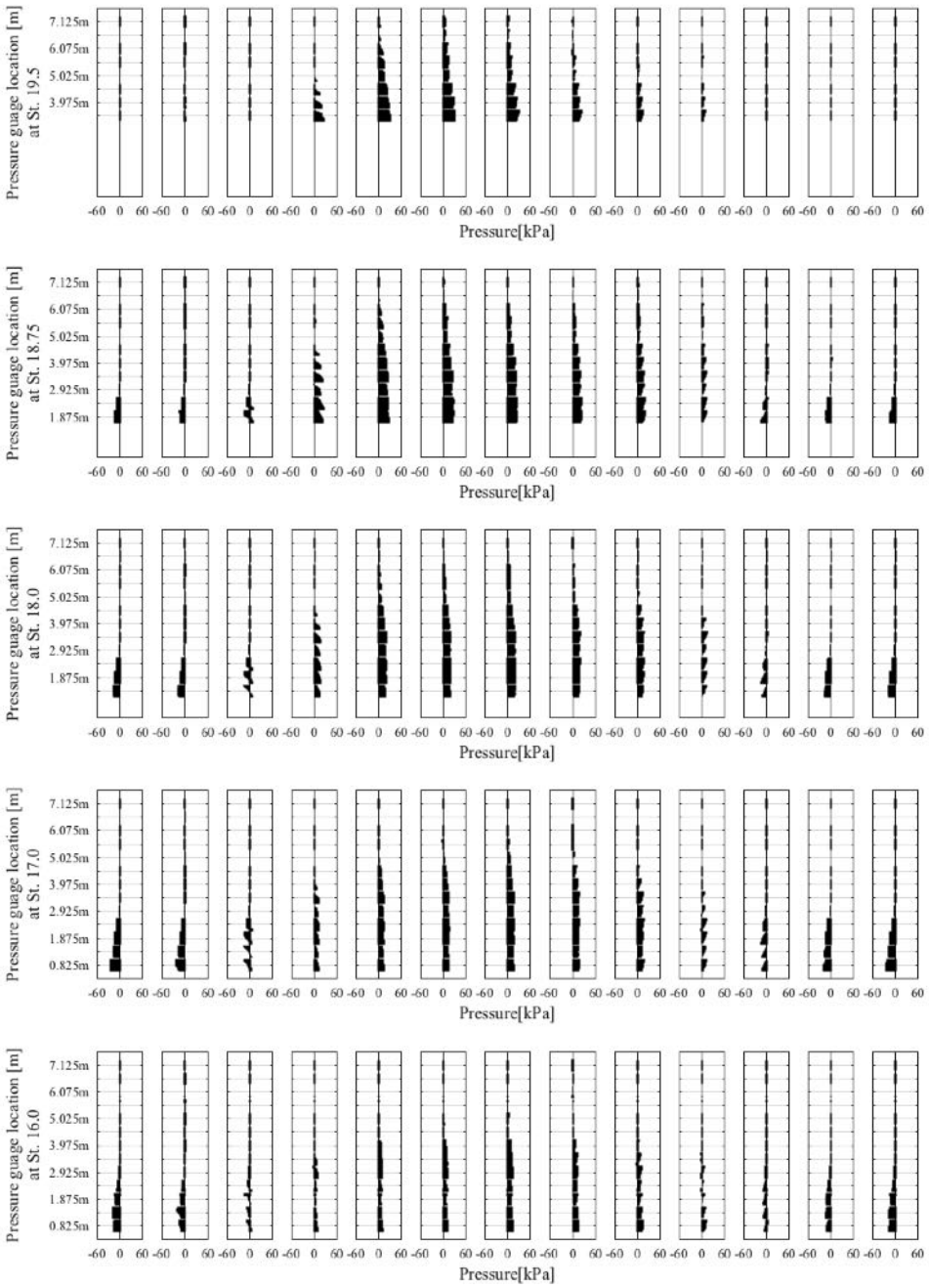

Figure A.4: The sequence history of pressure of the bow wave in intermediate waves (λ/L = 1.1) at Fn = 0.285

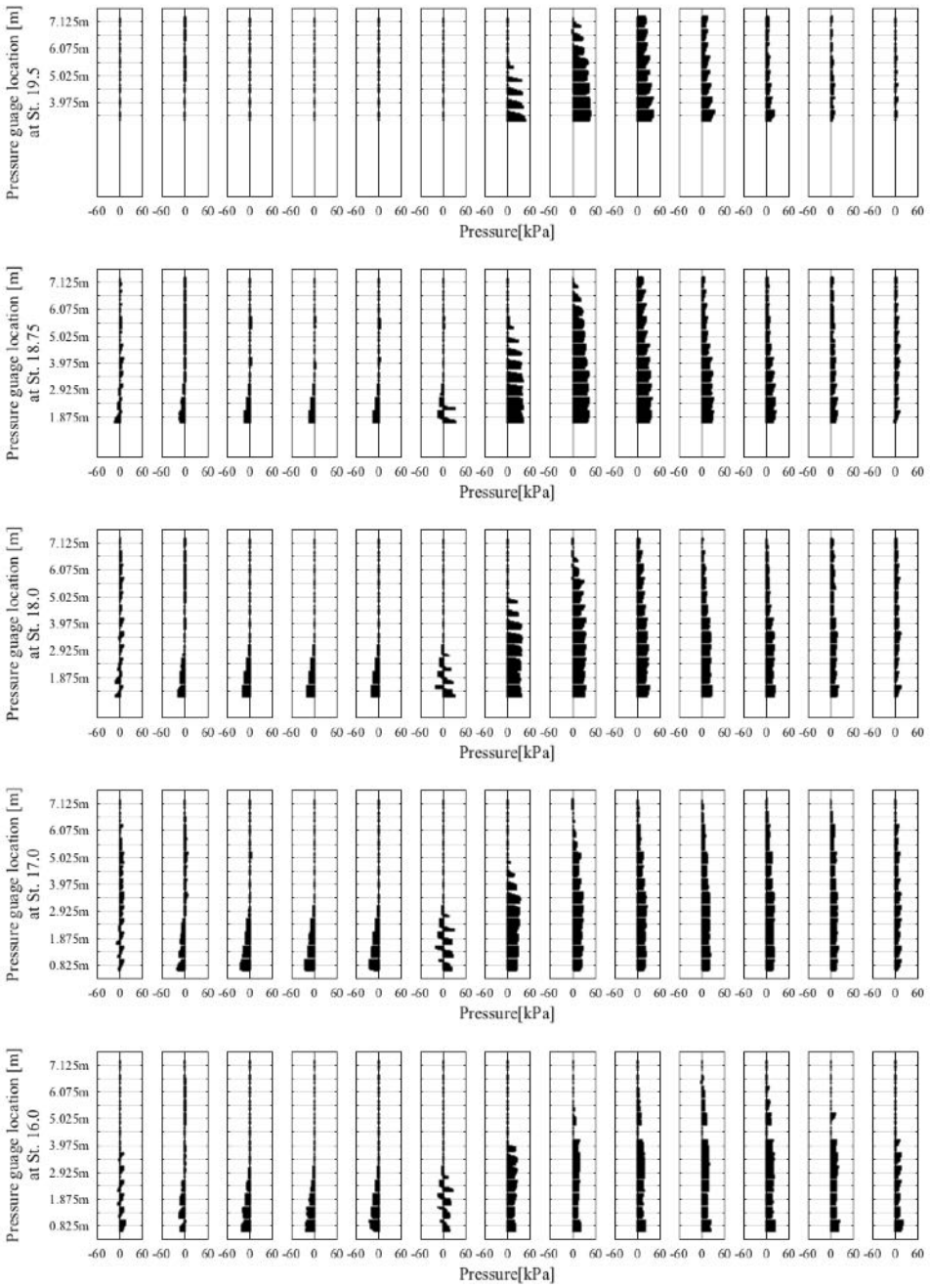

Figure A.5: The sequence history of pressure of the bow wave in intermediate waves (λ/L = 1.1) at Fn = 0.430

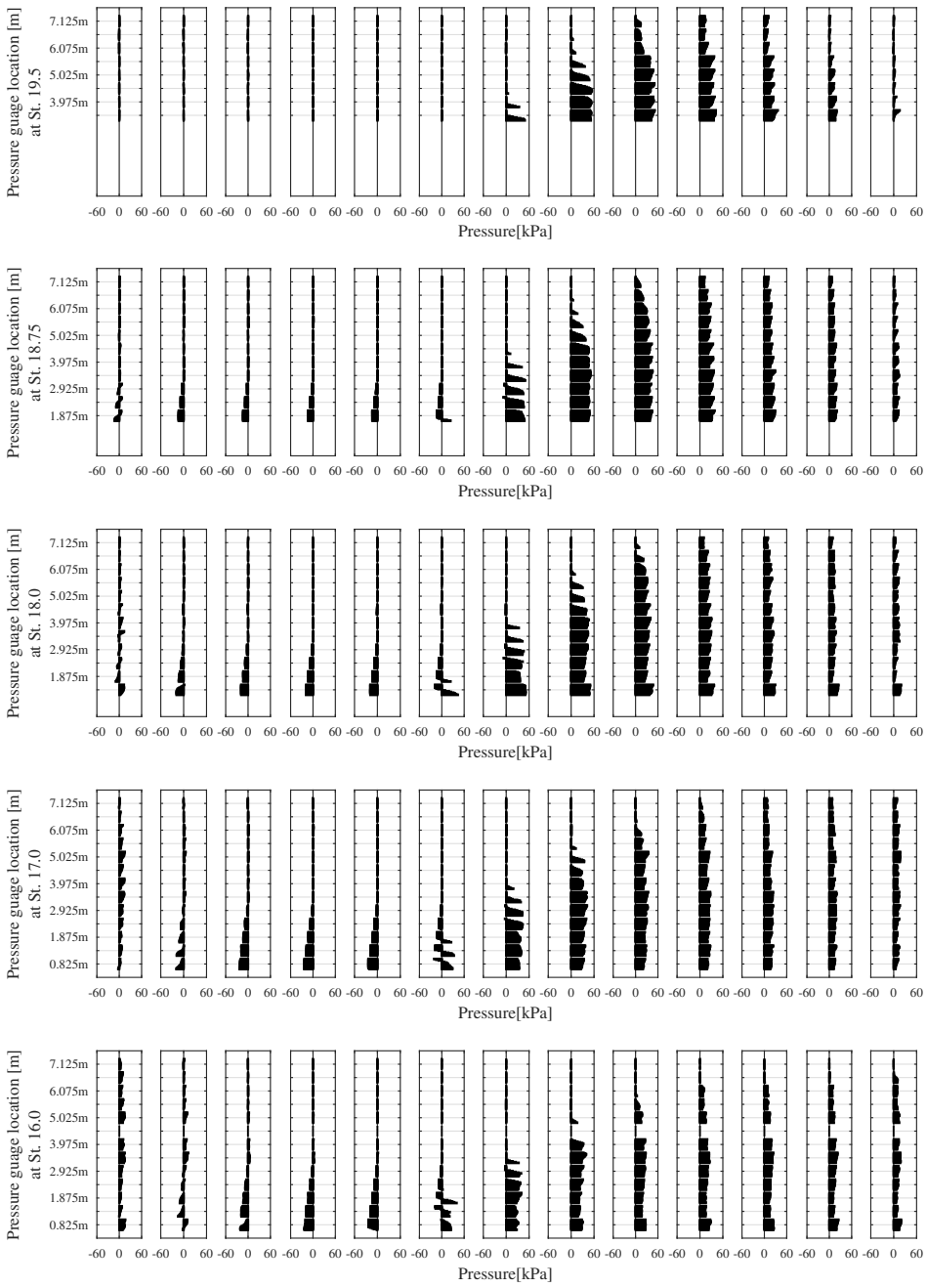

Figure A.6: The sequence history of pressure of the bow wave in intermediate waves (λ/L = 1.1) at Fn = 0.570

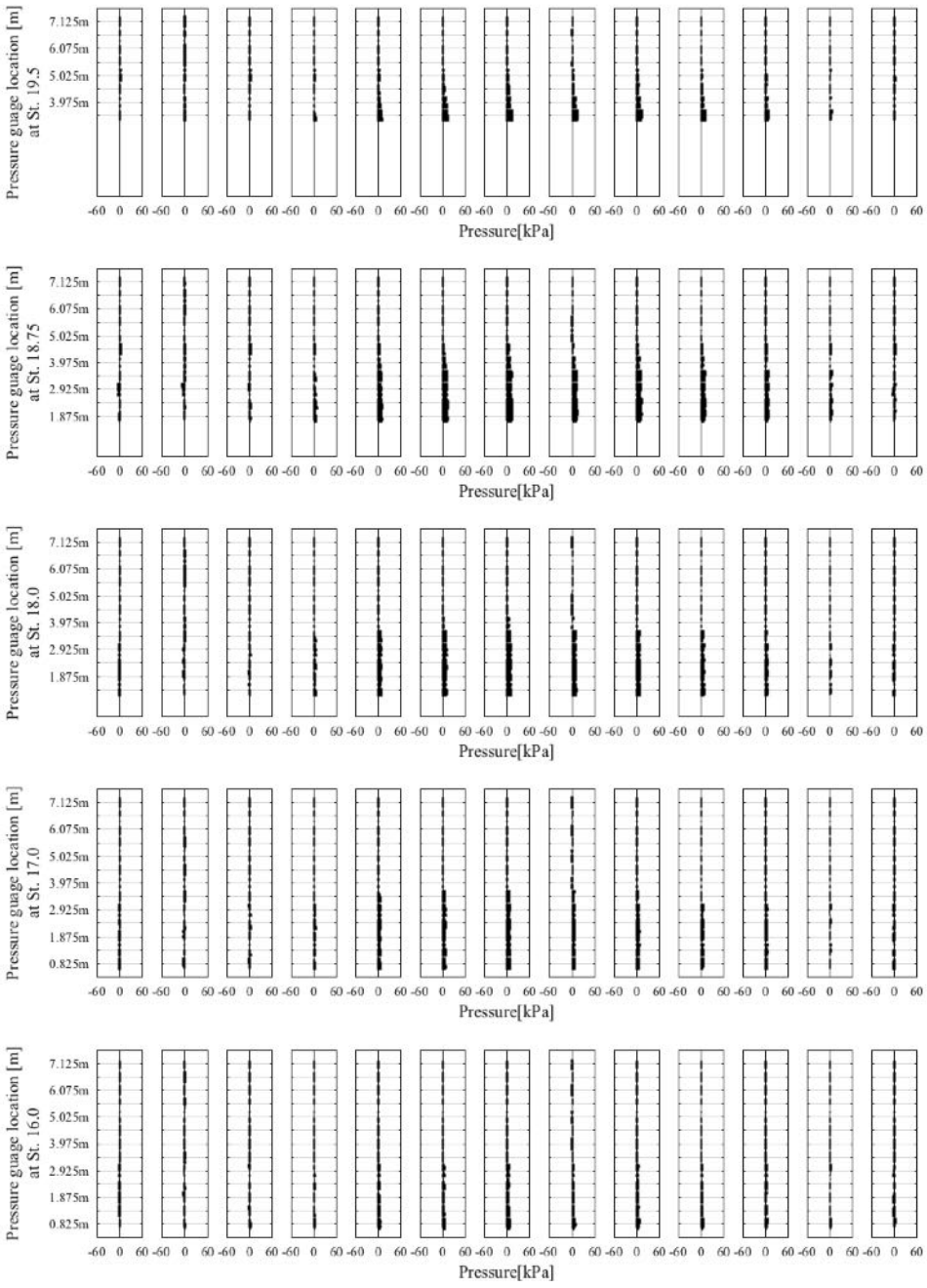

Figure A.7: The sequence history of pressure of the bow wave in long waves (λ/L = 2.0) at Fn = 0.285

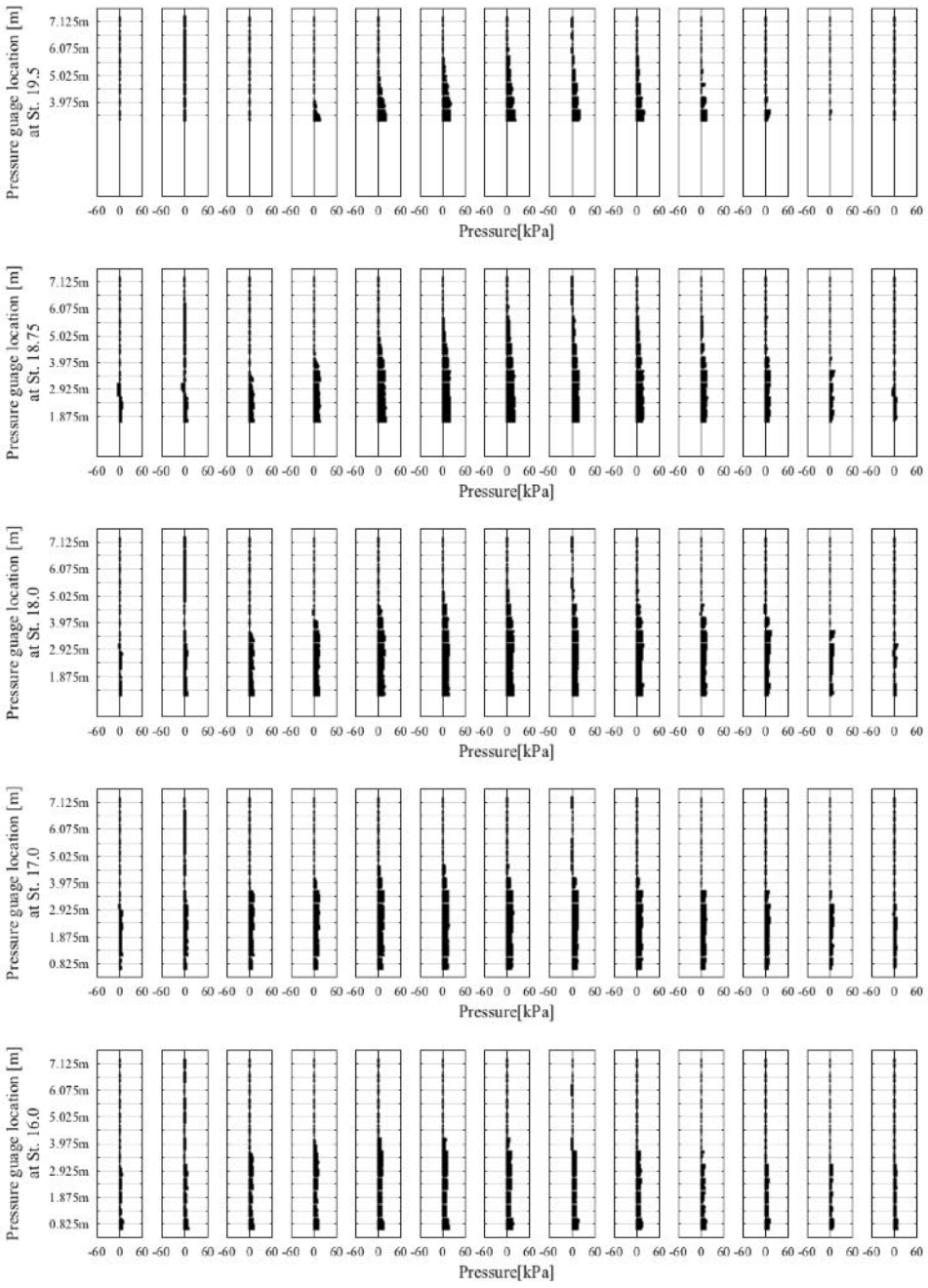

Figure A.8: The sequence history of pressure of the bow wave in long waves (λ/L = 2.0) at Fn = 0.430

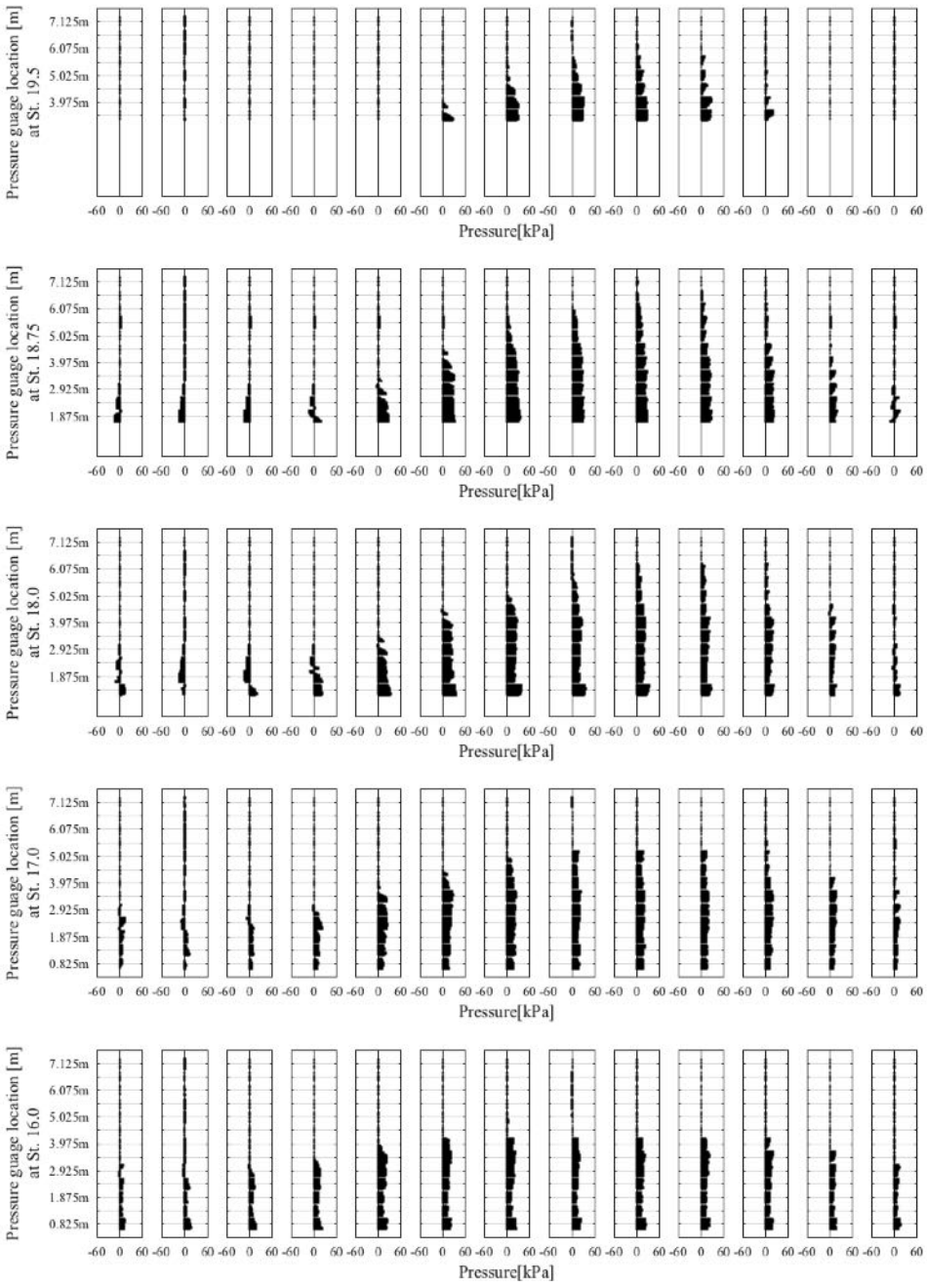

Figure A.9: The sequence history of pressure of the bow wave in long waves (λ/L = 2.0) at Fn = 0.570

B

ASSESSMENT OF AMPLITUDE EFFECT IN SHORT WAVES

The added resistance is known to be proportional to the squared of the relative wave elevation (ζ^2) in a linear condition where the bow waves are not broken. However, when the bow wave breaks, the quadratic relationship can no longer be maintained.

Appendix B evaluates the nonlinearity between pressure and wave height at the fast ship when the wave amplitude of short waves increases from 0.5 m to 1.0 m. The experiment is carried out under same settings as in Chapter 4. The amplitude

Table B.1: List of figures in Appendix B

No.	Type	Fn	λ/L	ζ_a [m]
Figure B.1	The sequence history of pressure	0.430	0.5	0.5
Figure B.2	The sequence history of pressure	0.430	0.5	1.0
Figure B.3	The sequence history of pressure	0.570	0.5	0.5
Figure B.4	The sequence history of pressure	0.570	0.5	1.0
Figure B.5	Pressure signals at St.18	0.430	0.5	0.5 and 1.0
Figure B.6	Pressure signals at St.18	0.570	0.5	0.5 and 1.0
Figure B.7	P-R diagram	0.430	0.5	0.5 and 1.0
Figure B.8	P-R diagram	0.570	0.5	0.5 and 1.0
Figure B.9	$\Delta\zeta$ in P-R diagram	0.430	0.5	0.5 and 1.0
Figure B.10	ΔCp in P-R diagram	0.570	0.5	0.5 and 1.0

of incident wave of 0.5 m is added. The relative wave elevation is measured at five stations, and the pressures with 0.525 m vertical steps are measured at the same time. The measured pressure and relative wave elevation are analyzed using the tools proposed in Chapter 4. The list of analysis graphs is shown in Table B.1.

Figures B.1, B.2, B.3 and B.4 show the sequence histories of the unsteady pressure and bow wave under different conditions of ship's speed and the incident wave's amplitude, respectively. The sequence history of pressure recognizes the effect of the bow wave in the hull pressure. The phenomena shown in these graphs are conditions under which the ship's motion response is ignored under short waves. Therefore, in this condition, only the pressure due to the incident wave applied to the hull is displayed. As the amplitude of the incident waves increases, the pressure acting at the top of the ship's draft (3.125 m) at each speed is distributed higher.

Figures B.5 and B.6 show a comparison of typical time series pressure signals. Each graph shows the change in the pressure signal as a function of the wave amplitude at station 18. In both graphs, the regular shape of the signal is destroyed as the wave amplitude increases.

Figures B.7 and B.8 show the relationship between measured pressure and relative wave elevation. As the incident wave's amplitude increases, the area of the diagram increases. The nonlinear relationship between the two signals is represented by the bulge of the graph. Nonlinearity is perceived intuitively through the bulge of the graph.

Figures B.9 and B.10 show the characteristic values of the bulge shape of the P-R diagram. The definitions of $\Delta\zeta$ and ΔCp are shown in Figure 4.13. As the P-R diagram expands, both values become larger. In Figures B.9 and B.10, the amplitude of the incident wave of 0.5 m is a solid black line, and the 1.0 m is a red dotted line. As the wave amplitude increases, the graphs of all stations in Figure B.9 and Figure B.10 move to the larger values. The nonlinear characteristic values are generally proportional to the increase in wave amplitude.

This analysis shows that as the wave height increases, the nonlinear relationship between pressure and relative wave elevation increases.

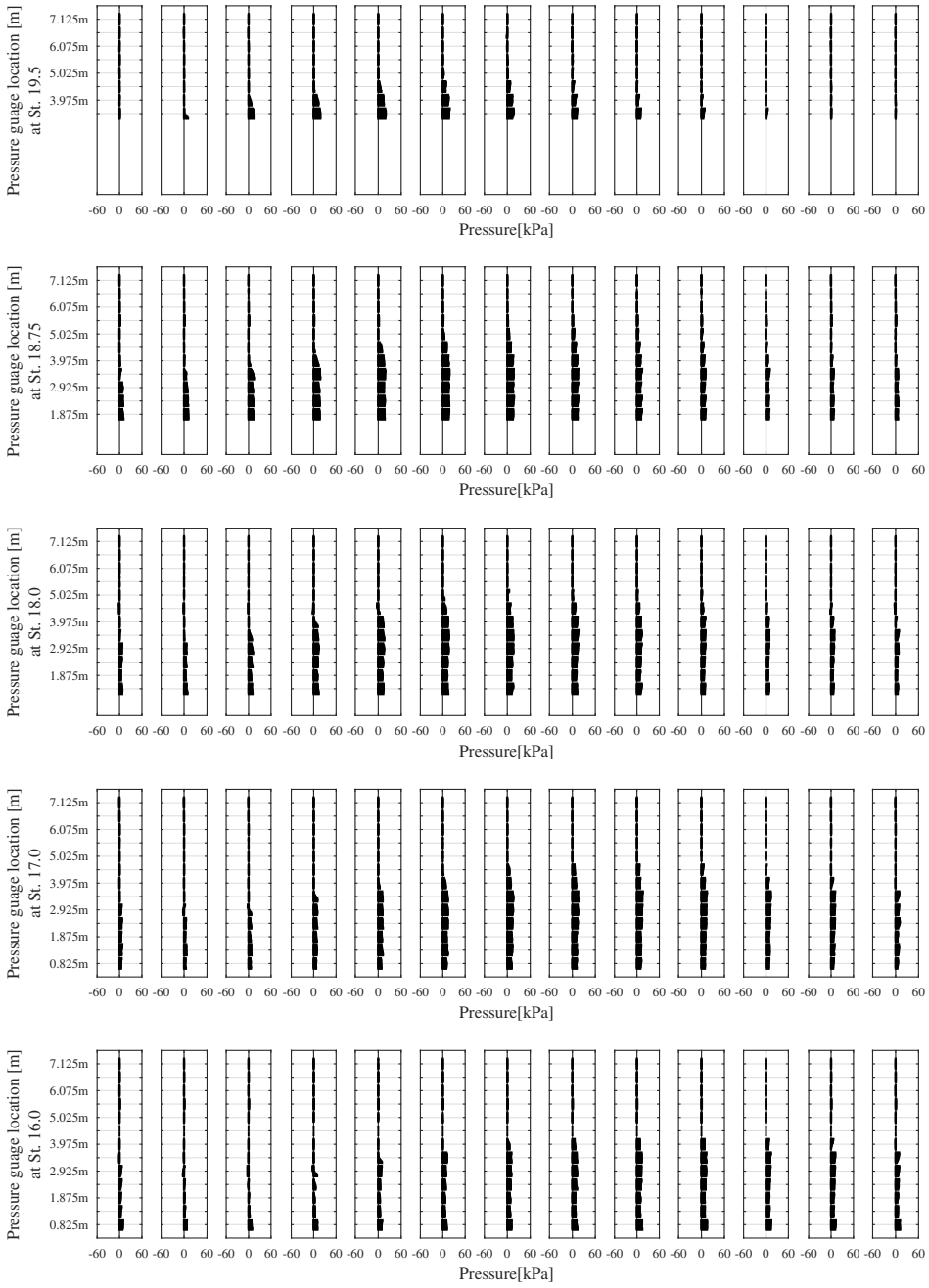

Figure B.1: The sequence history of pressure of the bow wave in short waves (λ/L = 0.5) in wave amplitude = 0.5 m at Fn = 0.430

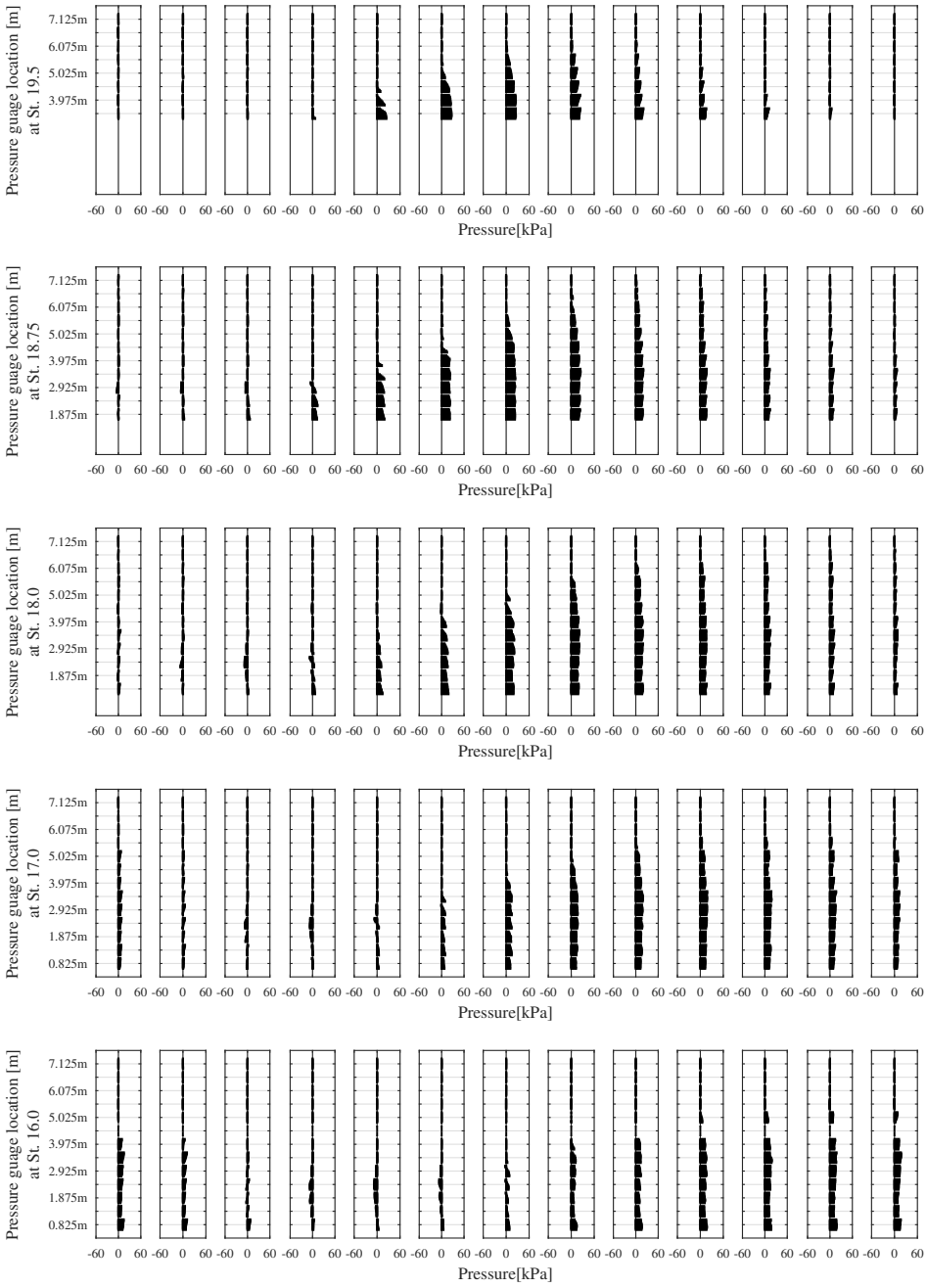

Figure B.2: The sequence history of pressure of the bow wave in short waves (λ/L = 0.5) in wave amplitude = 1.0 m at Fn = 0.430

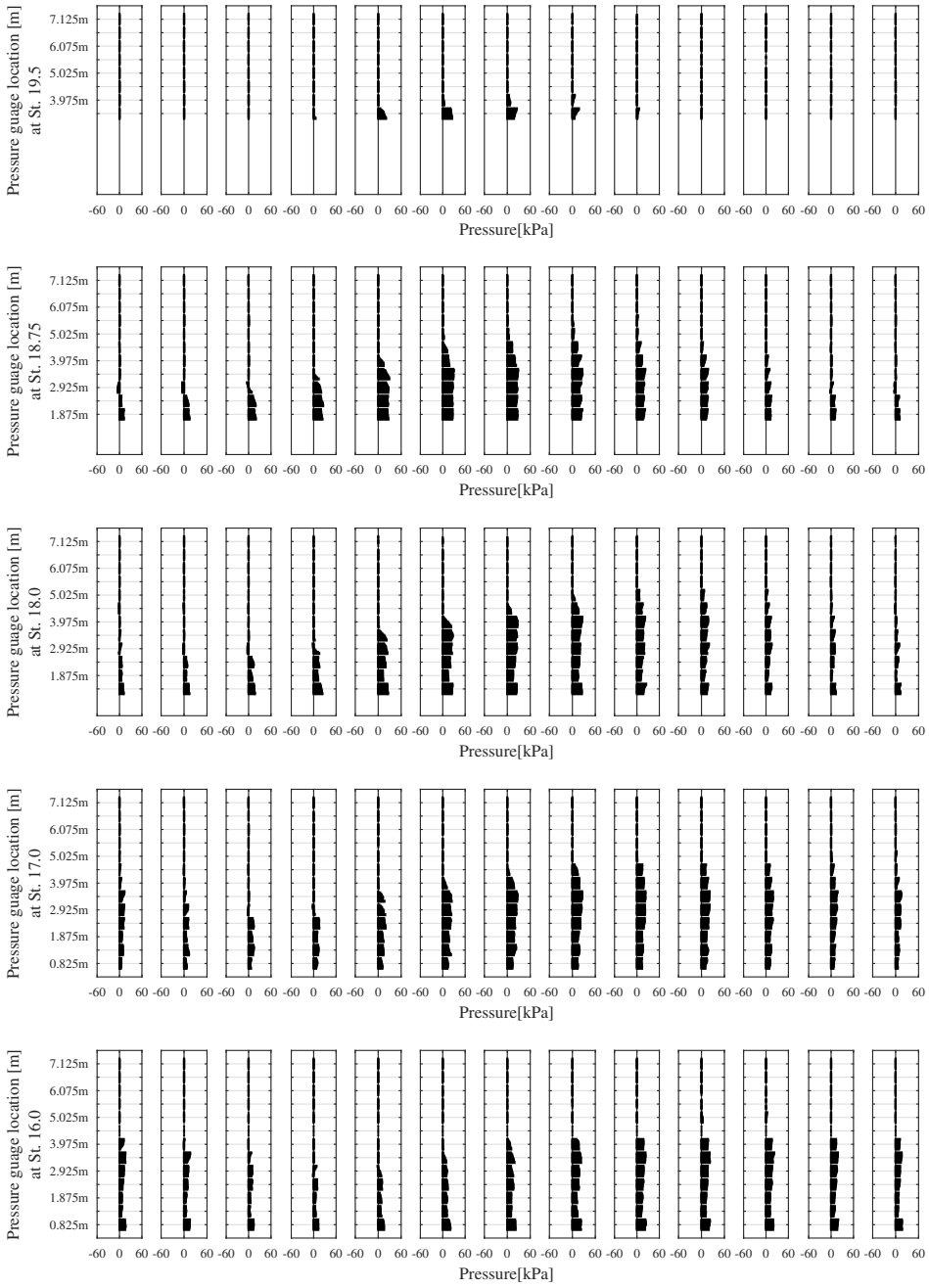

Figure B.3: The sequence history of pressure of the bow wave in short waves (λ/L = 0.5) in wave amplitude = 0.5 m at Fn = 0.570

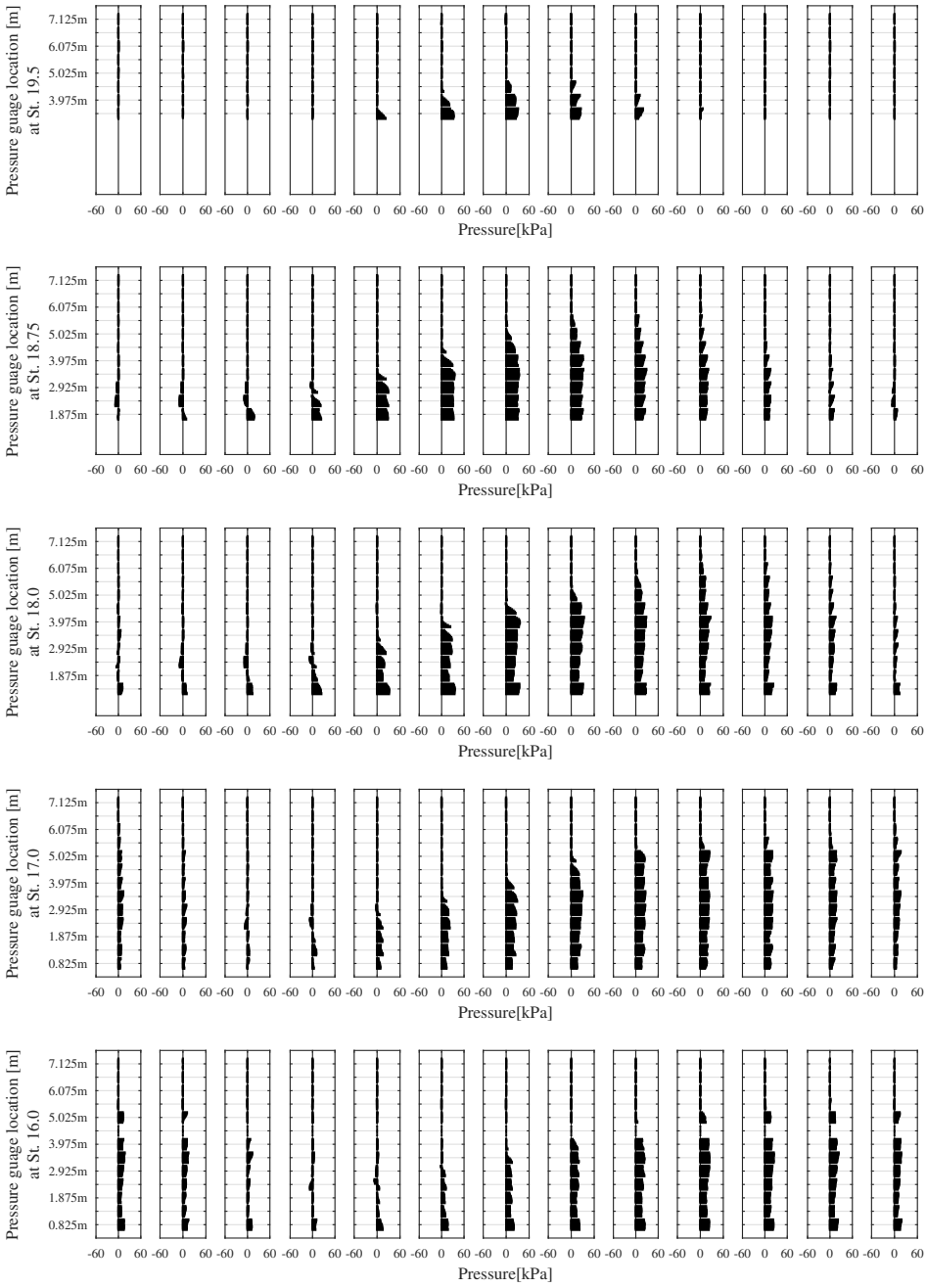

Figure B.4: The sequence history of pressure of the bow wave in short waves (λ/L = 0.5) in wave amplitude = 1.0 m at Fn = 0.570

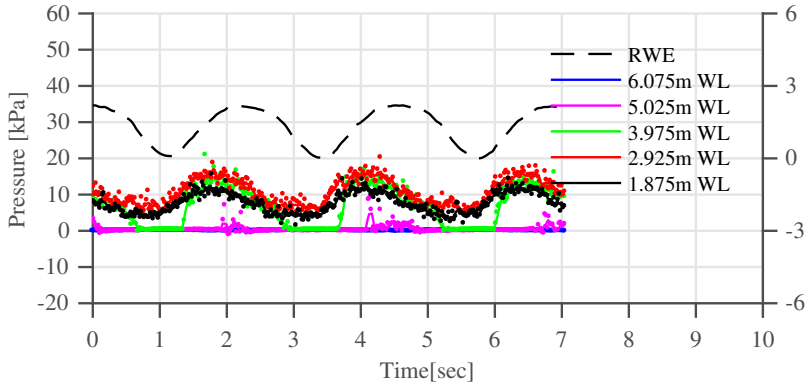

(a) Wave amplitude = 0.5 m

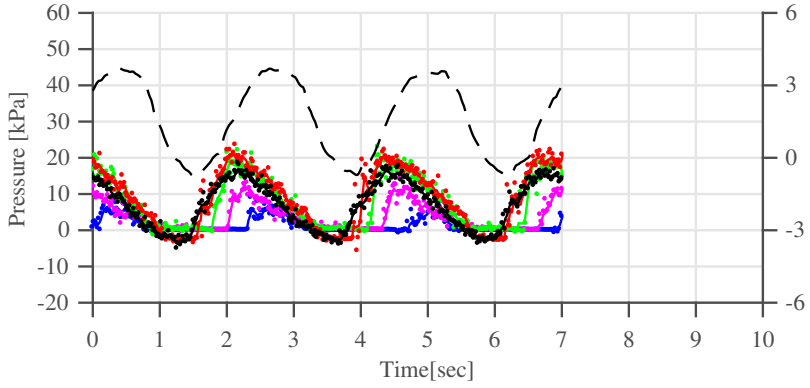

(b) Wave amplitude = 1.0 m

Figure B.5: An example of relative wave elevation (RWE) and pressure signals for three cycles. Pressure signals are smoothed with a time-based moving average filter of a five-point span over three speeds at station 18 in short waves (λ/L = 0.5) at Fn = 0.430

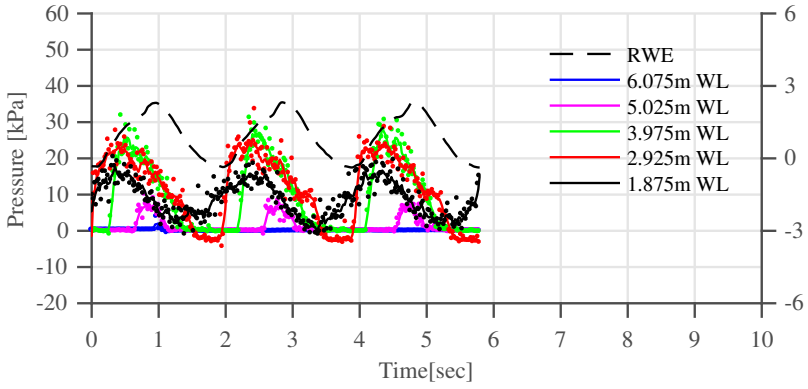

(a) Wave amplitude = 0.5 m

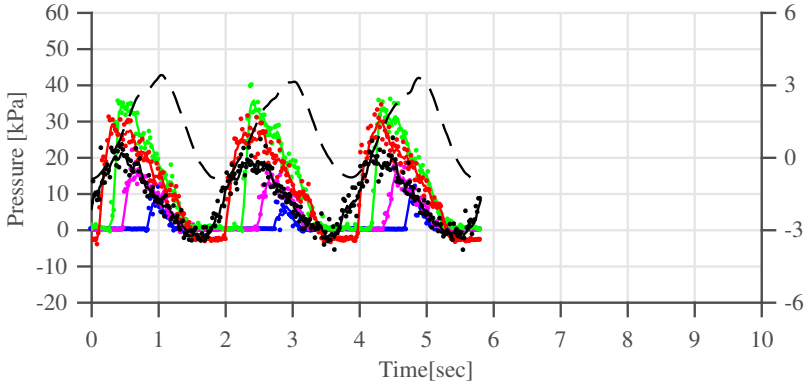

(b) Wave amplitude = 1.0 m

Figure B.6: An example of relative wave elevation (RWE) and pressure signals for three cycles. Pressure signals are smoothed with a time-based moving average filter of a five-point span over three speeds at station 18 in short waves (λ/L = 0.5) at Fn = 0.570

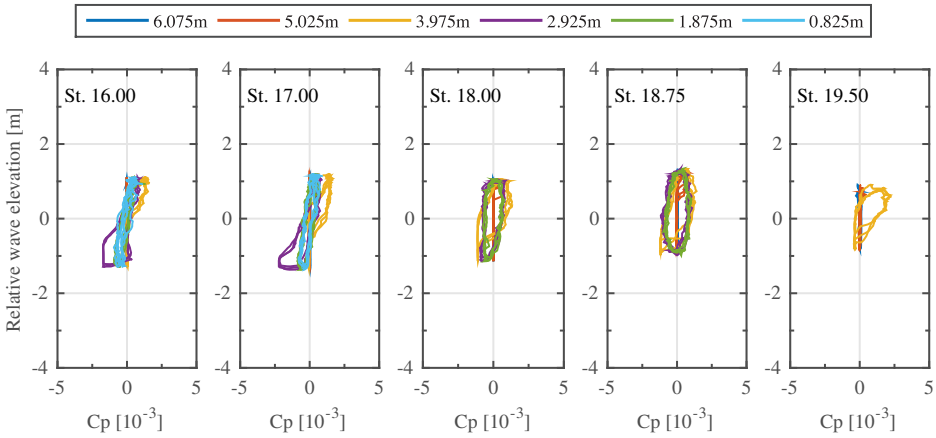

(a) Wave amplitude = 0.5 m

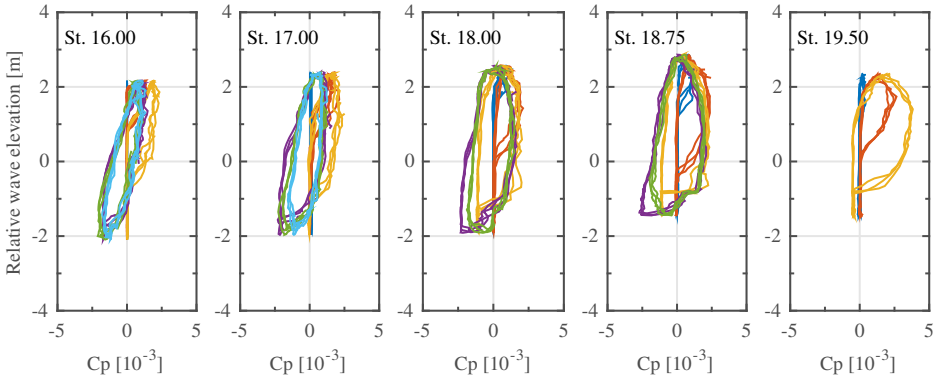

(b) Wave amplitude = 1.0 m

Figure B.7: The pressure and relative wave elevation diagram in short waves ($\lambda/L = 0.5$) at $Fn = 0.430$

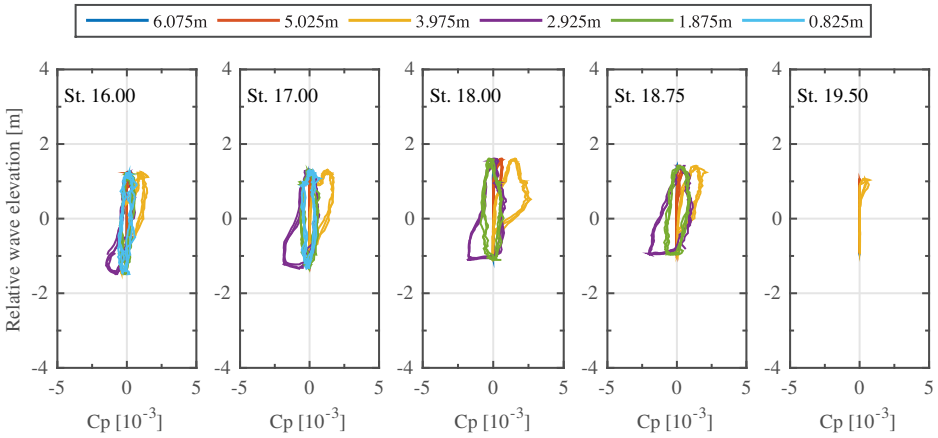

(a) Wave amplitude = 0.5 m

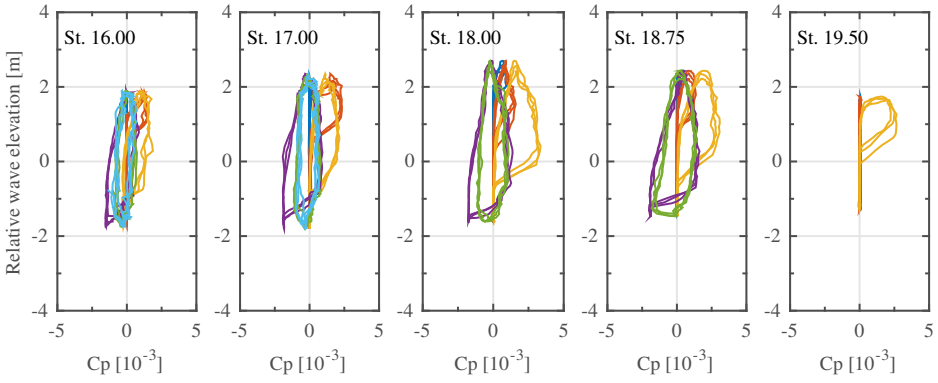

(b) Wave amplitude = 1.0 m

Figure B.8: The pressure and relative wave elevation diagram in short waves ($\lambda/L = 0.5$) at $Fn = 0.570$

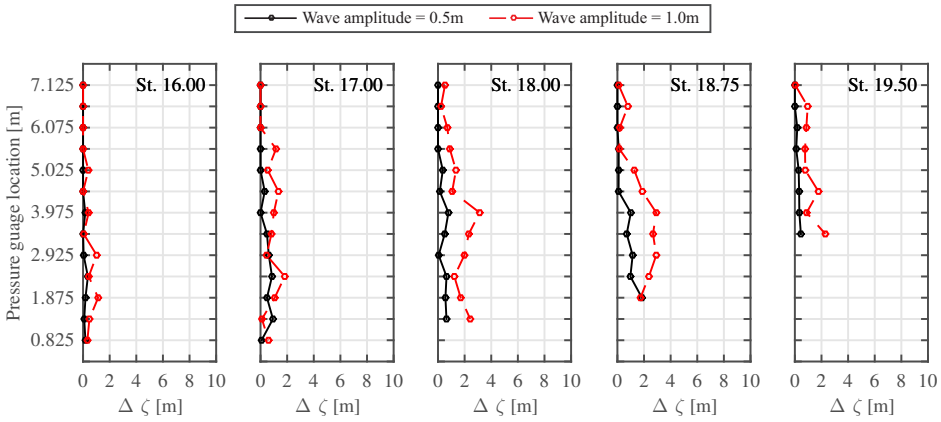

(a) $Fn = 0.430$

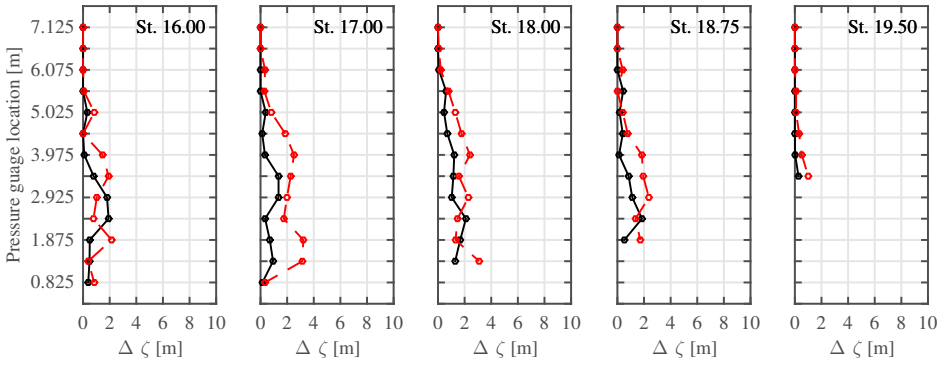

(b) $Fn = 0.570$

Figure B.9: The height difference ($\Delta\zeta$) between the highest relative wave elevation and the wave height on the maximum pressure in short waves (λ/L = 0.5)

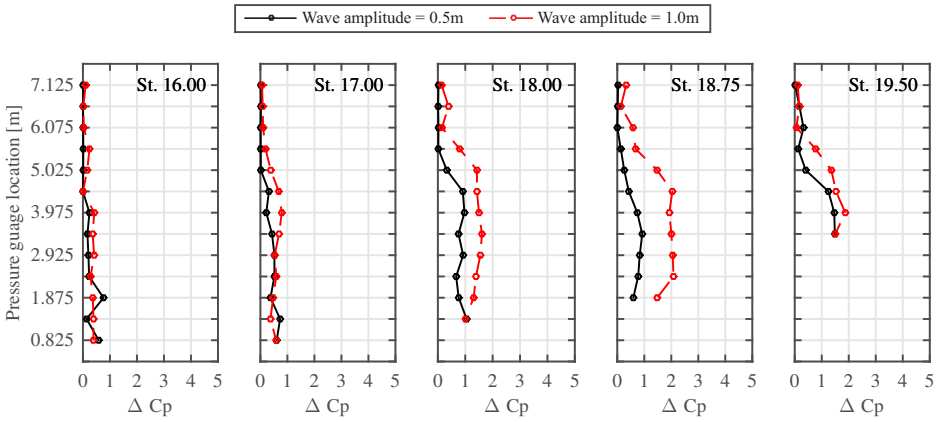

(a) Fn = 0.430

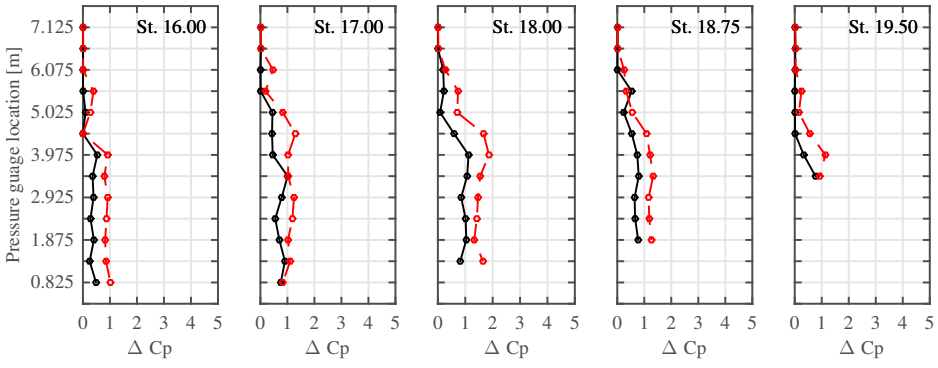

(b) Fn = 0.570

Figure B.10: The pressure drop (ΔCp) between the maximum pressure and the pressure at the highest relative wave elevation during upwash in short waves (λ/L = 0.5)

C

Assessment of amplitude effect in intermediate waves

Appendix B evaluates that the nonlinearity between pressure and relative wave elevation of the fast ship increases when the amplitude of short waves increases from 0.5 m to 1.0 m. Appendix C evaluates the nonlinearity of the intermediate waves as the amplitude of the wave increases from 0.5 m to 1.0 m. The amplitude of the incident wave of 0.5 m is added to the experiment in Chapter 4. The relative wave elevation is measured at five stations, and the pressures with 0.525 m vertical steps are measured at the same time. The measured pressure and relative wave elevation are analyzed using the tools proposed in Chapter 4. The list of analysis graphs is shown in Table C.1.

Figures C.1, C.2, C.3 and C.4 show the sequence histories of the unsteady pressure and bow wave under different conditions of ship's speed and the incident wave's amplitude, respectively. The sequence history of pressure indicates the impact of the bow wave in the hull pressure. Due to the large motion response in intermediate waves, the pressure acting on the hull and its variation are significant.

Figures C.5 and C.6 compare the pressure signals of a time series. Each graph shows the change in the pressure signal as a result of the wave amplitude at station 18. The slope of the pressure rise and fall increases as the wave amplitude increases.

Figures C.7 and C.8 show the relationship between measured pressure and relative wave elevation. At both speeds, the shape of the diagram has a significant

Table C.1: List of figures in Appendix C

No.	Type	Fn	λ/L	ζ_a [m]
Figure C.1	The sequence history of pressure	0.430	1.1	0.5
Figure C.2	The sequence history of pressure	0.430	1.1	1.0
Figure C.3	The sequence history of pressure	0.570	1.1	0.5
Figure C.4	The sequence history of pressure	0.570	1.1	1.0
Figure C.5	Pressure signals at St.18	0.430	1.1	0.5 and 1.0
Figure C.6	Pressure signals at St.18	0.570	1.1	0.5 and 1.0
Figure C.7	P-R diagram	0.430	1.1	0.5 and 1.0
Figure C.8	P-R diagram	0.570	1.1	0.5 and 1.0
Figure C.9	$\Delta\zeta$ in P-R diagram	0.430	1.1	0.5 and 1.0
Figure C.10	ΔCp in P-R diagram	0.570	1.1	0.5 and 1.0

correlation with the increase in wave amplitude. The nonlinearity is perceived intuitively as the bulge shape of the diagram increases.

Figure C.9 and Figure C.10 show the characteristic values ($\Delta\zeta$ and ΔCp) defined in Figure C.4 for the bulge shape of the P-R diagram. In Figures C.9 and C.10, the amplitude of the incident wave of 0.5 m is a black solid line, and the 1.0 m is a red dotted line. The stronger the counter-gradient in the upper right corner of the P-R diagram, the larger the value of both values. As in Appendix B, as the wave amplitude increases, the characteristic values at all stations in Figures C.9 and C.10 become larger.

Especially in Fn = 0.430, the change of the characteristic values with the increase of amplitude from 0.5 m to 1.0 m is detected. At station 16 and station 17, $\Delta\zeta$ and ΔCp of 0.5 m in Figure C.9 (a) and Figure C.10 (a) are negligible, but $\Delta\zeta$ and ΔCp of the amplitude of 1.0 m are increased to similar levels in the other stations.

Therefore, the increase in the amplitude of the incident waves expands the nonlinearity between pressure and relative wave elevation.

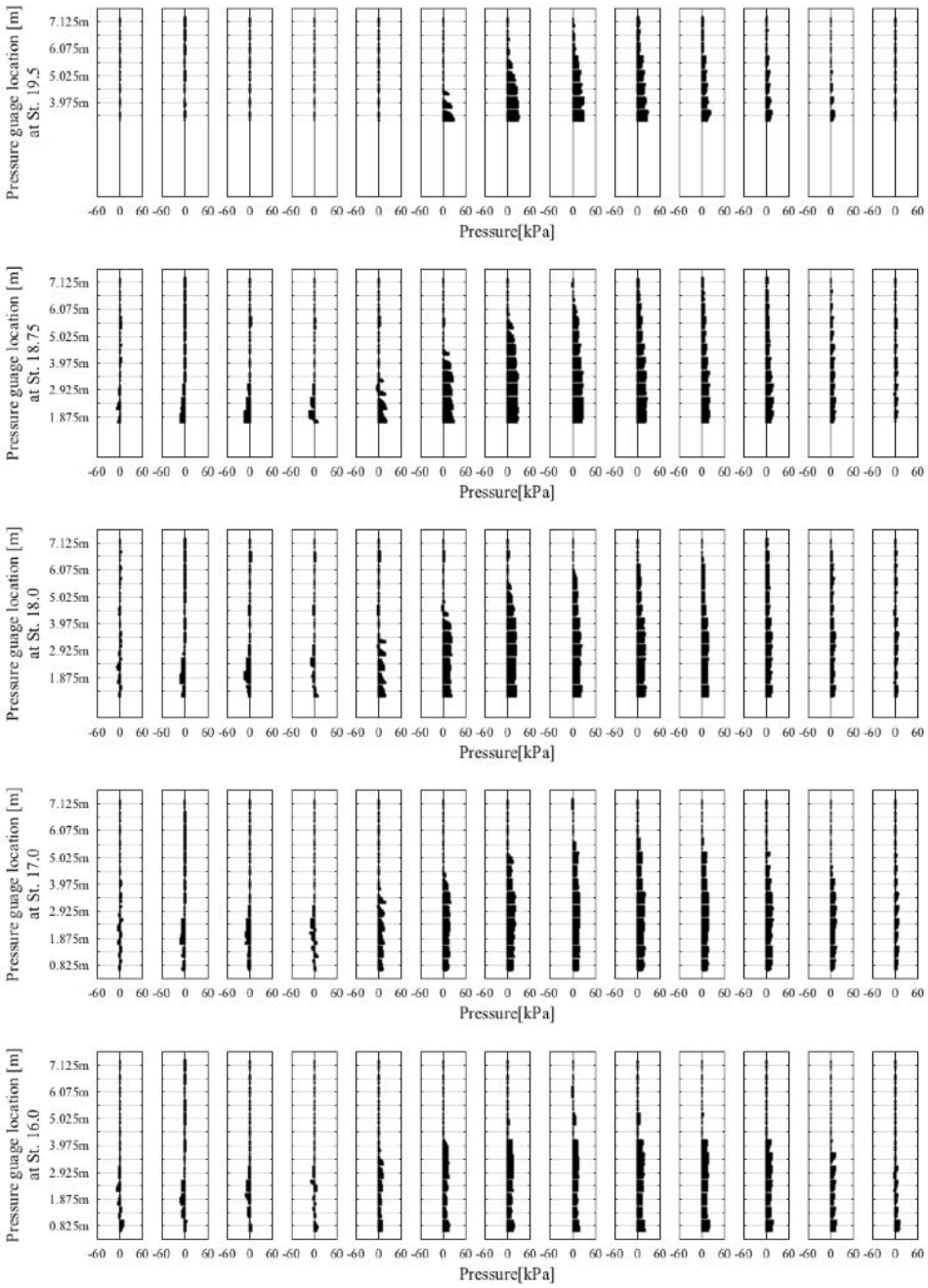

Figure C.1: The sequence history of pressure of the bow wave in intermediate waves (λ/L = 1.1) in wave amplitude = 0.5 m at Fn = 0.430

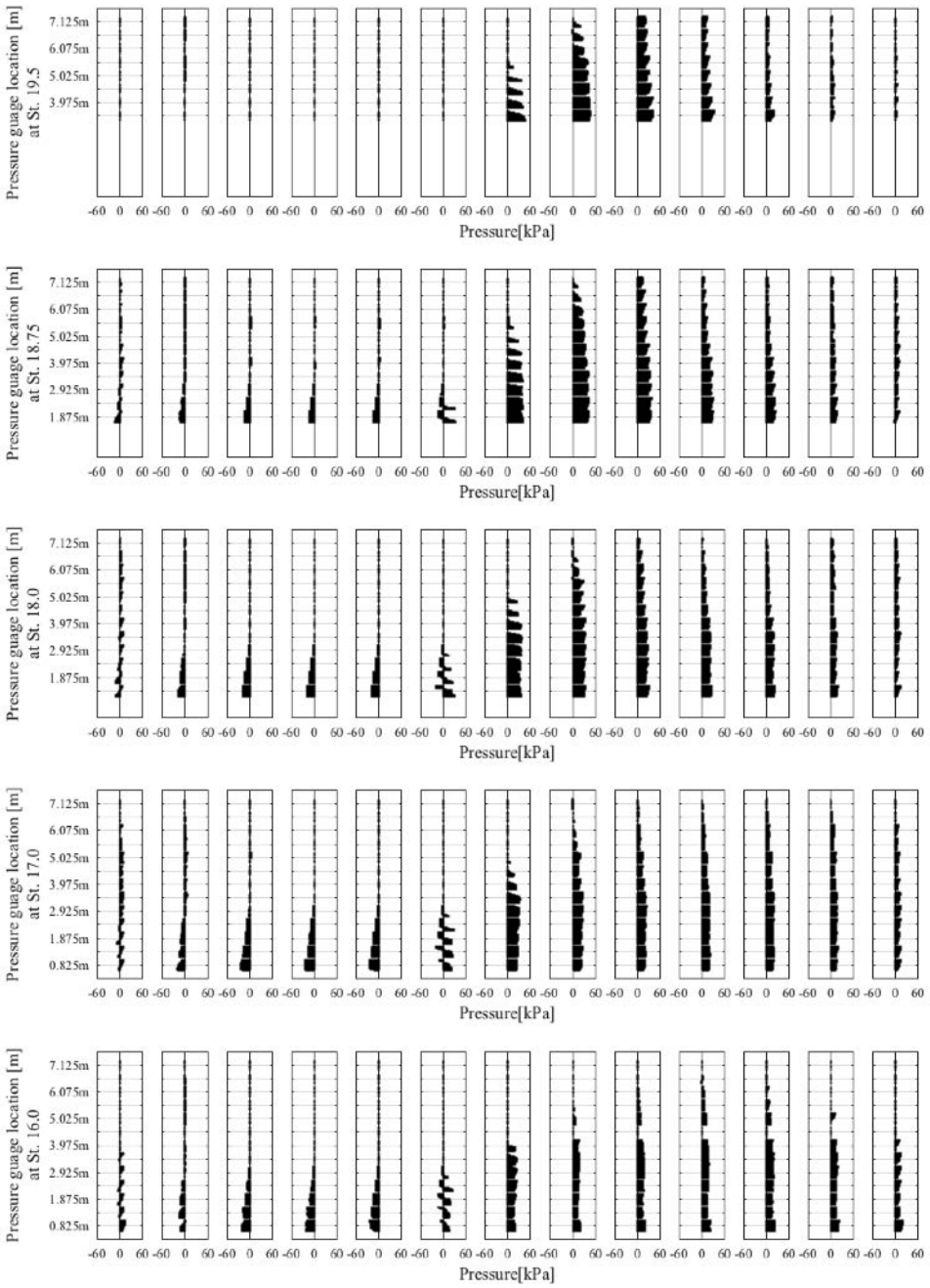

Figure C.2: The sequence history of pressure of the bow wave in intermediate waves (λ/L = 1.1) in wave amplitude = 1.0 m at Fn = 0.430

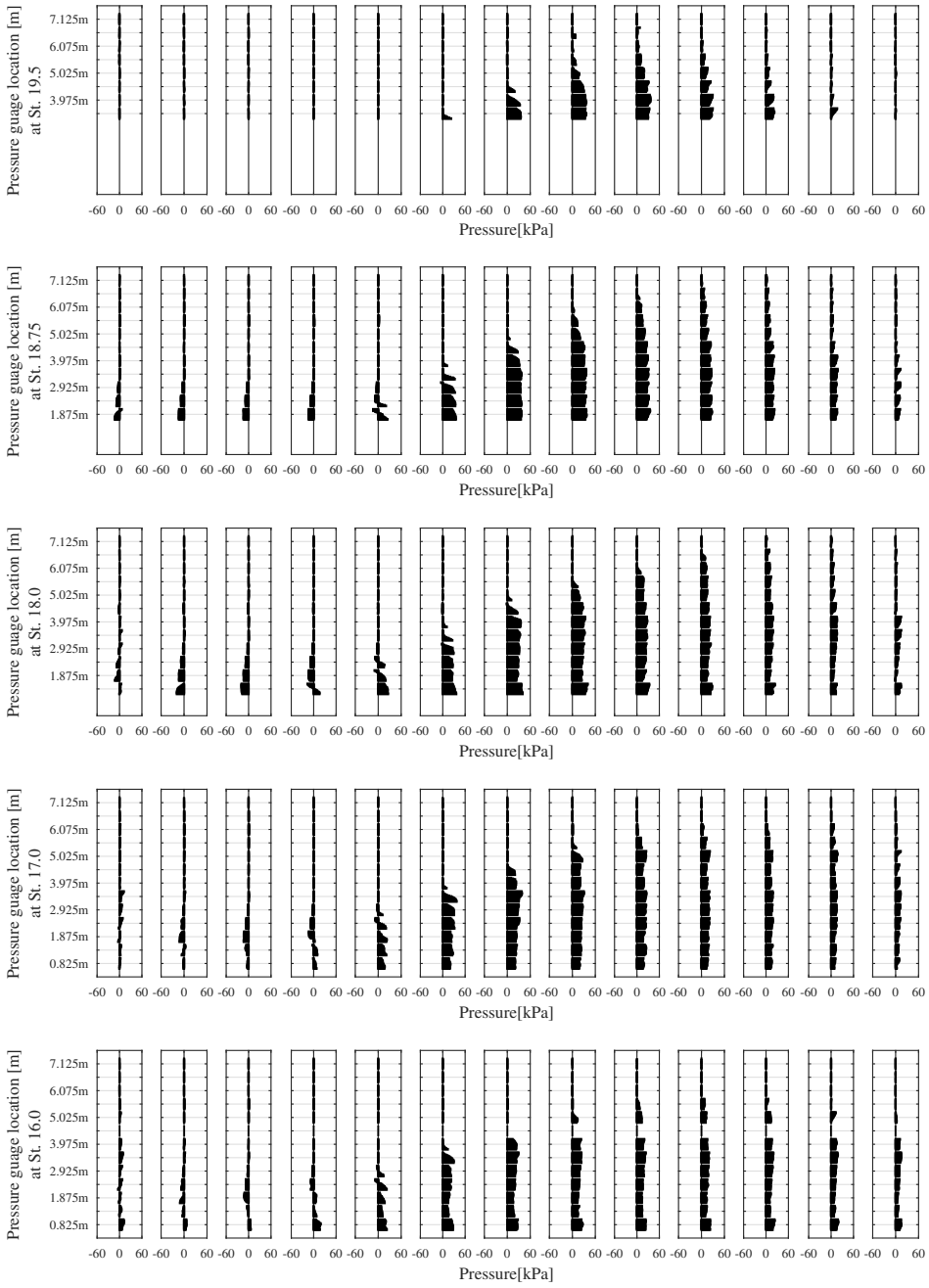

Figure C.3: The sequence history of pressure of the bow wave in intermediate waves (λ/L = 1.1) in wave amplitude = 0.5 m at Fn = 0.570

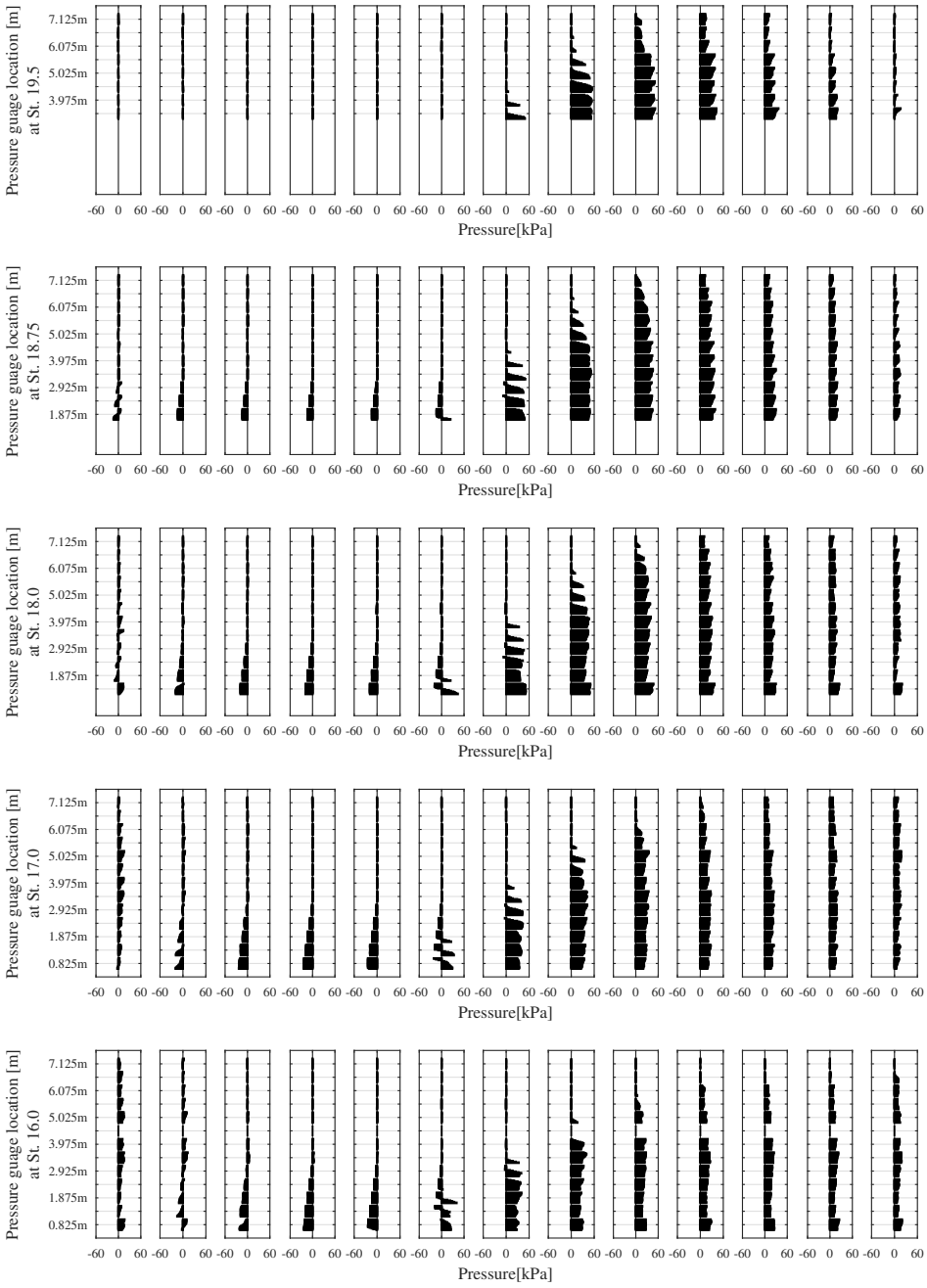

Figure C.4: The sequence history of pressure of the bow wave in intermediate waves (λ/L = 1.1) in wave amplitude = 1.0 m at Fn = 0.570

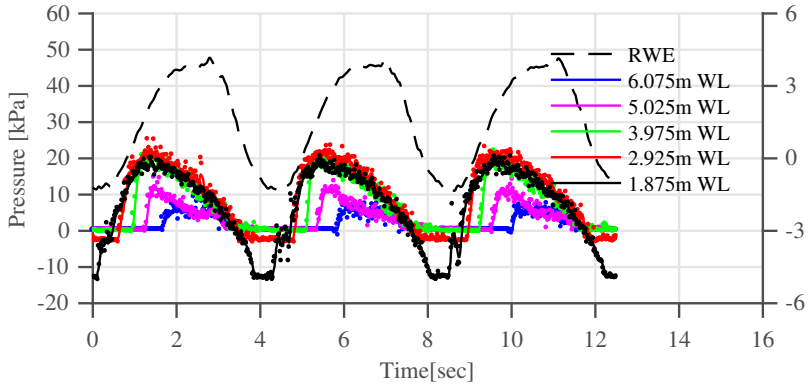

(a) Wave amplitude = 0.5 m

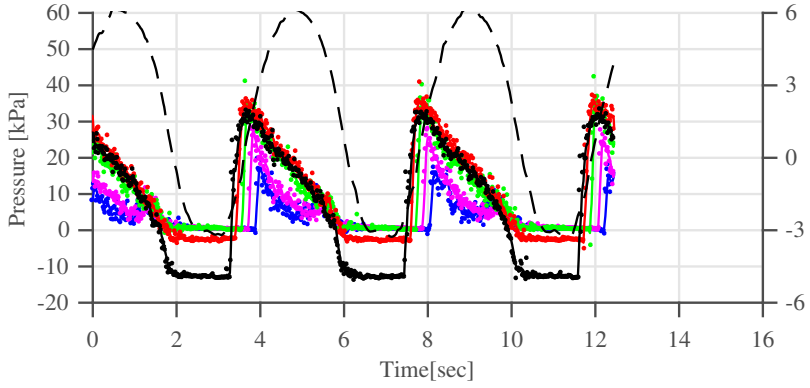

(b) Wave amplitude = 1.0 m

Figure C.5: An example of relative wave elevation (RWE) and pressure signals for three cycles. Pressure signals are smoothed with a time-based moving average filter of a five-point span over three speeds at station 18 in intermediate waves (λ/L = 1.1) at Fn = 0.430

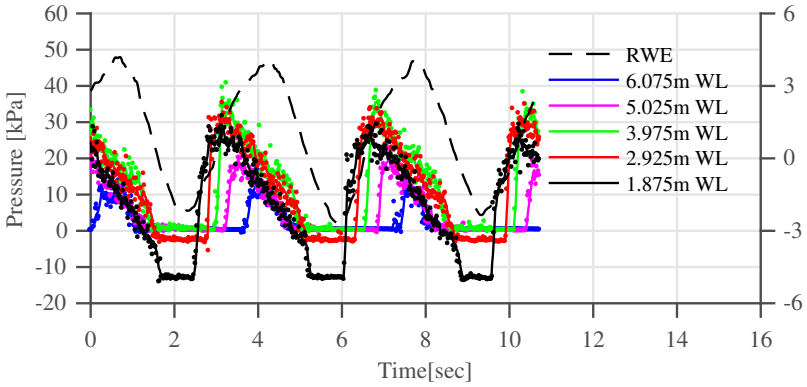

(a) Wave amplitude = 0.5 m

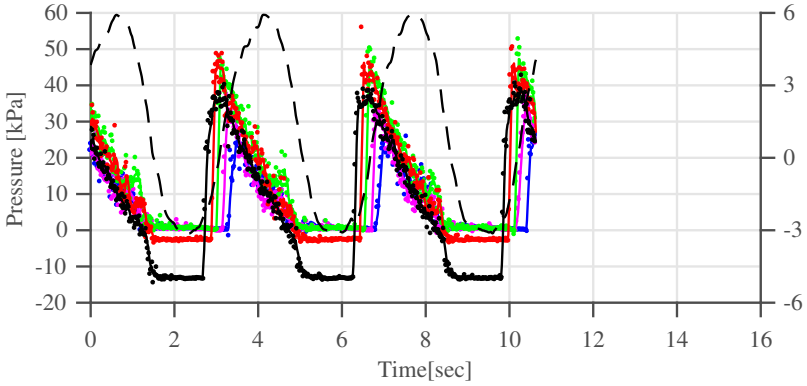

(b) Wave amplitude = 1.0 m

Figure C.6: An example of relative wave elevation (RWE) and pressure signals for three cycles. Pressure signals are smoothed with a time-based moving average filter of a five-point span over three speeds at station 18 in intermediate waves (λ/L = 1.1) at Fn = 0.570

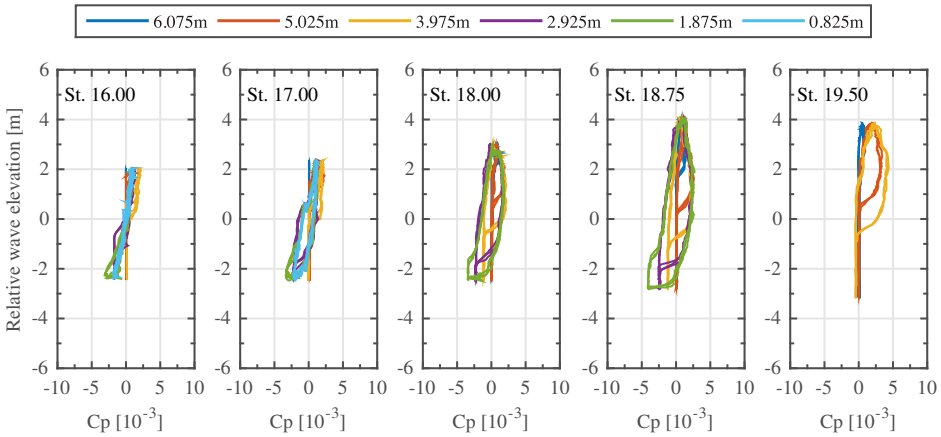

(a) Wave amplitude = 0.5 m

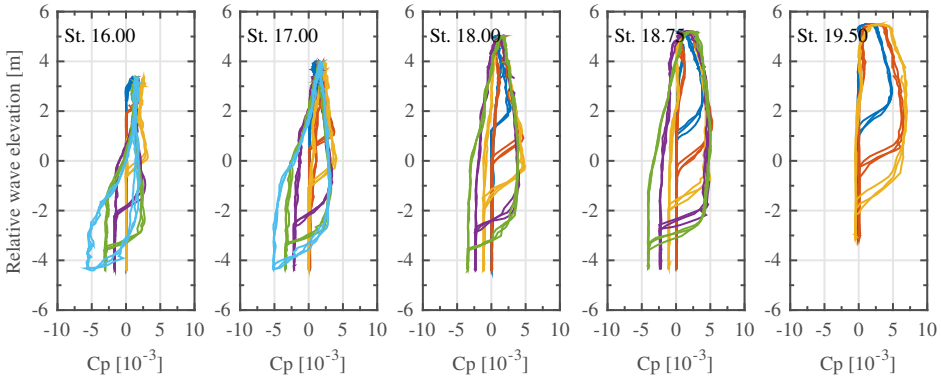

(b) Wave amplitude = 1.0 m

Figure C.7: The pressure and relative wave elevation diagram in intermediate waves (λ/L = 1.1) at Fn = 0.430

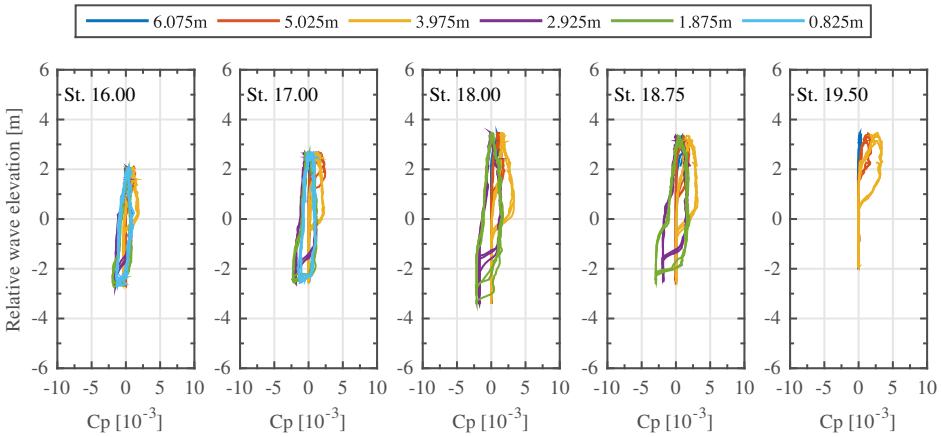

(a) wave amplitude = 0.5 m

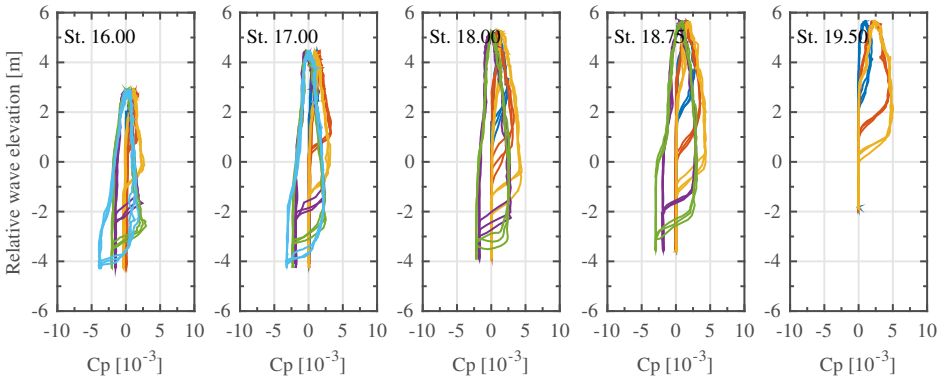

(b) wave amplitude = 1.0 m

Figure C.8: The pressure and relative wave elevation diagram in intermediate waves (λ/L = 1.1) at Fn = 0.570

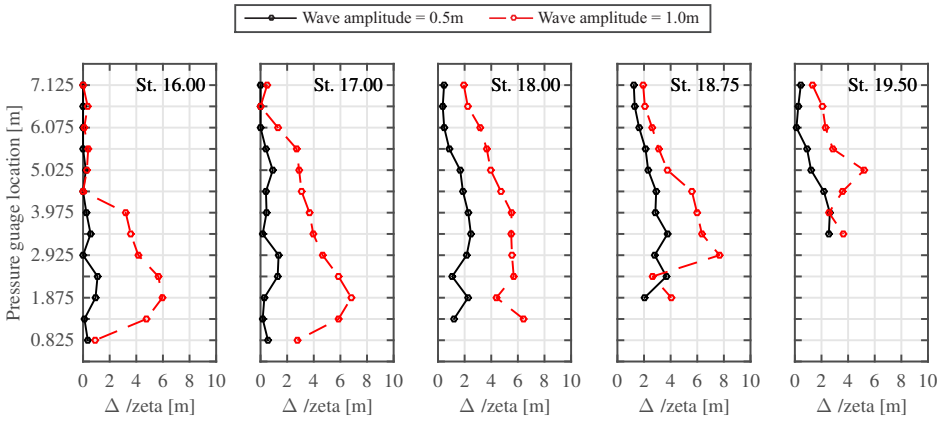

(a) $Fn = 0.430$

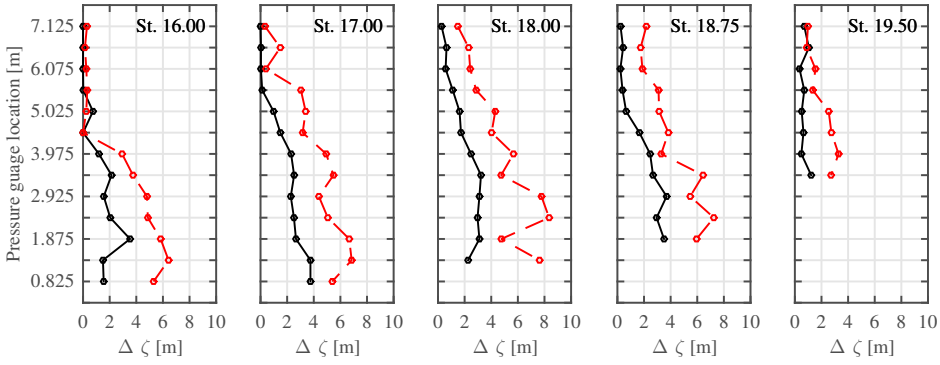

(b) $Fn = 0.570$

Figure C.9: The height difference ($\Delta\zeta$) between the highest relative wave elevation and the wave height on the maximum pressure in intermediate waves (λ/L = 1.1)

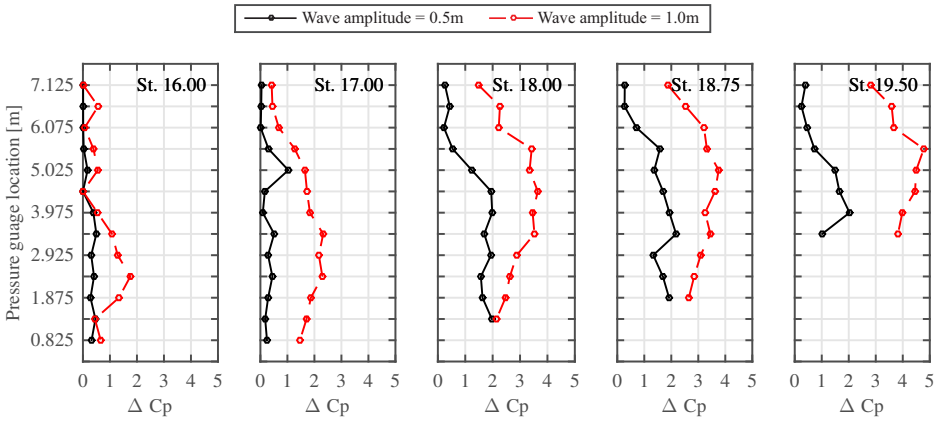

(a) $Fn = 0.430$

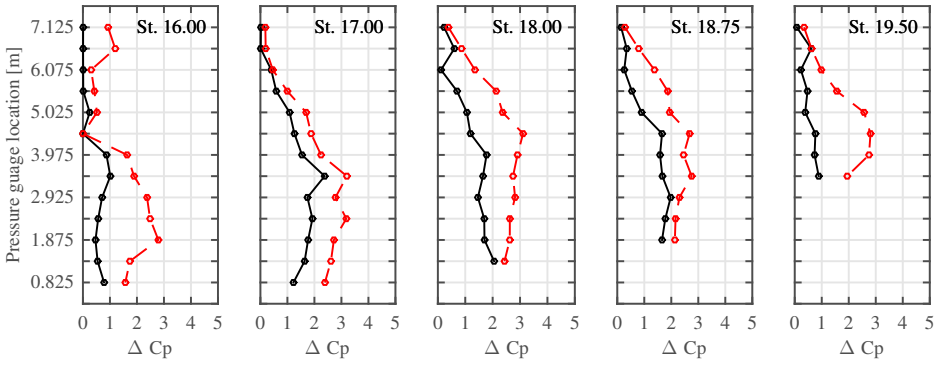

(b) $Fn = 0.570$

Figure C.10: The pressure drop (ΔCp) between the maximum pressure and the pressure at the highest relative wave elevation during upwash in intermediate waves (λ/L = 1.1)

REFERENCES

[1] IMO-MEPC, *Amendments to marpol annex vi on regulations for the prevention of air pollution from ships by inclusion of new regulations on energy efficiency for ships,* (2011).

[2] Y. Kim, D. Hayden, D. Fathi, G. Hermanski, P. de Jong, K. Tanizawa, G. Thomas, and W. Chengshen, *Seakeeping committee-final report and recommendations to the 27th ittct and recommendations to the 27th ittc,* in *Proceeding of 27th International Towing Tank Conference* (2014).

[3] B.-j. Guo and S. Steen, *Evaluation of added resistance of kvlcc2 in short waves,* Journal of Hydrodynamics, Ser. B **23**, 709 (2011).

[4] J. Ley, S. Sigmund, and O. el Moctar, *Numerical prediction of the added resistance of ships in waves,* in *ASME 2014 33rd International Conference on Ocean, Offshore and Arctic Engineering* (American Society of Mechanical Engineers, 2014).

[5] A. Papanikolaou, G. Zaraphonitis, E. Bitner-Gregersen, V. Shigunov, O. El Moctar, C. G. Soares, D. Reddy, and F. Sprenger, *Energy efficient safe ship operation (shopera),* Transportation Research Procedia **14**, 820 (2016).

[6] M. G. Seo, D. M. Park, K. K. Yang, and Y. Kim, *Comparative study on computation of ship added resistance in waves,* Ocean Engineering **73** (2013).

[7] H. Söding, V. Shigunov, T. E. Schellin, and O. el Moctar, *A rankine panel method for added resistance of ships in waves,* Journal of Offshore Mechanics and Arctic Engineering **136** (2014).

[8] H. Söding and V. Shigunov, *Added resistance of ships in waves,* Ship Technology Research **62**, 2 (2015).

[9] H. Maruo, *The drift of a body floating on waves,* Journal of Ship Research (1960).

[10] Strom-Tejsen, J. Hugh, Y. H. Yeh, and D. D. Moran, *Added resistance in waves,* Society of Naval Architects and Marine Engineers, Transactions **81**, 109 (1973).

[11] J. J. Blok, *The resistance increase of a ship in waves*, Ph.D. thesis, Delft University of Technology (1993).

[12] F. van Walree, D. Sgarioto, and T. Turner, *Validation of a time domain panel code for prediction of impulsive loads on high speed ships,* Symposium on Naval Hydrodynamics (2016).

[13] J. Gerritsma and W. Beukelman, *Analysis of the resistance increase in waves of a fast cargo ship,* International Shipbuilding Progress **19** (1972).

[14] H. Fujii and T. Takahashi, *Experimental study on the resistance increase of a ship in regular oblique waves,* in *Proceeding of 14th International Towing Tank Conference*, Vol. 4 (1975) pp. 351–360.

[15] S. Nakamura and S. Naito, *Propulsive performance of a container ship in waves,* Naval architecture and ocean engineering **15**, 24 (1977).

[16] J. M. J. Journée, *Experiments and calculations on 4 wigley hull forms in head waves,* Delft University of Technology, Report **909** (1992).

[17] M. Tsujimoto, *A practical correction method for added resistance in waves,* The Japan Society of Naval Architects and Ocean Engineers , 11 (2008).

[18] M. Kuroda, M. Tsujimoto, N. Sasaki, S. Ohmatsu, and K. Takagi, *Study on the bow shapes above the waterline in view of the powering and greenhouse gas emissions in actual seas,* Proceedings of the Institution of Mechanical Engineers, Part M: Journal of Engineering for the Maritime Environment **226**, 23 (2011).

[19] H. Maruo, *The excess resistance of a ship in rough seas* (International Shipbuilding Progress, 1957).

[20] C. D. Simonsen, J. F. Otzen, S. Joncquez, and F. Stern, *Efd and cfd for kcs heaving and pitching in regular head waves,* Journal of Marine Science and Technology **18**, 435 (2013).

[21] D. C. Kring, W. M. Milewski, and N. E. Fine, *Validation of a nurbs-based bem for multihull ship seakeeping,* in *25th Symposium on Naval Hydrodynamics, St. John's* (2004).

[22] D. M. Park, J. Lee, and Y. Kim, *Uncertainty analysis for added resistance experiment of kvlcc2 ship,* Ocean Engineering **95**, 143 (2015).

[23] D. M. Park, Y. Kim, M. G. Seo, and J. Lee, *Study on added resistance of a tanker in head waves at different drafts,* Ocean Engineering **111**, 569 (2016).

[24] M. P. Abdul Ghani and P. A. Wilson, *Experimental analysis of the seakeeping performance of catamaran forms with bulbous bows,* International Shipbuilding Progress , 1 (2017).

[25] Y. Watanabe, *Some contributions to the theory of rolling*, Vol. 80 (Trans. RINA, 1938) pp. 408–432.

[26] T. H. Havelock, *The resistance of a ship among waves,,* Proceedings of the Royal Society, Report A-161 (1937).

[27] T. H. Havelock, *The drifting force on a ship among waves,* The London (1942).

[28] J. M. J. Journée and W. W. Massie, *Offshore Hydromechanics* (Delft University of Technology, 2001).

[29] A. R. J. M. Lloyd, *Seakeeping: ship behaviour in rough weather* (Ellis Horwood, 1989).

[30] R. Hosoda, *The added resistance of ships in regular oblique waves,,* Japanese Society of Naval Architects **133**, 1 (1973).

[31] N. Salvesen, E. O. Tuck, and O. Faltinsen, *Ship motions and sea loads,* Trans SNAME (1970).

[32] N. Salvesen, E. O. Tuck, and O. Faltinsen, *Ship motions and sea loads,* Trans. SNAME **78**, 250 (1970).

[33] K. J. Bai and R. W. Yeung, *Numerical solutions to free-surface flow problems,* in *Proceedings of the 10th Symposium on Naval Hydrodynamics, Cambridge, MA* (1974) pp. 609–647.

[34] R. Brard, *The representation of a given ship form by singularity distributions when the boundary condition on the free surface is linearized,* Journal of Ship Research **16** (1972).

[35] M. D. Greenberg, *Applications of Green's functions in science and engineering* (Courier Dover Publications, 1971).

[36] M. A. Squires and P. A. Wilson, *An investigation into translating pulsating green'functions for ship motion prediction,* in *Proceedings of Computer Aided Design, Manufacture and Operation in the Marine and Offshore Industries(CADNO'92)* (Computational Mechanics Publications, 1992).

[37] G. X. Wu and R. E. Taylor, *The hydrodynamic force on an oscillating ship with low forward speed,* Journal of Fluid Mechanics **211**, 333 (1990).

[38] G. E. Gadd, *A method of computing the flow and surface wave pattern around full forms,* Trans. RINA 1976 , 207 (1976).

[39] C. W. Dawson, *A practical computer method for solving ship-wave problems,* in *Proceedings of the second international conference on numerical ship hydrodynamics* (1977) pp. 30–38.

[40] W. J. Piers, *Discretization schemes for the modelling of free water surface effects in first-order panel methods for hydrodynamic applications* (Nationaal Lucht-en Ruimtevaartlaboratorium, 1983).

[41] P. D. Sclavounos and D. E. Nakos, *Stability analysis of panel methods for free-surface flows with forward speed,* 17th Symposium on Naval Hydrodynamics (1989).

[42] D. E. Nakos and P. D. Sclavounos, *On steady and unsteady ship wave patterns,* Journal of Fluid Mechanics **215**, 263 (1990).

[43] H. C. Raven, *A solution method for the nonlinear ship wave resistance problem* (MARIN, 1996).

[44] T. H. J. Bunnik, *Seakeeping calculations for ships, taking into account the nonlinear steady waves*, Ph.D. thesis, Delft University of Technology (1999).

[45] R. Dallinga, T. Bunnik, and E. de Montgolfier, *Reducing added resistance of ships in waves,* Greenship , 1 (2011).

[46] W. P. A. Joosen, *Added resistance of ships in waves,* in *Proc 6th Symp Naval Hydrodynamics, Wasington, D.C.* (1966).

[47] M. Kashiwagi, T. Ikeda, T. Sasakawa, *et al.*, *Effects of forward speed of a ship on added resistance in waves,* International Journal of Offshore and Polar Engineering **20** (2010).

[48] S. A. G. Joncquez, H. B. Bingham, and P. Andersen, *Validation of added resistance computations by a potential-flow boundary-element method,* Symposium on Naval Hydrodynamics (2008).

[49] J. N. Newman, *Marine hydrodynamics,* (1977).

[50] M.-C. Fang and G.-R. Chen, *On the nonlinear hydrodynamic forces for a ship advancing in waves,* Ocean Engineering **33**, 2119 (2006).

[51] P. Boese, *Eine einfache methode zur berechnung der widerstandserhöhung eines schiffes im seegang*, Tech. Rep. (Ship Design and Ship Safety M-6, 1970).

[52] O. M. Faltinsen, K. J. Minsaas, N. Liapis, and S. Skjørdal, *Prediction of resistance and propulsion of a ship in a seaway,* Proceeding of 13th Symposium on Naval Hydrodynamics Tokyo (1980).

[53] K. H. Kim and Y. Kim, *Numerical study on added resistance of ships by using a time-domain rankine panel method,* Ocean Engineering **38**, 1357 (2011).

[54] J. Grue and E. Palm, *The mean drift force and yaw moment on marine structures in waves and current,* Journal of Fluid Mechanics (1993).

[55] H. K. Ye and C. C. Hsiung, *Computation of added wave resistance of a restrained floating body in the time-domain,* International shipbuilding progress (1997).

[56] K.-H. Kim, M.-G. Seo, and Y. Kim, *Numerical analysis on added resistance of ships,* International Journal of Offshore and Polar Engineering **22** (2012).

[57] M. Kuroda, M. Tsujimoto, T. Fujiwara, S. Ohmatsu, and K. Takagi, *Investigation on components of added resistance in short waves,* Journal of the Japan Society of Naval Architects and Ocean Engineers , 171 (2008).

[58] G. Bingjie and S. Steen, *Experiment on added resistance in short waves,* in *28th Symposium on Naval Hydrodynamics, Califormia, USA* (2010).

[59] W. Duan and C. Li, *Estimation of added resistance for large blunt ship in waves,* Journal of Marine Science and Application **12**, 1 (2013).

[60] M. Kashiwagi, *Prediction of surge and its effect on added resistance by means of the enhanced unified theory,* Trans. of West-Japan Soc. Nav. Arch. **89**, 77 (1995).

[61] M. G. Seo, K. K. Yang, D. M. Park, and Y. Kim, *Numerical analysis of added resistance on ships in short waves,* Ocean Engineering **87**, 97 (2014).

[62] H. Orihara and H. Miyata, *Evaluation of added resistance in regular incident waves by computational fluid dynamics motion simulation using an overlapping grid system,* Journal of Marine Science and Technology (2003).

[63] L. Larsson, F. Stern, and M. Visonneau, *Numerical ship hydrodynamics*, An assessment of the Gothenburg 2010 Workshop (Springer Science & Business Media, Dordrecht, 2013).

[64] H. Sadat-Hosseini, P.-C. Wu, P. M. Carrica, H. Kim, Y. Toda, and F. Stern, *Cfd verification and validation of added resistance and motions of kvlcc2 with fixed and free surge in short and long head waves,* Ocean Engineering **59**, 240 (2013).

[65] C. Hu, T. Mikami, and K. Yamamoto, *Prediction of added resistance in short waves by cfd simulation,* International Workshop on Water Waves and Floating Bodies , 1 (2014).

[66] O. E. Moctar, S. Sigmund, J. Ley, and T. E. Schellin, *Numerical and experimental analysis of added resistance of ships in waves,* Journal of Offshore Mechanics and Arctic Engineering (2016).

[67] A. Papanikolaou, G. Zaraphonitis, A. Maron, and T. Karayannis, *Nonlinear effects of vertical plane motions of ships with forward speed in waves,* Proceedings of fourth international osaka colloqium on seakeeping performance of ships, OC. Osaka (2000).

[68] W. Thomson, *On the waves produced by a single impulse in water of any depth, or in a dispersive medium,* (The Royal Society, 1887) pp. 80–83.

[69] H. Miyata, H. ORIHARA, and Y. SATO, *Nonlinear ship waves and computational fluid dynamics,* Proceedings of the Japan Academy, Series B **90**, 278 (2014).

[70] T. Inui, H. Miyata, and H. Kajitani, *Experimental investigations on the wave making in the near-field of ships,* (1979).

[71] H. Miyata, T. Inui, and H. Kajitani, *Free surface shock waves around ships and their effects on ship resistance,* J. Soc. Naval Arch. Japan (1980).

[72] H. Miyata and T. Inui, *Nonlinear ship waves,* Advances in Applied Mechanics (1984).

[73] Y. Toda, F. Stern, and J. Longo, *Mean-flow measurements in the boundary layer and wake and wave field of a series 60 cb=0.6 ship model. i : Froude numbers 0.16 and 0.316,* Journal of ship research **36**, 360 (1992).

[74] J. H. Duncan, *The breaking and non-breaking wave resistance of a two-dimensional hydrofoil,* Journal of Fluid Mechanics **126**, 507 (1983).

[75] A. Olivieri, F. Pistani, R. Wilson, E. F. Campana, and F. Stern, *Scars and vortices induced by ship bow and shoulder wave breaking,* Journal of Fluids Engineering **129**, 1445 (2007).

[76] R. R. Dong, J. Katz, and T. T. Huang, *On the structure of bow waves on a ship model,* Journal of Fluid Mechanics **346**, 77 (1997).

[77] G. I. Roth, D. T. Mascenik, and J. Katz, *Measurements of the flow structure and turbulence within a ship bow wave,* Physics of Fluids (1999).

[78] T. A. Waniewski, C. E. Brennen, and F. Raichlen, *Bow wave dynamics,* Journal of Fluid Mechanics (2002).

[79] A. Olivieri, F. Pistani, and A. Di Mascio, *Breaking wave at the bow of a fast displacement ship model,* Journal of Marine Science and Technology **8**, 68 (2003).

[80] A. Karion, T. C. Fu, T. Waniewski-Sur, J. R. Rice, D. C. Walker, and D. A. Furey, *Experiment to examine the effect of scale on a breaking bow wave*, Tech. Rep. (DTIC Document, 2004).

[81] E. Maxeiner, M. Shakeri, and J. H. Duncan, *A parametric study of breaking bow waves using a 2d + t technique,* Journal of Fluid Mechanics **687**, 540 (2011).

[82] S. Marrone, A. Colagrossi, M. Antuono, C. Lugni, and M. P. Tulin, *A 2d+t sph model to study the breaking wave pattern generated by fast ships,* Journal of Fluids and Structures **27**, 1199 (2011).

[83] G. B. Deng, E. Guilmineau, P. Queutey, and M. Visonneau, *Ship flow simulations with the ISIS CFD code* (CFD Workshop Tokyo, 2005).

[84] R. Luquet, E. Jacquin, P. E. Guillerm, and L. Gentaz, *RANSE with Free Surface Computations around fixed and Free DTMB 5415 model in Still Water and in Waves* (CFD Workshop, 2005).

[85] D. G. Dommermuth, T. O'Shea, K. Hendrickson, X. Dong, G. Weymouth, and D. K. P. Yue, *Modeling breaking ship waves for design and analysis of naval vessels challenge project C1V* (IEEE, 2005).

[86] P. M. Carrica, R. V. Wilson, and F. Stern, *Unsteady rans simulation of the ship forward speed diffraction problem,* Computers & Fluids **35**, 545 (2006).

[87] G. Weymouth, K. Hendrickson, D. K. P. Yue, T. OShea, D. G. Dommermuth, P. Adams, and M. Valenciano, *Modeling breaking ship waves for design and analysis of naval vessels,* Department of Defense - Proceedings of the HPCMP Users Group Conference 2007; High Performance Computing Modernization Program: A Bridge to Future Defense, DoD HPCMP UGC , 440 (2007).

[88] A. Colagrossi and M. Landrini, *Numerical simulation of interfacial flows by smoothed particle hydrodynamics,* Journal of Computational Physics **191**, 448 (2003).

[89] Longuet-Higgins, S. Michael, and E. D. Cokelet, *The deformation of steep surface waves on water-i. a numerical method of computation,* in *Proceedings of the Royal Society of London*, Vol. 350 (1976) pp. 1–26.

[90] F. Noblesse, D. Hendrix, L. Faul, and J. Slutsky, *Simple analytical expressions for the height, location, and steepness of a ship bow wave,* Journal of Ship Research **50**, 360 (2006).

[91] F. Noblesse, G. Delhommeau, M. Guilbaud, D. Hendrix, and C. Yang, *Simple analytical relations for ship bow waves,* Journal of Fluid Mechanics **600**, 105 (2008).

[92] G. Delhommeau, M. Guilbaud, L. David, C. Yang, and F. Noblesse, *Boundary between unsteady and overturning ship bow wave regimes,* Journal of Fluid Mechanics **620**, 167 (2009).

[93] P. R. Payne, *Contributions to planing theory,* Ocean Engineering (1995).

[94] J. J. Blok and W. Beukelman, *The high-speed displacement ship systematic series hull forms-seakeeping characteristics,* Transactions-Society of Naval Architects and Marine Engineers **92**, 125 (1984).

[95] J. J. Blok and J. Huisman, *Relative motions and swell-up for a frigate bow,* Royal Institution of Naval Architects Transactions **126** (1984).

[96] A. M. Ferguson and I. W. Dand, *Hull and bulbous bow interaction,* Publication of: Royal Institution of Naval Architects **112** (1970).

[97] A. R. J. M. Lloyd, J. O. Salsich, and J. J. Zseleczky, *The effect of bow shape on deck wetness in head seas,* Royal Institution of Naval Architects (1985).

[98] J. J. Blok and J. Huisman, *Relative motions and swell-up for a frigate bow,* Royal Institution of Naval Architects Transactions **126** (1984).

[99] M. A. Squires, *An investigation into the static and dynamic swell up effect for ship motions*, Ph.D. thesis, University of Southampton (1992).

[100] R. J. Rapp and W. K. Melville, *Laboratory measurements of deep-water breaking waves,* Philosophical Transactions of the Royal Society of London. Series A, Mathematical and Physical Sciences , 1 (1990).

[101] Y. Kayo and K. Takekuma, *On the free-surface shear flow related to bow wave-breaking of full ship models,* Journal of the society of Naval Architectects of Japan **149**, 11 (1981).

[102] M. A. Ali, K. Suzuki, and S. Miyauchi, *Study on bow wave breaking around ultra large block coefficient ship,* Journal of Naval Architecture and Marine Engineering **10**, 69 (2013).

[103] M. Kashiwagi, T. Sasakawa, and T. Wakabayashi, *Hydrodynamic study on added resistance by means of unsteady wave analysis method,* in *Proceedings of the Twenty-first International Offshore and Polar Engineering Conference* (International Society of Offshore and Polar Engineers, 2011).

[104] J. M. J. Journée, *Motions, resistance and propulsion of a ship in regular head waves,* Delft University of Technology, Report **428** (1976).

[105] J. A. Pinkster, *Low frequency second order wave exciting forces on floating structures*, Ph.D. thesis, Delft University of Technology (1980).

[106] G. K. Kapsenberg, A. B. Aalbers, A. Koops, and J. J. Blok, *Fast displacement ships: The marin systematic series* (Maritime Research Institute Netherlands, 2014).

[107] J. B. Hadler, *Coefficients for international towing tank conference 1957 model-ship correlation line*, Tech. Rep. (DTIC Document, 1958).

[108] G. K. Kapsenberg, *The marin systematic series fast displacement hulls,* Int. HISWA Symposium on Yacht Design and Yacht Construction (2012).

[109] B. Guo and S. Steen, *Experiment on added resistance in short waves,* Symposium on Naval Hydrodynamics , 1 (2010).

[110] S. Liu and A. Papanikolaou, *Fast approach to the estimation of the added resistance of ships in head waves,* Ocean Engineering **112**, 211 (2016).

[111] S. Liu, A. Papanikolaou, G. Zaraphonitis, *et al.*, *Practical approach to the added resistance of a ship in short waves,* in *The Twenty-fifth International Offshore and Polar Engineering Conference* (International Society of Offshore and Polar Engineers, 2015).

NOMENCLATURE

Abbreviations

2D	Two Dimensional
2D+T	Two-dimensional plus time
BEM	Boundary Element Method
CFD	Computational Fluid Dynamics
DNS	Direct Numerical Simulation
DTMB	David Taylor Model Basin
e.g.	For example
EEDI	Energy Efficiency Design Index
EEOI	Energy Efficiency Operation Index
EUT	Enhanced Unified Theory
FDS	Fast Displacement Ship
G-B method	Gerritsma and Beukelman method
GT	Gross Tonage
IMO	International Maritime Organization
ITTC	International Towing Tank Conference
KCS	Korea Container Ship
KVLCC	Korea Very Largy Croude oil Carrier
LPMC	Linear Potential Method Calculation
MARIN	Maritime Research Institute Netherlands
MEPC	Marine Environment Protection Committee
MRV	Regulation on Monitoring, Reporting and Verification
PIV	Particle Image Velocimetry

QTF	Quadratic Transfer Function
RANS	Reynolds-Average Navier-Stokes
RAO	Response Amplitude Operator
Ro-ro	Roll-on and roll-off
RWE	Relative Wave Elevation
SHOPERA	energy efficient safe SHip OPERAtion
SMB	Seakeeping and Maneuvering Basin
SPH	Smoothed Particle Hydrodynamics
St.	Station
URANSE	Unsteady Reynolds Average Navier-Stokes

Latin Letters

$\vec{n}$	Normal vector	$[-]$
$\vec{x}$	Coordinate vector	$[m]$
$\vec{\ddot{x}_g}$	Gravitational body accelerations	$[m/s^2]$
B	Ship breadth at still water	$[m]$
C_B	Block coefficient of the ship	$[-]$
C_f	Frictional resistance coefficient	$[-]$
C_r	Residual resistance coefficient	$[-]$
C_t	Total resistance coefficient	$[-]$
C_{px}	Pressure coefficient in longitudinal direction	$[-]$
CO_2	Carbon dioxide	
D	Ship depth	$[m]$
dS	Infinitesimal wetted hull surface	$[m^2]$
F	Force	$[N]$
Fn	Froude number	$[-]$
g	Gravitational constant	$[m/s^2]$
L	Ship length	$[m]$
Lpp	Ship length between perpendicular	$[m]$

M	Mass	$[kg]$
n_x	Normal vector in longitudinal direction	$[-]$
p	Pressure	$[Pa]$
p_{atm}	Constant atmospheric pressure	$[Pa]$
Rn	Reynolds number	$[-]$
S	Hull surface area	$[m^2]$
s	Smooth transition function	
U	Velocity of the ship	$[m/s^2]$
x	Longitudinal direction in Cartesian coordinates	$[m]$
x_g	Longitudinal center of gravity	$[m]$
y	Horizontal direction in Cartesian coordinates	$[m]$
y_g	Horizontal center of gravity	$[m]$
z	Vertical direction in Cartesian coordinates	$[m]$

Greek Letters

α	Total displacement vector	$[m]$
α_E	Waterline entrance angle	$[deg]$
α_{heave}	Vertical motion displacement by heave	$[deg]$
Δ	Difference	
η	Directional motion vector	$[m]$
λ	Wavelength	$[m]$
∇	Differential operator given in Cartesian coordinates	$[-]$
Ω	Rotational motion vector	$[deg]$
ϕ	Steady velocity potential	$[m^2/s]$
Ψ	Velocity potential	$[m^2/s]$
ρ	Fluid density	$[kg/m^3]$
θ_{pitch}	Angle of pitch motion	$[deg]$
θ_{roll}	Angle of roll motion	$[deg]$
φ	Unsteady velocity potential	$[m^2/s]$

ζ	Wave height	$[m]$
ζ_a	Amplitude of the incident wave	$[m]$
ζ_u	Unsteady wave height	$[m]$
ζ_{diff}	Diffracted wave height	$[m]$
ζ_{inc}	Incident wave height	$[m]$
ζ_{rad}	Radiated wave height	$[m]$

Subscripts

0	Initial condition
atm	Atmospheric
g	Gravitational
l	Line
$mean$	Average
p	Pressure
s	Steady
t	Time
u	Unsteady
wl	Waterline

Superscripts

(0)	Zeroth order
(1)	First order

Acknowledgements

I have greatly enjoyed my four years of research at the Delft University of Technology. Writing this dissertation was often challenging, but I have completed it with the help of many people around me, and I am glad to have accomplished this. I sincerely thank all those who have helped me to complete this thesis.

First, I would like to thank my family, who have always supported me during my time at Delft. Words cannot describe the wisdom, encouragement, and love that my wife, Myung-Ock Kim has given me. She took a break from her career in Korea so that we could live in the Netherlands, and she devoted herself to the care and support of our family. She helped me by reading the draft of my thesis and discussing its contents and language. I am glad that she is now free from the daily routines of caring for our son and me. She will always be my best friend and wisest teacher. I thank my son Eun-Woo and Eun-Seong for never minding my absence from home. When I was home, they would happily share their meals and even their desserts with me. Eun-Woo also contributed to my thesis by helping me select the font. I derived much joy from simply tucking Eun-Seong into his bed every day as he fell asleep. Our family in Korea has also supported us throughout. I thank my father in heaven. I always be grateful to my mother Mal-Young Ji and my sister Mun-Kyung Choi for their prayers and support. I am also grateful to my father-in-law In-Nam Kim and mother-in-law Ho-Kyung Lee for their prayers for our family's success and health.

I would like to express my deep gratitude to Professor Rene Huijsmans for granting and promoting my Ph.D. research at the Delft University of Technology. He has always guided my work and shared his wisdom to help me complete my dissertation in time. Our valuable discussions on various topics and data were crucial to completing this dissertation.

I also thank my co-promoter Dr. Peter Wellens for his many insightful suggestions and careful review of the draft of my thesis. His valuable comments greatly helped me in improving my thesis.

I would like to thank MARIN for providing the experimental data used in this thesis. Geert Kapsenberg helped me to use the test data and provided insightful feedback on my research proposal. Dr. Tim Bunnik helped me to use the linear potential program. Reint Dallinga guided me in the direction of this project at the beginning of my research.

Prof. Riaan van't Veer gave me an opportunity to review his numerical calculation code. This code helped me in understanding the connection between theory development and numerical analysis.

I would like to thank Prof. Younghwan Kim, one of the committee members. When I met him at the conference, he provided me with new information regarding my project, and he encouraged me to complete my thesis. Prof. Philip Wilson, another committee member, discussed my thesis with me and provided many helpful references. In fact, I thank all of the committee members for their valuable time in discussing and reviewing this thesis.

Professor Hyochul Kim, my teacher during my bachelor's and master's degree studies, gave me the strength and encouragement to finish my degree on time. He continues to inspire me with his enthusiasm for marine research.

Hyung-Taek Kim and Joo-Hyuck Choi shared opinions on the drafts and presentations of our projects; they also shared their respective experiences of studying in the United States and Denmark. Dr. Kyung-Gyu Yang spent two nights with me at a conference for reviewing the structure of my thesis.

I am grateful to all those who have helped me with specific aspects of this project. Dr. Won-Sup Lee helped me with the MATLAB code for handling the large dataset obtained from the model test. This code served as the basis for the data processing in my work and saved me a lot of time. Young-Sil Lee and Byeong-Woo Kim used Adobe Illustrator to produce clear figures from my hand-drawn images. Joo-Young Jung discussed the doctorate course and the English writing; she even lent me a desktop computer for free during my doctoral course.

During my years in Delft, I have benefited greatly from the valuable discussions and stories over coffee at the Towing Tank group. I had refreshing talks with group members about my project and even my personal life. Dr. Lex Kunning was kind enough to take the Towing Tank group on his yacht for our refreshing. Hans van der Hek's suggestions helped improve my family's quality of life in Delft. Frits Sterk discussed Dutch culture and politics with me. Peter Poot helped me to keep my thoughts and attitude positive. Piet de Heer occasionally provided chocolates and waffles during the coffee talks. Dr. Cornel Thill helped me to keep my works lighthearted. Dr. Sebastian discussed his work and shared many stories. Dr. Peter Naaijen followed my progress and occasionally shared his advice. Guido and I had many thoughts on Dutch life. Jasper always had a warm smile, and Jenifer always encouraged me. Nico reviewed my drafts and advised me on the English language. Matteo and Gunnar shared many coffee talks at towing tank.

I am grateful to my SHS colleagues who shared the same floor as the office. Our lunchtime talks were always interesting and helped me understand the cultures of different countries. My office colleague Tao Zou and I encouraged each other to successfully complete our degrees; we also spent much time discussing the culture of our different countries in the Netherlands.

I thank the people who helped me settle down in the Netherlands. Dr. Jie Dang recommended me to Professor Rene. He gave me a lot of advice when I started my research and family life in the Netherlands. Ye-Chan Yoon helped me and my family adjust to the Netherlands relatively quickly. Kyung-Ho Choe introduced me to many people in the Netherlands and also invited me to events I could attend.

I am particularly grateful to the DELft DOCtors (DELDOC) members who offered useful suggestions on the content and format of my thesis, including Eun-Chul Kang, Min-Young Kwon, Dr. Soo-Hyun Gong, Sang-Yup Kim, Dr. Seung-Hyun Kim, Dr. Sung-Chul Kim, Dr. Je-Kyung Ryu, Wan-Seo Park, Dr. Il-Yong Jung, and Seung-Kyu Ha. Moreover, the Korean student association at the Delft University of Technology helped me out whenever I needed.

I also thank the couples who spent their time with us in Delft. Dr. Myung-Jae Lee and Min-Young Cho shared much time with my family in Delft, and they discussed my family's daily life as well as my research. Dr. Doo-Yoon Kim shared his experiences in writing English theses, and his wife Mi-Jung Gim was always a delight. I am grateful to Dr. Jay Yoo and Sue-Kyung Chun as well as Yong-Yeon Bae and Bitna Oh for the delicious recipes and many travel stories they shared. I thank Jae-Ik Jung and Son-Hwa Yoon for sharing the information about family life in the Netherlands. I also thank Don-Sam Lim and Su-Jung Chae as well as Hyung-Jun Chun and Young-Mi Yoo for the love and encouragement they gave to my family in the Netherlands.

I am grateful to my many colleagues at Hyundai Maritime Research Institute (HMRI) for helping me to get my degree program funded by Hyundai Heavy Industries (HHI). They also helped me through many difficulties. Heung-Won Seo and Seok-Cheon Go contributed to this study and supported me in various ways, and they played crucial roles in my obtaining my doctoral degree. Dr. Hong-Gi Lee, Dr. Young-Jae Sung, Dr. Hyun-Ho Lee, Dr. Kyung-Soo Ahn helped me commit to starting my doctoral research. Yoon-Mo Lee handled the work I left behind at the company. Dr. Bong-Jun Chang encouraged me as well as my family life. Seok-Ho Son, and Dr. Bum-Woo Han provided much encouragement. Dr. Sang-Bong Lee worked in the neighboring office during his sabbatical at the TU Delft and discussed many aspects of my research. My achievements would not be possible without my research experience with my colleagues at HMRI.

I thank all of my family, friends and colleagues who have supported me through this journey. Finally, I apologize to anyone I may have forgotten to thank; I still owe them my deepest gratitude.

CURRICULUM VITÆ

BongJun Choi

BongJun Choi is a research engineer at Hyundai Heavy Industries (HHI). He was born on July 5, 1979, in Changwon, South Korea. In 2002 and 2004, he receives his Bachelor's and Master of Science degrees from Naval Architecture and Ocean Engineering at the Seoul National University. He studied experimental fluid dynamics at the Seoul National University's Towing Tank from 2000 to 2003. At the University, he participated in several experiments and the development of measurement devices such as the research of human-powered vessel, anti-rolling tank, and highly efficient rudder system.

Since January 2004, he continued his career as a researcher at the Towing Tank in the Maritime Research Institute of HHI. His main area of expertise in HHI has been to evaluate the power performance of the ship through experiments and numerical analyzes. He has focused his researches on the scale effect in the full-scale extrapolation from model tests, and the development of advanced measurement system. He also carried out hydrodynamics-based projects of the ship, such as hullform design and energy saving device development. He had a working experience in experimental fluid dynamics for twelve years before starting his doctoral research in 2013.

Since May 2013, he had been a Ph.D. researcher at the Delft University of Technology in the Netherlands with the financial support from HHI. He completed this thesis as a result of his Ph.D. research and has been returned to the Maritime Research Institute of the HHI for continuing his research in experimental fluid dynamics.

Career

2011-Present	Research Engineer Performance Evaluation Department Hyundai Maritime Research Institute Hyundai Heavy Industries Co., Ltd.
2013-2017	Director Korean Scientists and Engineers Association in the Netherlands (KOSEANL)
2009-2010	Senior Engineer Initial Design Department Shipbuilding Division Hyundai Heavy Industries Co., Ltd.
2004-2009	Researcher Resistance and Propulsion Research Department Hyundai Maritime Research Institute Hyundai Heavy Industries Co., Ltd.

Awards

2013	Full scholarship for graduate school (Ph.D.) Hyundai Heavy Industries Co., Ltd.
2007	Award for excellent researcher Hyundai Heavy Industries Co., Ltd.
2002	Full scholarship for graduate school (M.S.) Hyundai Heavy Industries Co., Ltd.
2002	1st prize in Human Powered Vessel Festival 2002 The Society of Naval Architects of Korea
2001	2nd prize in Human Powered Vessel Festival 2001 The Society of Naval Architects of Korea
2000	1st prize in Human Powered Vessel Festival 2000 The Society of Naval Architects of Korea

List of Publications

<Articles related to this thesis>

- **B. Choi**, R.H.M. Huijsmans, *Experimental assessment of effects of bow wave breaking on added resistance for the fast ship*, International Shipbuilding Progress, (2017 submitted)
- **B. Choi**, R.H.M. Huijsmans, *An analysis method to evaluate the added resistance in short waves considering bow wave breaking*, Proceedings of the 12th International Conference on Hydrodynamics, (2016)
- **B. Choi**, R.H.M. Huijsmans, *Experimental Investigation of Plunging Bow Wave Breaking in Short Waves*, Proceedings of the 31st Symposium on Naval Hydrodynamics, (2016)
- **B. Choi**, R.H.M. Huijsmans, *Intuitive discriminant method for the overturning bow wave breaking in short waves*, Europe-Korea Conference on Science and Technology 2016, (2016)

<Articles not related to this thesis>

- J.H. Kim, J.E. Choi, **B. Choi**, S.H. Chung, H.W. Seo, *Development of energy-saving devices for a full slow-speed ship through improving propulsion performance*, International Journal of Naval Architecture and Ocean Engineering, (2015)
- J.H. Kim, J.E. Choi, **B. Choi**, S.H. Chung, *Twisted rudder for reducing fuel-oil consumption*, International Journal of Naval Architecture and Ocean Engineering, Vol.6, pp.715-722, (2014)
- J.E. Choi, J.H. Kim, **B. Choi**, S.B. Lee, S.H. Chung and H.W. Seo, *Development of Energy-Saving Devices for a Full Slow-Speed Ship through Improving Propulsion Performance*, The 12th Symposium of Practical Design of Ships and other Floating Structures: PRADS 2013, (2013)
- J.E. Choi, J.H. Kim, H.G. Lee, **B. Choi**, D.H. Lee, *Computational predictions of ship-speed performance*, Journal of marine science and technology, Volume 14, (2009)

- J.E. Choi, J.H. Kim, D.H. Lee, **B. Choi**, *Speed-Power Prediction of a Large LNG Carrier Based on the Analysis of the CFD Results*, Proceedings of the Society of Naval Architects of Korea, (2007)
- **B. Choi**, J.M. Yang, H.W. Park, J.S. Kim, H.C. Kim, *Experimental Evaluation of High Performance Rudder Enhanced by Coanda Effect for VLCC at Low Speed Operation*, International Conference on Hydrodynamics 2004, (2004)
- **B. Choi**, H. Kim, *An Experimental Evaluation of the Coanda Jet Applied High Efficient Rudder System for VLCC*, Journal of Ship and Ocean Technology, Vol. 8, No. 2, Society of Naval Architects of Korea, (2004)
- **B. Choi**, H.W. Park, H. Kim, S.H. Lee, *An Experimental Evaluation on the Performance of High Lifting Rudder under Coanda Effect*, Proceedings of the 9th International Symposium on Practical Design of Ships and other Floating Structures, Vol.1, pp.329 336, (2004)
- **B. Choi**, H. Kim, *An Evaluation of High-Lifting Rudder Enhanced by the Coanda Effects on Maneuverability*, Proceedings of the Society of Naval Architects of Korea, pp.88 93, (2004)
- **B. Choi**, H. Kim, *An Experimental Evaluation of the Coanda Jet Applied High Efficient Rudder System for VLCC*, Proceedings of International Workshop on Frontier Technology in Ship and Ocean Engineering, (2003)
- J.M. Lew, H. Kim, **B. Choi**, *Design and Construction of Controlled Passive Anti-Rolling Tanks*, Proceedings of International Workshop on Frontier Technology in Ship and Ocean Engineering, (2003)
- **B. Choi**, H.W. Park, J.S. Kim, H. Kim, *Experimental Evaluation of Open Water Performances of High Lifting Rudder under Coanda Effect*, Proceedings of the Society of Naval Architects of Korea, pp.245-250, (2003)
- **B. Choi**, H.S. Ahn, J.S. Kim, H. Kim, *Design of high lift Rudder for model test*, Proceedings of the Society of Naval Architects of Korea, pp.307-311, (2003)
- J.M. Lew, **B. Choi**, H. Kim, *On the Passive type Anti-Rolling Tank and its Activation by Air Blower*, Journal of Ship and Ocean Technology, Vol. 7, (2003)
- J.M. Lew, H. Kim, **B. Choi**, *Development of Passive and Active Anti-Rolling Tanks*, Proceedings of The Fifth ISOPE Pacific/Asia Offshore Mechanics Symposium, (2002)
- J.M. Lew, H. Kim, **B. Choi**, *A Study on the Effects of the Period Adjustment Device of Anti-Rolling Tanks*, Proceedings of the Society of Naval Architects of Korea, pp.260 - 263, (2002)
- **B. Choi**, J.S. Kim, H.C. Kim, *Report on the Design and Construction of Human Powered Vessel-Poseria*, Proceedings of the Society of Naval Architects of Korea, (2001)